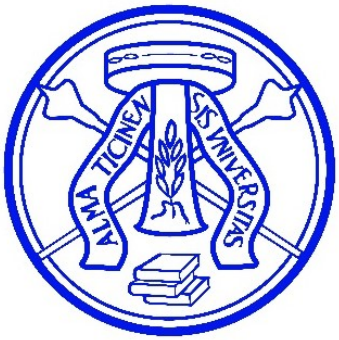

UNIVERSITÀ DEGLI STUDI DI PAVIA

DOTTORATO IN SCIENZE CHIMICHE E FARMACEUTICHE E INNOVAZIONE INDUSTRIALE

(XXXIV Ciclo)

Coordinatore: Chiar.mo Prof. Giorgio Colombo

"Sustainable Donor and Acceptor Components for Organic Photovoltaic Cells"

Tesi di Dottorato di

Giacomo Forti

A.A. 2020/2021

Tutor: Prof. Dario Pasini

Co-Tutor: Dott. Gabriele Bianchi

TABLE OF CONTENTS

CHAPTER 1: Introduction

1.1 ABBREVIATIONS

1.2. INTRODUCTION TO ORGANIC PHOTOVOLTAICS

1.3. NONFULLERENE ACCEPTORS (NFA_S)

1.3.1. MODIFICATION OF ELECTRON-DEFICIENT END-CAPPING GROUPS

1.3.2. STRUCTURAL MODIFICATION OF THE IDIC/ITIC AND Y6 CORE

1.4. SUSTAINABILITY, INDUSTRIAL CONSIDERATIONS, AND SCALABILITY OF NFAS.

1.5. FINAL REMARKS

CHAPTER 2: Sustainable synthetic approaches to the IDIC core through domino cyclization/deprotection reaction

2.1. INTRODUCTION

2.2. RESULTS AND DISCUSSION

2.3. CONCLUSION

2.4. EXPERIMENTAL PART

CHAPTER 3: Sustainable synthetic approaches to the IDIC core through domino cyclization/deprotection reaction

3.1 INTRODUCTION

3.2 RESULTS AND DISCUSSION

3.3. CONCLUSION

3.4. EXPERIMENTAL PART

CHAPTER 4: Synthesis of novel polymers no fullerene acceptors (PMSAs) based on anthradithiophene for bulk heterojunction solar cells (BHJs)

4.1 INTRODUCTION

4.2 RESULTS AND DISCUSSION

4.3. CONCLUSION

4.4. EXPERIMENTAL PART

CHAPTER 5: Synthesis of novel polymers no fullerene acceptors (PMSAs) via DARP

5.1 INTRODUCTION

5.2 RESULTS AND DISCUSSION

5.3. CONCLUSION

5.4. EXPERIMENTAL PART

6. Appendix

6.2 Chapter 2

6.3 Chapter 3

6.4 Chapter 4

6.5. Chapter 5

1.1→ ABBREVIATIONS

ADT	*Anthradithiophene*
aADT	*Angularly fused ADT*
lADT	*Linear fused ADT*
a-BC	*a 2-(3-oxo2,3-dihydro-1H-benzo [b]cyclopenta[d]thiophen-1-ylidene)*
BHJ_s	*Bulk Heterojunction solar cells*
BT	*benzothiadiazole*
BTA	*benzotriazole*
Bu_3SnCl	*Tributyltin chloride*
Bu_4NI	*Tetrabutylammonium iodide*
D-A	*Donor-Acceptor*
DMA	*Dimethylacetamide*
DMSO	*Dimethyl sulfoxide*
DHA	*Direct hetero arylation*
FA_s	*Fullerene acceptors*
FF(%)	*Fill-Factor*
GPC	*Gel permation chromatography*
GIWAXS	*Grazing-incidence small-angle X-ray scattering*
HOMO	*Highest occupied molecular orbital*
ITO	*Tin-doped indium oxide*
IC	*3-(Dicyanomethylidene)indan-1-one*
IDIC	*2,2'-((2Z,20Z)-((4,4,9,9-tetrahexyl-4,9- dihydro-s-indaceno[1,2-b:5,, 6-b']dithiophene-2,7-*

	diyl)bis(methanylylidene))bis(3-oxo-2,3-dihydro-1Hindene-2,1-diylidene))dimalononitrile
ITIC	*3,9-bis(2-methylene-(3-(1,1-dicyanomethylene)-indanone)-5,5,11,11-tetrakis(4-hexylphenyl)-dithieno[2,3-d:20 ,30 -d']-s-indaceno[1,2-b:5,6-b']dithiophene)*
ICT	*Internal charge transfer*
J_{sc}	*Short-circuit current*
LDA	*Lithium diisopropylamide*
LUMO	*Lowest unoccupied molecular orbital*
MoO_3	*Molybdenum Oxide*
NFA_s	*Non-fullerene acceptors*
NSS	*Number of synthetic steps*
NT	*2-octyldodecyl naphtho[1,2-b]thiophene-4-carboxylate*
ND2000	*Poly{[N,N'-bis(2-octyldodecyl)-naphthalene-1,4,5,8-bis(dicarboximide)-2,6-diyl]-alt-5,5'-(2,2'-bithiophene)}*
OD	*Optical density*
$OFET_s$	*Organic field-effect transistor*
$OLED_s$	*organic light-emitting devices*
OPV	*Organic photovoltaics*
PCE	*Power Conversion Efficiency*
PSC	*Polymer solar cell*
$PMAS_s$	*Polymer small molecule acceptors*
PC61BM	*[6,6]-phenyl-C61-butyric acid methyl esther*
PC71BM	*phenyl-[C71]-butyric acid methyl esther*

PM5	*Poly[[4,8-bis[5-(2-ethylhexyl)-2-thienyl]benzo[1,2-b:4,5-b']dithiophene-2,6-diyl]-2,5-thiophenediyl[5,7-bis(2-ethylhexyl)-4,8-dioxo-4H,8H-benzo[1,2-c:4,5-c']dithiophene-1,3-diyl]]*
PM6	*Poly[[4,8-bis[5-(2-ethylhexyl)-4-fluoro-2-thienyl]benzo[1,2-b:4,5-b']dithiophene-2,6-diyl]-2,5-thiophenediyl[5,7-bis(2-ethylhexyl)-4,8-dioxo-4H,8H-benzo[1,2-c:4,5-c']dithiophene-1,3-diyl]-2,5-thiophenediyl]*
$Pd_2(dba)_3$	*Tris(dibenzylideneacetone)dipalladium(0)*
$P(o\text{-}tolyl)_3$	*Tri(o-tolyl)phosphine*
$^{i}PrOH$	*Isopropyl alcohol*
PPV	*Poly(1,4-phenylene-vinylene)*
PEDOT:PSS	*Poly(3,4-ethylenedioxythiophene)-poly(styrenesulfonate)*
P3HT	*Poly(3-hexylthiophene-2,5-diyl)*
PDINN	*N,N'-Bis{3-[3-(Dimethylamino)propylamino]propyl}perylene-3,4,9,10-tetracarboxylic diimide*
SC	*Synthetic complexity*
TT	*Thieno[3,4-b]thiophene*
TMEDA	*N,N,N',N'-Tetramethyl ethylenediamine*
TGA	*Thermo gravimetric analysis*
Td	*Decomposition temperature*
V_{oc}	*Open-circuit voltage*
VT-NMR	*Varian temperature NMR*

Chapter 1

Introduction

This chapter is partly based on the following publication: *Recent Advances in Non-Fullerene Acceptors of the IDIC/ITIC Families for Bulk-Heterojunction Organic Solar Cells*', G. Forti, A. Nitti, P. Osw, G. Bianchi, R. Po, D. Pasini, *Int. J. Mol. Sci.* **2020**, *21*, 8085.

1.1→ INTRODUCTION TO ORGANIC PHOTOVOLTAICS

Since the industrial revolution, the world energy demand has been constantly increasing with our welfare, and consequently the demand for energy resources, in the first-place fossil fuels (coal, oil and natural gas). Considering that the United Nations have recently said that the population on the earth will reach almost 10 billion in 2050, energies policies should be guided to overcome the demand for the fossil fuels in favor of renewable energy (nuclear, hydroelectric, solar etc.), which are unlimited and much cleaner. The World Energy Agency data, over the past years, confirm a trend towards renewable energies (Figure 1.1).[1[

[1] BP Statistical Review of World Energy, **2019**. https://www.bp.com/en/global/corporate/energy-economics/statistical-review-of-world-energy.html

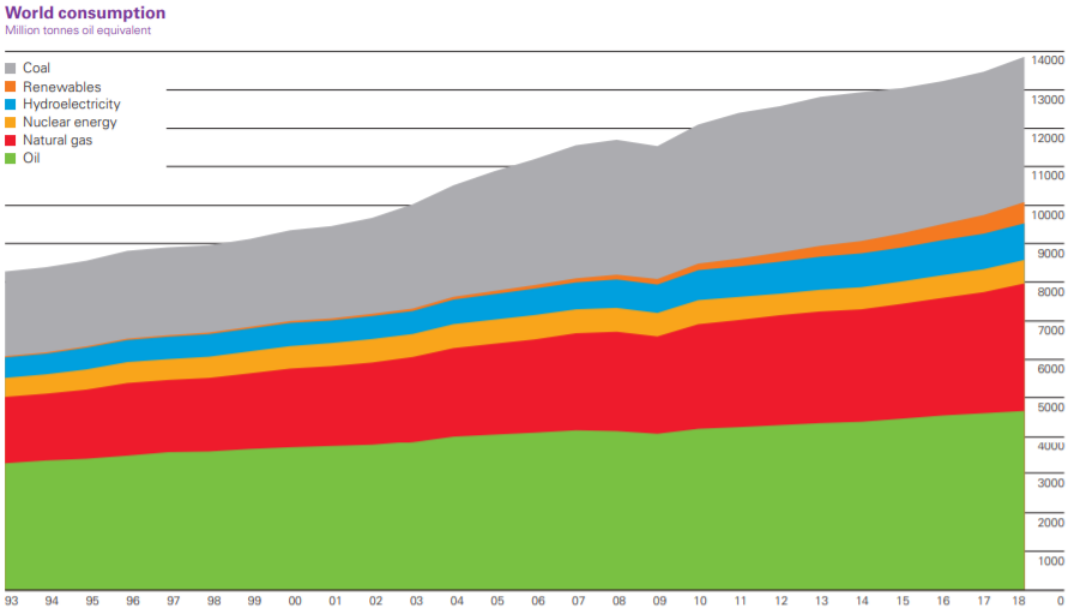

Figure 1.1: global trend of energy consumption from 1993 to 2018

From the graph, it is clear that the world energy demand in the past 30 years has grown intensively; despite hydroelectric and nuclear energy have the same trend, renewable energy sources have had a remarkable growth (Figure 1.2).

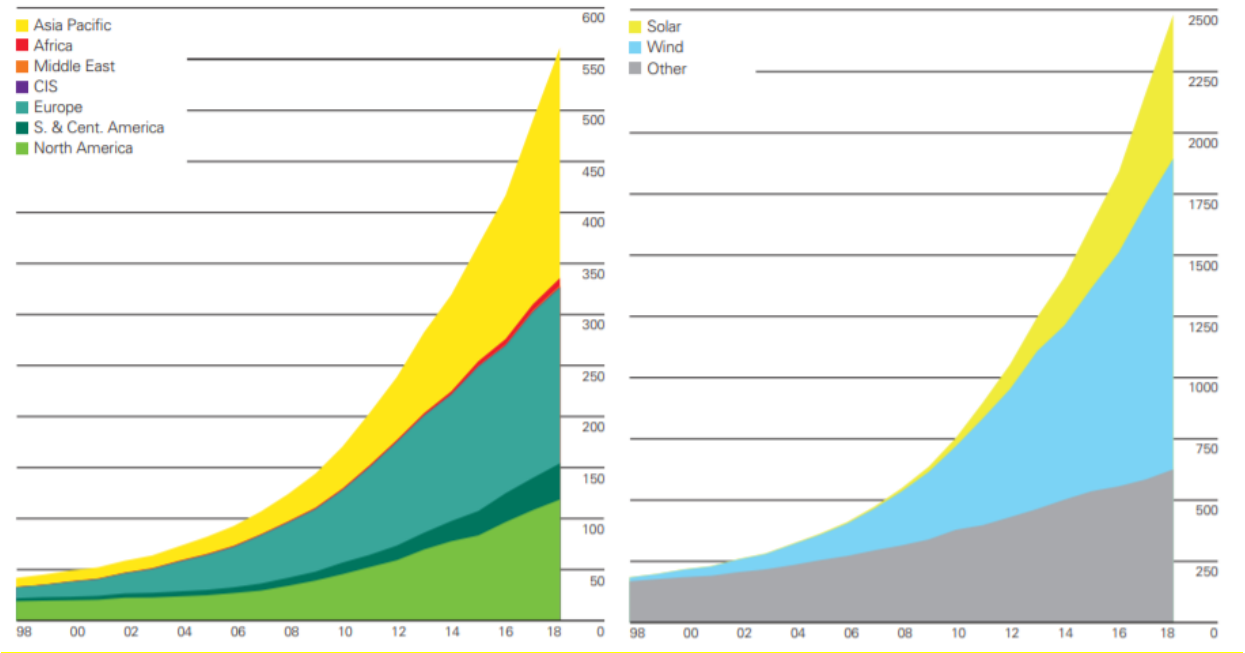

Figure 1.2 Left: World energy consumption of renewable energy from 1998 to 2018. Right: Renewables generation by source from 1998 to 2018.

Favorable world politics and a not optimal level of technology are some of the reasons that make the photovoltaic business very active both in selling massive technology and in investment for the development of innovative technologies in terms of power conversion efficiencies (PCE) and costs;[2] nonetheless, two major obstacles toward the final push of a widely spread use of solar energy must be overcome: a) low-cost production and b) disposal cost. Commercially available solar cells are devices constituted by light absorbing inorganic materials (crystalline or amorphous silicon doped so to generate a p–n junction) interposed between two electrodes, one of which is transparent to radiation in the visible region (Figure 1.3a). The physical principle behind light-harvesting is the photoelectric effect, the current generation when a metal is irradiated by light.[3] When an electromagnetic radiation hits the silicon-based light absorptive material with a hν energy, to promote an electronic transition from the valence band to the conduction band (Figure 1.3b), the excited electrons leave "holes" in the starting level. The electron mobility is responsible for the conduction of current between the two electrodes (Figure 1.3c). The silicon is then doped to produce a downward (p-doped) or upward (n-doped) shift of the valence and conduction bands of the semiconductor.[4]

---

[2] «IEA PVPS TRENDS IN PHOTOVOLTAIC APPLICATIONS» **2020**. https://iea-pvps.org/trends_reports/trends-in-pv-applications-2020/

[3] «The Nobel Prize in Physics,» **1921**. . [Online]. Available: (http://www.nobelprize.org/nobel_prizes/physics/laureates/1921/).

[4] D. W. C. Carlson, Topics in Applied Physics: Amorphous Semiconductors: Amorphous silicon solar cells, Springer, Berlin / Heidelberg, **1985**.

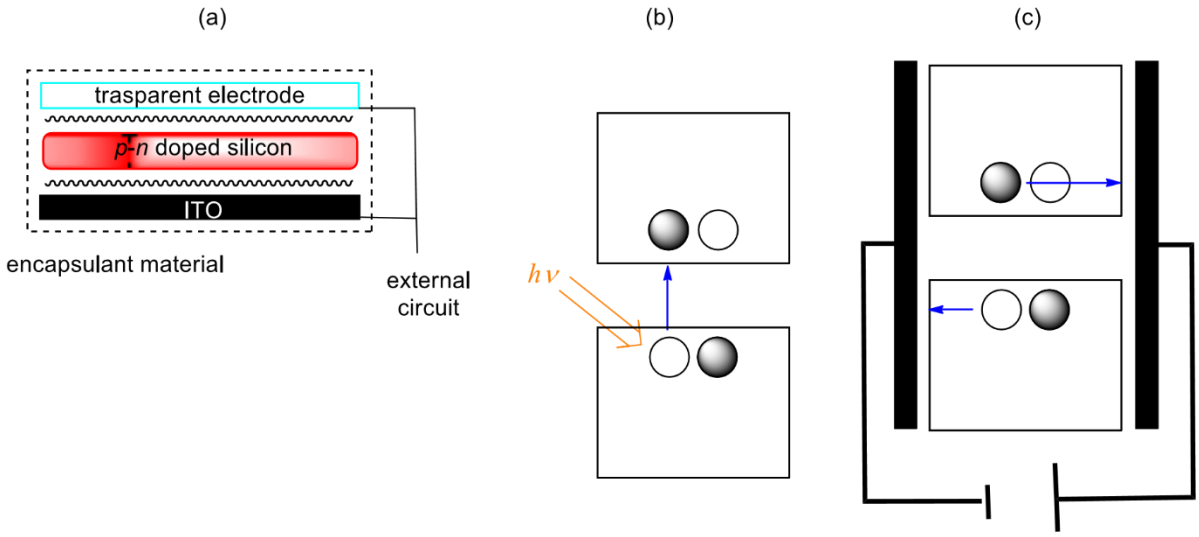

Figure1.3. Scheme of a typical silicon-based solar cell and fundamental mechanism of light-harvesting.

The best PCE performance achieved for this technology is 26%.[5] Silicon solar cells have disadvantages such as materials availability, efficiencies, durability, and life cycle constraints.[6] It is possible to build solar cells using different materials and architectures from the silicon-based solar cells. The fundamental constituent elements in a solar cell are represented by a light absorptive material which creates charge carriers, and by a pair of electrodes, one of which is transparent, to which the charge carriers need to be channelled. There are several types of photoactive layers; one of the new emerging fields is organic photovoltaics, where the photoactive layers are made by organic compounds. Organic solar cells use organic materials or organic polymers, that are solution processable at high throughput and are cheap to fabricate in large volumes, reducing productions costs. They can have specific advantages over silicon-

[5] K. Yoshikawa, H. Kawasaki, W. Yoshida, T. Irie, K. Konishi, K. Nakano, T. Uto, D. Adachi, M. Kanemastu, H. Uzu and K. Yamamoto, «Silicon heterojunction solar cell with interdigitated back contacts for a photoconversion efficiency over 26%» *Nat. Energy* **2017**, *2,* 17032.

[6] S. Almosni, A. Delammare, Z. Jehl, D. Suchet, L. Cojocaru, M. Giteau, B. Behaghel, A. Julian, C. Ibrahim, L. Tatry, H. Wang, T. Kubo, S. Uchida, H. Segawa, N. Miyashita, R. Tamaki, Y. Shoji, K. Yoshida, N. Ahsan, K. Watanabe, T. Inoue, M. Sugiyawa , Y. Nakano, T. Hamamura, T. Toupance, C. Olivier, S. Chambon, L. Vignau, C. Geffroy, E. Cloutet, G. Hadziioannou, N. Cavassilas, P. Rale, A. Cattoni, S. Collin, F. Gibelli, M. Paire, L. Lombez, D. Aureau, M. Bouttemy, A. Etcheberry, Y. Okada and J.-F. Guillemoles, «Material challenges for solar cells in the twentyfirst century: directions in emerging technologies» *Sci. Technol. Adv. Mater.* **2018**, *19,* 337.

based cells, such as low-cost fabrication, flexibility, low temperature process ability and roll to roll processing.[7]

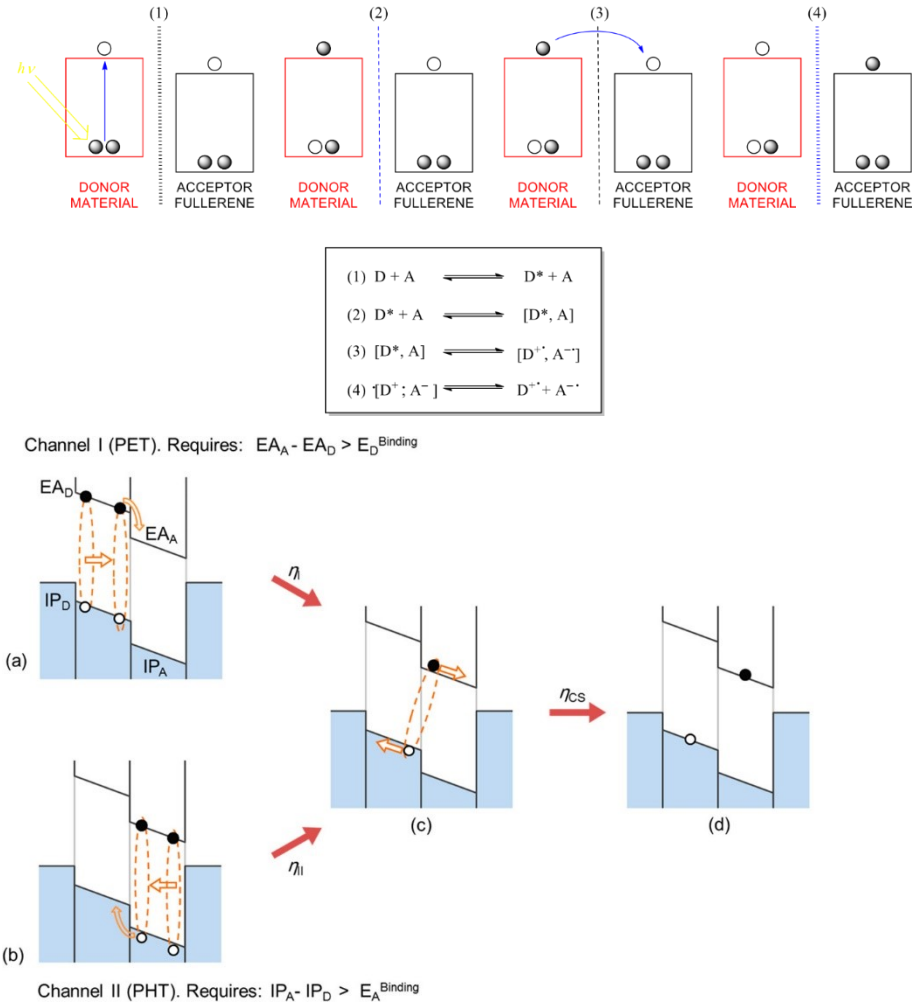

Figure 1.4: a) Channel I photoexcitation. (1) Photo absorption with formation of excitons; (2) diffusion of excitons toward the interface with fullerene; (3) dissociation with hole/electron pair formation; (4) migration toward electrodes. b) Channel II photoexcitation mechanism

Organic materials characteristically have a much lower dielectric constant than their inorganic counterparts, resulting in the generation of excitons (electron–hole pairs) upon photo absorption through the electron transfer from HOMO to LUMO levels, rather than free charge carriers. To promote current, these excitons must first be dissociated into free charge pairs. If the exciton is not able to dissociate within its lifetime, it will decay back to its ground state, resulting in the loss of the absorbed energy. In OPVs, exciton dissociation relies on the presence of a two-component system containing an electron donor and

[7] C. J. Brabec, «Organic photovoltaics: technology and market» *Sol. Energy Mater. Sol. Cells* **2004**, *83*, 273-292.

an electron acceptor that is similar to that of a p–n junction. The electron donor is typically characterized by a large ionization potential, while it is desirable for the electron acceptor to have a high electron affinity.[8] The main fundamental mechanism (Channel I) of operation by which light energy is converted into electrical energy in these devices occur in 4 distinct steps (Figure 1.4a); nevertheless, another possible mechanism (Channel II) by which light energy is converted into electrical energy can occur (Figure 1.4b).

Photo absorption of the donor material promotes the formation of an exciton. Exciton diffusion from the donor polymer to the interface with the fullerene acceptor compound follows, and by exciton dissociation electron charge carriers (−) in the acceptor material and hole (+) in the donor material are formed, which migrate to the electrodes with electricity generation in the external circuit.[9][10][11][12][13][14][15] Among all types of emerging OPV devices, polymer solar cells with BHJ architecture probably offer the best growth prospects due to the potential advantages including low cost, low toxicity, light weight and fast/cheap

[8] A. K. Mazzio and C. K. Luscombe, «The future of organic photovoltaics» *Chem. Soc. Rev.* **2015**, *44*, 78.

[9] D. Stoltzfus, J. Donaghey, A. Armin, E. P. Shaw, P. L. Burn and P. Meredith, «Charge Generation Pathways in Organic Solar Cells: Assessing the Contribution from the Electron Acceptor,» *Chem. Rev.* **2016***, 116,* 12920–12955.

[10] Y. H., L. Ye, H. Zhang, S. Li, S. Zhang and J. Hou, «Molecular Design of Benzodithiophene-Based Organic Photovoltaic Materials, *Chem. Rev.* **2016**, *116*, 7397–7457.

[11] X. Chen, G. Xu, G. Zeng, H. Gu, H. Chen, H. Xu, H. L. Y. Yao, J. Hou and Y. Li, «Realizing Ultrahigh Mechanical Flexibility and >15% Efficiency of Flexible Organic Solar Cells via a "Welding" Flexible Transparent Electrode» *Adv. Mater.* **2020***, 32,*1908478.

[12] F. Mateen, M. A. Saeed, J. W. Shim and S.-K. Hon, «Indoor/outdoor light-harvesting by coupling low-cost organic solar cell witha luminescent solar concentrator» *Solar Energy* **2020***, 207,* 379–387.

[13] Y.-X. Xu, C.-C. Chueh, H.-L. Yip, F.-Z. Ding, Y.-X. Li, C.-Z. Li, X. Li, W.-C. Chen and A. K.-Y. Jen, «Improved Charge Transport and Absorption Coefficient in Indacenodithieno[3,2-b]thiophene-based Ladder-Type Polymer Leading to Highly Efficient Polymer Solar Cells» *Adv. Mater.* **2012***, 24,* 6356–6361.

[14] J. J. Intemann, K. Yao, Y.-X. Li, H.-L. Yip, Y.-X. Xu, P.-W. Liang, C.-C. Chueh, F.-Z. Ding, X. Yang, X. Li, Y. Chen and J. A. K.-Y., «Highly Efficient Inverted Organic Solar Cells Through Material and Interfacial Engineering of Indacenodithieno[3,2-b]thiophene-Based Polymers and Devices» *.Adv. Funct. Mater.* **2014***, 24,* 1465–1473.

[15] Y. Li, K. Yao, H.-L. Yip, F.-Z. Ding, Y.-X. Xu, X. Li, Y. Chen and J. A. K.-Y., «Eleven-Membered Fused-Ring Low Band-Gap Polymer with Enhanced Charge Carrier Mobility and Photovoltaic Performance.» *Adv. Funct. Mater.* **2014***, 24,* 3631–3638.

manufacturing. [16] [17][18][19][20] Conventional BHJ-OSCs are typically based on a blend of bicontinuous and interpenetrating electron donor (D) and electron acceptor (A) materials. The absorption of photons creates excitons that dissociate into charge carriers (holes and electrons) at the D/A interface, and the opposite polarity carrier materials transport holes and electrons through the donor and acceptor channels to the anode and cathode, respectively, where they are collected to be used as electrical power source (Figure 1.5**)**.

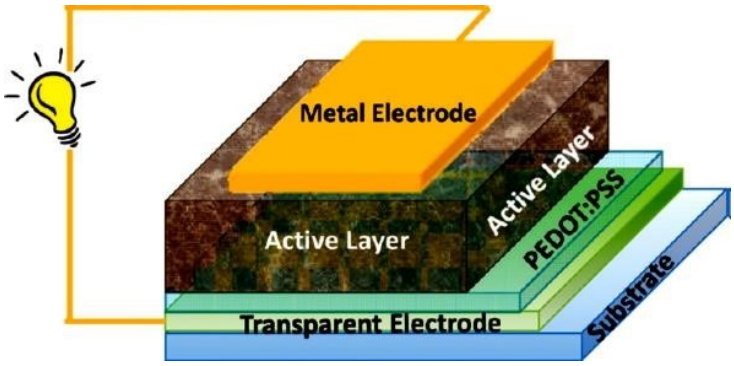

Figure 1.5. Architecture of Bulk Heterojunction solar cell.

Efficient exciton dissociation in charge carriers and efficient transport to the electrodes need to be achieved to obtain appreciable power conversion efficiencies (PCEs). Materials need to be chosen to obtain an exergonic driving force for charge separation ($\Delta GCS < 0$) and an efficient migration toward

[16] G. Wang, S. F. Melkonyan, A. Facchetti and T. J. Marks, «All-Polymer Solar Cells: Recent Progress, Challenges, and Prospects» *Angew. Chem. Int. Ed.* **2019***, 58,* 4129 –4142.

[17] L. X. Chen, «Organic Solar Cells: Recent Progress and Challenges» *ACS Energy Lett.* **2019***, 4,* 2537–2539.

[18] H. Yin, C. Yan, H. Hu, J. K. Z. X. Ho, G. Li and S. So, «Recent progress of all-polymer solar cells–From chemical structure and device physics to photovoltaic performance» *Mater. Sci. Eng. R Rep.* **2020***, 140,* 1005422.

[19] S. K. Karunakaran, G. M. Arumugam, W. Yang, S. Ge, S. N. Khan, X. Li and G. Yang, «Recent progress in inkjet-printed solar cells» *J. Mater. Chem. A* **2019***, 7,* 13873–13902.

[20] J. Qin, L. Lan, S. Chen, F. Huang, H. C. W. X. H. S. K. Shi and C. Yang, « Recent Progress in Flexible and Stretchable Organic Solar Cells» *Adv. Funct. Mater.* **2020***, 30,* 2002529.

[21] A. Nitti, M. Signorile, M. Boiocchi, G. Bianchi, R. Po and D. Pasini, «Conjugated Thiophene-Fused Isatin Dyes through Intramolecular Direct Arylation.» *J. Org. Chem.* **2016***, 81,* 11035–11042.

[22] A. Nitti, G. Bianchi, R. Po, T. M. Swager and D. Pasini, «Domino Direct Arylation and Cross-Aldol for Rapid Construction of Extended Polycyclic π-Scaffolds.» *J. Am. Chem. Soc.* **2017***, 139,* 8788–8791.

the electrodes. Typical electron donor polymers exhibit a conjugated backbone on which pendant alkyl side chains, necessary for solubilization in organic solvents and processability, are present. One of the prototypical and widely used donor material is poly(3-hexylthiophene-2,5-diyl) (P3HT), a regioregular polymer easily obtainable through several ways.[23][24][25][26][27][28]

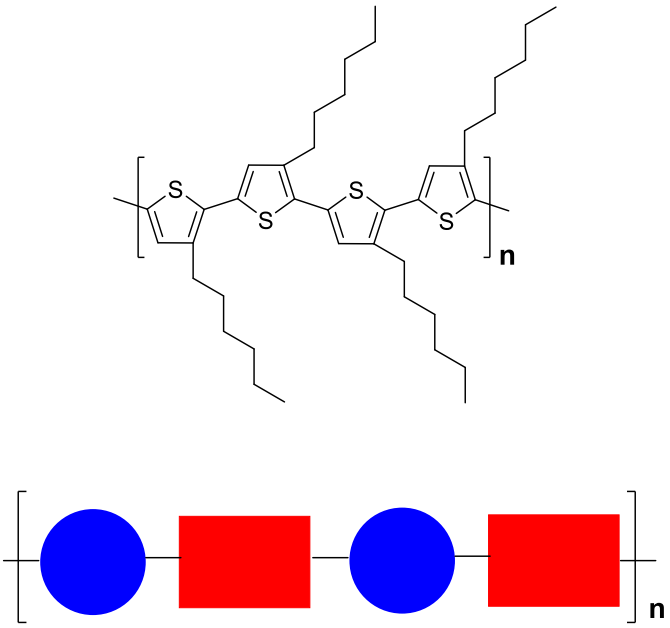

Figure 1.6. Top: P3HT. Bottom: Donor (Blue)acceptor (Red) copolymer

[23] R. McCullough and R. D. Lowe, «Enhanced Electrical Conductivity in Regioselectively Synthesized Poly(3-al kylthiophenes)» *J. Chem. Soc.* **1992**, 70−72.

[24] A. T. Che and D. R. Rieke, «The first regioregular head-to-tail poly(3-hexylthiophene-2,5-diyl) and a regiorandom isopolymer: nickel versus palladium catalysis of 2(5)-bromo-5(2)-(bromozincio)-3-hexylthiophene polymerization» *J. Am. Chem. Soc.* **1992**, *114,* 10087–10088.

[25] Q. Wang, R. Takita, Y. Kikuzaki and F. Ozawa, «Palladium-Catalyzed Dehydrohalogenative Polycondensation of 2-Bromo-3-hexylthiophene: An Efficient Approach to Head-to-Tail Poly(3-hexylthiophene)» *J. Am. Chem. Soc.* **2010**, *132,* 11420–11421.

[26] Q. Wang, M. Wakioka and F. Ozawa, «Synthesis of End-capped Regioregular Poly(3-hexylthiophene)s via Direct Arylation» *Macromol. Rapid Commun.* **2012**, *33,* 1203−1207.

[27] S. Holliday, R. Ashraf, A. Wadsworth, D. Baran, S. A. Yousaf, C. Nielsen, C.-H. Tan, S. D. Dimitrov, Z. . Shang, N. Gasperini, M. Alamoudi, F. Laguai, C. J. Brabec, A. Salleo, J. R. Durrant and I. McCulloch, «High-efficiency and air-stable P3HT-based polymer solar cells with a new non-fullerene acceptor» *Nat. Commun.* **2016**, *7,* 11585.

[28] C. Yang, S. Zhang, J. Ren, M. Gao, P. Bi, L. Ye and J. Hou, «Molecular design of a non-fullerene acceptor enables a P3HT-based organic solar cell with 9.46% efficiency» *Energy Environ. Sci.* **2020**,*13,* 2864−2869.

Despite the cheap synthesis and high mobilities μh, P3HT has a rather high E_{HOMO} (ca. 5.1 eV), which leads to a low V_{OC}, limiting its solar cell performance. Higher performance donor materials have an alternating D and A building blocks on the backbone, to ensure a fine tuning of the photophysical and photovoltaics properties (Figure 1.6).[29][30]

OSCs have been traditionally based on fullerene electron acceptors (FAs). 6,6-Phenyl C_{61} butyric acid methyl ester (PC61BM) and its C_{70}-based homologue (PC71BM) are the most successful and widely used FAs for solution-processed BHJ OSCs, and played a central role in the development of increasingly better performing devices, with PCE up to 10%.[31] Their specific advantages can be summarized as follows: (i) strong tendency to accept electrons from common donor semiconductors; (ii) high electron mobility even in the phase segregated form; (iii) ability to form favourable nanoscale morphological networks with donor materials; (iv) isotropy of charge transport; and (v) reversible electrochemical reduction.[32][33]

Record efficiencies in OSCs have been the result of the development of new electron donor materials with improved properties, such as better spectral sensitivity, enhanced hole transport, and more favourable HOMO/LUMO energy levels, better matching with $PC_{61}BM$ or $PC_{71}BM$ HOMO/LUMO levels. However, FAs possess several drawbacks such as a) weak absorption in the visible region, b)

[29] K. He, P. Kumar, Y. Yuan and Y. Li, «Wide bandgap polymer donors for high efficiency non-fullerene acceptor based organic solar cells» *Mater. Adv.* **2021***, 2,* 115.

[30] J. B. Park, J.-W. Ha, I. W. Jung and D.-H. Hwang, «High-Performance Nonfullerene Organic Photovoltaic Cells Using a TPD-Based Wide Bandgap Donor Polymer» *ACS Appl. Energy Mater.* **2019***, 2,* 5692–5697.

[31] C. L. Chochos, A. Katsouras, N. Gasparini, C. Koulogiannis, T. Ameri, C. J. Brabec and A. Avgeropoulos, «Rational Design of High-Performance Wide-Bandgap (≈2 eV) Polymer Semiconductors as Electron Donors in Organic Photovoltaics Exhibiting High Open Circuit Voltages (≈1 V)» *Macromol. Rapid Commun.* **2017***, 38,* 1600614.

[32] Y. Cai, X. Zhang, X. Xue, D. Wei, H. L. and Y. Sun, «High-Performance Wide-Bandgap Copolymers Based on Indacenodithiophene and Indacenodithieno[3,2-b]thiophene Units» *J. Mater. Chem. C* **2017***, 5,* 7777–7783.

[33] N. Gasparini, A. Katsouras, M. I. Prodromidis, A. Avgeropoulos, D. Baran, M. Salvador, S. Fladischer, E. Spiecker, C. L. Chochos, T. Ameri and C. J. Brabec, «Photophysics of Molecular-Weight-Induced Losses in Indacenodithienothiophene-Based Solar Cells.» *Adv. Funct. Mater.* **2015***, 25,* 4898–4907.

limited tunability in terms of spectral absorption, c) high synthetic costs and d) morphological instability, decreasing the device performance.[34]

1.3→ NONFULLERENE ACCEPTORS (NFAs)

The focus in the development of OSCs has shifted to non-fullerene electron acceptors (NFAs) in combination with a polymeric electron donor in BHJ OSCs. In fact, the PCEs of such cells have increased dramatically since 2015, now reaching a high value of over 18%.[3536] An ideal NFA should exhibit (a) strong absorption coefficients in regions of the visible and NIR spectrum that are complementary to those in which the available electron donor polymers absorb; (b) suitably matched energy levels for achieving exergonic charge separation with donors; (c) the ability to form appropriate morphologies for charge separation and suitable percolation pathways for charge transport; and (d) good molecular and morphological thermal and photostability. NFAs have a long history; indeed, the first reported bilayer OSCs used a perylene-based acceptor,[37] and some early BHJ OSCs used electron-rich and electron-deficient poly(phenylenevinylene)s.[38] A wide variety of material classes have been examined as

[34] C. B. Nielsen, S. Holliday, H.-Y. Chen, S. J. Cryer and I. McCulloch, «Non-Fullerene Electron Acceptors for Use in Organic Solar Cells» *Acc. Chem. Res.* **2015***, 48,* 2803−2812.

[35] Y. Qin, Y. Chang, X. Zhu, X. Gu, L. Guo, L. Zhang, Q. Wang, J. Zhang, X. Zhang, X. Liu, K. Lu, E. Zhou, Z. Wei and X. Sun, «18.4% efficiency achieved by the cathode interface engineering in non-fullerene polymer solar cells» *NanoToday* **2021***, 41,* 101289.

[36] Y. Lin, Y. Firdaus, F. H. Isikgor, M. I. Nugraha, E. Yengel, G. T. Harrison, R. Hallani, A. El-Labban, H. Faber, C. Ma, X. Zheng, A. Subbiah, C. T. Howells, O. M. Bakr, I. McCulloch, S. De Wolf, L. Tsetseris and T. D. Anthopoulos, «Self-Assembled Monolayer Enables Hole Transport Layer-Free Organic Solar Cells with 18% Efficiency and Improved Operational Stability» *ACS Energy Lett.* **2020***, 5,* 2935–2944.

[37] C. W. Tang, «Two-layer organic photovoltaic cell» *Appl. Phys. Lett*. **1986**, *48*, 183–185.

[38] J. Hou, O. Inganäs, R. Friend and F. Gao, «Organic solar cells based on non-fullerene acceptors» *Nat. Mater.* **2018***, 17,* 119–128.

NFAs.[3940414243] Many of the advances in NFA-containing OSCs are attributable to two classes of materials: rylene di-imides and fused-ring electron acceptors (FREAs).[4445464748] By far the best NFA-containing OSCs performances were achieved using FREAs, well-defined organic compounds characterized by a push–pull architecture in which π-extended donating cores with four or more aromatic fused rings are flanked by two electron-withdrawing units (A–D–A molecular structures) or by introduction of an electron deficient core in the middle of the molecule (A-D-A-D-A). Aromatic fused rings have been widely applied in the construction of high-mobility organic semiconductors because the extended conjugation in fused rings is beneficial to forming effective interchain π–π overlaps and enhancing intermolecular charge transport. Typical fused rings have high planarity and suffer from strong aggregation, leading to the formation of large crystalline domains. The introduction of rigid out-of-plane

[39] D. Srivani, A. Agarwal, S. Bhosale, A. Puvad, W. Xiang, R. Evans, A. Gupta e S. Bhosale, «Naphthalene diimide-based non-fullerene acceptors flanked by open-ended and aromatizable acceptor functionalities» *Chem. Commun.* **2017***, 53,* 11157–11160.

[40] M. Sung, M. Huang, S. Moon, T. Lee, S. Park, J. Kim, S. Kwon, H. Choi and Y. Kim, «Naphthalene diimide-based small molecule acceptors for fullerene-free organic solar cells» *Sol. Energy* **2017***, 150,* 90–95.

[41] R. Jina, F. Wang, R. Guana, X. Zhenga and T. Zhang, «Design of perylene-diimides-based small-molecules semiconductors for organic solar cells» *Mol. Phys.* **2017***, 115,* 1591–1597.

[42] J. Jo, J. Jung, H.-W. Wang, P. Kim, T. Russell and W. Jo, «Fluorination of Polythiophene Derivatives for High Performance Organic Photovoltaics» *Chem. Mater.* **2015***, 27,* 4865–4870.

[43] W. Jung and W. Jo, «Low-Bandgap Small Molecules as NonFullerene Electron Acceptors Composed of Benzothiadiazole and Diketopyrrolopyrrole for All Organic Solar Cells» *Chem. Mater.* **2015***, 27,* 6038–6043.

[44] F. Zhao, S. Dai, Y. Wu, Q. Zhang, J. Wang, L. Jiang, Q. Ling, Z. Wei, W. Ma, W. You *et al.* «Single-Junction Binary-Blend Nonfullerene Polymer Solar Cells with 12.1% Efficiency» *Adv. Mater.* **2017***, 29,* 1700144.

[45] Y. Cui, H. Yao, B. Gao, Y. Qin, S. Zhang, B. Yang, C. He, B. Xu and J. Hou, « Fine-Tuned Photoactive and Interconnection Layers for Achieving over 13% Efficiency in a Fullerene-Free Tandem Organic Solar Cell» *J. Am. Chem. Soc.* **2017***, 139,* 7302–7309.

[46] D. Xie, T. Liu, W. Gao, C. Zhong, L. Huo, Z. Luo, K. Wu, W. Xiong, F. Liu, Y. Sun *et al.* «A Novel Thiophene-Fused Ending Group Enabling an Excellent Small Molecule Acceptor for High-Performance Fullerene-Free Polymer Solar Cells with 11.8% Efficiency» *Solar RRL* **2017***, 1,* 1700044.

[47] J. Wang, W. Wang, X. Wang, Y. Wu, Q. Zhang, C. Yan, W. Ma, W. You and X. Zhan, «Enhancing Performance of Nonfullerene Acceptors via Side-Chain Conjugation Strategy» *Adv. Mater.* **2017***, 29,* 1702125.

[48] Y. Lin, Q. He, F. Zhao, L. Huo, J. Mai, X. Lu, C.-J. Su, T. Li, J. Wang and J. Zhu, «A Facile Planar Fused-Ring Electron Acceptor for As-Cast Polymer Solar Cells with 8.71% Efficiency» *J. Am. Chem. Soc.* **2016***, 138,* 2973–2976.

side chains onto the fused rings avoids the formation of large crystalline domains, and it optimizes the exciton diffusion/separation efficiencies. Meanwhile, the introduction of electron-withdrawing moieties (such as imide, amide, and cyano groups) end-capping the π-conjugated core can cause efficient mixing in forming the molecular orbitals, leading to stabilization of the molecular LUMO and reduction of the molecular HOMO–LUMO gap to red-shift absorbance. Amongst FREAs, the **IDIC/ITIC** and **Y6** families of NFAs stood out in the last five years in terms of performances, due to their absorption near the NIR, favourable charge mobility and optimal morphology with the donor component. The prototypical **IDIC**[48], **ITIC**[49] and **Y6**[50] molecules, namely, 2,2'-((2Z,20Z)-((4,4,9,9-tetrahexyl-4,9-dihydro-s-indaceno[1,2-b:5,, 6-b']dithiophene-2,7-diyl)bis(methanylylidene))bis(3-oxo-2,3-dihydro-1Hindene-2,1-diylidene))dimalononitrile (IDIC), 3,9-bis(2-methylene-(3-(1,1-dicyanomethylene)-indanone)-5,5,11,11-tetrakis(4-hexylphenyl)-dithieno[2,3-d:20 ,30 -d']-s-indaceno[1,2-b:5,6-b']dithiophene) (ITIC) and 2,2'-((2Z,2'Z)-((12,13-bis(2-ethylhexyl)-3,9-diundecyl-12,13-dihydro-[1,2,5]thiadiazolo[3,4-e]thieno [2",3'':4',5']thieno [2',3':4,5]pyrrolo[3,2-g]thieno[2',3':4,5]thieno[3,2-b]indole-2,10-diyl)bis(methanylylidene))bis(5,6-difluoro-3-oxo-2,3-dihydro-1H-indene-2,1-diylidene))dimalononitrile **a0**, **b0** and **c0**, respectively, are shown in (Figure 1.7).

[49] Y. Lin, J. Wang, Z.-G. Zhang, H. Bai, Y. Li, D. Zhu e X. Zhan, «An Electron Acceptor Challenging Fullerenes for Efficient Polymer Solar Cells» *Adv. Mater.* **2015***, 27,* 1170–1174.

[50] J. Yuan, Y. Zhang, L. Zhou, G. Zhang, H.-L. Yip, T.-K. Lau, X. Lu, C. Zhu, H. Peng, P. Johnson *et al.* «Single-Junction Organic Solar Cell with over 15% Efficiency Using Fused-Ring Acceptor with Electron-Deficient Core» *Joule* **2019***, 3,* 1140–1151.

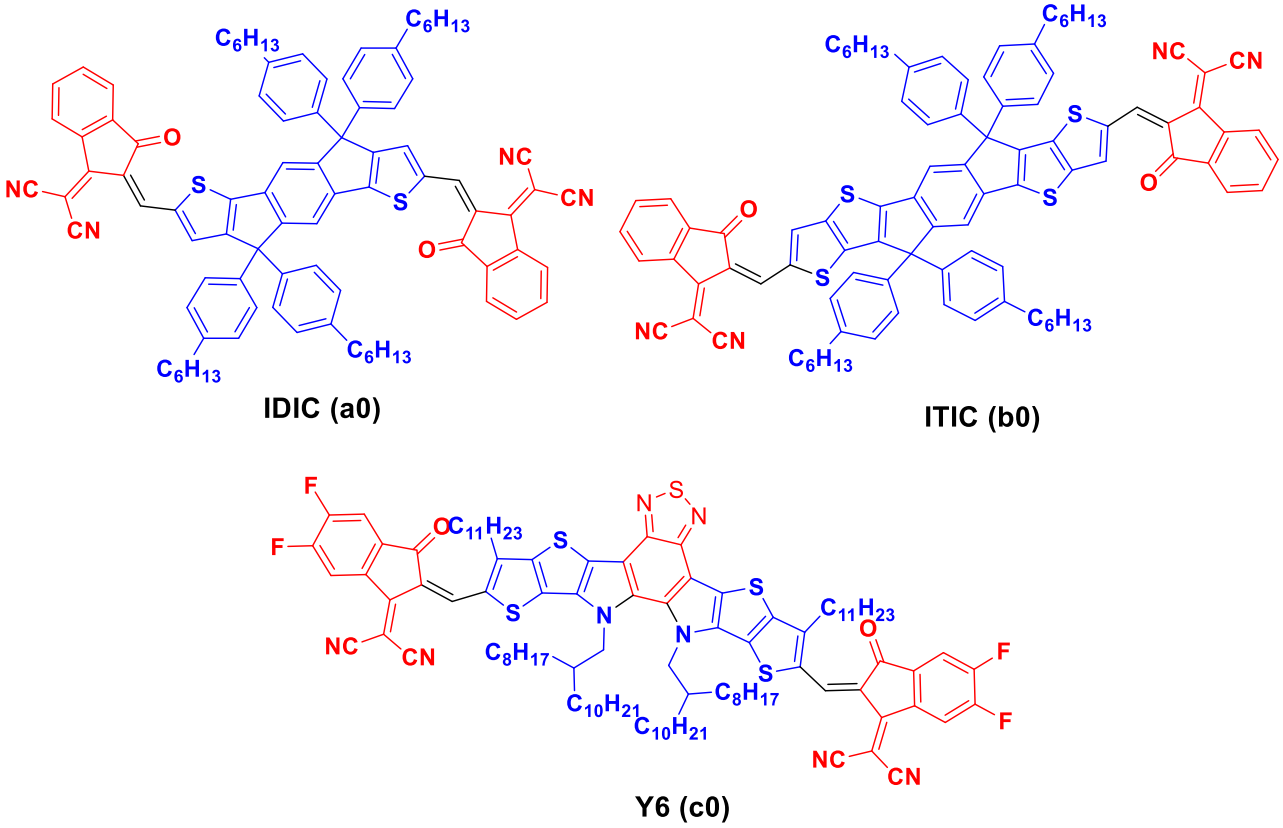

Figure 1.7. ITIC/IDIC and Y6.

Since the discovery of the **ITIC** and then **Y6**, several efforts have been put into the modification and functionalization of these two main NFAs family. The two main strategies to achieve it, can be summarized as A) core modification, B) end groups modification. Modifications of the lateral solubilizing chains have shown to bring minimal changes to the photovoltaic performances, and such studies are not commented here. We focus our attention on the rational design of the modifications carried out on the **IDIC/ITIC** and **Y6 NFAs**, and on the outcome in terms of the photovoltaic performance.

1.3.1→ MODIFICATION OF ELECTRON-DEFICIENT END-CAPPING GROUPS

End-capping groups are extremely important for the optical and electrochemical properties of the NFAs for the following reasons: (a) they retrieve electron density from the electron-rich core, generating a push–pull effect responsible for the light absorption in the region of 600–800 nm as well as a spatial

confinement of the LUMO orbitals over them;[51] (b) they contribute to the interaction between the acceptors and the donor,[52] and to the overall morphological properties of the active layer.[53] Compounds obtained from the formal modification of the basic structure of compound **a0** are identified with the letter **a**, whereas compounds obtained from the formal modifications of the basic structure of compound **b0** are identified with the letter **b**. The most important modifications of the end-capping groups in the last two years are shown in (Figure 1.8), and their properties are summarized in (Table 1.1).

The three main parameters to compare different cells are J_{SC}, the short circuit current: V_{OC}, the open-circuit voltage and FF(%), the fill factor. All three of them need to be maximized to improve the PCE value. Numerous studies have demonstrated that V_{OC} depends on the energy gap between the HOMO level of the donor and the LUMO level of the acceptor of the BHJ. [54] J_{SC} is primarily dependent on factors related to the efficiencies of each stage in the photovoltaic process, including the efficiency of light absorption, exciton diffusion, exciton dissociation, recombination, charge transport, and charge collection. The FF(%) gives an indication of how easily and what fraction of the generated charges can be removed from a cell and, in the ideal case, will have a value of unity. Tang et al.[5556] recently synthesized two novel NFAs, **a1** and **a2**, formally derived from **a0**. They have similar π-electron-deficient spacers: a benzotriazole for **a1** and a benzothiadiazole for **a2**, as well as different end groups: **a1** presents a dicyano-functionalized rhodanine, while **a2** has a rhodanine. Absorption spectra of **a2** are

[51] Z. Fei, F. Eisner, X. Jiao, M. Azzouzi, J. Röhr, Y. Han, M. Shahid, A. Chesman, C. Easton, C. McNeill *et al.* «An Alkylated Indacenodithieno[3,2-b]thiophene-Based Nonfullerene Acceptor with High Crystallinity Exhibiting Single Junction Solar Cell Efficiencies Greater than 13% with Low Voltage Losses» *Adv. Mater.* **2018***, 30,* 1705209.

[52] Z. Zhang, S. Guang, J. Yu, H. Wang, J. Cao, F. Du, X. Wang and W. Tang, «Over 15.5% efficiency organic solar cells with triple side chain engineered ITIC» *Sci. Bull.* **2020***, 65,* 1533–1536.

[53] C. Yang, S. Zhang, J. Ren, M. Gao, P. Bi, L. Ye and J. Hou, «Molecular design of a non-fullerene acceptor enables a P3HT-based organic solar cell with 9.46% efficiency» *Energy Environ. Sci.* **2020***, 13,* 2864–2869.

[54] N. Elumalai and A. Uddin, «Open circuit voltage of organic solar cells: An in-depth review» *Energy Environ. Sci.* **2016***, 9,* 391–410.

[55] A. Tang, B. Xiao, Y. Wang, F. Gao, K. Tajima, H. Bin, Z.-G. Zhang, Y. Li, Z. Wei and E. Zhou, «Simultaneously Achieved High Open-Circuit Voltage and Efficient Charge Generation by Fine-Tuning Charge-Transfer Driving Force in Nonfullerene Polymer Solar Cells» *Adv. Funct. Mater.* **2018***, 28,* 1704507.

[56] L.-M. Tang, J. Xiaob, W.-Y. Baia, Q.-Y. Lia, H.-C. Wanga, M.-S. Miaoc, H.-L. Yipb and Y.-X. Xua, «End-chain effects of non-fullerene acceptors on polymer solar cells» *Org. Electron* **2019***, 64,* 1–6.

red shifted with respect to **a1**, with an absorption maximum essentially identical to **b0**. Compound **a2** has substantially higher HOMO and lower LUMO levels with respect to **a1**.

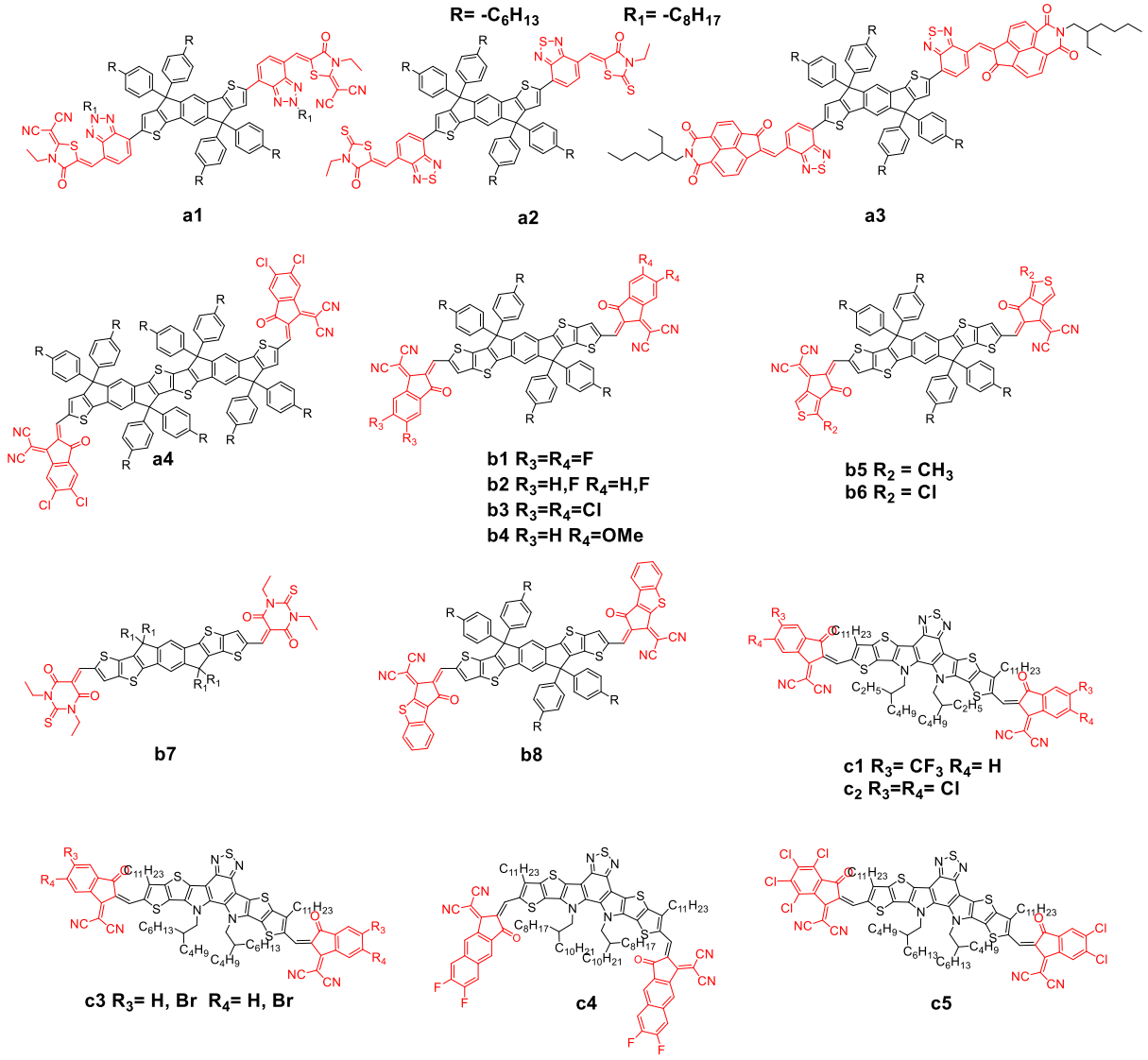

Figure 1.8: Principal End-cap modification

Table 1.1. Optical and electrochemical properties of acceptors **a0–a4** and **b0–b8**.

Entry	*Compounds*	*Td (°C)*[a]	*λ sol max (nm)*[b]	*λ Film max (nm)*[c]	*EG^{OPT} (eV)*[d]	*ε (λ_{max})*[e]	*HOMO (eV)*[f]	*LUMO (eV)*[f]	*μ SCLC ($cm^2 \cdot V^{-1} \cdot s^{-1}$)*[g]	*Ref.*
1	**a0**		664	716	1.62	$2.4x10^5$	-5.69	-3.91	$1.1x10^{-3}$	48
2	**a1**	396	613	636	1.27	$1.14x10^5$	-5.49	-3.57.	-	55
3	**a2**		662	688	1.47		-5.31	-3.70	-	56
4	**a3**	354	628	660	1.32	$8.8x10^4$	-5.38	-3.68	$1.44x10^{-4}$	57
5	**a4**	362	715	754	1.55	$2.1x10^5$	-5.35	-3.91	$2.36x10^{-3}$	58
6	**b0**	345	664	702	1.59	1.310^5	-5.48	-3.83	$3.0x10^{-4}$	49
7	**b1**	-	-	717	-	$1.16x10^5$	-5.66	-4.14	$5.05x10^{-4}$	59
8	**b2**		677	720	1.57	-	-5.67	-4.02	$3.26x10^{-4}$	60
9	**b3**	-	-	746	1.48	1.4x	-5.75	-4.09	-	61
10	**b4**	-	671	695	1.63	$1.9x10^5$	-5.61	-3.92	-	62
11	**b5**	-	674	718	1.58	$2.1x10^5$	-5.57	-3.92	$8.4x10^{-4}$	63
12	**b6**	-	709	746	1.58	$2.3x10^5$	-5.58	-4.01	$7.8x10^{-4}$	64
13	**b7**	-	621	654	1.75	$2.6x10^5$	-5.81	-3.97	$1.8x10^{-4}$	65
14	**b8**	433	664	691	1.59	$1.5x10^5$	-5.49	-3.90		66
15	**c0**	318	731	821	1.33	1.07×10^5	-5.65	-4.10	2.35×10^{-4}	50
16	**c1**	300	744	837	1.30	2.15×10^5	-5.45	-3.96	4.5×10^{-4}	67

17	**c2**	-	746	825	-	1.09×10^5	-5.65	-3.63	1.58×10^{-4}	68
18	**c3**		734	820		1.65×10^5	-5.56	-4.07		69
19	**c4**	330	762	837	1.32	-	-5.58	-3.98	$8.42\text{x}10^{-4}$	70
20	**c5**	330	-	-	-	-	-5.65	-4.01	8.29×10^{-4}	71

a) Decomposition temperature; *b*) λ_{max} in solution; *c*) λ_{max} in thin films; *d*) optical band gap in thin films; *e*) extinction coefficient at $\boldsymbol{\lambda}_{max}$ in $M^{-1}\cdot L^{-1}$; *f*) determined in solution by cyclic voltammetry; *g*) electron mobility.

The photovoltaic properties of the best devices for NFAs shown in Figure 1.8 are reported in Table 1.2, alongside the indication of the reference and the acronym of the donor polymer used in combination with the NFA to produce the bilayer cell. **a2** showed higher Jsc compared with **a1**, presumably because of a better positioned LUMO, causing a positive difference in terms of PCE (entries 2 and 3 in Table 1.2). It is noteworthy that **a1** has the highest V_{OC} reported in Table 2, which, according to the authors, is a result of the optimal energy level matching the used donor polymer.

Table 1.2. Photovoltaic properties of best devices incorporating NFA acceptors shown in (Figure 1.8).

Entry	*Device*	*Voc (V)*[a]	*Jsc (mA·cm^{-2})*[b]	*FF (%)*[c]	*PCE (%)*[d]	*Ref.*
1	**PDBT-T1:a0**	0.89	14.61	63.0	8.19	48
2	**J61: a1**	1.15	10.84	66.17	8.25	55
3	**PTB7-Th: a2**	1.04	13.57	62.64	8.82	56
4	**PBDB-T: a3**	1.04	17.34	60.0	10.08	57
5	**PBDB-T: a4**	0.85	18.9	66.6	10.7	58
6	**PTB7-TH: b0**	0.81	14.21	59.1	6.80	49
7	**PBDB-T-SF: b1**	0.88	20.88	71.3	13.1	59
8	**PBT1-C: b2**	0.90	16.50	70.8	10.54	60

9	**PBDB-T-2F: b3**	0.79	22.67	75.2	13.45	61
10	**PBDB-T: b4**	0.93	18.11	71.52	12.07	62
11	**J71: b5**	0.92	18.41	74.2	12.5	63
12	**PM6: b6**	0.91	20.1	74.1	13.6	64
13	**PBDB-T: b7**	0.98	15.80	69.0	10.08	65
14	**PBDB-T: b8**	0.94	19.90	64.51	12.07	66
15	**PM6:c0**	0.86	24.3	73.2	15.3	50
16	**PM6:c1**	0.85	25.19	72.82	15.59	67
17	**PM6:c2**	0.867	25.4	75.o	16.5	68
18	**PM6:c3**	0.88	25.03	73.13	16.11	69
19	**PM6:c4**	0.83	27.8	69.5	16.0	70
20	**PM6:c5**	0.945	24.07	72.02	16.37	71

a) open circuit voltage, *b*) short-circuit current density, *c*) fill factor, *d*) power conversion efficiency.

Kolhe *et al*.[57] reported earlier this year the synthesis of a novel NFA, **a3**, which contains the unusual naphthaleneimide mono-ketone as the electron rich end-capping group. **a3** showed an absorption maximum at a lower wavelength with respect to **a2**, demonstrating that the modified naphthalene imide does not possess an optimal electron withdrawing character. Moreover, the absorption coefficient and the electron mobility data are considerably lower than most other NFAs in Table 1. Nevertheless, BHJ cells with **a3**, using a different donor polymer, gave higher PCE than to **a1** and **a2**. Qu *et al.*[58] recently reported the synthesis of a novel NFA, **a4**, formally derived from the substitution of the benzene core of a0 with a thienothiophene unit as central core and chlorinated end groups. **A4** showed a remarkable red

[57] N. Kolhe, S. West, D. Tran, X. Ding, D. Kuzuhara, N. Yoshimoto, T. Koganezawa and S. Jenekhe, «Designing High Performance Nonfullerene Electron Acceptors with Rylene Imides for Efficient Organic Photovoltaics» *Chem. Mater.* **2020***, 32,* 195–204.

[58] J. Qu, Q. Zhao, J. Zhou, H. Lai, T. Liu, D. Li, W. Chen, Z. Xie and F. He, «Multiple Fused Ring-Based Near-Infrared Nonfullerene Acceptors with an Interpenetrated Charge-Transfer Network» *Chem. Mater.* **2019**, *31*, 1664–1671.

shift vs. **a1–3**, while the HOMO/LUMO levels showed a higher energy level for the HOMO, resulting in a lower optical bandgap compared to the previously discussed cases. In terms of photovoltaic properties, **a4** did not show an optimal V_{OC}, but excellent J_{SC} resulting in comparable PCEs. Modifications of the end-capping units of the prototypical ITIC **b0** have been reported for a few years by means of di- or tetra-fluorine substitution of the hydrogen of the benzene unit in the modified indanedione terminal units (compounds **b1** and **b2**).[5960] Zhang et al.[61] recently reported the synthesis of a novel NFA, **b3**, which is essentially the chlorinated version of **b1**. **B3** showed a remarkable red shift, a higher dipole moment and a higher intramolecular charge transfer (ICT) with respect to **b1**. HOMO/LUMO levels are considerably lower in absolute energy compared to those of **b1** and **b2**. The presence of chlorine atoms, as suggested by the authors, also caused more pronounced molecular stacking, which helps to expand the absorption spectrum and affords very high absorption coefficients. The rather low V_{OC} is largely compensated by high values of J_{sc} (see also the high absorbance coefficient) and FF(%), affording record efficiencies for devices made with **b3**. Last year, Li *et al*.[62] reported the synthesis of a novel asymmetric NFA, **b4**, which contains two methoxy units in one of the end-capping groups with respect to **b0**. The authors explain their choice as on this basis of the following: (a) generation of a permanent dipole moment over the whole molecule, with NFA of the kind A1–D–A2; (b) fine tuning of energy levels; and (c) facile and cost-effective synthesis. **B4** showed a blue-shifted absorption spectrum (in thin films) with respect to **b0** ascribed to the electron-donating capacity of the methoxy groups, resulting in deeper lying HOMO and LUMO levels, but with similar energy gap. In terms of photovoltaic properties, **b4**, with respect to **b0**, showed higher V_{OC} as a consequence of the better match with the donor polymer and higher J_{sc} and FF(%) (Table 1.2 entry 10). The authors ascribe this to the presence of the enhanced dipole moment, which enables effective tuning of the molecular binding energy, crystallization properties, and morphology of the blend films, allowing a close molecular packing

[59] W. Zhao, S. Li, H. Yao, S. Zhang, Y. Zhang, B. Yang and J. Hou, «Molecular Optimization Enables over 13% Efficiency in Organic Solar Cells» *J. Am. Chem. Soc.* **2017***, 139,* 7148−7151.

[60] X. Li, C. Li, L. Ye, K. Weng, H. Fu, H. Ryu, D. Wei, X. Sun, H. Woo and Y. Sun, «Asymmetric A–D–p–A-type nonfullerene small molecule acceptors for efficient organic solar cells,» *J. Mater. Chem. A* **2019***, 7,* 19348–19354.

[61] H. Zhang, H. Yao, J. Hou, J. Zhu, J. Zhang, W. Li, R. Yu, B. Gao, S. Zhang and J. Hou, «Over 14% Efficiency in Organic Solar Cells Enabled by Chlorinated Nonfullerene Small-Molecule Acceptors» *Adv. Mater.* **2018***, 30,* 1800613.

[62] M. Li, Y. Zhou, J. Zhang, J. Song and Z. Bo, «Tuning the dipole moments of nonfullerene acceptors with an asymmetric terminal strategy for highly efficient organic solar cells» *J. Mater. Chem. A* **2019***, 7,* 8889–8896..

and an efficient charge transport. Luo *et al*.[63][64] reported the synthesis of two novel NFAs **b5** and **b6**, which contain thiophene-fused end-capping groups, differing only in the substituent on the α-position of the terminal thiophene residue, a methyl group for **b5** and a chlorine atom for **b6**. The authors observed markedly different photophysical and photovoltaic properties in these NFAs. **B5** and **b6** showed an increasing level of red shifting with respect to **b0** and, accordingly, lower HOMO/LUMO energy gaps. In terms of photovoltaic properties **b5** and **b6**, although compared in combination with different donor polymers, gave some of the best performances in the field to date for binary BHJ cells. The authors ascribe the results to balanced hole and electron mobilities, low recombination, more effective carrier extraction and a good morphology of the active layers. Firdaus *et al*.[65] reported the synthesis of a novel NFA, **b7**, which contains 3-diethyl-2-thiobarbituric acid as end groups. **B7** is blue-shifted compared to b0; this is ascribed to the different electron withdrawing ability of the end-capping units, which do not allow for optimal push–pull molecular profiles. In any case, photovoltaic efficiencies were over 10%. Last year, Chang *et al.*[66] reported the synthesis of a novel NFA, **b8**, which contains a 2-(3-oxo2,3-dihydro-1H-benzo [b]cyclopenta[d]thiophen-1-ylidene) (α-BC) moiety as the electron-deficient end-capping group. **b8** showed similar absorption properties with respect to **b0**. The α-BC moieties promote a large dipole between the electron-rich benzothiophene and electron-withdrawing dicyanovinylidene moieties, which enhance π–π interactions. In terms of photovoltaic properties, **b8** showed better parameters and PCE than those of **b0**, which, according to the authors, can be attributed to the better packaging and shorter π–π stacking distances.

---

[63] Z. Luo, H. Bin, T. Liu, Z.-G. Zhang, Y. Yang, C. Zhong, B. Qiu, G. Li, W. Gao and D. Xie, «Fine-Tuning of Molecular Packing and Energy Level through Methyl Substitution Enabling Excellent Small Molecule Acceptors for Nonfullerene Polymer Solar Cells with Efficiency up to 12.54%» *Adv. Mater.* **2018***, 30,* 1706124.

[64] Z. Luo, T. Liu, Y. Wang, G. Zhang, R. Sun, Z. Chen, C. Zhong, J. Wu, Y. Chen, M. Zhang *et al.* «Reduced Energy Loss Enabled by a Chlorinated Thiophene-Fused Ending-Group Small Molecular Acceptor for Efficient Nonfullerene Organic Solar Cells with 13.6%» *Adv. Energy Mater.* **2019***, 9,* 1900041.

[65] Y. Firdaus, Q. He, Y. Lin, F. Nugroho, V. Le Corre, E. Yengel, A. Balawi, A. Seitkhan, F. Laquai, C. Langhammer *et al.* «Novel wide-bandgap non-fullerene acceptors for efficient tandem organic solar cells» *J. Mater. Chem. A* **2020***, 8,* 1164–1175.

[66] S.-L. Chang, K.-E. Hung, F.-Y. Cao, K.-H. Huang, C.-S. Hsu, C.-Y. Liao, C.-H. Lee and Y.-J. Cheng, «Isomerically Pure Benzothiophene-Incorporated Acceptor: Achieving Improved Voc and Jsc of Nonfullerene Organic Solar Cells via End Group Manipulation» *ACS Appl. Mater. Interfaces* **2019***, 11,* 33179–33187.

Lai, H. *et al.*[67] last year reported the synthesis of **c1**, which contain a trifluoromethyl-IC core as electron-deficient end group. **c1** showed better photophysical properties compared to **c0**, in particular, an ultra-narrow bandgap which is the lowest bandgap observed for **Y6** family, and a slightly higher PCE. According to the authors, -CF_3 groups are able to provide a 3D packing of the molecule, with close π-π stacking, resulting in better morphological properties. Cui, Y. *et al.*[68] recently reported the synthesis of **c2**, which is formally the tetra chloro version of **c0**. **c2** showed similar photophysical properties when compared with **c0**, with a slightly red-shifted UV and a downshifted LUMO compared to **c0**; however, it possesses a higher PCE compared to **c0**. According to the authors, this can be ascribed to the lower energy loss which increases Voc. Wang, H. *et al.* [69] reported last year the synthesis of **c3**, which contain a brominated-IC as electron-deficient end-cap group. **c3** showed similar photophysical properties compared to **c0**; despite that, **c3** posseses a slightly higher PCE with respect to **c0**, probably as a consequence of a well-balanced electron/hole mobility, an optimized film morphology, an outstanding quenching efficiency, a high charge dissociation, and a high charge collection efficiency. Li, G. *et al.* [70] this year reported the synthesis of **c4**, which bears difluorinated naphthalene electron-deficient end-cap groups. **c4** showed a slightly red-shifted absorption profile compared to **c0** due to the π-extension of the end-cap group, but a similar bandgap. Regarding the photovoltaic properties, **c4** showed higher J_{sc} and PCE, presumably as a consequence of larger π-overlaps between the extended EGs, better film morphology and a well-balanced charge mobility. Li, S. *et al.* [71] last year reported the synthesis of **c5**, which possesses an asymmetric structure bearing two chlorinated electron-deficient end-groups. **C5**

[67] H. Lai, Q. Zhao, Z. Chen, H. Chen, P. Chao, Y. Zhu, Y. Lang, N. Zhen, D. Mo, Y. Zhang and F. He, «Trifluoromethylation Enables a 3D Interpenetrated Low-Band-Gap Acceptor for Efficient Organic Solar Cells» *Joule,* **2020***, 4,* 688–700.

[68] Y. Cui, H. Yao, J. Zhang, T. Zhang, Y. Wang, L. Hong, K. Xian, B. Xu, S. Zhang, P. Ling, Z. Wei, F. Gao and J. Hou, «Over 16% efficiency organic photovoltaic cells enabled by a chlorinated acceptor with increased open-circuit voltages» *Nat. Comm.* **2019***, 10,* 2515.

[69] H. Wang, T. Liu, J. Zhou, D. Mo, L. Han, H. Lai, H. Chen, N. Zheng, Y. Zhu, Z. Xie and F. He, «Bromination: An Alternative Strategy for Non-Fullerene Small Molecule Acceptors» *Adv. Sci.* **2020***, 7,* 1903784.

[70] G. Li, X. Zhang, O. L. Jones, J. M. Alzola, S. Mukherjee, L.-W. Feng, W. Zhu, C. L. Stern, W. Huang, J. Yu, V. K. Sangwan, D. M. DeLongchamp, K. L. Kohlstedt, M. R. Wasielewski, G. C. Schatz, A. Facchetti and T. J. Marks, «Systematic Merging of Nonfullerene Acceptor π-Extension and Tetrafluorination Strategies Affords Polymer Solar Cells with >16%» *J. Am. Chem. Soc.* **2021***, 143,* 6123−6139.

[71] S. Li, L. Zhan, Y. Jin, G. Zhou, T.-K. Lau, R. Qin, M. Shi, C.-Z. LI, H. Zhu, X. Lu, F. Zhang and H. Chen, «Asymmetric Electron Acceptors for High-Efficiency and Low-Energy-Loss Organic Photovoltaics» *Adv. Mater.* **2020***, 32,* 2001160.

showed identical HOMO/LUMO levels when compared to **c0** but a much higher electron-mobility. In terms of photovoltaic properties, **c5** possesses a much higher Voc but similar J_{sc} and FF(%) compared to **c0**, which can be ascribed to a lower nonradiative loss resulting in a much higher PCE.

1.3.2→ STRUCTURAL MODIFICATION OF THE IDIC/ITIC AND Y6 CORE

The modification of the planar conjugated structure is one of the possible strategies to promote fine tuning of the optoelectronic and photovoltaic properties of the **IDIC/ITIC** and **Y6** families. Many recent reports have investigated the modification of these core by means of variations in the (a) central benzene ring, or (b) lateral thiophene or thienothienophene moieties for IDIC/ITIC or by modification of the (a) electron-deficient core and (b) thienothienophene moieties for the **Y6** familiy. The most important modifications to the central core and lateral moieties are shown in Figure 1.9 and Figure 1.10. The optical and electrochemical properties are summarized in Tables 1.3–1.6.

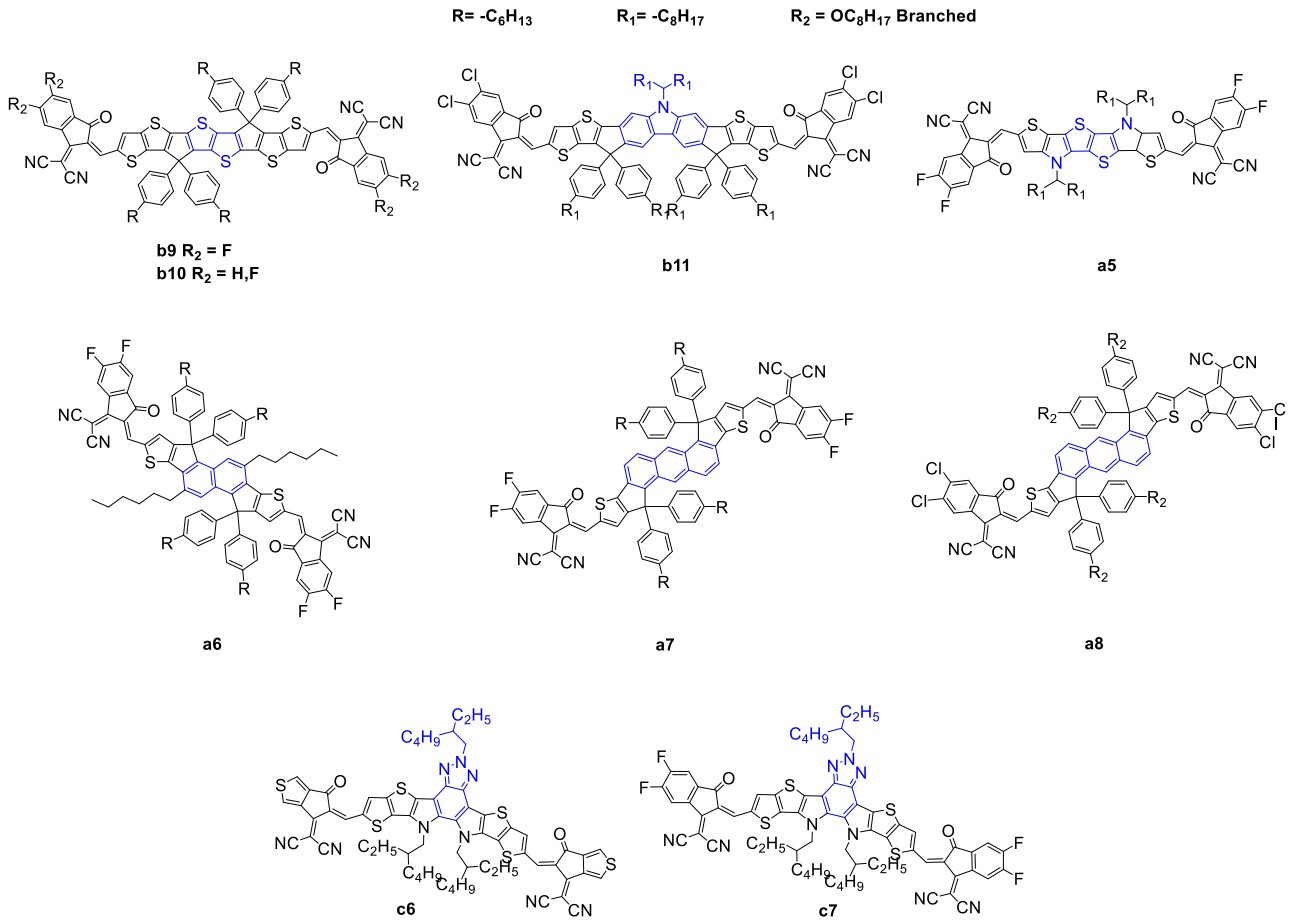

Figure 1.9. Structure of the acceptors of the IDIC/ITIC and Y6 families, where the central core of **a0, b0** and **c0** has been modified.

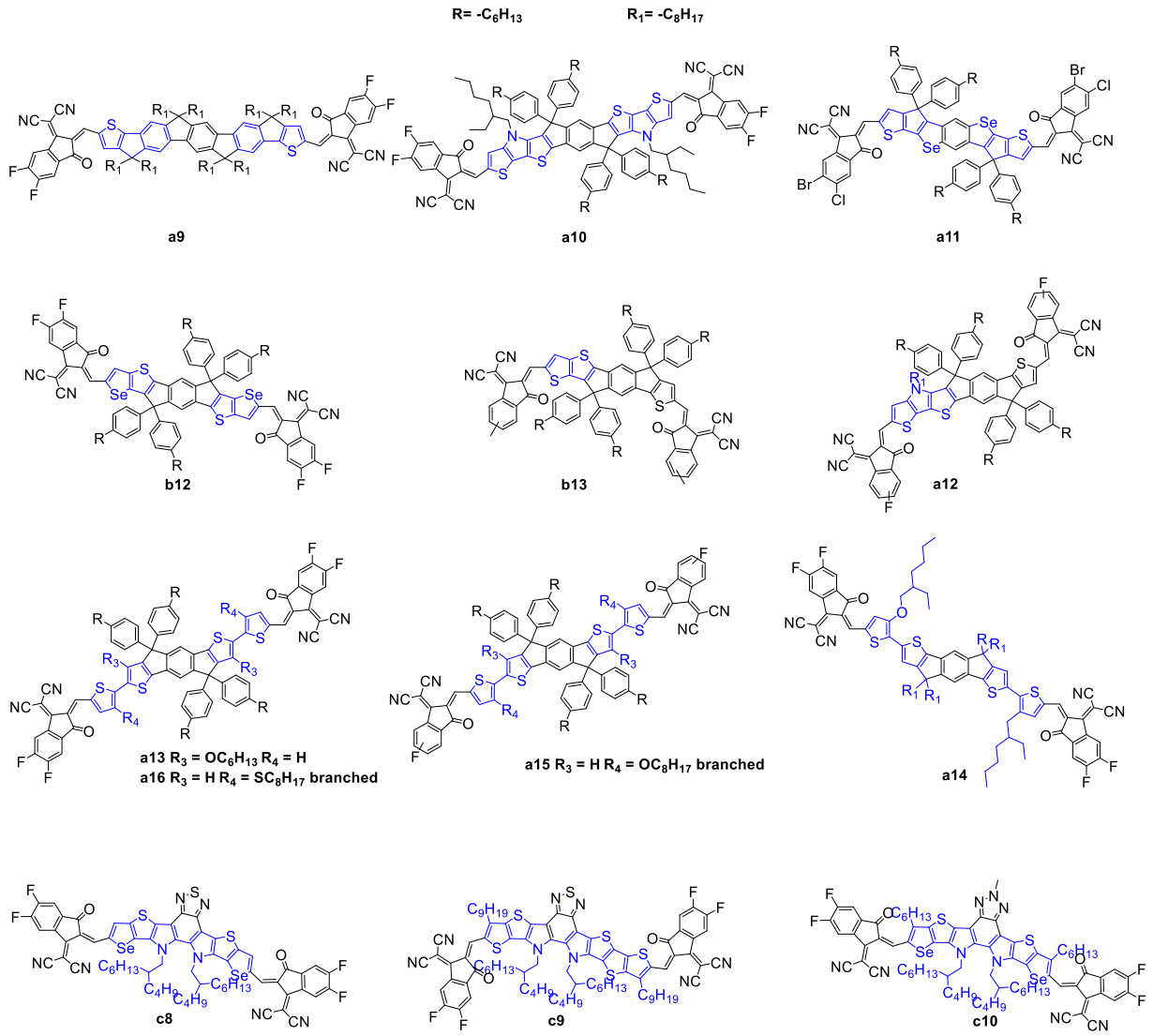

Figure 1.10. Structure of the acceptors of the IDIC/ITIC and Y6 families, where the central core of **a0, b0** and **c0** has been modified.

Table 1.3. Optical and electrochemical properties of acceptors **a5-a8**, **b9-b11** and **c6-c7**

Entry	*Compounds*	*Td (◦C)[a]*	*λ sol max (nm)[b]*	*λ Film max (nm)[c]*	*EG^{OPT} (eV)[d]*	*ε (λmax) ($M^{-1}·L^{-1}$)*	*HOMO (eV)[f]*	*LUMO (eV)[f]*	*μ SCLC ($cm^2·V^{-1}·s^{-1}$) [g]*	*Ref.*
1	**a0**		664	716	1.62	2.4×10^5	-5.69	-3.91	1.1×10^{-3}	*48*
2	**a5**	-	-	-	1.32	-	-5.52	-4.11	3.94×10^{-4}	75
3	**a6**	384	696	730	1.55	1.8×10^5	-5.41	-3.78	1×10^{-3}	76
4	**a7**	-	718	778	1.68	-	-5.69	-4.01	-	77
5	**a8**	-	691	709	1.60	2.2×10^5	-5.71	-3.89	-	78

6	**b0**	345	664	702	1.59	1.3×10^5	-5.48	-3.83	3.0×10^{-4}	49
7	**b9**	331	788	862	1.27	2.3×10^5	–5.43	–4.00	1.5×10^{-3}	72
8	**b10**	328	782	836	1.32	2.0×10^5	–5.36	–3.92	1.2×10^{-3}	73
9	**b11**	338	690	753	1.47	2.3×10^5	-5.72	-4.03	-	74
10	**c0**	318	731	821	1.33	1.07×10^5	-5.65	-4.10	2.35×10^{-4}	50
11	**c6**	350	758	827	1.40	-	-5.43	-4.04	2.08×10^{-4}	79
12	**c7**	-	802	851	1.31	-	-5.56	-4.11	3.01×10^{-4}	80

a) Decomposition temperature; *b*) λ_{max} in solution; *c*) λ_{max} in thin films; *d*) optical band gap in thin films; *e*) extinction coefficient at $\boldsymbol{\lambda}_{max}$; *f*) determined in solution by cyclic voltammetry; *g*) electron mobility.

Table 1.4. Photovoltaic properties of best devices incorporating NFA acceptors shown in Figure 1.9.

Entry	Device	Voc (V)[a]	Jsc ($mA\cdot cm^{-2}$)[b]	FF (%)[c]	PCE (%)[d]	Ref.
1	**PDBT-T1:a0**	0.89	14.6	63.0	8.2	*48*
2	**PBDB-T:a5**	0.78	23.2	73.0	13.2	75
3	**FTAZ:a6**	0.90	19.7	69.3	12.3	76
4	**PBDB-TF:a7**	0.93	19.0	73.9	13.1	77
5	**PBDB-TF:a8**	0.90	19.5	75.5	13.3	78
6	**PTB7-TH:b0**	0.81	14.2	59.1	6.8	49
7	**PTB7-Th:b9**	0.64	25.1	67.6	10.9	72
8	**PTB7-Th:b10**	0.74	24.0	67.1	12.0	73
9	**PM6:b11**	0.92	22.6	74.0	15.4	74
10	**PM6:c0**	0.86	24.3	73.2	15.3	50
11	**PM5:c6**	0.81	22.0	71.1	13.40	79
12	**PM6:c7**	0.83	25.2	68.5	14.4	80

a) open circuit voltage, *b*) short-circuit current density, *c*) fill factor, *d*) power conversion efficiency.

Table 1.5. Optical and electrochemical properties of acceptors **a9-a16**, **b12-b13** and **c8-c10**

Entry	*Compounds*	*Td (°C)[a]*	*λ sol max (nm)[b]*	*λ Film max (nm)[c]*	*EG^{OPT} (eV)[d]*	*ε (λmax) ($M^{-1}\cdot L^{-1}$)*	*HOMO (eV)[f]*	*LUMO (eV)[f]*	*μ SCLC ($cm^2\cdot V^{-1}\cdot s^{-1}$)[g]*	*Ref.*
1	**a0**	-	664	716	1.62	2.4×10^5	-5.69	-3.91	1.1×10^{-3}	*48*
2	**a9**	-	678	704	1.61	-	-5.71	-3.96	3.53×10^{-4}	*81*
3	**a10**	377	769	821	1.39	3.51×10^5	-5.42	-3.95	-	*82*
4	**a11**	350	736	793	1.39	-	-5.64	-3.95	-	*83*
5	**a12**	350	739	775	1.44	-	-5.51	-3.96	-	*86*
6	**a13**	-	723	765	1.44	9.9×10^4	-5.54	-3.94	-	*87*

7	**a14**	-	790	850	1.28	1.32×10^5	−5.44	−4.15	-	*88*
8	**a15**	345	794	839	1.31	-	-5.34	-4.06		*89*
9	**a16**	334	751	831	1.30	-	-5.54	-4.05	2.65×10^{-4}	*90*
10	**b0**	345	664	702	1.59	1.3×10^5	-5.48	-3.83	3.0×10^{-4}	*49*
11	**b12**	-	698	752	1.44	$2.14\text{x}10^5$	-5.52	-3.90	-	*84*
12	**b13**	300	664	696	1.65	2.00×10^5	–5.60	–3.87	9.64×10^{-4}	*85*
13	**c0**	318	731	821	1.33	1.07×10^5	-5.65	-4.10	2.35×10^{-4}	*50*
14	**c8**	-	749	844	1.30	$2.05\text{x}10^5$	-5.59	-3.97	1.1×10^{-4}	*91*
15	**c9**	-	735	794	1.34	$2.30\text{x}10^5$	-5.63	-3.88	$6.15\text{x}10^{-4}$	*92*
16	**c10**	-	770	877	1.25	-	-5.60	-3.90	2.8×10^{-4}	*93*

a) Decomposition temperature; *b*) λ_{max} in solution; *c*) λ_{max} in thin films; *d*) optical band gap in thin films; *e*) extinction coefficient at $\boldsymbol{\lambda}_{max}$; *f*) determined in solution by cyclic voltammetry; *g*) electron mobility.

Table 1.6. Photovoltaic properties of best devices incorporating NFA acceptors shown in Figure 1.10.

Entry	Device	Voc (V)[a]	Jsc ($mA\cdot cm^{-2}$)[b]	FF (%)[c]	PCE (%)[d]	Ref.
1	**PDBT-T1:a0**	0.89	14.61	63.0	8.19	*48*
2	**PBDB-T2F:a9**	0.980	17.60	76.0	13.1	*81*
3	**PBDB-T:a10**	0.852	21.9	69.8	13.1	*82*
4	**PM7:a11**	0.830	22.91	76.5	14.54	*83*
5	**PBDB-T:a12**	0.860	22.4	72.4	14.0	*86*
7	**PBDB-T:a13**	0.850	20.87	72.0	12.79	*87*
8	**PTB7-Th:a14**	0.74	26.30	67.0	13.1	*88*
9	**PTB7-Th:a15**	0.817	21.90	65.0	12.1	*89*
10	**PTB7-Th:a16**	0.750	25.3	69.3	13.2	*90*
11	**PTB7-TH:b0**	0.81	14.21	59.1	6.80	*49*
12	**PBDB-T-2F:b12**	0.846	20.21	75.2	13.05	*84*
13	**PBDB-T:b13**	0.910	16.02	76.8	11.2	*85*
14	**PM6:c0**	0.86	24.3	73.2	15.3	*50*
15	**PM6:c8**	0.820	27.03	72.00	15.96	*91*
16	**PM6:c9**	0.888	24.6	76.3	16.7	*92*
17	**PM6:c10**	0.804	27.72	76.35	17.02	*93*

a) open circuit voltage, *b*) short-circuit current density, *c*) fill factor, *d*) power conversion efficiency.

.

Dai *et al.* [72] reported the synthesis of a novel thienothiophene (TT) core **b9**. The introduction of the TT moiety increases the electron density and extends the conjugation of the core compared to the classical benzene ring. The UV-Vis spectra of **b9** showed a remarkable redshift, with higher maximum extinction coefficient, a lower optical bandgap originated from a lower LUMO level and a higher electron mobility with respect to the prototypical ITIC **b0**. The authors also reported a simultaneously enhance of V_{OC} and J_{sc} and consequently a higher PCE with respect to **b0**, other materials and parameters equal. Li *et al.* [73] recently reported the synthesis of a novel NFA b10 which possesses essentially the same structure of b9 but differs in terms of the endcapping groups: b10 possesses two fluorine atoms instead of four of **b9**. **b10** has an absorption spectrum with a remarkable redshift due to the halogenated endcapping groups and a higher (almost double) maximum extinction coefficient respect to ITIC **b0**; moreover, it has a higher HOMO and a lower LUMO which provoke a lower optical bandgap. In terms of photovoltaics properties, **b9** and **b10** showed higher PCE compared with those of **b0**; the authors explained it as a consequence of complementary absorption with the donor, higher and more balanced charge mobility and a higher domain purity which suppresses the bimolecular recombination and promotes charge transport and consequently increase the PCE. Chen *et al.*[74] reported the synthesis of a novel NFA **b11** with a carbazole moiety instead of a benzene ring, combined with chlorine-substituted endcapping group. The carbazole moiety has a strongly electron donating capacity and consequently the resulting core is richer in term of electron density. Such core substitution, however, gives rise in **b11** to substantial redshift, higher HOMO and lower LUMO with respect to **b0**, and, in addition to the expected lower optical bandgap and a higher extinction coefficient at the absorption maxima. In terms of photovoltaics property, **b11** showed higher V_{OC} and FF(%) compared to those of **b0**, presumably as a consequence, as suggested by the authors, of higher electron/hole mobilities. The carbazole based acceptor achieved the highest PCE for the binary BHJs reported so far in the literature with this class of NFAs (entry 13 in

[72] S. Dai, T. Li, W. Wang, Y. Xiao, T. Lau, Z. Li, K. Liu, X. Lu and X. Zhan, «Enhancing the Performance of Polymer Solar Cells via Core Engineering of NIR-Absorbing Electron Acceptors» *Adv. Mater.* **2018***, 30,* 1706571.

[73] T. Li, S. Dai, Z. Ke, L. Yang, J. Wang, C. Yan, W. Ma and X. Zhan, «Fused Tris(thienothiophene)-Based Electron Acceptor with Strong Near-Infrared Absorption for High-Performance As-Cast Solar Cells» *Adv. Mater.* **2018***, 30,* 1705969.

[74] T.-W. Chen, K.-L. Peng, Y.-W. Li, Y.-J. Su, K.-J. Ma, L. Hong, C.-C. Chang, J. Hou and C.-S. Hsu, «A chlorinated nonacyclic carbazole-based acceptor affords over 15% efficiency in organic solar cells» *J. Mater. Chem. A* **2020***, 8,* 1131.

Table 4). Huang *et al.* [75] reported the synthesis of a novel NFA, **a5**, with a tetrathiophene central core in a structure with high planarity, resulting in an extended and electron rich core compared with that of **a0**. The visible spectrum of **a5** showed a remarkable redshift and a reduced HOMO/LUMO gap. In terms of photovoltaics property (Table 2, entry 3), **a5** showed much higher J_{sc} and FF(%) with respect to **a0**, as a result, as claimed by the authors, of higher electron mobility and a lower level of charge recombination. Zhu *et al.*[76] reported the synthesis of a novel NFA with a naphthalene core **a6**; the optoelectronic properties are essentially those of the **a0**, apart from deeper HOMO and LUMO levels, probably better matching the donor polymer, resulting in better performances in terms of photovoltaics properties. An anthracene moiety was also proposed as a core by Yao *et al.*[77] and Feng *et al.* [78] (compounds **a7-8**). These scaffolds present an extension of the conjugation resulting in a red-shifted UV-Vis spectra and good extinction coefficients at λ_{max}. HOMO/LUMO energy differences, however, resulted to be higher for **a7** and **a8** than for **a0**. In terms of photovoltaics properties, however, **a7-8** showed better performances compared to those of **a0**, with higher values for all relevant parameters V_{OC}, J_{sc}, FF(%) and PCE. Yuan *et al.*[79] in the past years synthetized **c6**, which bearing a benzotriazole (BTA) as electron-deficient central core instead of the classical benzothiadiazole (BT). **c6** showed a slightly red-shift (solution) and an higher bandgap compared to **c0**, and with respet to the photovoltaic properties, **c6** possesses lower Voc, J_{sc} and

[75] C. Huang, X. Liao, K. Gao, L. Zuo, F. Lin, X. Shi, C.-Z. Li, H. Liu, L. X., F. Liu, Y. Chen, H. Chen and A. K.-Y. Jen, «Highly Efficient Organic Solar Cells Based on S,N-Heteroacene NonFullerene Acceptors» *Chem. Mater.* **2018***, 30,* 5429−5434.

[76] J. Zhu, Z. Ke, Q. Zhang, J. Wang, S. Dai, Y. Wu, Y. Xu, Y. Lin, W. Ma, W. You and X. Zhan, «Naphthodithiophene-Based Nonfullerene Acceptor for High-Performance Organic Photovoltaics: Effect of Extended Conjugation» *Adv. Mater.* **2018***, 30,* 1704713.

[77] C. Yao, B. Liu, Y. Zhu, L. Hong, J. Miao, J. Hou, F. He and H. Meng, «Highly fluorescent anthracene derivative as a non-fullerene acceptor in OSCs with small non-radiative energy loss of 0.22 eV and high PCEs of over 13%» *J. Mater. Chem. A* **2019***, 7,* 10212-10216.

[78] H. Feng, Y.-Q.-Q. Yi, X. Ke, J. Yan, Y. Zhang, X. Wan, C. Li, N. Zheng, Z. Xie and Y. Chen, «New Anthracene-Fused Nonfullerene Acceptors for High-Efficiency Organic Solar Cells: Energy Level Modulations Enabling Match of Donor and Acceptor» *Adv. Energy Mater.* **2019***, 9,* 1803541.

[79] J. Yuan, T. Huang, P. Cheng, Y. Zou, H. Zhang, J. L. Yang, S-Y. Chang, Z. Zhang, W. Huang, R. Wang, D. Meng, F. Gao and Y. Yang «Enabling low voltage losses and high photocurrent in fullerene-free organic photovoltaics» *Nat. Commun.,* **2019***, 10,* 570.

FF(%) which result in a lower PCE. Wang *et al.*[80] in the past years synthesized **c7**, which can be formally derived from **Y6** by substitution of the central electron-deficient BT core with BTA. **c7** showed a remarkable red shift in both solution and film compared and a higher electron mobility compared to **c0**, while it possesses the same bandgap. Regarding the photovoltaic properties, **c7** possess a slightly lower Voc and FF(%), resulting in a lower PCE compared to **c0**. The modification of the lateral moieties has also been addressed (figure 1.10). Liu *et al.*[81] reported the synthesis of a novel NFA (**a9**) in which the two thiophene units of **a0** have been substituted with fluorene-type moieties. This substitution should affect the optoelectronic properties, and indeed the UV spectra is slightly red shifted with respect to **a0** in solution, but such red shift is not confirmed in thin films (Tables 1.5 and 1.6). Interestingly, **a9** possesses a lower electron mobility, but higher photovoltaic parameters than those of **a0**; the authors explained it as a consequence of a better complementary absorption with the donor, a suppressed nonradioactive recombination loss, uniform and much decreased phase-separated-morphology and a more efficiently suppressed charge recombination. Sun *et al*. [82] reported the synthesis of a novel NFA **a10** in which the lateral thiophene moieties have been substituted with dithienopyrrole moieties. The core extension in **a10** allowed a remarkable red shift of the UV spectra to the NIR, with higher maximum molar absorption coefficient; moreover, the introduction of a much more electron rich core lead a substantially higher HOMO, a lower optical bandgap and a higher electron mobility compared with those of **a0**. In terms of photovoltaics property **a10** showed better photovoltaic parameters than **a0**. Wan *et*

[80] R. Wang, J. Yuan, R. Wang, G. Han, T. Huang, W. Huang, J. Xue, H-C, Wang, C. Zhang, C. Zhu, P. Cheng, D. Meng, Y. Yin, K-H, Wei, Y. Zou and Y. Yang. «Rational Tuning of Molecular Interaction and Energy Level Alignment Enables High-Performance Organic Photovoltaics» *Adv. Mater.* **2019***, 31,* 1904215.

[81] G. Liu, J. Jia, K. Zhang, X. Jia, Q. Z. W. Yin, L. Li, F. Huang and Y. Cao, «15% Efficiency Tandem Organic Solar Cell Based on a Novel Highly Efficient Wide-Bandgap Nonfullerene Acceptor with Low Energy Loss.,» *Adv. Energy Mater.* **2019***, 9,* 180365.

[82] J. Sun, X. Ma, Z. Zhang, J. Yu, J. Zhou, X. Yin, L. Yang, R. Geng, R. Zhu, F. Zhang and W. Tang, «Side chain engineering on Dithieno[3,2-b:2',3'-d]pyrrol Fused Nonfullerene Acceptors Enabling Over 13% Efficiency for Organic Solar Cells» *Mater. Chem. Front.* **2019***,3,* 702-708.

al.[83] [84] and Lin *et al.*[84] reported the synthesis of two novel NFAs **a11** and **b12**. These acceptors, despite the different halides in the endcapping groups, have a regioisomeric scaffold. **a11** and **b12** present a remarkable and slightly red-shift UV spectra compared with a0 and **b0**, respectively, induced by the introduction of the Selenium heterocycle. In terms of photovoltaics properties, interestingly **a11** showed higher PCE than **b12**.

Asymmetric scaffolds represent an interesting strategy to promote a fine tune of the optoelectronic properties and a way to achieve high performance OSCs. Gao *et al.*[85] reported the synthesis of a novel NFA **b13** with an asymmetrical scaffold: it can be categorized as an ITIC with a thiophene instead of a thienothiophene. **b13** showed basically the same UV spectra with a slightly higher molar extinction coefficient, moreover, **b13** has a higher HOMO and a comparable LUMO with respect to **b0**. Interestingly, the authors observed that the asymmetric scaffold of **b13** possessed a higher dipole moment, leading to a high polarity molecule, which could be useful to increase the solubility of these molecules in much more polar solvent than the conventional ones used in the device fabrication. In terms of photovoltaic properties, **b13** showed higher values for all parameters *vs.* **b0**, and consequently higher PCE. The authors explained these results as a consequence of higher and more balanced carrier mobilities, better dissociation probability and charge collection ability, minor bimolecular recombination, and an excellent morphology. Yang *et al*.[86] last year reported the synthesis of a novel asymmetric NFA **a12**, which possesses a dithienopyrrole moiety. **a12** showed a remarkable red shift compared to **a0**, and, in terms of photovoltaic properties, it showed higher values for all parameters vs. **a0**, and consequently higher PCE.

---

[83] S.-S. Wan, X. Xu, Z. Jiang, J. Yuan, A. Mahmood, G.-Z. Yuan, K.-K. Liu, W. Ma, Q. Peng and J.-L. Wang, «A bromine and chlorine concurrently functionalized end group for benzo[1,2-b:4,5-b′]diselenophene-based non-fluorinated acceptors: a new hybrid strategy to balance the crystallinity and miscibility of blend films for enabling highly efficient polymer solar cells» *J. Mater. Chem. A* **2020***, 8,* 4856-4867.

[84] F. Lin, L. Zuo, K. Gao, M. Zhang, S. B. Jo, F. Liu and A. K.-Y. Jen, «Regio-Specific Selenium Substitution in Non-Fullerene Acceptors for Efficient Organic Solar Cells» *Chem. Mater.* **2019***, 31,* 6770−6778.

[85] W. Gao, M. Zhang, T. Liu, R. Ming, Q. An, K. Wu, D. Xie, Z. Luo, C. Zhong, F. Liu, F. Zhang, H. Yan and C. Yang, «Asymmetrical Ladder-Type Donor-Induced Polar Small Molecule Acceptor to Promote Fill Factors Approaching 77% for High-Performance Nonfullerene Polymer Solar Cells» *Adv. Mater.* **2018***, 30,* 1800052.

[86] L. Yang, X. Song, J. Yu, H. Wang, Z. Zhang, R. Geng, J. Cao, D. Baran and W. Tang, «Tuning of the conformation of asymmetric nonfullerene acceptors for efficient organic solar cells» *J. Mater. Chem. A* **2019***,7,* 22279.

NFAs molecules must be soluble in the common organic solvents to be processable. Alkyl side chains ensure a good solubility in these solvents; the introduction of alkyl chains is however associated with other problems such as impeding the ordered packing of molecules, which decreases the charge transport ability, lowers carrier mobility, and deteriorates device performance. Liu *et al*. [87] synthesized a novel NFA **a13** which bears two hexyloxy groups at its central core to modulate the photophysical, photovoltaic and morphological properties. The introduction of the side chains and the two terminal thiophene rings of **a13** provoke a remarkable red shift with respect to **a0**. In terms of photovoltaic properties, **a13** shows higher values for all parameters vs. **a0**, and consequently higher PCE. It is worth noting that the photovoltaic performances were achieved with spin-coated active layers; no extra treatment such as using additives or annealing was needed. Lee *et al.* [88] synthesized a novel NFA **a14** which possesses an asymmetrical side chain substitution pattern. **a14** showed a remarkable red shifted UV/Vis spectrum compared to **a0**, while, in terms of HOMO/LUMO levels, **a14** showed a lower optical bandgap. In terms of photovoltaic properties, it showed higher values for all parameters vs. **a0**, and consequently higher PCE as a primary consequence of favourable BHJ morphology for efficient charge separation and transport. Lee *et al*. [89] and Chen *et al* [90] expended this work by synthesizing two novel NFAs **a15** and **a16** which contain the same side chains but different heteroatoms onto the flanking thiophene rings. Both acceptors showed remarkable, red-shifted UV/Vis spectra compared to those of **a0**. The optical bandgaps are essentially the same for both acceptors. In terms of photovoltaic properties, they showed higher values for all parameters vs. **a0**, and consequently higher PCE. The authors claim an efficient wavelength collection near NIR, a favorable BHJ morphology, and a well-ordered molecular orientation and tight face-on packing.

---

[87] Y. Liu, M. Li, X. Zhou, Q.-Q. Jia, S. Feng, P. Jiang, X. Xu, W. Ma, H.-B. Li and Z. Bo, «Nonfullerene Acceptors with Enhanced Solubility and Ordered Packing for HighEfficiency Polymer Solar Cells» *ACS Energy Lett.* **2018***, 3,* 1832−1839.

[88] J. Lee, S. Song, J. Huang, Z. Du, H. Lee, Z. Zhu, S.-J. Ko, T.-Q. Nguyen, J. Y. Kim, K. Cho and G. C. Bazan, «Bandgap Tailored Nonfullerene Acceptors for Low-Energy-Loss Near-Infrared Organic Photovoltaics» *ACS Materials Lett.* **2020***, 2,* 395−402.

[89] J. Lee, S.-J. Ko, M. Seifrid, H. Lee, C. McDowell, B. R. Luginbuhl, A. Karki, K. Cho, T.-Q. Nguyen and C. Bazan G, «Design of Nonfullerene Acceptors with Near-Infrared Light Absorption Capabilities» *Adv. Energy Mater.* **2018***, 8,* 1801209.

[90] J. Chen, G. Li, Q. Zhu, X. Guo, Q. Fan, W. Ma and M. Zhang, «Highly efficient near-infrared and semitransparent polymer solar cells based on an ultra-narrow bandgap nonfullerene acceptor» *J. Mater. Chem. A* **2019***, 7,* 3745–3751.

Jen *et al.*[919293] last year reported the synthesis of three novel NFAs: **c8**, which can be formally derived from **Y6** by substitution of a thiophene with a selenophene in the elctron-rich thienothiophene moiety; **c9**, which possesses an asymmetric scaffold based on Y6-like structure; and **c10** which possesses a BTA as electron-deficient core. Despite **c9** which showed a slightly blue-shift in both solution and film UV, **c8** and **c10** possess a remarkable red-shift in both solution and thin films compared to **c0**. The narrow bandgap related to **c10** is noteworthy, since in our knowledge is the narrowest bandgap reported for NFA molecules. In terms of photovoltaic properties, all the above NFAs showed better photovoltaic performance: **c10** possesses a remarkably high PCE, one the highest so far. According to the authors, all these NFAs possesses a well-defined morphology as well as well-balance charge mobility, which result in better photophysical and photovoltaics properties.

1.4→ SUSTAINABILITY, INDUSTRIAL CONSIDERATIONS, AND SCALABILITY OF NFAS.

The sustainability of these materials plays an important role, since one of the selling points for OPV is costs, environmental issues (especially when compared with lead-based perovskites) and scalability. Three main factors must be taken into consideration a) atom economy, which was developed by Barry Trost and can be seen as "what atoms of the reactants are incorporated into the final desired product(s) and what atoms are wasted ", b) step economy, which is related to the steps required for a given molecule and c) E-factor which is the ratio between mass of waste and mass of product (Equation 1.1).[949596]

---

[91] F. Lin, K. Jiang, W. Kaminsky, Z. Zhu and A. K.-Y. Jen, «A Non-fullerene Acceptor with Enhanced Intermolecular π-Core Interaction for High-Performance Organic Solar Cells» *J. Am. Chem. Soc.* **2020***, 142,* 15246–15251.

[92] W. Gao, H. Fu, Y. Li, F. Lin, R. Sun, Z. Wu, X. Wu, C. Zhong, J. Min, J. Luo, H. Y. Woo, Z. Zhu and J. K.-Y. Alex, «Asymmetric Acceptors Enabling Organic Solar Cells to Achieve an over 17% Efficiency: Conformation Effects on Regulating Molecular Properties and Suppressing Nonradiative Energy Loss» *Adv. Energy Mater.* **2020***, 11,* 2003177.

[93] F. Qi, K. Jiang, F. Lin, W. Ziang, H. Zhang, W. Gao, Y. Li, Z. Cai, H. Y. Woo, Z. Zhu and J. K.-Y. Alex, «Over 17% Efficiency Binary Organic Solar Cells with Photoresponses Reaching 1000 nm Enabled by Selenophene-Fused Nonfullerene Acceptors» *ACS Energy Lett.* **2021***, 6,* 9–15.

[94] P. T. Anastas and J. C. Warner, Green Chemistry: Theory and Practice, Oxford University Press: New York, **1998**.

[95] B. M. Trost, «The Atom Economy-A Search for Synthetic Efficiency» *Science* **1991***, 254,* 1471-1477.

[96] R. Sheldon, «E Factors, green chemistry and catalysis: An odyssey» *Chem. Commun.* **2008***, 3352-3365.*

$$\text{E-factor} = \frac{Mass\ of\ waste}{Mass\ of\ products}$$

Equation 1.1: E-factor formula

For instance, NFA **Y6** and donor polymer **PM6**, the most promising acceptor/donor component for OPV (Figure 1.11) require many synthetic steps, harsh conditions, and toxic reagent for their synthesis.[5197]

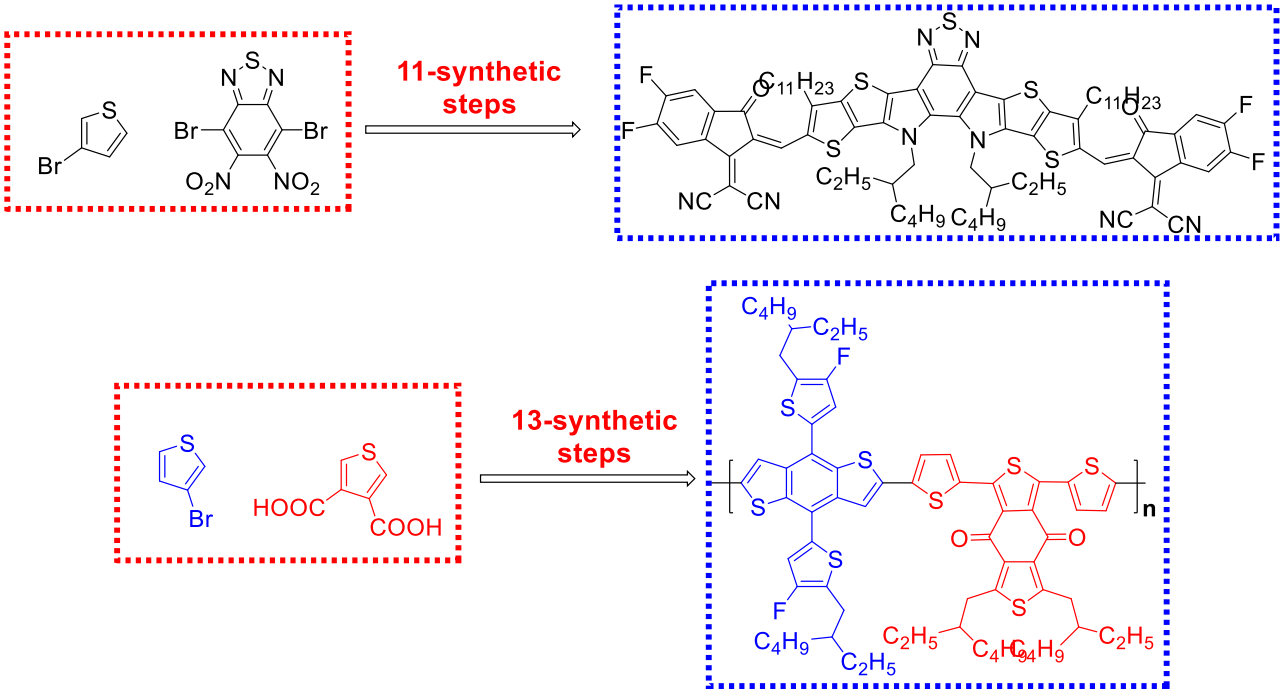

Figure 1.11. number of synthetic steps for Y6 and PM6

Efforts must focus on novel ways to produce high performance materials with less synthetic steps, non-toxic reagents, high atom/steps economy and low E-factor. The cost of fabricating a photovoltaic module entails different contributions, but the higher costs are associated to the active layer materials.[98] The comparison between OSC systems is often made by considering the best PCE of devices characterizing each specific combination of polymer donor and acceptor. Although this metric is undoubtedly important,

[97] M. Zhang, X. Guo, S. Zhang and J. Hou, «Synergistic Effect of Fluorination on Molecular Energy Level Modulation in Highly Efficient Photovoltaic Polymers» *Adv. Mater.* **2014**, *26,* 1118–1123.

[98] J. Min, Y. N. Luponosov, C. Cui, B. Kan, H. Chen, X. Wan, Y. Chen, S. A. Ponomarenko, Y. Li and C. J. Brabec, «Evaluation of Electron Donor Materials for Solution-Processed Organic Solar Cells via a Novel Figure of Merit» *Adv. Energy Mater.* **2017**, *7,* 1700465.

other parameters for the determination of the potential of OSC materials for industrialization are essential to be considered. The cost of the materials, and more specifically of the donor and acceptor employed is in turn primarily dependent on their synthetic accessibility, which broadly speaking is related to the number of synthetic steps (NSS) required.[99] Po *et al.* a few years ago, investigated quantitative metrics in an attempt to rationalize and quantify the synthetic complexities of donor and acceptor components for OSCs.[100] They have calculated the synthetic complexity (SC) data and the cost per gram of material for a series of recent NFAs reported in this chapter, and the data are reported in Table 1.7. The synthetic complexities are rather high for all substrates evaluated, essentially as the consequence of the relevant NSS (9–15) required to afford the target molecules. Low values for NSS, such as in the case of entry 2, can result in high costs, depending on the costs of the starting materials.

Table 1.7. Synthetic complexities and relevant parameters for a series of NFAs described in this chapter.

Entry	NFA	NSS	*SC*	*Cost (Euro/g)*
1	**b1**	12	72	58
2	**b0**	9	68	113
3	**a2**	15	97	105
4	**a15**	15	91	115

The (photo)stability of solar devices is one of the pillars for the deployment of the OPV technology.[101] Guo *et al.*[101] have published a study where a wide range of non-fullerene acceptors have been ranked

[99] F. Machui, M. Hösel, N. Li, G. D. Spyropoulos, T. Ameri, R. R. Sondergaard, M. Jorgensen, A. Scheel, D. Gaiser, K. Kreul, D. Lenssen, M. Legros, N. Lemaitre, M. Vilkman, M. Va¨lima¨ki, S. Nordman, C. J. Brabec and F. C. Krebs, «Cost analysis of roll-to-roll fabricated ITO free single and tandem organic solar modules based on data from manufacture» *Energy Environ. Sci.,* **2014***, 7,* 2792–2802.

[100] R. Po, G. Bianchi, C. Carbonera and A. Pellegrino, «All That Glisters Is Not Gold": An Analysis of the Synthetic Complexity of Efficient Polymer Donors for Polymer Solar Cells» *Macromolecules* **2015***, 48,* 453–461.

[101] J. Guo, Y. Wu, R. Sun, W. Wang, J. Guo, Q. Wu, X. Tang, C. Sun, Z. Luo, K. Chang, Z. Z., J. Yuan, T. Li, W. Tang, E. Zhou, Z. Xiao, L. Ding, Y. Zou, X. Zhan, C. Yang, Z. Li, C. J. Brabec, Y. Li and J. Min, «Suppressing photo-oxidation of

according to their photobleaching rate. They found out that IDIC derivatives are less photodegradable than ITIC derivatives, with optical density (OD) losses per hour lower than 0.3%. For comparison, the OD loss per hour of ITIC is about 12%; derivatives with electron-withdrawing groups on the terminal moieties are more stable, while derivatives with electron-rich substituents are much more prone to degradation. The introduction of an electron-withdrawing benzothiadiazole ring between the indacenodithiophene core and the dicyanoindanone terminals (i.e. the IDTBR family of acceptors, for example **a2**) further increases the stability, that makes these materials the most interesting for modules manufacturing (providing that the energy level matching with the donor is satisfactory).[102] In any case, the findings described above provide a rule of design of acceptors useful for further OPV materials development. The optimal thickness of the active layer of polymer solar cells based on NFAs is typically around 100 nm,[103] usually attributed to the ideal morphology consisting in a bicontinuous network of small molecule domains around 15-20 nm. Higher thicknesses generally lead to enhanced bimolecular recombination, low charge mobilities and low FF(%) values. However, two issues exist with these low thicknesses. First, thin films are not able to absorb all photons of the solar spectrum, leading to low *J*sc values. The final PCE is therefore a trade-off between the decrease of FF with the active layer thickness, and the increase of J_{sc}. In addition, it is also very difficult for roll-to-roll productions based on printing techniques to reach thin films over a large area in an uniform way. In fact, thin films are very susceptible to film defects (with possible shunts), not tolerant to thickness variation, and less reproducible. Ideally, thicknesses of at least 250-300 nm would be required for the scale up. The literature reports a relatively low number of studies (about 50 papers) on devices based on NFA with thick active layers where good efficiencies are maintained. These devices are the result of careful and delicate optimization of the active layer morphology. From this point of view, IDTBR (**a2**) is again one of the more robust acceptors, with PCE as high as 8.1% for 1010 nm thick devices.[104] IDIC type acceptors provide devices with 8.5% PCE

non-fullerene acceptors and their blends in organic solar cells by exploring material design and employing friendly stabilizers» *J. Mater. Chem. A* **2019***, 7,* 25088.

[102] S. Strohm, F. Machui, S. Langner, P. Kubis, N. Gasperini, M. Salvador, I. McCulloch, E. H.-J. and C. J. Brabec, «P3HT: non-fullerene acceptor based large area, semi-transparent PV modules with power conversion efficiencies of 5%, processed by industrially scalable methods» *Energy Environ. Sci.* **2018***, 11,* 2225-2234.

[103] A. Yin, D. Zhang, S. H. Cheung, S. K. So, Z. Fu, L. H. F. Ying, H. Zhou and Y. Zhang, «On the understanding of energetic disorder, charge recombination and voltage losses in all-polymer solar cells» *J Mater. Chem. C.* **2018***, 6,* 7855-7863.

[104] Z. Whang, X. Liu, H. Jiang, X. Zhou, L. Zhang, F. Pan, X. Qiao, D. Ma, W. Ma, L. Ding, Y. Cao and J. Chen, «A ternary organic solar cell with 300 nm thick active layer shows over 14% efficiency» *Sol. RRL* **2019***, 3,* 1900079.

at 530 nm thickness (for comparison the PCE at 105 nm is 12.2%)[105], while in the case of ITIC-type acceptor, a device with 8.9% at 500 nm has been reported (12.7% at 141 nm). [106]

1.5→ FINAL REMARKS

Since their discovery, NFAs have been boosted the device's photovoltaic performances up to 17%, thank to a carefully optimization and investigation of the core, side chains and end-cap groups. Nevertheless, while much effort has been put into the synthesis of high performance NFAs, less effort has been made to find sustainable synthesis to reduce the cost/g required for monomers. Industrial as well as sustainable point of views must be considered into the development of new NFAs.

[105] S. Li, L. Ye, W. Zhao, X. Liu, J. Zhu, H. Ade and J. Hou, «Design of a New Small-Molecule Electron Acceptor Enables Efficient Polymer Solar Cells with High Fill Factor» *Adv. Mater.* **2017***, 29,* 1704051.

[106] L. Zhang, H. Zhao, B. Li, J. Yuan, X. Xu, J. Wu, K. Zhou, X. Guo, M. Zhang and W. Ma, «A blade-coated highly efficient thick active layer for non-fullerene organic solar cells» *J. Mater. Chem A* **2019***, 7,* 22265-22273.

Chapter 2

Sustainable synthetic approaches to the IDIC core through domino cyclization/deprotection reactions

This chapter is partly based on the following publication: *Sustainable synthetic approaches to the IDIC core through domino cyclization/deprotection reactions*, G. Forti, A. Nitti, G. Bianchi, R. Po, D. Pasini, *submitted*.

2.1→ INTRODUCTION

Among the organic photovoltaics device, Bulk Heterojunction Solar cells (BHJs) are the most promising technology for the solar energy conversion, due to their high efficiency, flexibility, stretchability and the possibility to integrate them in many architectures.[107][108][109] BHJ normally possess a "sandwich" structure, where the photoactive layer is usually made by a blend mixture of an electron donor material, usually a polythiophene, and an electron acceptor small molecule (SMA), usually a nonfullerene acceptor (NFA), encapsulated between two interlayers, an electron transporting layer (ETL) and an hole transporting layer

[107] E. Dauzon, X. Sallenave, C. Plesse, F. Goubard, A. Amassian and T. D. Anthopoulos, «Pushing the Limits of Flexibility and Stretchability of Solar Cells: A Review,» *Adv. Mater.* **2021***, 33,* 2101469.

[108] M. Seri, F. Mercuri, G. Ruani, Y. Feng, M. Li, Z.-X. Xu and M. Muccini, «Toward Real Setting Applications of Organic and Perovskite Solar Cells: A Comparative Review,» *Energy Technol.* **2021***, 9,* 2000901.

[109] J. Yao, B. Qiu, Z.-G. Zhang, L. Xue, R. Wang, C. Zhang, S. Chen, Q. Zhou, C. Sun, C. Yang, M. Xiao, L. Meng and Y. Li, «Cathode engineering with perylene-diimide interlayer enabling over 17% efficiency single-junction organic solar cells,» *Nat. Commun.,* **2020***, 11,* 2726.

(HTL).[110][111] In the past decade, several efforts have been made for the developing of new nonfullerene electron acceptors components (NFAs). The major breakthrough arrived in 2015 with the discovery of ITIC/IDIC family as high performance NFAs, and since then several molecules bearing the indaceno core have been synthetized by modification of the central electron rich core, side chains and end-cap groups.[49,59,61,87112113] Despite that, synthesis of the indaceno core and its functionalization remain a challenge in terms of sustainable chemistry. Two main strategies have been reported, and they require several steps, harsh conditions, and toxic reagents, so that a large scale production, despite the high performance shown into devices, remain infeasible.[114][115] Here we propose a novel synthesis for the IDIC Core (**Figure 2.1**), which starts from relatively cheap starting materials and allow us to assemble a fully functionalized IDIC core with a reduction of synthetic steps compared to the synthetic routes reported in the literature. We base our approach on two main aspects: a) avoid the use of tin derivatives, whose byproducts are well known to be toxic, and b) the use of cascade reaction to reduce the number of synthetic steps.

2.2→ RESULTS AND DISCUSSION

[110] H. Zhang, Y. Li, X. Zhang, Y. Zhang and H. Zhou, «Role of interface properties in organic solar cells: from substrate engineering to bulk-heterojunction interfacial morphology» *Mater. Chem. Front.,* **2020***, 4,* 2863-2880.

[111] X. Xu, D. L, J. Yuan, Y. Zhou and Y. Zou, «Recent advances in stability of organic solar cells,» *EnergyChem.,* **2021***, 3,* 100046.

[112] G. Forti, A. Nitti, P. Osw, G. Bianchi, R. Po e D. Pasini, «Recent Advances in Non-Fullerene Acceptors of the IDIC/ITIC Families for Bulk-Heterojunction Organic Solar Cells» *Int. J. Mol. Sci.* **2020***, 21,* 8085.

[113] Y. Li, W. K. Tatum, J. W. Onorato, S. D. Barajas, Y. Y. Yang and C. K. Luscombe, «An indacenodithiophene-based semiconducting polymer with high ductility for stretchable organic electronics» *Polym. Chem.,* **2017***, 8,* 5185–5193.

[114] Y. Zhang, J. Zou, H.-L. Yip, K.-S. Chen, D. F. Zeigler, Y. Sun and A. K.-Y. Jen, « Indacenodithiophene and Quinoxaline-Based Conjugated Polymers for Highly Efficient Polymer Solar Cells» *Chem. Mater.* **2011***, 23,* 92289–92291.

[115] H. 13. Chen, A. Wadsworth, C. Ma, A. Nanni, W. Zhang, M. Nikolka, A. T. M. Luci, M. L. A. Perdigão, K. J. Thorley, C. Cendra, B. Larson, G. Rumbles, T. D. Anthopoulos, G. Costantini, H. Sirringhaus and I. McCulloch, «The Effect of Ring Expansion in Thienobenzo[b]indacenodithiophene Polymers for Organic Field-Effect Transistors» *J. Am. Chem. Soc.* **2019***, 141,* 18806–18813.

The two main routes for the synthesis of the IDIC core present in the literature are described in Figure 2.1. They both involve an initial Stille coupling of a monostannylated thiophene residue. Li's route is then followed by a series of steps involving ester hydrolysis, an intramolecular acid catalyzed cyclization and a reduction, followed by the alkylation of the newly formed CH_2 positions with long alkyl chains for imparting overall solubility and processability to the final product. Zhang's route, instead, proceeds through the formation of a tertiary alcohol, via the attack of an organometallic species to the ester, which is followed by an acid catalyzed cyclization, which allows to have aryl substituents directly placed onto the IDIC skeleton, to impart solubility and avoid intermolecular aggregation. Our approach started with the choice of a particular zinc derivative as starting material, which bears a protected acetal moiety and allow us to bypass the conventional route based on Stille in favour of an eco-friendlier Negishi reaction for the synthesis of both derivatives **1a** and **1b** (Scheme 2.1). Moreover, the presence of the acetal moiety with an acid-labile protecting group ensures, in the final acid-catalyzed cyclization step, its deprotection, to restore the aldehyde functionality, consequently allowing a reduction of the synthetic steps. In the case of derivative **1a**, the Negishi protocol afforded the title compound in essentially quantitative yield, after purification of the reaction mixture by column chromatography. In the case of **1b**, the reaction was selective towards the functionalization of the iodide aryl substituents, with an overall yield of 70% after purification by column chromatography.

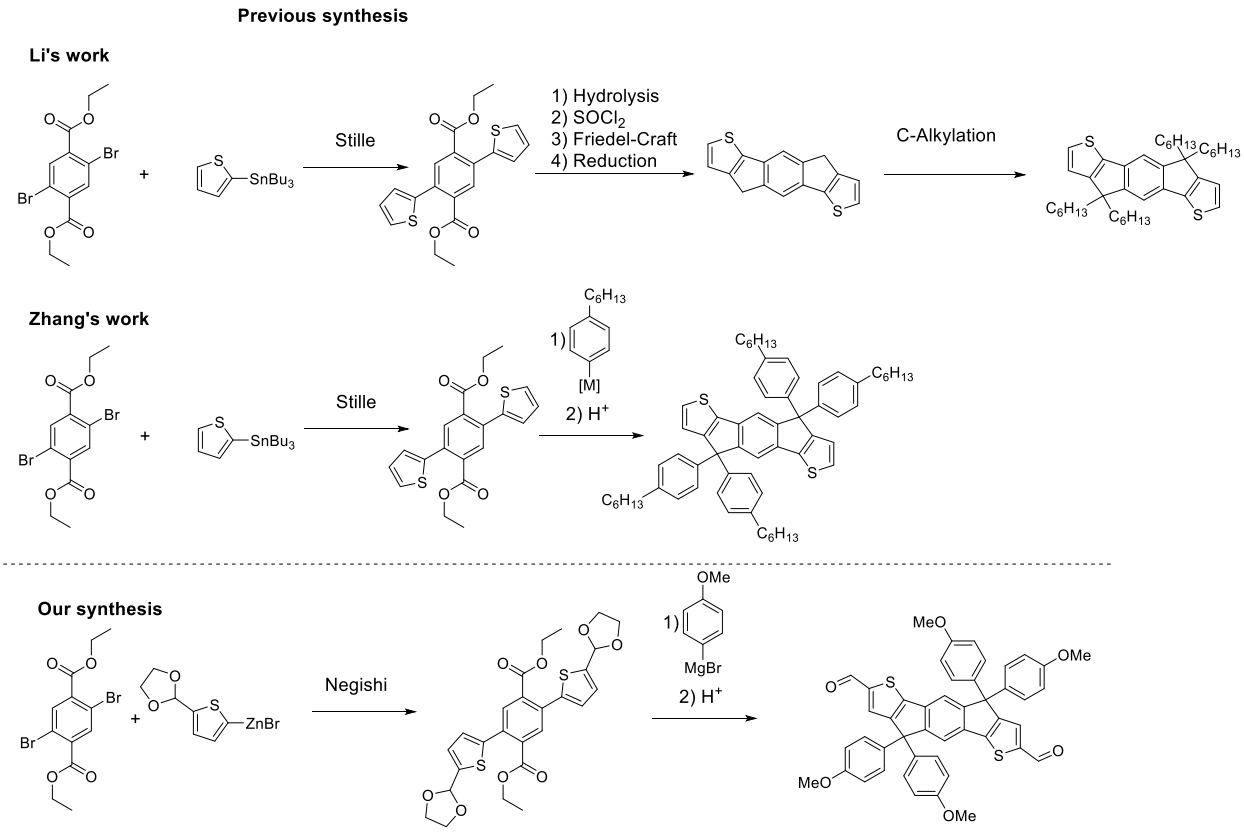

Figure 2.1. Previous syntheses and our approach

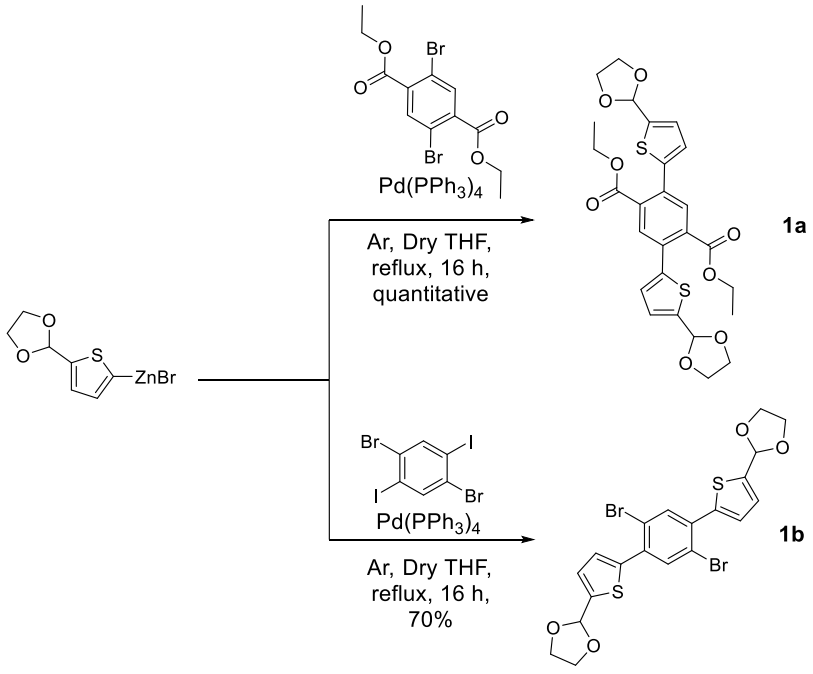

Scheme 2.1: Negishi coupling for derivatives 1a and 1b

The corresponding acetal **1a** was tested in the next step, the nucleophilic attack by the Grignard reagent, followed by a cascade intramolecular cyclization/deprotection to give the corresponding IDIC core **2a** (Scheme 2.2)

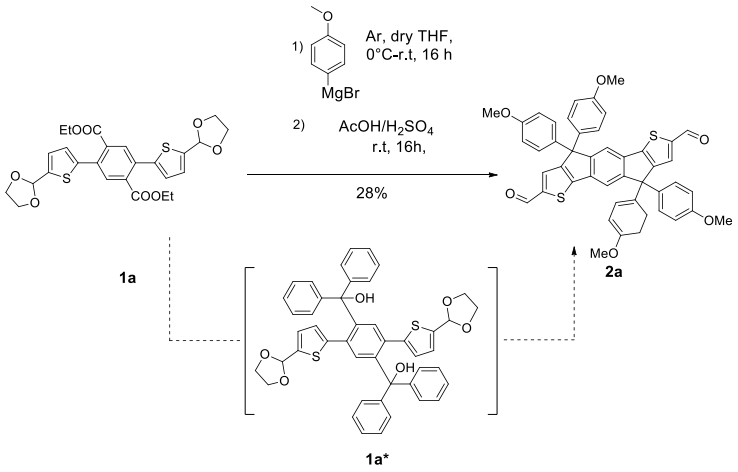

Scheme 2.2: one pot cyclization/ deprotection step

The cyclization/deprotection step has been extensively studied to find the most suitable conditions, as reported in Table 2.1. Noteworthy, in the classical conditions reported in literature (entries 1 and 2) the reaction proceed with a very low yield; lowering the temperature (entry 3), allowed us to obtain derivative **2a**, albeit in modest yield. We investigated the possibility to promote this reaction using different source of acids: we tried SiO_2 and amberlyst as proton sources (entries 4 and 5), however, after 16 h we did not observe the formation of derivative **2a**. Also, in the case of $BF_3.OEt_2$, after 2 h we observed only degradation products.

Table 2.1. Cyclization conditions for the synthesis of 2a

Entry	***H^+***	***Conditions***	***Yield***
1	HCl/AcOH	Reflux, 3 h	7%
2	H_2SO_4/AcOH	Reflux, 3 h	7%
3	H_2SO_4/AcOH	r.t 16 h	28%
4	SiO_2 /H_2O	r.t 16 h	-

5	Amberlyst	r.t, 16 h	-
6	$BF_3.OEt_2$	0°C to r.t 2 h	-

We ascribe the low yields as the consequence of competitive reaction pathways: deprotection and cyclization. Indeed, if the first reaction which takes place is deprotection (**Path A**), the produced aldehyde reduces the electron density over the thiophene ring and does not allow the intramolecular cyclization, while when the first reaction is the cyclization (**Path B**), the cascade reaction is ensured (Scheme 2.3).

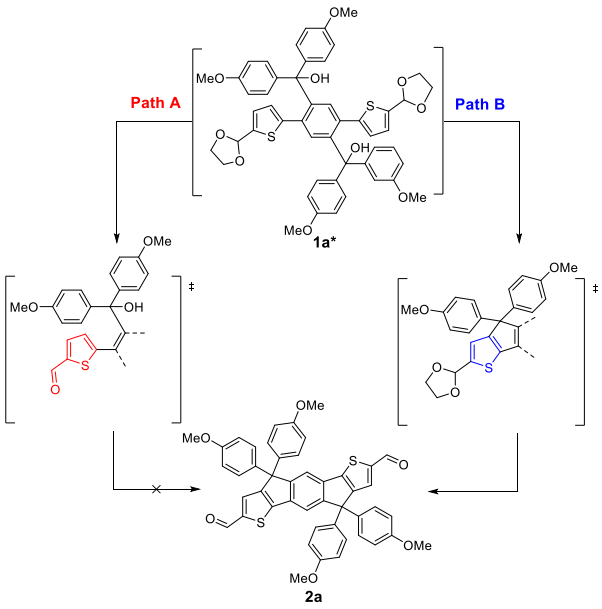

Scheme 2.3. Pathways for cyclization/ deprotection step for the synthesis of compound 2a

Since the deprotection of the acetal functionality requires the stoichiometric addition of water, we performed the reaction in our best conditions (entry 3) in the presence of molecular sieves, with the aim of activating the acetal deprotection in the acquoeus work-up procedures, only after the successful cyclization had occurred. Unfortunately, also in this case yields were not improved.

In the light of the overall improved sustainability of the OPV process, solubility and processability of the components in green solvents such as alcohols are desirable. In our approach to develop an alcoholic soluble IDIC core, we deprotected molecule **2a** to restore the phenolic moiety; the demethylation reaction

was carried out in presence of BBr_3 to give us the corresponding molecule **3a** (Scheme 2.4) in good, isolated yields. The free phenol functionalities could in our view functional as a solubilizing anchor for the overall core, because of their enhanced polaritiy and the possibility of their basification and formation of organic salts of tunable solubility in different solvents, because of the structure of the cationic counterpart.

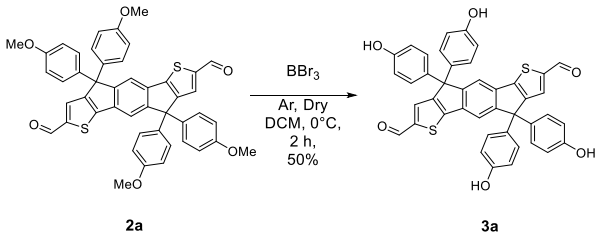

Scheme 2.4. Demethylation step for the synthesis of 3a

For the second acetal **1b** we envisaged a different path. Our strategy was thought to modify the central core of IDIC by the introduction of a spiro moiety which has been reported for the first time by Xie *et al.*[116]. Therefore, we tried to generate the corresponding lithium derivate **1b*** followed by reaction with fluorenone derivative to give the tert-alcohol **2b**, which would have been further cyclized to form the IDIC core **3b** (Scheme 2.5).

[116] L. Xie, J. Xiao, L. Wu, W. Zhang, Z. Ge and S. Tan, «Synthesis,and photovoltaic properties of small molecule electron acceptors with twin spiro-type core structure» *Dyes and Pigments,* **2019***, 168,* 197–204.

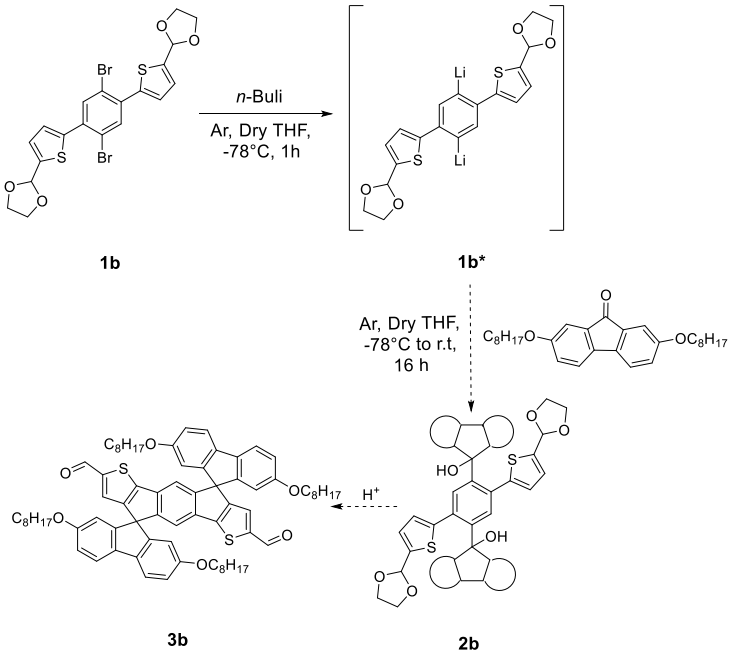

Scheme 2.5: one pot cyclization/deprotection

However, despite several attempts, we were never able to isolate **3b**, but instead we observed several side products difficult to characterize. We ascribed this luck of reactivity, as reported for the derivative **2a**, due to the competition between deprotection and cyclization, with the former which, when occurring before, switches off the reactivity of the electron-rich thiophene moiety for the latter cyclization. In the case of acetal **1b**, since the correct product **3b** could not be obtained, pathway **A** seems to be the only one operating (Scheme 2.6).

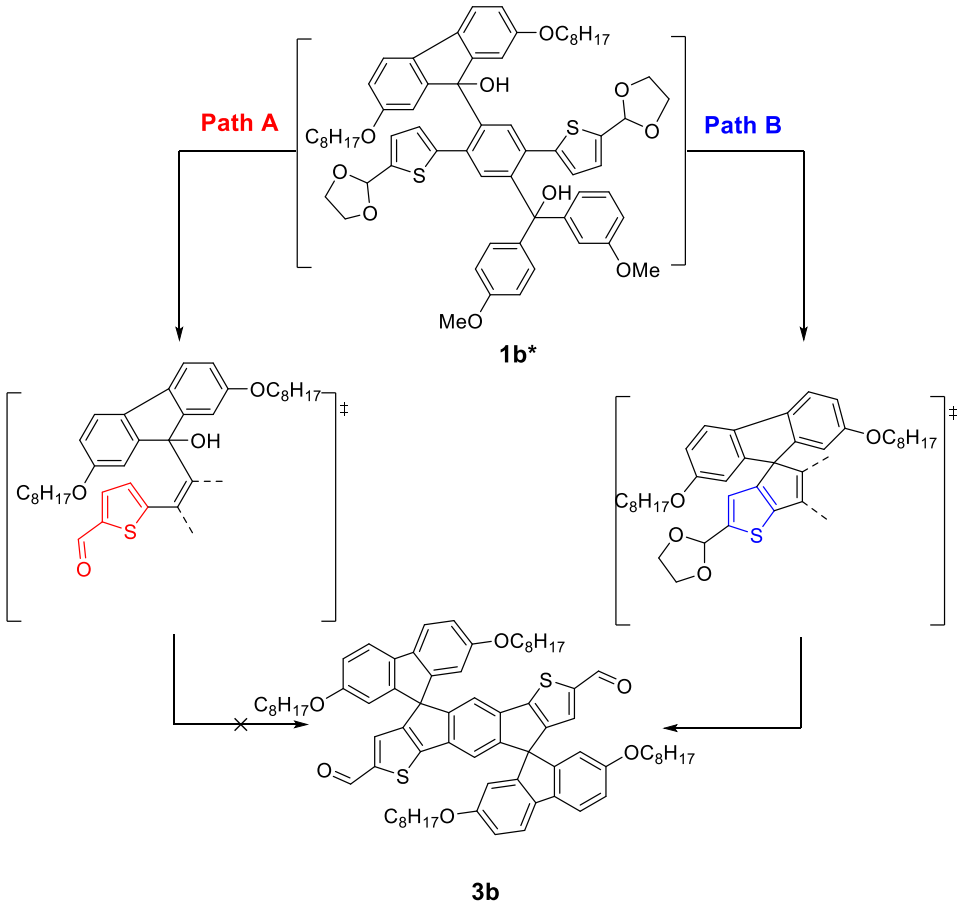

Scheme 2.6. Pathways for cyclization/ deprotection step.

Our synthesis for molecule **2a** possesses an overall E-*f*actor of **201.83** while the conventional synthesis calculated possesses **176.88**. Nevertheless, despite a slightly higher E-*f*actor value than **IDIC**, our approach in only 3 steps allow us to obtain a fully conjugate **IDIC-CHO** core, avoiding the further formylation step required for the classical synthesis, through an innovative and much more sustainable synthesis, which in our knowledge has never been reported so far.

2.3→ CONCLUSION

We have successfully developed a novel strategy for IDT core **3a**, which avoided tin derivatives and allowed us to reduce the synthetic steps required for its synthesis, by a subsequential cyclization deprotection reaction. The synthetic pathway is more sustainable, also because it makes use of commercially available zinc derivatives, which are considerably more ecofriendly than tin derivatives

used in the Stille coupling of the conventional approach reported in the literature. We also investigated the possibility to apply this strategy for the synthesis of derivative **2b**, unfortunately without any success. Further studies will focus on the possible application of this strategy for the synthesis of new NFAs core.

2.4→ EXPERIMENTAL PART

1.General experimental

All commercially available reagents and solvents were purchased from Sigma-Aldrich, Fluorochem, Alfa Aesar. Flash chromatography was carried out using Merck silica gel 60 (pore size 60 Å, 270-400 Mesh). ^{1}H and ^{13}C NMR spectra were recorded from solutions in deuterated solvents on 300 Bruker or 400 Jeol spectrometers with the residual solvent as the internal standard. d. Mass spectra of pure compounds were recorded using an Electron Spray Ionization Agilent Technologies mass spectrometer, Direct Exposure Probe mass spectrometer, GC-MS ThermoScientific spectrometer.

2. Synthesis of New Compounds

Synthesis of diethyl 2,5-bis(5-(1,3-dioxolan-2-yl)thiophen-2-yl)terephthalate (1a).

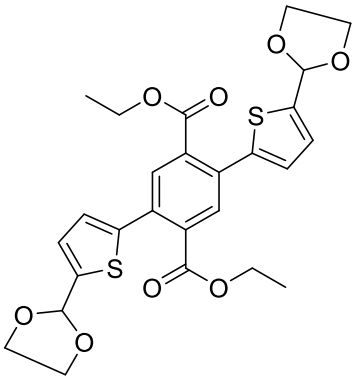

In a dry Schlenk, under Ar, were added added diethyl 2,5-dibromoterephthalate (1g, 2.63 mmol) and (5-(1,3-dioxolan-2-yl)thiophen-2-yl)zinc(II) chloride (11.5 mL, 5.8 mmol) and $Pd(PPh_3)_4$ (122 mg, 0.105 mmol) in previously degassed dry THF (20 mL, 0.15 M). The resulting black solution was refluxed under stirring for 16 h. After 16 h the reaction was stopped, and the resulting solution was extracted three times with DCM/$NaHCO_3$ solution The combined organic phases, was dried over Na_2SO_4 then, solvent solvent was removed under reduced pressure.to give a black solid. The resulting dark solid was purified by flash chromatography [Basic SiO_2, 7:3 v/v (Hex/EtOAc)] to give a yellow solid compound (quantitative yield).

^{1}H NMR (300 MHz, $CDCl_3$): δ= 7.84 (s, 2H), 7.13-7.11 (d, 2H, J = 3.62 Hz), 6.98-6.96 (d, 2H, J = 3.53 Hz), 6.31 (s, 2H), 4.25-3.97 (m, 12H), 1.21-1.14 (t, 6H, J = 14Hz), 13C NMR (101 MHz, CDCl3): δ= 167.31, 142.91,141.23, 133.81, 133.26, 131.82, 126.33, 126.22, 107.5, 65.15, 61.17, 13.68. ESI-MS: 553 [M+Na^+]

Synthesis of 2,2'-((2,5-dibromo-1,4-phenylene)bis(thiophene-5,2-diyl))bis(1,3-dioxolane) (1b)

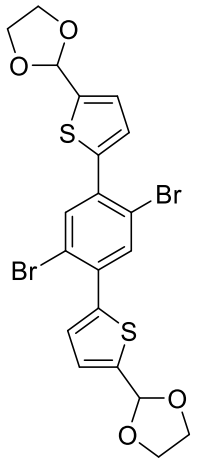

In a dry schlenk under Ar, were added 1,4-dibromo-2,5-diiodobenzene (100 mg, 0.20 mmol), (5-(1,3-dioxolan-2-yl)thiophen-2-yl)tributylstannane (0.9 mL, 0.45 mmol), and $Pd(PPh_3)_4$ (12 mg, 0.010 mmol) in 2 mL of degassed dry THF. The resulting black solution was stirred for 1 days at 60°C. After 1 day the reaction was stopped and the resulting reaction mixture was extracted with DCM/ $NaHCO_3$ solution three times. The combined organic phases were dried over Na_2SO_4 then, solvent was removed under reduced pressure.to give a black solid. The desired compound was purified by flash chromatography [Basic SiO_2, eluents 9:1 to 8:2 (Hexane/EtOAc)] to give a light-yellow solid (73% yield). ^{1}H NMR (400 MHz, $CDCl_3$): δ= 7.77(s, 1H), 7.25-7.24 (d, 1H, J = 4Hz), 7.17-7.16 (d, 1H, J = 4Hz), 6.13 (s, 1H), 4.21-4.00 (m, 4H). 13C NMR (101 MHz, CDCl3): δ= 143.33, 140.54, 136.01, 135.74, 128.11, 126.25, 121.16, 100.21, 65.35, 65.28. ESI-MS: 1111 [2M+Na]

Synthesis of 4,4,9,9-tetrakis(4-methoxyphenyl)-4,9-dihydro-s-indaceno[1,2-b:5,6-b']dithiophene-2,7-dicarbaldehyde (3a).

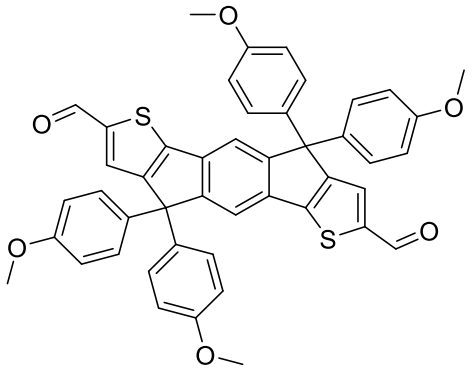

In a dry Schlenk under Ar was added **1** (246 mg, 0.46 mmol) in dry THF solution (3 mL, 0.15 M), the resulting light-yellow solution was cooled to 0°C, then was added dropwise under stirring (4-methoxyphenyl) magnesium bromide (4.10 mL, 2.05 mmol). Immediately the solution changed its colour from light yellow to red. The resulting red solution was allowed to reach r.t under stirring for 16 h. After 16 h the reaction was stopped, and the resulting red solution was quenched with a $NaHCO_3$ solution, then a quick extraction with DCM/H_2O, give an orange solid. The resulting orange solid was dissolved at r.t in AcOH followed by a catalytic amount of H_2SO_4 conc, immediately the resulting solution changed its colour from orange to violet. After 16 hours under stirring at r.t, the resulting violet solution was quenched with an aqueous solution of $NaHCO_3$ and extracted three times with DCM/H_2O. The combined organic phases were dried over Na_2SO_4 then, solvent was removed under reduced pressure to give an orange solid. The resulting orange solid was purified by flash chromatography [7:3 v/v (Hex/EtOAc)] to give a yellow solid compound 2 (95 mg, 28% yield).

^{1}H NMR (300 MHz, $CDCl_3$): δ= 9.87 (s, 2H), 7.63 (s, 2H), 7.58 (s, 2H), 7.18-7.14 (d, 8H, J = 8.8 Hz), 6.84-6.80 (d, 8H, J = 8.8 Hz), 3.78 (s, 12H) ppm. ^{13}C NMR (75 MHz, $CDCl_3$) δ= 182.69, 158.77, 157.14, 155.38, 149.98, 146.44, 135.70, 135.23, 131.57, 128.71, 118.83, 113.92, 62.14, 55.17 ppm.

ESI-MS: 747.33 g/mol [M+1]

Synthesis of 4,4,9,9-tetrakis(4-hydroxyphenyl)-4,9-dihydro-s-indaceno[1,2-b:5,6-b']dithiophene-2,7-dicarbaldehyde (4a).

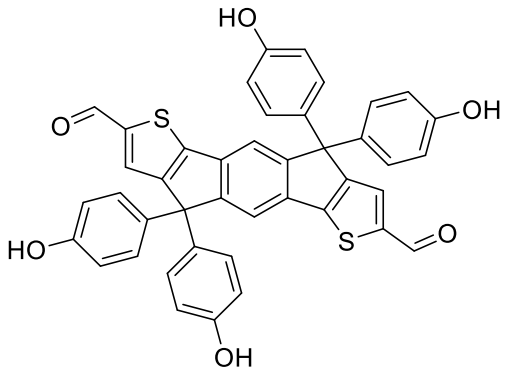

In a dry Schlenk under Ar, was added 2 (95 mg, 0.127 mmol) in dry DCM (1.2 mL, 0.1 M), the resulting light-yellow solution was cooled to 0°C, then was added dropwise under stirring BBr_3 (0.980 mmol, 170 µL). Immediately the solution changed its colour from light yellow to dark red. The resulting dark red solution was allowed to reach r.t under stirring for 2 h. After 2 h the reaction was stopped, and the resulting dark blue solution was extracted three times with EtOAc/H_2O.The combined organic phases, was dried over Na_2SO_4 then, the solvent was removed under reduced pressure.to give a dark red solid. The resulting dark red solid was purified by precipitation in Hexane from THF, to give a red solid compound 3 (44 mg, 50% yield).

^{1}H NMR (300 MHz, Acetone-d_6): δ= 9.91 (s, 2H), 8.35 (s, 4H), 7.96 (s, 2H), 7.90 (s, 2H), 7.15-7.11 (d, 8H, J = 8.5 Hz), 6.77-6.73 (d, 8H, J = 8.6 Hz). ^{13}C NMR (75 MHz, Acetone-d_6): δ= 184.41, 157.91, 148.18, 135.78, 133.48, 130.17, 119.79, 118.69, 116.55, 55.32 ppm.

Chapter 3

Anthradithiophene-based organic semiconductors through regiodirected double annulations

This chapter is partly based on the following publication: *Anthradithiophene-based organic semiconductors through regiodirected double annulations,'* A. Nitti, G. Forti, G. Bianchi, C. Botta, F. Tinti, M. Gazzano, N. Camaioni, R. Po, D. Pasini,* *J. Mater. Chem. C* **2021**, *9*, 9302−9308.

3.1→ INTRODUCTION

Organic molecules comprising extended, π-conjugated, fused aromatic rings have been the subject of a longstanding interest, as intriguing organic materials with rich optoelectronic properties and with potential applications as organic semiconductors.[117][118] Particular attention has been paid to systems composed of laterally fused benzene rings, called acenes. Pentacene, the major representative of this group, shows high hole mobilities at room temperature, but it has several shortcomings, such as poor solubility, limited stability and unfavorable packing in the solid state. All higher acenes can in fact be unstable and reactive, and often heteroatoms are introduced within the π-extended system to overcome this problem.[119] Thienoacenes, comprising fused thiophene rings in the typical ladder-type molecular

[117] M. Bendikov, F. Wudl and D. F. Perepichka, «Tetrathiafulvalenes, Oli-goacenenes, and Their Buckminsterfullerene Derivatives: The Brick and Mortar of Organic Electronics» *Chem. Rev.* **2004***, 104,* 4891−4946.

[118] J. Wu, W. Pisula and K. Müllen, «Graphenes as Potential Material for Electronics» *Chem. Rev.* **2007***, 107,* 718−747.

[119] J. E. Anthony, «Functionalized Acenes and Heteroacenes for Organic Electronics» *Chem. Rev.* **2006***, 106,* 5028−5048.

structure of acenes, are one of the most promising class of semiconducting heteroacenes.[120][121] The presence of multiple intermolecular interactions (including S···S, S···C and C/H···π interactions) gives them high charge transfer mobility and superior morphological and optoelectronic properties.[122][123] Their use, as a single component or combined with other units, in oligomeric and polymeric molecular architectures, for the fabrication of organic electronic solid-state devices such as organic field-effect transistors (OFETs),[124][125] organic light-emitting diodes (OLEDs),[126] and organic photovoltaic cells (OPVs),[127][128] has been demonstrated. Among various thienoacenes, anthradithiophene derivatives

[120] J. Poater, R. Visser, M. Sola and F. M. Bickelhaupt, «Polycyclic Ben-zenoids: Why Kinked is More Stable than Straight» *J. Org. Chem.* **2007***, 72,* 1134–1142.

[121] V. Coropceanu, O. Kwon, B. Wex, B. R. Kaafarani, N. E. Gruhn, J. C. Durivage, D. C. Neckers and B. J.-L., «Vibronic Coupling in Organic Semiconductors: The Case of Fused Polycyclic Benzene–Thiophene Structures» *Chem. Eur. J.* **2006***, 12,* 2073–2080.

[122] V. Coropceanu, J. Cornil, D. A. O. Y. da Silva Filho, R. Silbey and J.-L. Brédas, «Charge transport in organic semiconductors» *Chem. Rev.* **2007***, 107,* 926−952.

[123] K. Takimiya, S. Shinamura, I. Osaka and E. Miyazaki, «Thienoacene-Based Organic Semiconductors» *Adv. Mater.* **2011***, 23,* 4347–4370.

[124] T. Ishida, Y. Sawanaka, R. Toyama, Z. Ji, H. Mori and Y. Nishihara, «Synthesis of Dinaphtho[2,3-d:2’,3’-d’]anthra[1,2-b:5,6-b’]dithiophene (DNADT) Derivatives: Effect of Alkyl Chains on Transistor Properties» *Int. J. Mol. Sci.* **2020***, 21,* 2447.

[125] K. Hyodo, S. Nishinaga, Y. Sawanaka, T. Ishida, H. Mori and Y. Nishihara, «Synthesis and Physicochemical Properties of Dibenzo[2,3-d:2′,3′-d′]anthra[1,2-b:5,6-b′]dithiophene (DBADT) and Its De-rivatives: Effect of Substituents on Their Molecular Orientation and Transistor Properties» *J. Org. Chem.* **2019***, 84,* 698−709.

[126] Q. Ye, Z. Zhang, Z. M. Png, W. T. Neo, T. Lin, H. Zeng, H. Xu and J. Xu, «Cyclization of Tetraaryl-Substituted Benzoquinones and Hydro-quinones through the Scholl Reaction» *J. Org. Chem.* **2016***, 81,* 9219−9226.

[127] C. Li, N. Zheng, H. Chen, J. Huang, Z. Mao, L. Zheng, C. Weng, S. Tana and G. Yu, «Synthesis, characterization, and field-effect transistor properties of tetrathienoanthracenebased copolymers using a two-dimensional π-conjugation extension strategy: a potential build-ing block for high-mobility polymer semiconductors» *Polym. Chem.* **2015***, 6,* 5393–5404.

[128] J.-S. Wu, C.-T. Lin, C.-L. Wang and Y.-J. H. C.-S. Cheng, «New Angu-lar-Shaped and Isomerically Pure Anthradithiophene with Lat-eral Aliphatic Side Chains for Conjugated Polymers: Synthesis, Characterization, and Implications for Solution-Prossessed» *Organic Field-Effect Transistors and Photovoltaics. Chem. Mater.* **2012***, 24,* 2391−2399.

(Figure 3.1), isoelectronic analogues of pentacene, have been previously used for the fabrication of OFET devices.[129][130][131]

[132][133][134] The reactive thiophene α-positions at both ends of the molecular framework make ADT-based compounds suitable and versatile for their incorporation into oligomers and polymer backbones. In addition to linear-fused ADT systems (lADT), angularly fused ADT (aADT) have been reported. The synthesis of lADT has been achieved in not less than 5 synthetic steps, yielding both the *syn* or the *anti* regioisomer (the sulfur atom of the thiophene moieties pointing to the same or to opposite directions).[135][136] Several synthetic methodologies have been reported in the literature for the synthesis of aADT, and their retrosynthetic disconnections are reported in Figure 3.1$_a$. The aADT scaffold could be obtained by Bronsted or Lewis acid-mediated Friedel-Crafts cyclization on alkynes or epoxides

[129] J. G. Laquindanum, H. E. Katz and A. J. Lovinger, «Synthesis, Morphology, and Field-Effect Mobility of Anthradithiophenes» *J. Am. Chem. Soc.* **1998***, 120,* 664–672.

[130] M. M. Payne, S. R. Parkin, J. E. Anthony, C.-C. Kuo and T. N. Jackson, «Organic Field-Effect Transistors from Solution-Deposited Func-tionalized Acenes with Mobilities as High as 1 cm2/V·s» *J. Am. Chem. Soc.* **2005***, 127,* 4986–4987.

[131] K. C. Dickey, J. E. Anthony and Y. L. Loo, «Improving Organic Thin-Film Transistor Performance through Solvent-Vapor Annealing of Solu-tion-Processable Triethylsilylethynyl Anthradithiophene» *Adv. Mater.* **2006***, 18,* 1721.

[132] N. Sooji, J. Jaeyoung, J. E. Anthony, J.-J. Park, C. E. Park and K. Kim, «High-Performance Triethylsilylethynyl Anthradithiophene Tran-sistors Prepared without Solvent Vapor Annealing: The Effects of Self-Assembly during Dip-Coating» *ACS Appl. Mater. & Interf.* **2013***, 5,* 2146–2154.

[133] B. R. Conrad, C. K. Chan, M. A. Loth, S. R. Parkin, X. Zhang, D. M. DeLongchamp, J. E. Anthony and D. J. Gundlach, «Characteriza-tion of a soluble anthradithiophene derivative» *App. Phys. Lett.* **2010***, 97,* 133306.

[134] K. C. Dickey, S. Subramanian, J. E. Anthony, L. H. Han, S. Chen and Y. L. Loo, «Large-area patterning of a solution-processable organic semiconductor to reduce parasitic leakage and off currents in thin-film transistors» *Appl. Phys. Lett.* **2007***, 90,* 24410.

[135] M. Mamada, T. Minamiki, H. Katagiri and S. Tokito, «Synthesis, Physical Properties, and Field-Effect Mobility of Isomerically Pure syn-/anti-Anthradithiophene Derivatives» *Org. Lett.* **2012***, 14,* 4062–4065.

[136] B. Tylleman, C. M. L. Vande Velde, J.-Y. Balandier, S. Stas, S. Sergeyev and Y. H. Geerts, «Synthesis of Isomerically Pure anti-Anthradithiophene Derivatives» *Org. Lett.* **2011***, 13,* 5208–5211.

intermediates,[137][138][139][140] [2+2+2] base catalyzed annulation with alkynes bearing aliphatic side chains,[141] Scholl cyclization with Lewis acids on tetrasubstituted benzene with aryl moieties,[132][142][143][144][145] as well as oxidative photocyclization (disconnection strategy 1).[146][147] Pd-activated [148][149] or light-driven [150] C-H

[137] K. Hyodo, S. Nishinaga, Y. Sawanaka, T. Ishida, H. Mori and Y. Nishihara, «Synthesis and Physicochemical Properties of Dibenzo[2,3-d:2′,3′-d′]anthra[1,2-b:5,6-b′]dithiophene (DBADT) and Its Derivatives: Effect of Substituents on Their Molecular Orientation and Transis-tor Properties» *J. Org. Chem.* **2019***, 84,* 698–709.

[138] S. Nishinaga, Y. Sawanaka, R. Toyama, T. Ishida, H. Mori and Y. Nishi-hara, «Synthesis and Transistor Characteristics of Dinaph-tho[2,3-d:2′,3′-d′]anthra[1,2-b:5,6-b′]dithiophene (DNADT)» *Chem. Lett.* **2018***, 47,* 1409–1411.

[139] W.-L. Liau, T.-H. Lee, J.-T. Chen and C.-S. Hsu, «The synthesis of anthradithiophene-based liquid crystals and their applications in organic thin film transistors» *J. Mater. Chem. C* **2016***, 4,* 2284–2288.

[140] M. B. Goldfinger, K. B. Crawford and T. M. Swager, «Directed Electrophilic Cyclizations: Efficient Methodology for the Synthesis of Fused Polycyclic Aromatics» *J. Am. Chem. Soc.* **1997***, 119,* 4578–4593.

[141] H. Hanamura, M. Watanabe, M. Tanabiki, H. Saito, H. Sugita and K. Mikami, « Synthesis of dithieno[2,3-d:2′,3′-d']anthra[1,2-b:5,6-b']dithiophene (DTADT) units: Structure, polymerization, DFT study, and OFET application» *Polymer* **2020***, 206,* 122888.

[142] Y. Li, A. Concellón, C.-J. Lin, N. A. Romero, S. Lin and S. T. M., «Thiophene-fused polyaromatics: synthesis, columnar liquid crystal, fluorescence and electrochemical properties» *Chem. Sci.* **2020***, 11,* 4695–4701.

[143] T. Hirano, H. Hanamura, M. Inoue, S. Ueda, M. Watanabe, M. Tana-biki and K. Mikami, «Synthesis of soluble, air-stable fully conjugated ladder polymers» *Polymer* **2019**, *177*, 282–289.

[144] H. Komiyama, C. Adahi and T. Yasuda, «Tetrathienoanthracene-based π-Extended Narrow-band-gap Molecules: Synthesis, Physico-chemical, and Photovoltaic Properties» *Chem. Lett.* **2017***, 46,* 29–31.

[145] F. He, W. Wang, W. Chen, T. Xu, S. B. Darling, J. Strzalka, Y. Liu and L. Yu, «Tetrathienoanthracene-Based Copolymers for Efficient So-lar Cells» *J. Am. Chem. Soc.* **2011***, 133,* 3284–3287.

[146] A. Pietrangelo, B. O. Patrick, M. J. MacLachlan and M. O. Wolf, «Conjugated Thiophene-Containing Oligoacenes Through Photocycliza-tion: Bent Acenedithiophenes and a Thiahelicene» *J. Org. Chem.* **2009***, 74,* 4918–4926.

[147] A. Pietrangelo, M. J. MacLachlan, M. O. Wolf and B. O. Patrick, «Synthesis and Structures of Novel Luminescent Bent Acenedithiophenes» *Org. Lett.* **2007***, 9,* 3571–3573.

[148] E. Sankar, P. Raju, J. Karunakaran and A. K. Mohanakrishnan, «Syn-thetic Utility of Arylmethylsulfones: Annulative π-Extension of Aromatics and Heteroaromatics Involving Pd(0)-Catalyzed Heck Coupling Reactions» *J. Org. Chem.* **2017***, 82,* 13583−13593.

[149] J. Huang, Z. Chen, J. Yang, H. Ju, W. Zhang and G. Yu, «Semiconducting Properties and Geometry-Directed Self-Assembly of Heptacyclic Anthradithiophene Diimide-Based Polymers» *Chem. Mater.* **2019***, 31,* 2507–2515.

[150] P. Sarkar, B. K. Das, D. Chakraborty and K. Muthamma, «Carboheli-cenes and thiahelicene from phthalaldehydes through Perkin approach» *J. Mol. Struct.* **2019***, 1195,* 309–314.

activation (disconnection 2), or Suzuki annulation [151] and thienannulation reactions, [152153] respectively (disconnection approaches 3 and 4). All such approaches require several steps, they are not really scalable and sustainable at the industrial level, confining ADT-based compounds to the realm of academic studies.

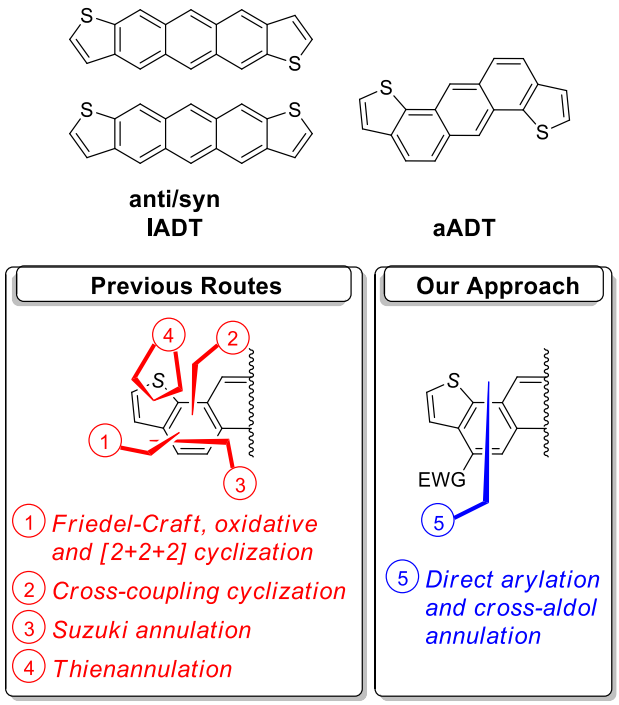

Figure 3.1. Top: the structures of linear and angular ADTs. Bottom: the comparison of the previously reported synthetic methodologies for the synthesis of aADT scaffolds and the synthetic approach adopted in this work.

[151] L.) Biniek, B. C. Schroeder, J. E. Donaghey, N. Yaacobi-Gross, R. S. Ashraf, Y. W. Soon, C. B. Nielsen, J. R. Durrant, T. D. Anthopoulos and I. McCulloch, «New Fused Bis-Thienobenzothienothiophene Copolymers and Their Use in Organic Solar Cells and Transistors» *Macromolecules* **2013**, *46,* 727−735.

[152] C. Zeng, C. Xiao, X. Feng, L. Zhang, W. Jiang and Z. Wang, «Electron-Transporting Bis(heterotetracenes) with Tunable Helical Packing» *Angew. Chem. Int. Ed.* **2018**, *57,* 10933–10937.

[153] J. Wu, D. He, Y. Wang, F. Su, Z. Guo, J. Lin and H.-J. Zhang, «Selective Ortho-π-Extension of Perylene Diimides for Rylene Dyes» *Org. Lett.* **2018**, *20,* 6117−6120.

Our group have recently demonstrated the broad applicability of an annulation[154][155][156] protocol combining, in a one-pot procedure, direct arylation and cross aldol condensations. The regiospecific direct arylation drives the subsequent cross-aldol condensation, which proceeds under the same basic conditions, and the overall protocol has been applied to the synthesis of extended aromatics wherein the thiophene ring is annulated with furans, pyridines, indoles, benzothiophenes and benzofurans.[22][157][158]

[159][160][161] In our previous contributions, the DHA-cross aldol protocol was confined to one annulation reaction.

3.2.→ RESULTS AND DISCUSSION

In this chapter, we report on the efficient double annulation for the synthesis of aADT derivatives (disconnection approach 5 in Figure 3.1), and its derivatives. The synthetic protocol is high yielding and regiospecific and allows the regiodirected synthesis of the aADT scaffold. We elaborate such scaffold by means of functionalization of the α-position of the terminal thiophene residues; we incorporate aADT as the core or as endcapping unit in π-extended oligomers of up to 11 aromatic rings in sequence and

---

[154] J. Yu, H. Yan and C. Zhu, «Synthesis of Multiply Substituted Polycyclic Aromatic Hydrocarbons by Iridium-Catalyzed Annulation of Ring-Fused Benzocyclobutenol with Alkyne through C−C Bond Cleavage» *Angew. Chem. Int. Ed.* **2016**, *55,*1143–1146.

[155] Y. Koga, T. Kaneda, Y. Saito, K. Murakami and K. Itami, «Synthesis of partially and fully fused polyaromatics by annulative chlorophenylene dimerization» *Science,* **2018**, *359,* 435–439.

[156] B. VanVeller, D. Robinson and T. M. Swager, «Triptycene Diols: A Strategy for Planar π-Systems Demonstrated by the Catalytic Conversion of a PPE into a PPV» *Angew Chem Int Ed* **2012**, *51,* 1182–1186.

[157] P. Osw, A. Nitti, S. I. Etkind, M. N. Abdullah, J. Mwaura, A. Galbiati and D. Pasini, «Synthesis and Evaluation of Scalable D-A-D π-Extended Oligomers as p-Type Organic Materials for Bulk-Heterojunction Solar Cells,» *Polymers,* **2020**, *12,* 720.

[158] A.) Nitti, P. Osw, M. N. Abdullah, A. Galbiati and D. Pasini, «Scalable Synthesis of Naphthothiophene-based D-π-D Extended Oligomers through Cascade Direct Arylation Processes» *Synlett,* **2018**, *29,* 2577–2581.

[159] A. Nitti, F. Debattista, L. Abbondanza, G. Bianchi, R. Po and D. Pasini, «Donor–acceptor conjugated copolymers incorporating tetra-fluorobenzene as the π-electron deficient unit» *J. Polym. Sci. Pol. Chem.* **2017**, *55,* 1601-1610.

[160] WO2019/175367A1

[161] A. Nitti, G. Bianchi, R. Po and D. Pasini, «Scalable Synthesis of Naph-thothiophene and Benzodithiophene Scaffolds as π-Conjugated Synthons for Organic Materials» *Synthesis* **2019**, *51,* 677–682.

demonstrate their potential as organic semiconductors.[162][163][164][165] Moreover, we report on the use of ADT as the core for the synthesis of novel non fullerene acceptors to be used in bulk heterojunction solar cells (BHJs). Due to patentability reasons of the presented results, the chemical stracutre of the synthetized acceptors have been partially masked.

3.2.1. Synthesis of aADT and oligomeric derivatives. The annulation protocol takes advantage of our previously published optimized experimental conditions, in which a 3-thiopheneacetic acid residue is reacted with (hetero)aryl *ortho*-bromoaldehydes to yield a variety of annulated structures (Scheme 3.1 top). The key for the high yielding of the process is the use the thiophene substrate as the free carboxylic acid derivative, so that the direct-arylation step occurs before the intramolecular cross-aldol condensation, aided from a chelating effect of the substrate on the transition metal catalyst, and effectively generating a new, condensed aromatic ring within the π-system. A double annulation procedure could afford, in a rapid, sustainable and scalable manner, thiophene-endcapped symmetrical π-systems amenable to further incorporation into oligomeric or polymeric structures.

---

[162] A. Punzi, A. Operamolla, O. H. Omar, F. Brunetti, A. D. Scaccabarozzi, G. M. Farinola and N. Stingelin, «Designing Small Molecules as Ternary Energy-Cascade Additives for Polymer:Fullerene Solar Cell Blends» *Chem. Mater.* **2018***, 30,* 2213.

[163] H. Hu, K. Jiang, G. Yang, J. Liu, Z. Li, H. Lin, Y. Liu, J. Zhao, J. Zhang, F. Huang, Y. Qu, W. Ma and H. Yan, «Terthiophene-Based D–A Polymer with an Asymmetric Arrangement of Alkyl Chains That Enables Efficient Polymer Solar Cells» *J. Am. Chem. Soc.* **2015***, 137,* 14149–14157.

[164] W. Zhu, Y. Wu, S. Wang, W. Li, X. Li, J. Chen, Z.-S. Wang and H. Tian, «Organic D-A-π-A Solar Cell Sensitizers with Improved Stability and Spectral Response» *Adv. Funct. Mater.* **2011***, 21,* 756–763.

[165] L. Chen, B. Zhang, Y. Cheng, Z. Xie, L. Wang, X. Jing and F. Wang, «Pure and Saturated Red Electroluminescent Polyfluorenes with Dopant/Host System and PLED Effi ciency/Color Purity Trade-Offs» *Adv. Funct. Mater.* **2010***, 20,* 3143–3153.

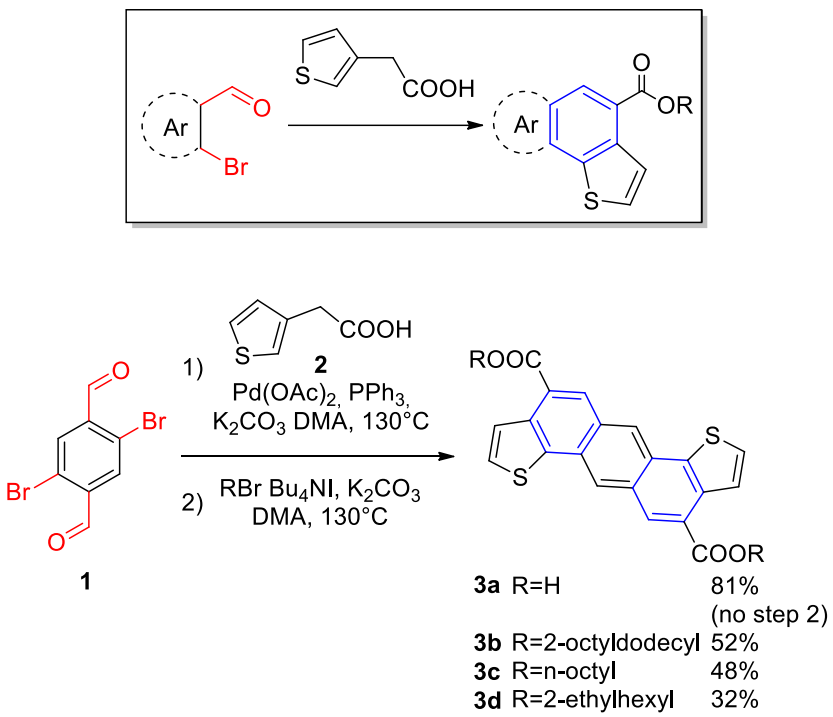

E factor for **3a** = ***2.3*** E factor for **3b** = ***16.9***

Scheme 3.1. Top: general approach to regiodirected annulations. Bottom: synthesis of angularly fused ADT **3**.

One of the possible simplest substrates, namely 2,5-dibromotherephthaladehyde **1,** was reacted with 2 equivalents of 3-thiopheneacetic acid **2**, affording the doubly annulated aADT compounds as the free carboxylic acid derivative (**3a**) or, after a subsequent alkylation protocol, as the ester derivatives **3b-3d** (Scheme 3.1). The Pd^{2+} catalyst was used in combination with an excess of potassium carbonate as the base, needed for the direct arylation step but also catalyzing the cross-aldol condensation, in dimethylacetamide (DMA) at 130°C. The dicarboxylic anthradithiophene **3a** was isolated in 81% yield after precipitation from HCl aqueous solution and Soxhlet purification and extraction in acetone. Interestingly, the ^1H NMR in D_2O of the crude reaction mixture (Figure 3.S1 in the Supporting Information) demonstrates the highly efficient double annulation protocol, as there is essentially no evidence of monofunctionalization or other byproducts after removal of the reaction solvent. Better results were obtained by isolating the carboxylic acid derivative **3a** and then conducting the alkylation in presence of K_2CO_3 and Bu_4NI (conditions reported in Scheme 3.1). Compound **3b** was obtained by alkylation step in 52% yield after a simple filtration on a silica gel pad and further purification by

precipitation in ^{i}PrOH. Ester derivatives **3c-d** were obtained in similar yields following this procedure. Extensive optimization of the esterification was conducted, as summarized in Table 3.S1. The reaction could be conducted one-pot, without isolating the free carboxylic acid intermediate, but in this case product **3b** was isolated in lower yields (37%). The use of the acid chloride (generated using $SOCl_2$ from **3a** in refluxing toluene) and 2-octyldodecyl alcohol with base scavengers/activators afforded aADT derivative **3b** in lower yields and a more difficult and lengthy purification procedure by column chromatography. The use of an ester derivative, 2-octyldodecyl thiopheneacetate, instead of thiopheneacetic acid afforded a poorly regiodirected mixture of compounds, including product **3b** in low yields (8%). This last experiment confirms our previously reported observation regarding the decisive role of the free carboxylate functionality on the thiophene residue in regiodirecting and facilitating the DHA step vs. the cross-aldol final annulative step. Compounds **3a-d** were fully characterized (see SI). The protocol shows a very low synthetic complexity and it requires only two steps starting from relatively inexpensive reagents. Our synthesis of aADT **3b** could be easily scaled up to 25 g batches in our laboratiories. Impressive E factors of 2.3 and 16.9 could be calculated for the synthesis of **3a** and **3b** (see Scheme 3.1 and Table 3.S2). The dicarboxylic acid **3a** is insoluble in common organic solvents, except for DMSO, it is poorly soluble in DMF but it is soluble in water as the carboxylate salt. Compound **3b**, on the contrary, is soluble in typical organic solvents except for acetone and alcoholic solvents. Compound **3b** was used for the synthesis of oligomers incorporating a 5,6-difluorobenzo[*c*][1,2,5]thiadiazole (BT) core and 2-octyldodecyl naphtho[1,2-b]thiophene-4-carboxylate (NT) residues. The choice of the cores responds to the call for synthetic simplicity, scalability and sustainability of the building blocks to be used for the development of new semiconducting organic materials. NT derivatives, due to their high planarity and conjugation, are suitable end-capping units for the rapid construction of oligomers incorporating ADT unit as the central core. On the other end, the BT scaffold has considerable utility as the electron-withdrawing comonomer in n-type conjugated polymers and oligomers for OPVs[160 170 171] and OLEDs.[172166167] Towards this end, initial attempts were conducted in order to functionalize the two α-thiophene terminal positions by bromination (Scheme 3.2).

[166] S. Yao, B. Kim, X. Yue, M. Colon Gomez, M. Bondar and K. Belfield, «Synthesis of Near-Infrared Fluorescent Two-Photon-Absorbing Fluorenyl Benzothiadiazole and Benzoselenadiazole Derivatives» *ACS Omega* **2016***, 1,* 1149–1156.

[167] S. Ellinger, K. Graham, P. Shi, R. Farley, T. Steckler, R. Brookins, P. Taranekar, J. Mei, L. Padilha and T. Ensley, «Donor–Acceptor–Donor-based-Conjugated Oligomers for Nonlinear Optics and Near-IR Emission» *Chem. Mater.* **2011***, 23,* 3805.

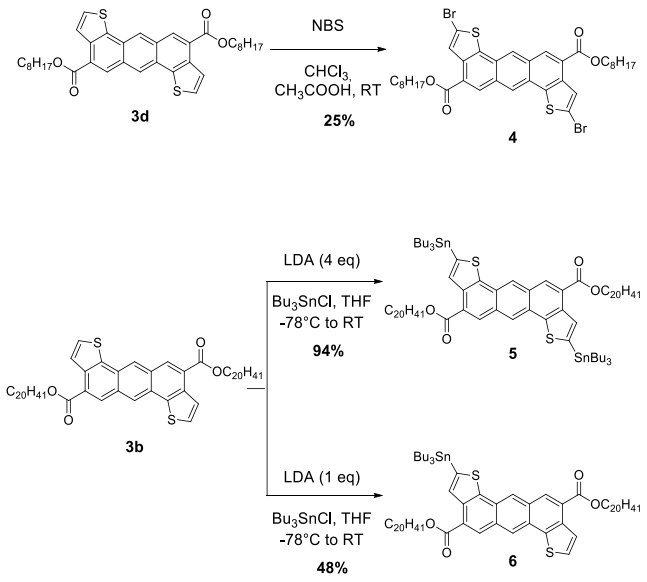

Scheme 3.2. Bromination and stannylation of aADT esters

Both **3a** and **3b** were subjected to typical brominating agents (NBS or Br_2) in several solvent systems (Table 3.S3), but the reactions conducted on either compound did not afford the desired product: in the former case probably as a result of the insolubility of the compound, whereas in the latter we rationalized the failure is related to steric hindrance of the bulky branched C_{20} side chains. In fact, using derivative **3d**, bearing 2-ethylhexyl branched C_8 chains, the dibromo derivative was obtained, although in low yields (25%). The difficulties to obtain brominated ADT derivatives in good yields directed us towards stannylation of **3b**, in order to activate Stille cross-coupling procedures for the functionalization of ADT derivatives. Mono- and di-stannylated derivatives **5** and **6**, with two and one tributylstannyl groups, respectively, were obtained in 94% and 48% yields using LDA as lithiating agent (several equivalents for **5** and 1 equivalent for **6**) in THF at -78°C and Bu_3SnCl as the electrophile. The reaction for **5** could be successfully scaled up to the gram scale after extensive optimization, as shown in Table 3.2.

Initially, using classical conditions reported for α-lithiation/stannylation of thiophene (entry **1**) we did not isolate any intermediate **5.** A further increase in concentration (entry **2**) allowed us to isolate the desired product in very low yield. Interestingly, we observed that ADT-COOR tend to precipitate at -78°C, for this reason we tried the reaction at 0°C (entry **3**). Although higher temperatures for lithiation are known to promote side reactions, we recovered in this case the starting material ADT-COOR. We ascribe the low yield to the tendency that ADT possess to precipitate at low temperature, but further increases in both LDA and molarity concentration (entry **4**, **5** and **6**) allowed us to get high yields of the

desired product, probably due to the shifts of the equilibrium between stannylated intermediate **5** and **3b**. Finally, we were able to further improve the yields by adding LDA at -40°C then stirring at -78°C before quenching of the anion with the addition of Bu_3SnCl (entry **7**).

Table 3.1. Optimization of stannylation conditions for ADT-COOR **3b**.

Entry	***Reagent***	***T(°C)***	***ADT Conc.***	***Yield***
1*	LDA (4 eq.)	-78 to r.t	0.010 M	-
2	LDA (4 eq.)	-78 to r.t	0.017 M	10 %
3*	LDA (4 eq.)	0°C (30 min) to r.t	0.017 M	-
4	LDA (4 eq.)	-78 to r.t	0.030 M	4 %
5	LDA (8 eq.)	-78 to r.t	0.030 M	36 %
6	LDA (8 eq.)	-78 to r.t	0.040 M	76 %
7	LDA (4eq.)	-40 to -78 then r.t	0.025 M	94 %

* Starting material was recovered

Stille reaction of **5** and **6** in presence of **7** and **8** gave oligomers **9** and **10** in 71% and 76% yields, respectively, after simple purifications on silica gel (Scheme 3.3). Oligomers **9** and **10** were perfectly soluble in common organic solvents and were fully characterized (see appendix for copies of spectroscopic data). Representative ^1H NMR spectra (Figure 3.3) for compounds **3b** and **9** show the relative simplicity of the patterns, because of the C_{2h} symmetry of the molecular structure. In agreement with our previous observations, the β–hydrogen atoms of the annulated thiophene-fused moieties in **3b**

are more deshielded when compared to α–hydrogen (the opposite occurs in thiophene residues), since they are in direct conjugation with the electron withdrawing ester moieties.[168]

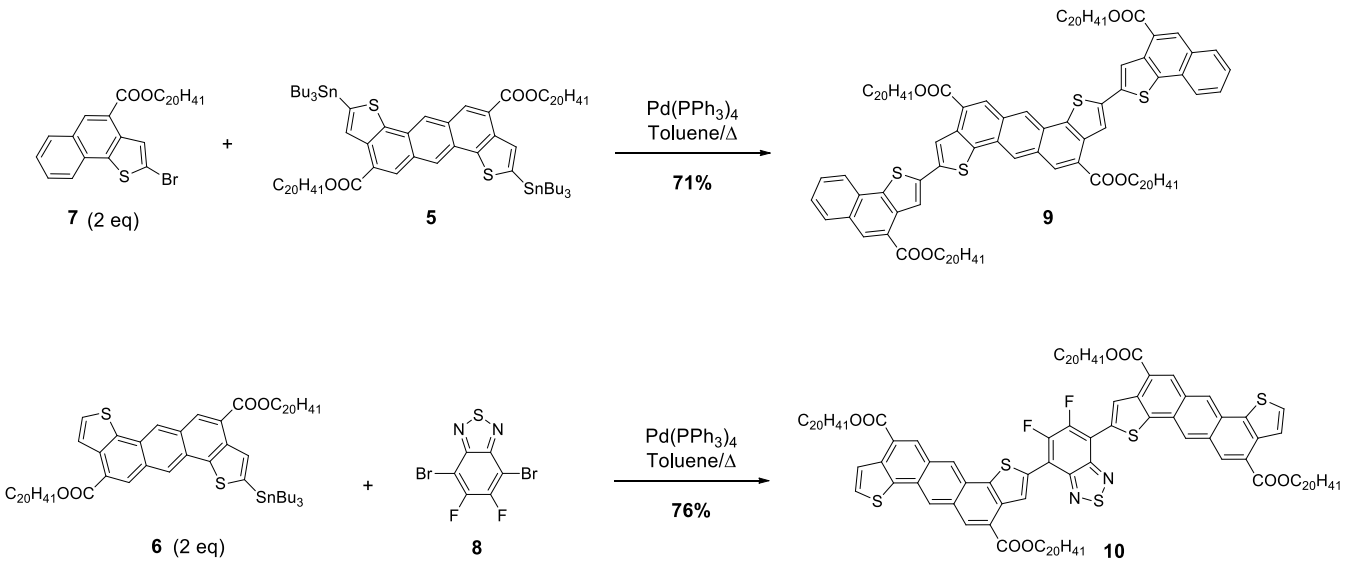

Scheme 3.3. Synthesis of ADT-based oligomers **9** and **10**.

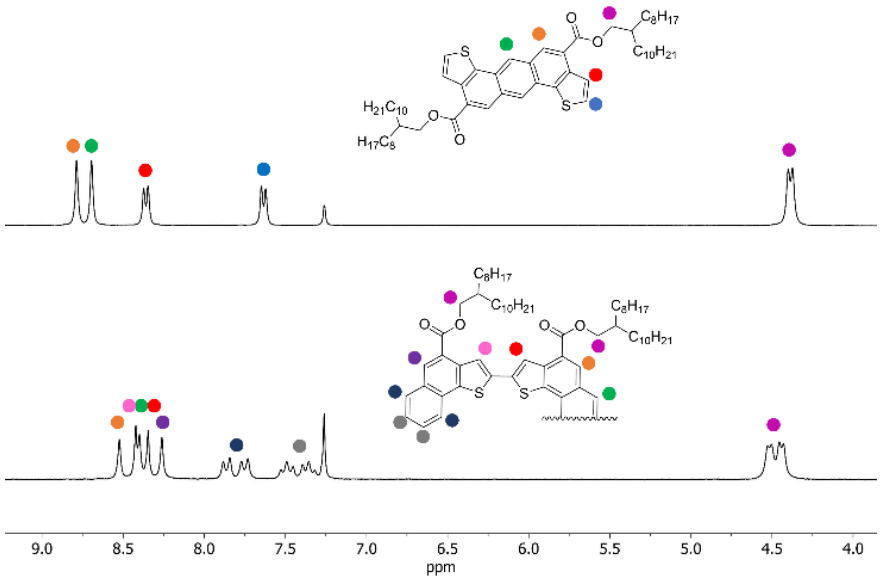

Figure 3.3. Aromatic region of the ^{1}H NMR spectra ($CDCl_3$, 400 MHz) of compounds **3b** (top) and **9** (bottom).

[168] A. Nitti, P. Osw, G. Calcagno, C. Botta, S. I. Etkind, G. Bianchi, R. Po, T. M. Swager and D. Pasini, «One-Pot Regiodirected Annulations for the Rapid Synthesis of π-Extended Oligomers» *Org. Lett.* **2020**, *22,* 3263–3267.

Optical, electrochemical and charge mobility properties. The UV-Vis and PL spectra of **3b**, **9** and **10** in solution or thin films are shown in Figure 3.4, while the CV voltammograms recorded in solutions are reported in the appendix (Figures 3.S2-S4). The relevant photophysical data are summarized in Table 3.1. The maximum absorption of **3b** is observed at λ_{max} = 328 nm with a narrow bandwidth, which is 25 nm redshifted relative to that of the corresponding anthraditiophene derivative lacking the electron withdrawing ester moieties (aADT in Figure 1, λ_{max} = 304 nm). The spectrum of **3b** showed structured, narrow bandwidth peaks in the 350-400 nm region, with low molar absorbivities, typical of fused acenes, and similarly to aADT.[152]

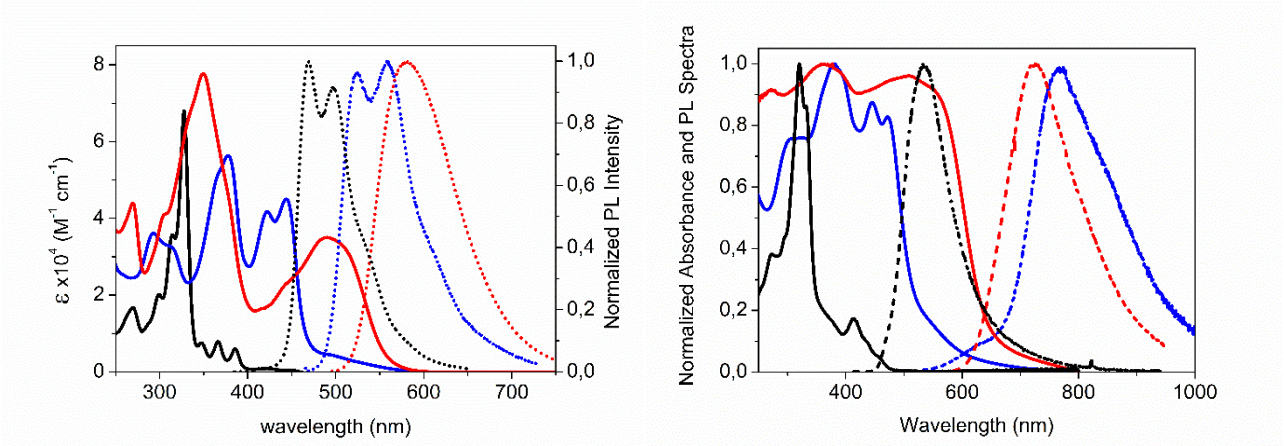

Figure 3.4. UV-Vis (solid) and normalized PL spectra (dot) of compound **3b** (black), **9** (blue) and **10** (red) in CH_2Cl_2 (10^{-5} mol·L^{-1}) (left), and in thin films (right).

Table 3.2. Photophysical properties in solution and thin films of compounds **3b**, **9** and **10**.

Compounds	Solution[1]					Film[2]			
	λ_{abs} (nm)	$\varepsilon\times10^4$ ($M^{-1}cm^{-1}$)	λ_{em} (nm)	QY[3] (%)	τ[4] (ns)	λ_{max} (nm)	E_g^{opt} (nm)	λ_{em} (nm)	QY (%)
aADT[4]	304	1.45	408	36	-	413	-	-	-
3b	328	6.79	468	23	18.3	413	3.20	535	5
9	444	4.49	524	3	1.92	471	2.31	766	<0.1

10	490	3.50	581	23	1.44	511	1.90	723	<0.1

[1] In $CHCl_3$ (10^{-5} M). [2] Obtained by casting of CH_2Cl_2 solutions (ca. 10^{-3} M) of the chromophores. [3]Fluorescence quantum yield. [4] Fluorescence lifetime. [4] Data taken from ref. 30

The absorption spectra of **9** and **10** show broader bands when compared to **3b** (Figure 3.4 top), because of their more flexible structures, induced by the aryl-aryl bonds, around which free rotation, cross-talking and conjugation between the differing chromophores is allowed. The absorption maxima in both compounds **9** and **10** are red shifted with respect to **3b**, and the insertion of the strong electron-withdrawing BT unit in **10** affords a "push-pull" character, with a charge-transfer band centered at 490 nm. Emission spectroscopy for **3b** showed the presence of a bimodal emission peak, with a quantum yield in solution in line with the reported value for aADT (see Table 3.2). Compounds **9** and **10** exhibit broad emission bands, typical of conjugated oligomers with substantial degrees of conformational freedom, centered at 524 and 581 nm, respectively. They are weakly fluorescent in solution with large Stokes shifts (over 80 nm) and with nanosecond lifetimes (Figures 3.S5-S6 in the appendix). Absorption and emission spectra were also recorded in thin films (Figure 3.4 left), and substantially red-shifted profiles with respect to solution for all compounds could be observed. For oligomer **9**, the redshift is much more pronounced than for **10**, resulting in a lower energy emission in the former, presumably due to more favourable packing interactions in the solid state. The compounds are weakly (in the case of **3b**) or nonfluorescent in the solid state. The HOMO and LUMO molecular orbital levels determined by cyclic voltammetry are graphically represented in Figure 3.5. ADT **3b** showed HOMO-LUMO levels substantially lower than available data for structurally related aADT derivatives lacking the electron withdrawing ester residues (DBADT, -5-50 and -2.53 eV for HOMO and LUMO, respectively).[143] Oligomers **9** and **10** exhibit non completely reversible oxidation and reduction waves, with HOMO-LUMO energy level differences at 2.22 eV and 1.96 eV, in close agreement with the optical gaps. Density functional theory (DFT) calculations on ADT monomer **3b**, as well as oligomers **9** and **10** revealed that all molecules exhibit highly planar geometries. In compound **3b**, the electron density coefficients for the HOMO orbital are higher on peripheral thiophene rings, whereas the LUMO is centered on the anthracene core. In compound **9** the HOMO shows delocalized electron density on the ADT central core as well as on thiophene rings of naphthothiophene units, while the LUMO electronic structure is localized on the ADT central core. For compound **10**, as expected for a "push-pull" structure, the HOMO electronic structure is centered on the peripheral ADT units, while the LUMO, is centered on the BT core.

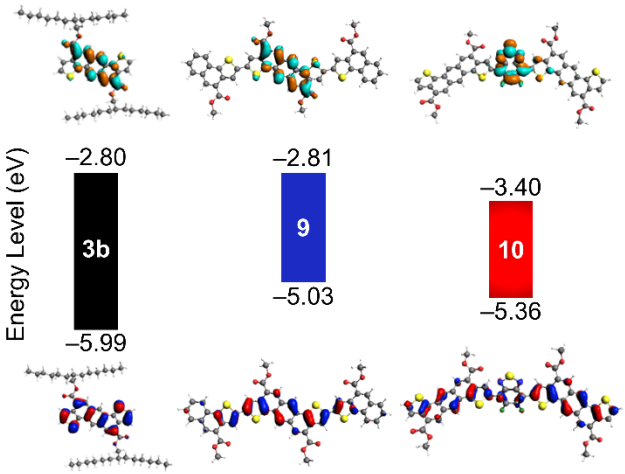

Figure 3.5. HOMO and LUMO levels (obtained by cyclic voltammetry) of compounds **3b** (black), **9** (blue) and **10** (red)and frontier molecular orbitals obtained by DFT calculations.

Most heteroacenes, including known aADT derivatives,[137 143 169] have electronic structures compatible with p-type semiconducting materials, and have been characterized in OFET applications. In order to verify the potential of our novel aADT scaffolds, we prepared hole-only devices for charge-carrier mobility measurements, with the sandwich structure ITO/PEDOT:PSS/organic compound/MoO_3/Au and with a spin-coated organic layer. Reliable results were obtained for oligomer **9**, showing excellent film-forming properties from chloroform-solution deposition and a HOMO energy level well aligned with the work function of gold, acting as the hole-injecting electrode in the device structure. The bulk hole mobility (μ) for oligomer **9** was investigated as a function of the electric field (E) by means of impedance spectroscopy measurements. Under high-injection conditions, the capacitance minima are observed in the frequency range 10^4 – 10^5 Hz, for a thickness of the oligomer film of 600 nm, in agreement with expectations (Figure 3.S7 in the appendix). The hole mobility of spin-coated oligomer **9** exhibits an almost field-independent behavior (Figure 3.7), suggesting a low energetic disorder.[170] The mean value of the data shown in Figure 3.7 is 2.5×10^{-5} $cm^2\cdot V^{-1}\cdot s^{-1}$, a remarkable value for the bulk mobility of a

[169] M.-C. Chen, C. Kim, S.-Y. Chen, Y.-J. Chiang, M.-C. Chung, A. Facchetti and T. J. Marks, «Functionalized anthradithiophenes for organic field-effect transistors» *J. Mater. Chem.* **2008**, *18,* 1029–1036.

[170] S. Martin, A. Kambili and A. T. Walker, «temperature and field dependence of the mobility of highly ordered conjugated polymer films» *Phys. Rev. B.* **2003**, *67,* 165214.

low-molecular weight and spin-coated compound, in line with "workhorse" polymers used in the field.[171] Given the rough independence on electric field, the hole mobility was also confirmed from the current-density *versus* voltage (*J-V*) characteristic of the hole-only device made of oligomer **9**.

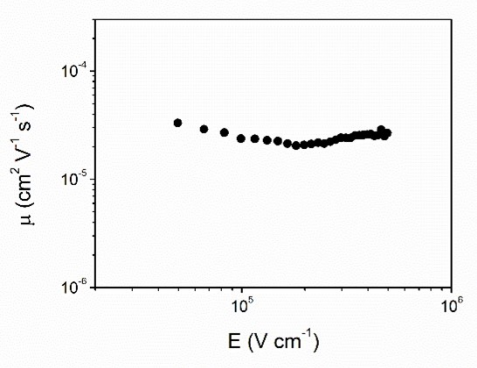

Figure 3.7. Bulk hole mobility as a function of the electric field, obtained from impedance measurements, for a hole-only device made of oligomer **9** (600 nm thick).

3.2.2. Synthesis of novel NFAs based on ADT core

All NFAs to date have some common features such as a) an electron-rich π-core, b) alkyl side chains for solubility and c) electron-deficient end-cap groups (Figure 3.8, top).[173 174 175 176 177] Despite several effort to modify/functionalize these molecules, their synthesis remains challenging and potentially difficult for large scale up. Here we present three new electron rich synthons based on the ADT scaffold (Figure 3.8, bottom) [178], as cores for NFAs.

[171] C. Tanase, E. J. Meijer, B. P. W. M. and D. M. De Leeuw, «Unification of the Hole Transport in Polymeric Field-Effect Transistors and Light-Emitting Diodes» *Phys. Rev. Lett.* **2003***, 91,* 216601.

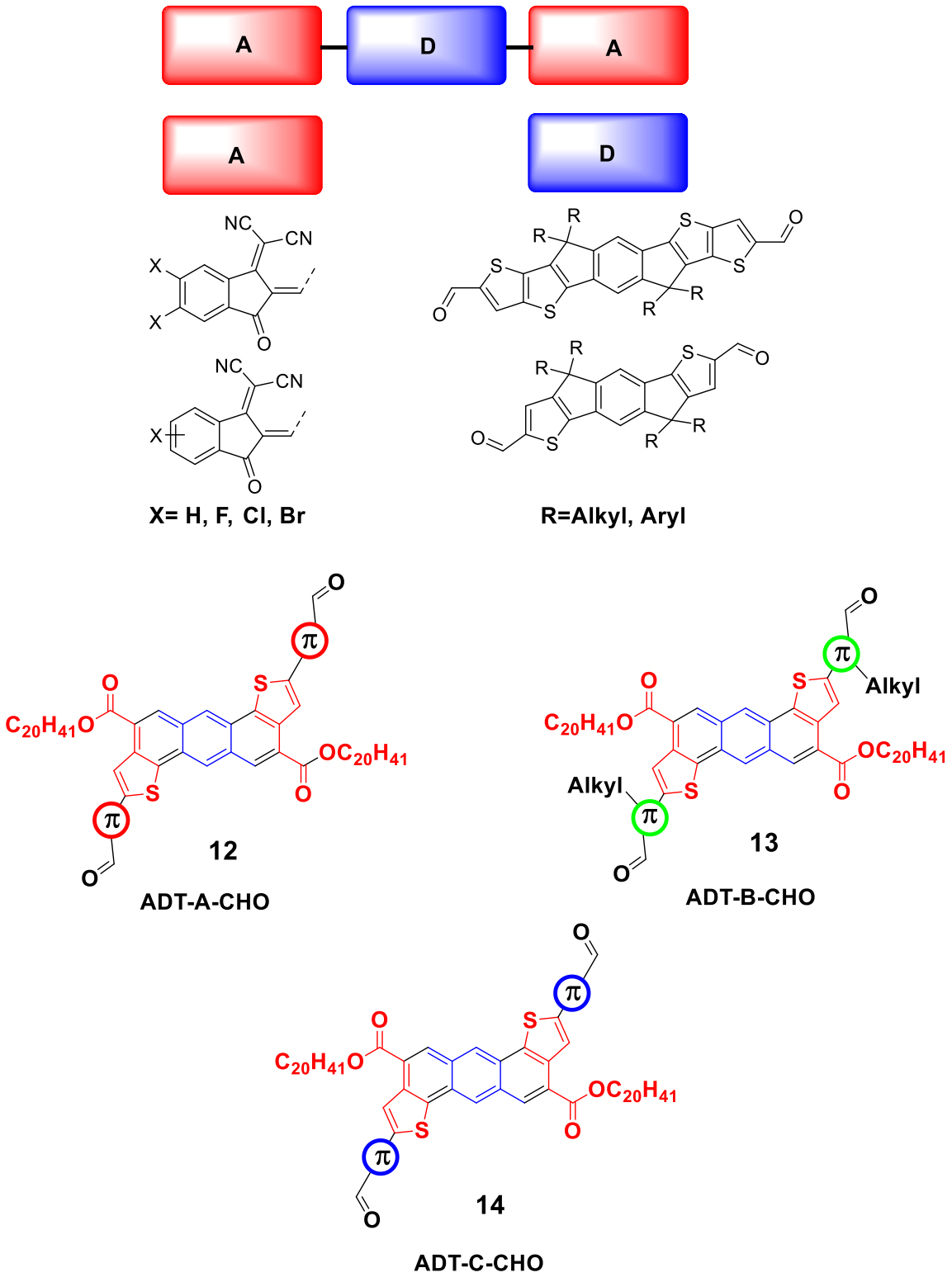

Figure 3.8. Top: general push-pull structure; bottom: general structures of ADT-A-CHO (**12**) , ADT-B-CHO (**13**) and ADT-C-CHO (**14**).

Our ADT scaffold, compared with those already reported, offers several advantages: a) fully conjugated pentacyclic structure, b) long ester side chains, and c) possibility to be synthesized in multigram scale, which makes it suitable for an industrial scale-up. The retro-synthetic pathway for the aldehydes (Scheme 3.4) starts from ADT-COOR (**3b**) which has been stannylated in presence of LDA to generate intermediate **5** followed by Stille cross-coupling with aldehyde **a**, **b** and **c** to afford the molecules **12, 13** and **14**.

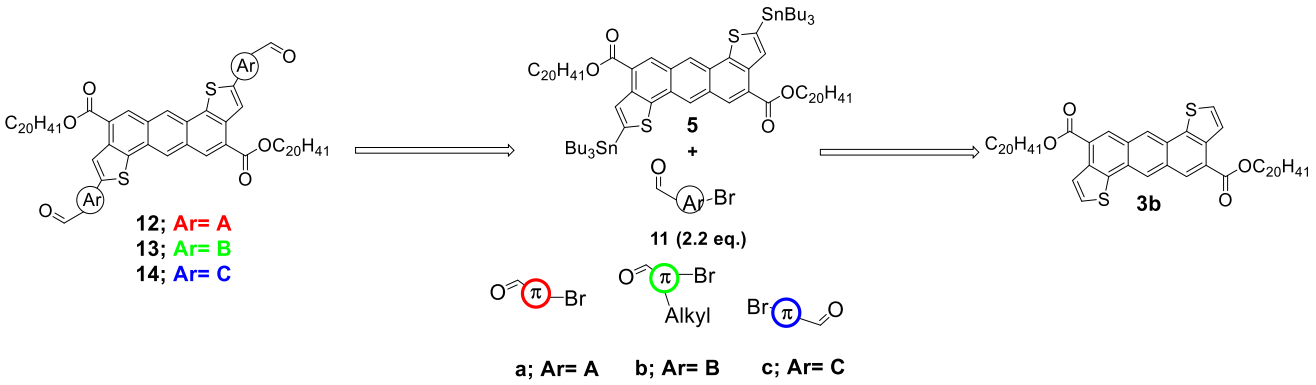

Scheme 3.4. Retro-synthetic pathway towards compounds **12-14**.

Stille cross-coupling was carried out in presence of $Pd(PPh_3)_4$ as source of Pd^0 without any phosphine (Scheme 3.5). Interestingly while molecule **12** and **14**, despite their different structures, were isolated in very high yield after chromatographic column, molecule **13** did not react in the same conditions reported for molecule **12**. Increasing the reaction temperature to 110°C, as used for derivative **14**, allowed us to isolate molecule **13** in modest yield after purification. We ascribe this luck of reactivity due to the presence of the alkyl side chain into π-spacer ring, which probably increase the activation energy required for the process.

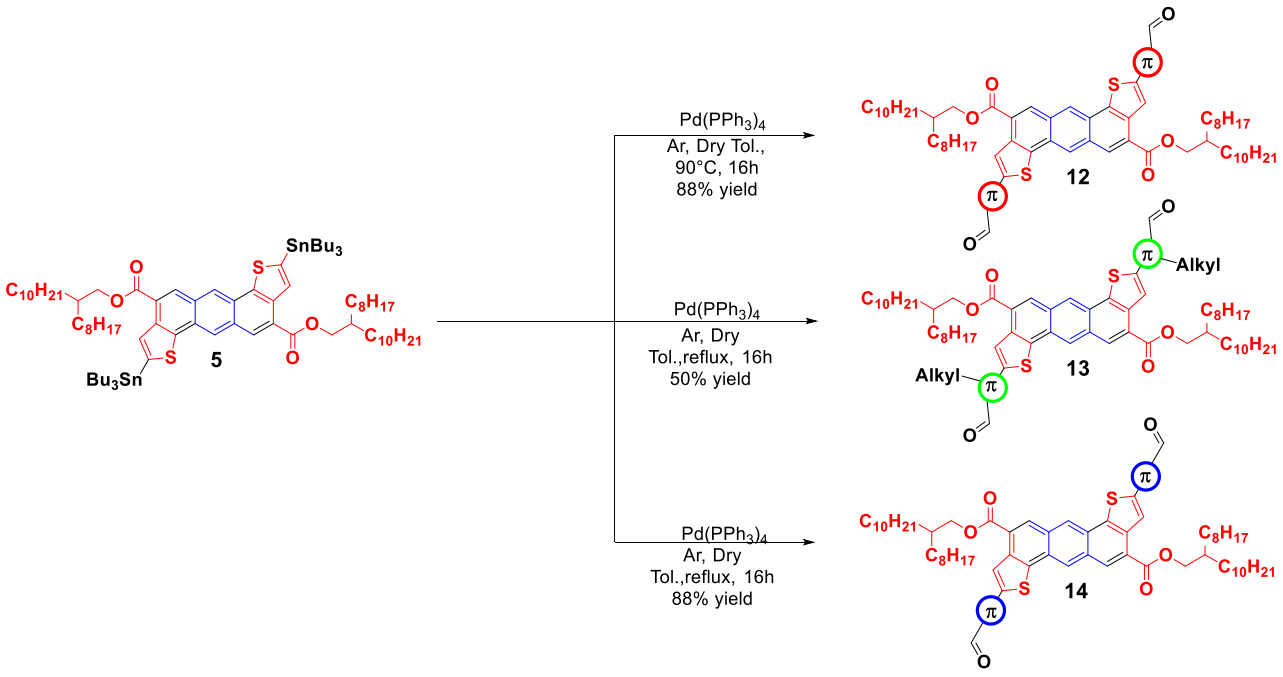

Scheme 3.5. Functionalization of the ADT scaffold by Stille reactions

We also investigated the possibility to obtain molecule **14** *via* C-H activation (Scheme 3.6, top) to avoid the tin intermediate as well as toxic tin-based byproducts, promoting a much cleaner and easiest route for its synthesis. The use of direct arylation methodologies, however, as reported in many papers, can give rise to several problems such as a) lack of selectivity and b) substrate dependency, still limiting its applicability for some monomers and/or positions. We successfully achieved this route using the conditions reported by Renyolds, J. R *et al*,[172] demonstrating the feasibility of the direct arylation reaction (DArP) in combination with the ADT scaffold (Scheme 3.6, bottom). It is noteworthy that DArP reactions showed a slightly higher yield compared to Stille.

[172] J. F. Ponder, H. Chen, A. M. T. Luci, S. Moro, M. Turano, A. L. Hobson, G. S. Collier, L. M. A. Perdigão, M. Moser, W. Zhang, G. Costantini, J. R. Renyolds and I. McCulloch, «Low-Defect, High Molecular Weight Indacenodithiophene (IDT) Polymers Via a C–H Activation: Evaluation of a Simpler and Greener Approach to Organic Electronic Materials» *ACS Mater. Lett.* **2021**, *3,* 1503-1512.

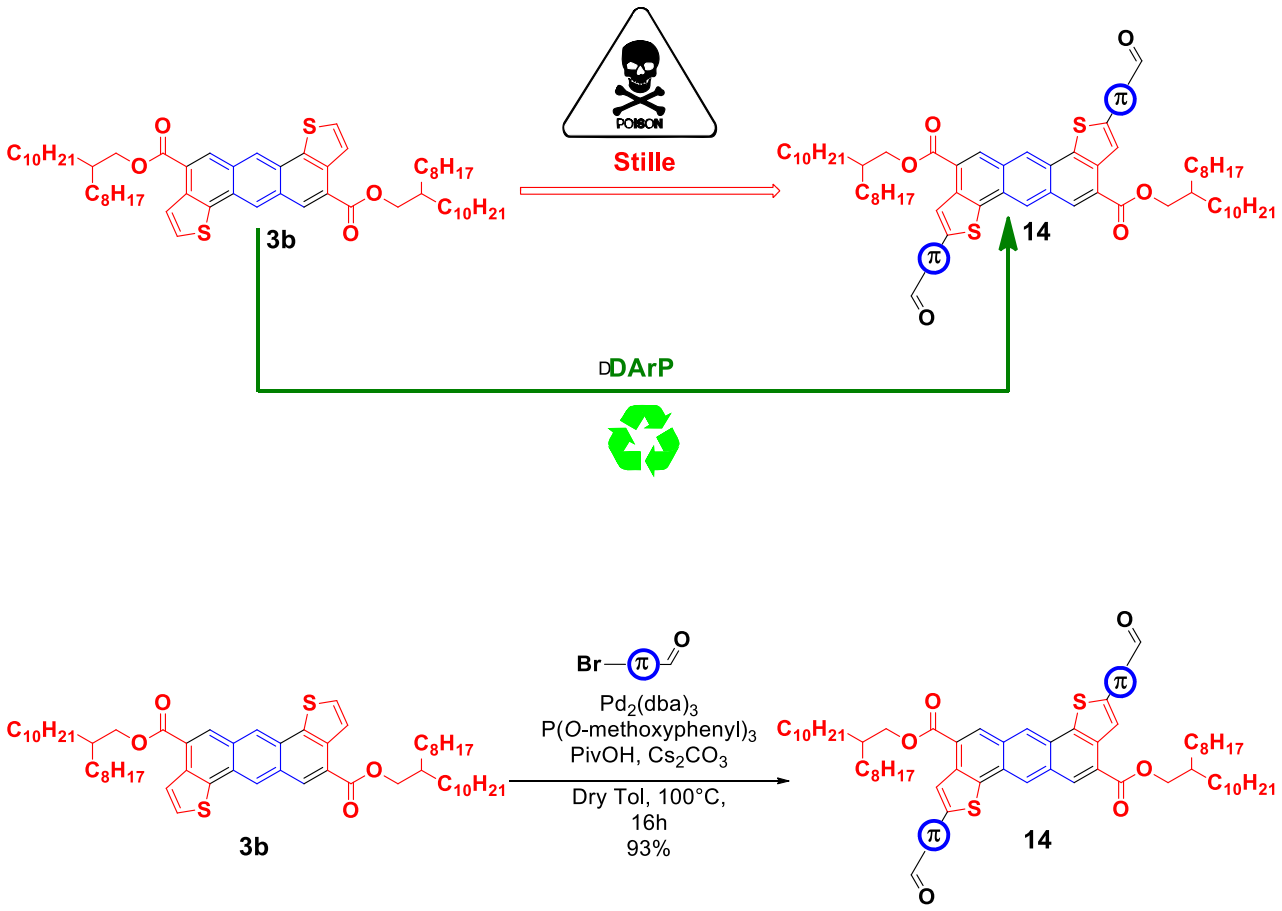

Scheme 3.6. DArP reaction for the synthesis of compound **14**.

Interested in the possibility to develop new NFAs based on ADT, we decided to introduce the end-cap electron poor core by Knoevenagel reaction as reported in the Scheme 3.7.

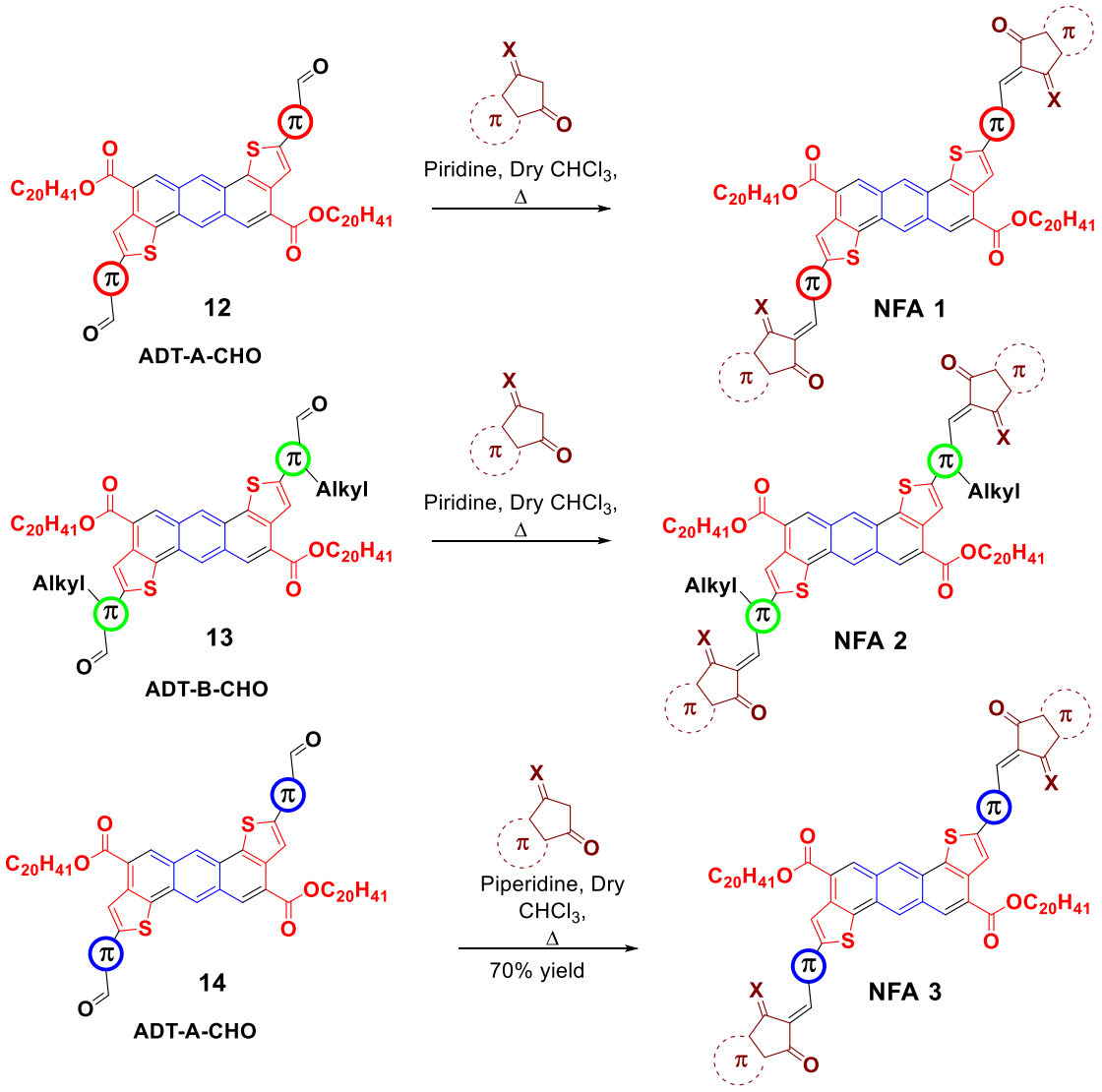

Scheme 3.7. Knoevenagel reactions for the synthesis of NFAs 1-3.

Despite intermediate **12** and **13** possess a very good solubility in common organic solvents, **NFAs 1** and **2** did not possess any appreciable solubility, so that their isolation and characterization could not be achieved, and proof of the obtainment of the final compounds could be confirmed only by MALDI. On the contrary, final **NFA 3**, obtained using a different end-cap unit, showed much better solubility in the same solvents, and could be fully characterized by NMR spectroscopy. We believe that, upon condensation with end-cap core, **NFAs 1** and **2** tend to form strong π-π interactions, which result in a lower solubility, while molecule **NFA 3,** which possess a different end-cap unit, does not suffer this problem allowing a better solubility.

NMR, Uv/Vis and PL properties. Despite the presence in all intermediate molecules of an aldehyde fucntional group, molecule **14** showed a remarkable shift at low fields of its signals compared to molecules **12** and **13** (Figure 3.9), because of the presence of a strong electron-withdrawing spacer ring compared to those used in molecules **12** and **13**.

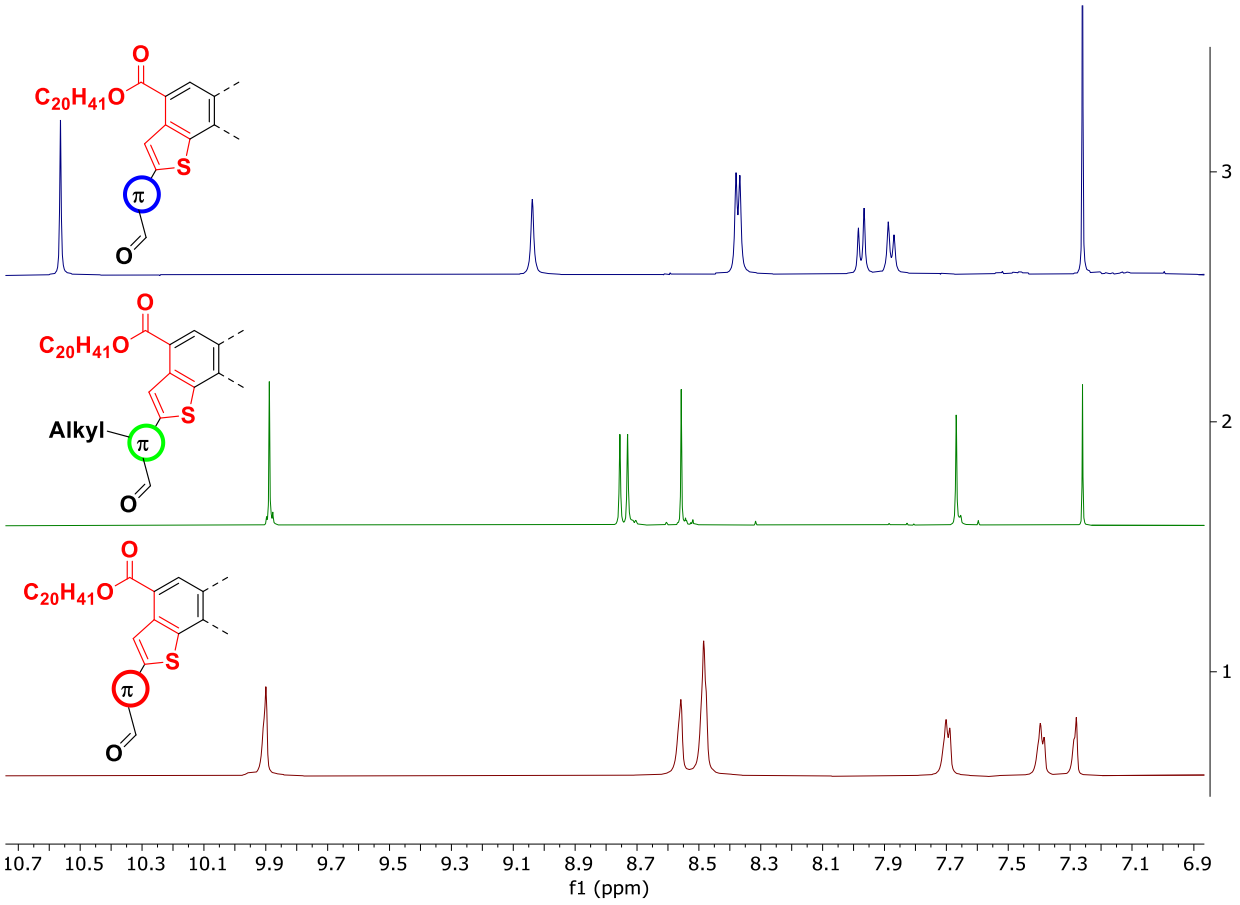

Figure 3.9. ^{1}H NMR spectra of compounds (from top to bottom): **14**, **13** and **12**.

To understand in deep the difference between our aldehydes, and how different end ring can afflict electronic properties, we measured their UV/PL spectra in both solution and film (Figure 3.10). While molecule **12** showed in solution a narrow absorption profile located at 449 nm and slightly red-shifted in cast film (452 nm), molecule **14**, due to the presence of electron-withdrawing spacer ring, showed a remarkable red-shift in both solution and cast film with a broader and much higher absorption profile located respectively at 507 nm and 554 nm.

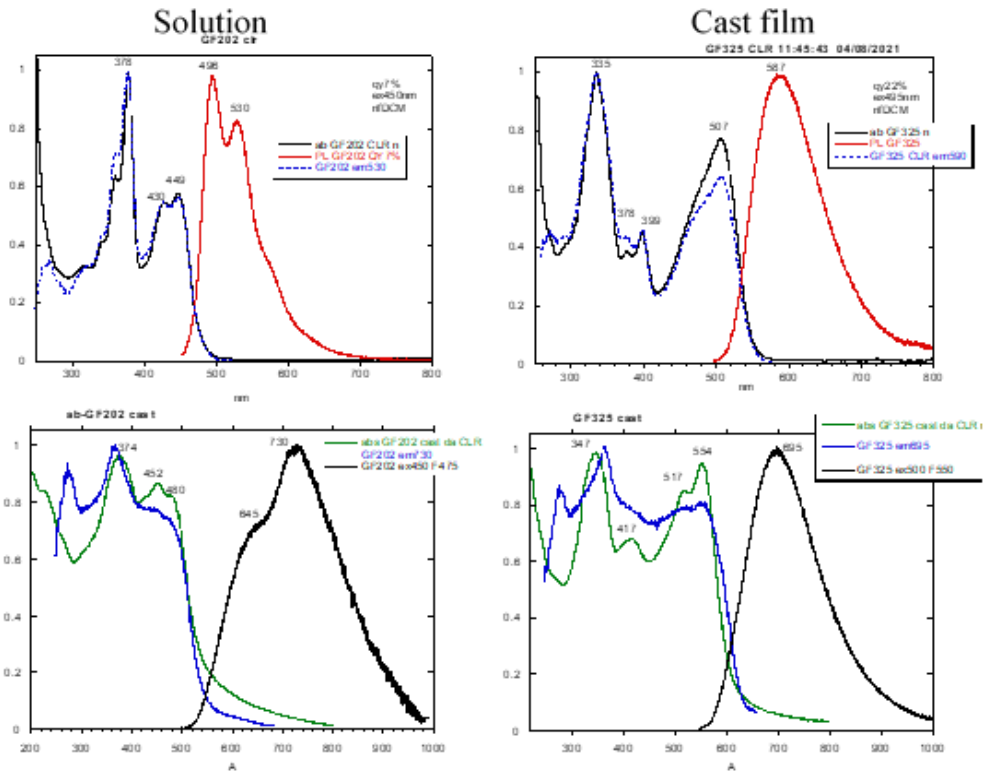

Figure 3.10. Uv/PL in solution and cast film for molecules **12** and **14**

3.3→ CONCLUSIONS

We have reported a scalable synthesis of novel ADT derivatives through an efficient methodology, the DHA-cross aldol reaction, through which a regioselective double annulation of a simple benzene derivative is obtained in high yields. The green metrics for such syntheses are unprecedentedly low. We have proven that the novel aADT scaffold is amenable to regioselective substitution on the two a-thiophene positions, to introduce selectively one or two reactive functionalities. Two types of π-oligomers have been synthesized in high yields, in which ADT moieties are either endcapped with electron-donating naphthothiophene units, to form a p-type oligomer, or used as terminal groups, with electron-withdrawing benzothiadiazole units, to form an n-type material. The energy levels of the esterified aADT scaffold demonstrate that it can be considered as a moderate electron donor. Its incorporation into oligomers brings about the formation of semiconducting materials, with the p-type oligomer showing good film forming properties and respectable mobilities. The combination of the aADT scaffold with suitable comonomers will bring a novel generation of scalable and sustainable

polymers to be used in all the "big three" (OPV, OLED, OFET) of organic electronics. Our efforts in this context are being addressed and will be presented in the near future.

We successfully achieved the synthesis of three novel π-extended dialdehydes with tunable electronic and absorption characteristics, based on the ADT scaffold. The compounds were obtained via Stille reaction, and we demonstrated the feasibility of direct arylation for their synthesis. They showed comparable absorption profiles with the most common electron rich core used in NFA, as well as good solubility in halogenated solvents. We were able to synthesize the first NFA, **NFA 3**, based on the ADT core without chromatographic column in high yield. **NFA 3** will be further studied to evaluate its photo-physical and photovoltaic properties.

3.4→ EXPERIMENTAL PART

1. General Experimental

All commercially available reagents and solvents were purchased from Sigma-Aldrich, Fluorochem and Alfa Aesar. They were all used as received. 2,5-Dibromoterephthalaldehyde **1**[173] and compound **7** were synthesized according to literature.[174] Flash chromatography was carried out using Merck silica gel 60 (pore size 60 Å, 270-400 Mesh). ^{1}H and ^{13}C NMR spectra were recorded from solutions in deuterated solvents on 300 Bruker or 400 Jeol spectrometers with the residual solvent as the internal standard. Mass spectra of pure compounds were recorded using an Electron Spray Ionization Agilent Technologies mass spectrometer, Direct Exposure Probe mass spectrometer, GC-MS ThermoScientific spectrometer and a Bruker Autoflex MALDI-TOF in reflectron mode with or without trans-2-(3-(4-tert-Butylphenyl)-2-methyl-2-propenylidene)malononitrile (DCTB) as the matrix. The spectra were recorded also without the matrix, giving in most cases equivalent results due to the direct formation of the radical cation of the relevant species. The UV-Vis spectroscopic studies were recorded using JASCO V-550 spectrophotometer. The photoluminescence experiments and lifetime experiments were recorded using

[173] Prusinowska, N.; Bardzinski, M.; Janiak, A.; Skowronek, P.; Kwit, M. «Sterically Crowded Trianglimines-Synthesis, Structure, Solid-State Self-Assembly, and Unexpected Chiroptical Properties. *Chem. Asian J.* **2018**, *13*, 2691 –2699

[174] Nitti, A.; Bianchi, G.; Po, R.; Pasini, D. «Scalable Synthesis of Naphthothiophene and Benzodithiophene Scaffolds as π-Conjugated Synthons for Organic Materials. *Synthesis* **2019**, *51*, 677–682

Horiba Fluorolog®-3 Model FL3-22iHR. Cyclic voltammetry experiments were carried out using a Epsilon-Eclipse potentiostat with a polished glassy carbon working electrode, platinum counter electrode, silver pseudo-reference electrode, and tetrabutylammonium hexofluorophosphate (recrystallized three times from EtOH) as a supporting electrolyte. Sample concentrations were between 0.2 and 1.0 mM in CH_2Cl_2. All electrochemical measurements were referenced to the Fc/Fc^+ redox couple. Band gaps were estimated using the onset of the initial oxidation and reduction events, and E_{HOMO} and E_{LUMO} were estimated given an E_{HOMO} of 4.80 eV for ferrocene. In all figures the first scan is shown, which is similar to subsequent scans.[175] Theoretical energy calculations were performed with density functional theory (DFT) calculations using the DFT/B3LYP framework with the DZP basis set. Solubilizing alkyl groups were replaced with methyl groups in oligomers **9** and **10** for simplicity.

Hole Mobility Measurements. Hole-only devices were prepared for the investigation of mobility of positive charge carriers. The devices had the sandwiched structure ITO/PEDOT:PSS/PDTIDTBT/MoO3/Au, where ITO is indium tin oxide and PEDOT:PSS is poly(3,4-ethylenedioxythiophene)/polystyrene sulphonic acid (CLEVIOS P VP AI 4083, H.C. Starck). ITO-coated glass substrates were first cleaned in detergent and water, then ultrasonicated in acetone and isopropyl alcohol for 15 min each. The layer of PEDOT:PSS (~ 40 nm) was spin-coated at 4000 rpm onto the ITO-glass substrates, and baked in an oven at 120 °C for 10 min. The oligomer layer was deposited by spin-coating (280 rpm) from a chloroform solution (40 g/L) to a thickness of 600 nm. The MoO_3 layer (5 nm) and the Au top electrode (100 nm) were thermally evaporated at a base pressure of $4x10^{-6}$ mbar through a shadow mask defining a device active area of 8 mm^2. The electrical characterization of hole-only devices was carried out at room temperature in an Ar-filled glove-box. J-V characteristics were taken using a digital source meter (Keithley model 2400) and Impedance Spectroscopy measurements were performed using an Agilent 4294A impedance analyzer. The impedance measurements were done in the frequency range 40 Hz–1 MHz, with an amplitude of the harmonic voltage modulation of 20 mV. The DC bias was varied in the range 0 V–30 V.

[175] Osw, P.; Nitti, A.; Etkind, S. I.; Abdullah, M. N.; Mwaura, J.; Galbiati, A.; Pasini, D. «Synthesis and Evaluation of Scalable D-A-D π-Extended Oligomers as p-Type Organic Materials for Bulk-Heterojunction Solar Cells» *Polymers* **2020**, *12*, 720

The transit time of charge carriers τ can be inferred from the peak frequency of the negative differential subsceptance or from the peak frequency of the imaginary part of impedance (*ImZ*).[176] Figure S7 shows the frequency dependence of *ImZ*, at various values of the dc bias, for a hole-only device based on oligomer **9**, indicating that clear peaks were observed, shifting toward higher frequencies as the dc voltage was increased. The transit time of charge carriers was obtained from the peak frequency through $\tau = k\tau_p$, where τ_p is the time constant corresponding to the peak frequency of *ImZ* and k a constant dependent on the dispersion degree. The value of 0.44 was assumed for k, which has been reported for a moderate degree of dispersion.[177] The values of hole mobility μ was calculated by using the well-known expression $\mu = d / (E\,\tau)$, where d is the film thickness. As shown in Figure S7, the hole mobility of spin-coated oligomer **9** exhibits an almost field-independent behavior, suggesting a low energetic disorder.[178] The mean value of the data shown in Figure 5 is 2.45 x 10^{-5} cm^2 V^{-1} s^{-1}, a remarkable value for the bulk mobility of a low-molecular weight and spin-coated compound.

Given the rough independence on field, the hole mobility was also extracted from the current-density *versus* voltage (*J-V*) characteristic of the hole-only device made of oligomer **9**. In figure S7, J is reported as a function of square V, showing the excellent linear behavior expected for the space-charge-limited current in an one-carrier only device, as predicted by the Mott-Gurney low:[179]

$$J = \frac{9}{8}\varepsilon\varepsilon_0\mu\frac{V^2}{d^3}$$

where ε and ε_0 are the relative dielectric constant and the permittivity in vacuum, respectively. By plotting J as a function of V^2, the slope of the line is strictly correlated with mobility. A value of 2.38×10^{-5} cm^2

---

[176] a) Tanase, C.; Meijer, E. J.; Blom, P. W. M.; De Leeuw, D. M. «Unification of the Hole Transport in Polymeric Field-Effect Transistors and Light-Emitting Diodes» *Phys. Rev. Lett.*, 2003, **91**, 216601; (b) Kassing, R. «Calculation of the frequency dependence of the admittance of SCLC diodes» *Phys. status solidi*, **1975**, *28*, 107–117.

[177] Tripathi, D. C.; Tripathi, A. K.; Mohapatra, Y. N. «Mobility determination using frequency dependence of imaginary part of impedance (Im Z) for organic and polymeric thin films» *Appl. Phys. Lett.*, **2011**, *98*, 33304

[178] Martin, S. J.; Kambili, A.; Walker, A.B. «Temperature and field dependence of the mobility of highly ordered conjugated polymer films» *Phys. Rev. B.* **2003**, *67*, 165214.

[179] Lampert, M.A.; Park, P. «*Current Injection is Solids*» Academic Press, New York, **1970**

V^{-1} s^{-1} was calculated by assuming $\varepsilon = 3$, in excellent agreement with the mean hole mobility obtained with impedance spectroscopy.

2. Synthesis of New Compounds

Anthra[1,2-b:5,6-b']dithiophene-4,10-dicarboxylic acid (3a)

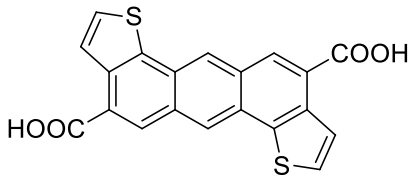

A three-necked flask equipped with condenser and mechanical stirring was charged in argon atmosphere with 3-thiopheneacetic acid (28.4 g, 0.2 mol, 2 eq), $Pd(OAc)_2$ (2.25 g, 0.01 mol, 0.01 eq), PPh_3 (5.25 g, 0.02 mol, 0.1 eq), K_2CO_3 (55.3 g, 0.4 mol, 4 eq) and dry DMAc (2 L). The reaction mixture was warmed to 110 °C and 2,5-dibromoterephthalaldehyde **1** (29.2 g, 0.1 mol, 1 eq) was added portionwise in 10 min under inert atmosphere. The reaction mixture was kept at the same temperature under stirring for 24 h, and then the reaction solvent was removed under reduced pressure. The dark crude reaction mixture was dissolved in distilled water (1 L) and HCl conc (50 mL) was added dropwise until full acidity (pH = 1). The precipitate was filtered under reduced pressure and washed with MeOH (500 mL). The dark powder was purified by Soxhlet extraction with acetone for 24 h to give **3a** as a black powder (26.9 g, 81%). ^{1}H NMR (300 MHz, DMSO-*d*$_6$) δ: 13.37 (s, 2H), 9.19 (s, 2H), 8.90 (s, 2H), 8.31 (d, J = 5.4 Hz, 2H), 8.01 (d, J = 5.4 Hz, 2H). ^{13}C NMR (101 MHz, DMSO-*d*$_6$) δ: 167.9, 138.7, 134.8, 131.1, 130.1, 128.2, 127.6, 126.4, 125.8, 125.0. ESI-MS: 377 [M - 1]$^-$.

General procedure for the alkylation of compound 3a. *Synthesis of compound* **3b**. 9-(bromomethyl)nonadecane (36.1 g, 100 mmol, 2 eq) was added to a solution of compound **3a** (18.9 g, 50 mmol, 1 eq), Bu_4NI (3.69 g, 10 mmol, 0.2 eq), K_2CO_3 (13.82 g, 100 mmol, 2 eq) in dry DMAc (500 mL) under inert atmosphere and then stirred at 130 °C for 48 h. After removal of solvent under reduced pressure, the crude reaction mixture was dissolved in hexane:AcOEt (98:2) and filtered through a short silica gel path (4 cm). The organic solvent was removed under reduced pressure, the crude reaction mixture was dissolved in $CHCl_3$ and precipitated in EtOH and ^{i}PrOH (twice) to give **3b** as a yellow powder (23.9 g, 51%).

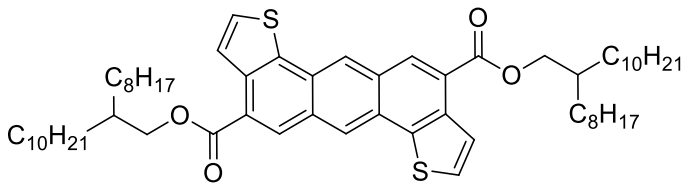

*Bis(2-octyldodecyl) anthra[1,2-b:5,6-b']dithiophene-4,10-dicarboxylate (***3b***)*. Yellow powder (51%). ^{1}H NMR (300 MHz, $CDCl_3$) δ: 8.79 (s, 2H), 8.69 (s, 2H), 8.36 (d, J = 5.3 Hz, 2H), 7.63 (d, J = 5.3 Hz, 2H), 4.39 (d, J = 5.1 Hz, 4H), 1.92 (s, 2H), 1.57 – 1.13 (m, 64H), 0.95 – 0.75 (m, 12H). ^{13}C NMR (75 MHz, $CDCl_3$) δ: 166.6, 139.1, 134.6, 130.9, 130.0, 128.6, 126.6, 125.7, 125.2, 124.6, 77.2, 76.7, 76.3, 67.8, 37.3, 31.6, 31.4, 29.8, 29.4, 29.4, 29.3, 29.1, 26.6, 22.4, 13.8. DEP-MS (*m/z)*: 938. Anal. calcd. for $C_{60}H_{90}O_4S_2$: C 76.7; H 9.7; found: C 76.8; H 9.7.

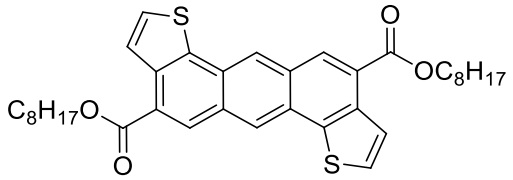

*Bis(n-octyl) anthra[1,2-b:5,6-b']dithiophene-4,10-dicarboxylate (***3c***)*. Yellow powder (48%). ^{1}H NMR (300 MHz, $CDCl_3$) δ: 8.77 (s, 2H), 8.69 (s, 2H), 8.34 (d, J = 5.3 Hz, 2H), 7.62 (d, J = 5.3 Hz, 2H), 4.46 (t, J = 6.7 Hz, 4H), 1.89 (t, J = 6.9 Hz, 4H), 1.57 – 1.19 (m, 20H), 0.97 – 0.84 (m, 6H). ^{13}C NMR (75 MHz, $CDCl_3$) δ: 166.6, 139.1, 134.6, 130.9, 130.0, 128.6, 126.6, 125.7, 125.2, 124.6, 65.7, 32.0, 29.5, 29.4, 29.0, 26.3, 22.9, 14.3. DEP-MS (*m/z)*: 602, 546, 490, 446, 334. Anal. calcd. for $C_{36}H_{42}O_4S_2$: C 71.7; H 7.0; found: C 71.8; H 7.1.

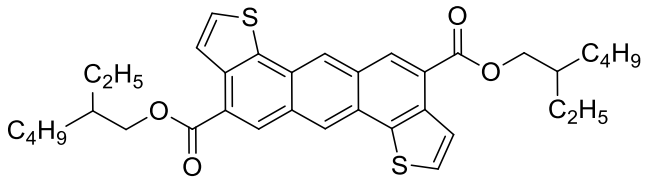

*Bis(2-etylhexyl) anthra[1,2-b:5,6-b']dithiophene-4,10-dicarboxylate (***3d***)*. Yellow powder (32%). ^{1}H NMR (300 MHz, $CDCl_3$) δ: 8.77 (s, 2H), 8.69 (s, 2H), 8.34 (d, J = 5.3 Hz, 2H), 7.62 (d, J = 5.3 Hz, 2H), 4.39 (d, J = 5.1 Hz, 4H), 1.92 (s, 2H), 1.57 – 1.13 (m, 16H), 0.95 – 0.75 (m, 12H). ^{13}C NMR (75 MHz, $CDCl_3$) δ: 165.6, 139.1, 133.9, 131.0, 130.3, 128.6, 126.6, 125.8, 125.2, 124.3, 65.6, 32.1, 29.5, 29.4, 29.1, 26.3, 22.9, 14.5. DEP-MS: *m/z*: 602, 378. Anal. calcd. for $C_{36}H_{42}O_4S_2$: C 71.7; H 7.0; found: C 71.7; H 7.1.

Bis(2-ethylhexyl) 2,8-dibromoanthra[1,2-b:5,6-b']dithiophene-4,10-dicarboxylate (4).

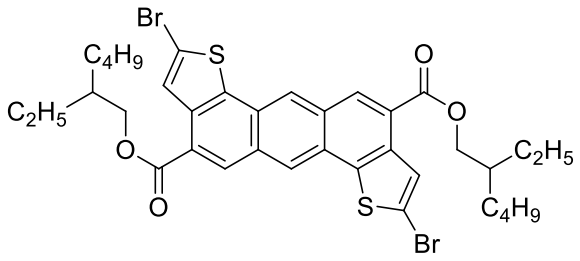

N-Bromosuccinimide (71 mg, 0.4 mmol, 4 eq) was added to a solution of compound **3d** (60 mg, 0.1 mmol, 1 eq) in a mixture of $CHCl_3$ and AcOH (8:2, 1 mL) under inert atmosphere. The reaction mixture was kept under stirring at room temperature for 24 h. After removal of the solvent under reduced pressure, the crude reaction mixture was dissolved in hexane:AcOEt (98:2) and filtered through a short silica gel path (4 cm). The organic solvent was removed under reduced pressure to give **4** as a yellow powder (18 mg, 25%). ^{1}H NMR (300 MHz, $CDCl_3$) δ: 8.63 (s, 2H), 8.57 (s, 2H), 8.34 (s, 2H), 4.43 (d, J = 5.1 Hz, 4H), 1.92 (s, 2H), 1.57 – 1.13 (m, 16H), 0.95 – 0.75 (m, 12H). ^{13}C NMR (75 MHz, $CDCl_3$) δ: 165.6, 139.1, 133.9, 131.0, 130.3, 128.6, 126.6, 125.8, 125.2, 124.3, 65.6, 32.1, 29.5, 29.4, 29.1, 26.3, 22.9, 14.5. DEP-MS: *m/z*: 760, 682, 535. Anal. calcd. for $C_{36}H_{40}Br_2O_4S_2$: C 56.9, H 5.3; found: C 56.8; H 5.4.

Bis(2-octyldodecyl) 2,8-bis(tributylstannyl)anthra[1,2-*b*:5,6-*b*′]dithiophene-4,10-dicarboxylate (5)

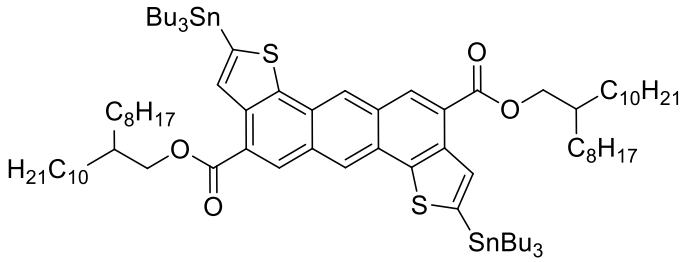

A solution of compound **3b** (1 g, 1.06 mmol, 1eq) in dry THF (25 mL) under argon was cooled to -40 °C. After 15 min, a solution of LDA (1 M in hexane, 4.26 mL, 4.26 mmol, 4 eq) was added dropwise and the resulting red solution was further down to -78°C for 2h, then Bu_3SnCl (722 µL, 2.66 mmol, 2.5 eq) was added in one portion. The reaction mixture was kept at -78°C for 30 min, and then it was warmed to room temperature and stirred overnight. The reaction mixture was quenched with H_2O (20 mL), most of the organic solvent was removed under reduced pressure, and the aqueous phase extracted with Et_2O (3 x 20 mL). the combined organic phase was dried (Na_2SO_4). After removal of the solvent under reduced pressure, the reaction mixture was purified by flash chromatography on neutral alumina (*n*-hexane as the eluent) affording **5** as a pale yellow oil (1.51 g, 94%). ^{1}H NMR (400 MHz, $CDCl_3$) δ: 8.91 (s, 2H), 8.73 (s, 2H), 8.41 (s, 2H), 4.44 (d, J = 5.1 Hz, 4H), 1.92 (s, 2H), 1.57 – 1.13 (m, 16H), 0.95 – 0.75 (m, 12H).

^{13}C NMR (75 MHz, $CDCl_3$) δ: 167.7, 149.8, 145.0, 139.7, 136.4, 135.0, 131.3, 130.4, 128.9, 125.5, 65.6, 32.1, 29.5, 29.4, 29.1, 26.3, 22.9, 14.5. APCI-MS: *m/z* 1518 $[M]^+$.

bis(2-octyldodecyl) 2-(tributylstannyl)anthra[1,2-*b*:5,6-*b'*]dithiophene-4,10-dicarboxylate (6).

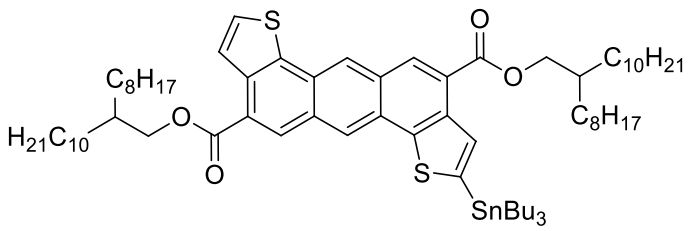

A solution of compound **5d** (1 g, 1.06 mmol, 1eq) in dry THF (25 mL) under argon atmosphere was cooled to -78°C. After 15 min LDA (1 M in hexane, 1.59 mL, 1.59 mmol, 1.5 eq) was added dropwise and kept for 2h at the same temperature, then Bu_4SnCl (288 μL, 1.59 mmol, 1.5 eq) was added in one portion. The reaction mixture was kept at -78°C for 30 min, and then it was warmed to room temperature and stirred overnight. The reaction mixture was quenched with H_2O (20 mL), most of the organic solvent was removed under reduced pressure, and the aqueous phase extracted with Et_2O (3 x 20 mL). the combined organic phase was dried (Na_2SO_4). After removal of the solvent under reduced pressure, the reaction mixture was purified by flash chromatography on neutral alumina (*n*-hexane as the eluent) affording pure compound **6** as a pale yellow oil (627 mg, 48%).^{1}H NMR (400 MHz, $CDCl_3$) δ: 8.90 (s, 1H), 8.75 (s, 1H), 8.72 (s, 1H), 8.43 (s, 1H), 8.38 (d, J = 5.4 Hz, 1H), 7.64 (d, J = 5.4 Hz, 1H), 4.40 (t, J = 5.2 Hz, 4H), 1.96 – 1.87 (m, 2H), 1.73 – 1.19 (m, 76H), 0.94 (t, J = 7.3 Hz, 9H), 0.94 – 0.77 (m, 12H). ^{13}C NMR (101 MHz, $CDCl_3$) δ: 167.1, 166.8, 144.4, 139.3, 139.2, 134.5, 134.4, 131.0, 130.6, 130.1, 129.9, 128.5, 126.6, 125.7, 125.5, 125.2, 125.1, 124.5, 68.3, 37.7, 34.4, 32.0, 31.7, 31.7, 30.5, 30.2, 30.1, 29.8, 29.6, 29.5, 29.2, 27.4, 27.0, 27.0, 22.8, 14.2, 13.8, 11.2.

bis(2-octyldodecyl) 2,8-bis(4-(((2-octyldodecyl)oxy)carbonyl)naphtho[1,2-b]thiophen-2-yl)anthra[1,2-b:5,6-b']dithiophene-4,10-dicarboxylate (9).

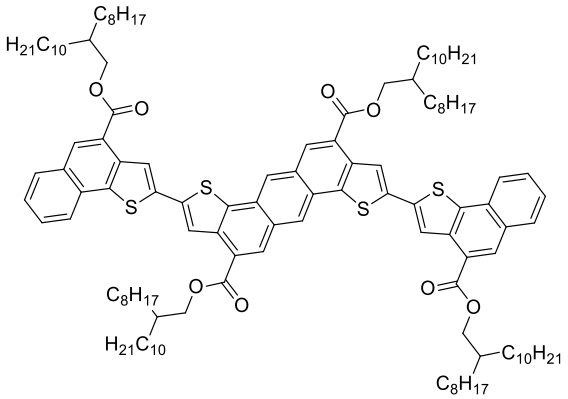

A solution of compound **5** (303 mg, 0.2 mmol, 1 eq), 2-octyldodecyl 2-bromonaphtho[1,2-b]thiophene-4-carboxylate **7** (235 mg, 0.4 mmol, 2 eq) in dry toluene (2 mL)was degassed for 5 min under argon atmosphere. $Pd(PPh_3)_4$ (4.62 mg, 4 □mol, 0.02 eq) was added in one portion, and the solution was further degassed for 10 min. The reaction mixture was heated at reflux under stirring for 24 h. The reaction solvent was removed under reduced pressure and the reaction mixture was purified by flash chromatography (SiO_2; petroleum ether:CH_2Cl_2 8:2), to obtain compound **9** as a dark yellow solid (277 mg, 71%). ^{1}H NMR (400 MHz, $CDCl_3$) δ: 8.40 (s, 2H), 8.28 (s, 2H), 8.20 (s, 2H), 8.18 (s, 2H), 8.13 (s, 2H), 7.74 (d, J = 8.0 Hz, 4H), 7.62 (d, J = 8.0 Hz, 4H), 7.39 (t, J = 7.4 Hz, 4H), 7.25 (t, J = 7.4 Hz, 4H), 4.52 (d, J = 5.0 Hz, 4H), 4.44 (d, J = 5.4 Hz, 4H), 2.12 – 2.02 (m, 2H), 1.98 (d, J = 5.3 Hz, 2H), 1.66 – 1.13 (m, 128H), 0.82 (dd, J = 12.9, 6.0 Hz, 24H). ^{13}C NMR (101 MHz, $CDCl_3$) δ: 166.3, 166.1, 138.3, 138.2, 137.2, 137.1, 135.7, 134.7, 131.0, 130.4, 130.1, 129.5, 129.4, 128.6, 127.3, 125.8, 124.4, 124.2, 123.7, 123.3, 123.2, 123.0, 68.5, 68.2, 37.8, 32.1, 32.1, 32.1, 31.9, 31.8, 30.4, 30.0, 29.9, 29.9, 29.8, 29.6, 29.5 27.2, 22.8, 22.8, 14.2. MALDI-TOF: $[M]^+$ = 1953.

tetrakis(2-octyldodecyl) 2,2'-(benzo[c][1,2,5]thiadiazole-4,7-diyl)bis(anthra[1,2-b:5,6-b']dithiophene-4,10-dicarboxylate) **(10).**

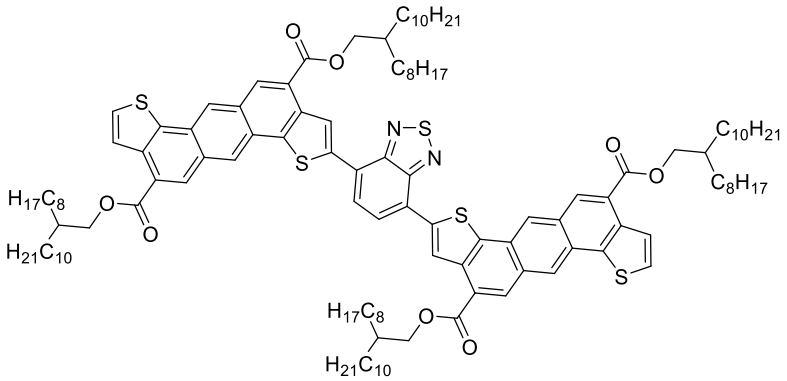

A solution of compound **6** (303 mg, 0.2 mmol, 1 eq), 4,7-dibromo-5,6-difluorobenzo[*c*][1,2,5]thiadiazole **8** (235 mg, 0.4 mmol, 2 eq) in dry toluene (2 mL) was degassed for 5 min under argon atmosphere. $Pd(PPh_3)_4$ (4.62 mg, 4 □mol, 0.02 eq) was added in one portion, and the solution was further degassed for 10 min. The reaction mixture was heated at reflux under stirring for 24 h. The reaction solvent was removed under reduced pressure and the reaction mixture was purified by flash chromatography (SiO_2; petroleum ether:CH_2Cl_2 8:2), to obtain compound **10** as a dark red solid (277 mg, 76%). ^{1}H NMR (400 MHz, $CDCl_3$) δ: 8.77 (s, 0H), 8.33 – 8.17 (m, 0H), 8.07 (s, 0H), 7.81 (d, J = 22.4 Hz, 0H), 7.33 (d, J = 5.1 Hz, 0H), 4.53 (d, J = 5.5 Hz, 0H), 4.26 (d, J = 4.3 Hz, 0H), 2.11 (d, J = 5.6 Hz, 0H), 1.97 – 1.79 (m, 0H), 1.80 – 1.09 (m, 8H), 0.98 – 0.75 (m, 1H). ^{13}C NMR (101 MHz, $CDCl_3$) δ: 165.73, 138.39, 133.98,

133.26, 130.74, 130.50, 129.41, 129.27, 129.05, 128.98, 127.70, 126.48, 126.39, 124.96, 124.35, 124.07, 123.75, 123.42, 68.58, 37.79, 37.58, 32.14, 31.67, 31.50, 30.46, 30.27, 30.02, 29.90, 29.67, 29.56, 29.54, 29.47, 27.11, 26.92, 22.85, 14.25. MALDI-TOF: [*M*]=2045.

Synthesis of intermediate (12)

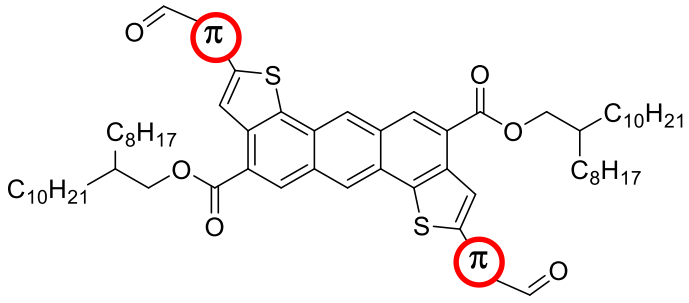

In a dried two neck round bottom flask under Ar, were compound **5** (116 mg, 0.0764 mmol) and aldehyde **a** (32 mg, 0.168 mmol) in dry Toluene (5 mL, 0.015 M), the resulting dark brown solution was degassed for 15 min with Ar, then was added $Pd(PPh_3)_4$ (4.41 mg, 0.00382 mmol), after that, the solution was heated to 90 °C for 48 h. After 48 h the resulting dark red solution was extracted with DCM/H_2O, then the combined organic phase was dried over Na_2SO_4 and the solvent was distilled in vacuo.to give a dark red solid. The corresponding solid was purified by flash chromatography (9:1 to 7:3 v/v Hex/EtOAc) to give pure compound **13** as orange solid (75 mg, 88% yield) ^{1}H NMR (300 MHz, CDCl3): δ= 9.91 (s, 2H), 8.56 (s, 2H), 8.49 (s, 4H), 7.70-7.69 (d, 2H, J= 3Hz), 7.40-7.38 (d, 2H, J= 6Hz), 4.44-4.43 (m, 4H), 2.02-1.94 (m, 2H), 1.57-1.32 (m, 66H) 0.90-0.87 (t, 12H, J= 9Hz) ppm, ^{13}C NMR (75 MHz, CDCl3) δ= 182.12, 165.78, 146,37, 142.64, 139.00, 136.85, 135.55, 135.00, 131.14, 129.81, 127.68, 125.22, 124.80, 124.75, 124.48, 68.52, 37.50, 31.80, 31.51, 30.06, 29.96, 29.60, 29.56, 29.25, 26.80, 22.57, 22.55, 13.98 ppm. MS (MALDI-TOF): [M]=1158.5

Synthesis of intermediate (13)

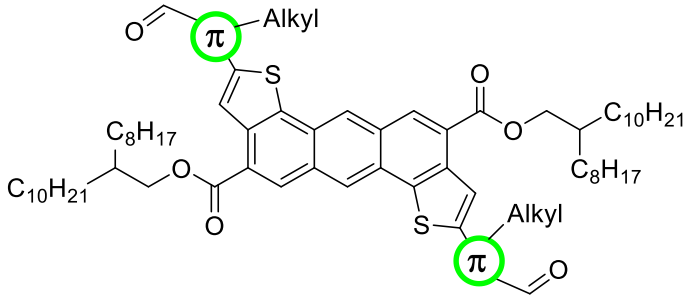

In a dried two neck round bottom flask under Ar, were added compound **5** (340 mg, 0.224 mmol) and aldehyde **b** (160 mg, 0.527 mmol) in dry Toluene (16 mL, 0.015 M), the resulting dark brown solution was degassed for 15 min with Ar, then was added $Pd(PPh_3)_4$ (13 mg, 0.0112 mmol) and the solution was heated to reflux °C for 48 h. After 48 h the resulting dark red solution was extracted with DCM/H_2O, then the combined organic phase was dried, and the solvent was distilled in vacuo to give a dark red solid. The corresponding solid was purified by flash chromatography (95:5 v/v Hex/EtOAc) to give pure compound **14** as orange solid (160 mg, 50% yield) ^1H NMR (300 MHz, CDCl3): δ= 9.91 (s, 2H), 8.78 (s, 2H), 8.75 (s, 2H), 8.58 (s, 2H), 7.69 (s, 2H), 4.44-4.43 (d, 4H, J= 3Hz)), 3.00-2.98 (d, 4H, J= 6Hz), 1.97-1.94 (m, 2H), 1.82-1.76 (m, 2H), 1.52-1.26 (m, 86H), 0.91-0.87 (m, 18H) ppm. ^{13}C NMR (75 MHz, CDCl3) δ= 182.49, 166.12, 141.70, 141.44, 140.69, 139.68, 138.76, 134.96, 134.92, 131.22, 130.10, 128.11, 126.67, 125.11, 124.81, 68.56, 37.59, 31.91, 31.88, 31.55, 30.04, 30.03, 29.70, 29.68, 29.63, 29.50, 29.48, 29.45, 29.36, 29.35, 29.26, 26.85, 22.67, 14.11, 14.09 ppm. MS (MALDI-TOF): [M]=1382.7)

Synthesis of intermediate (14)

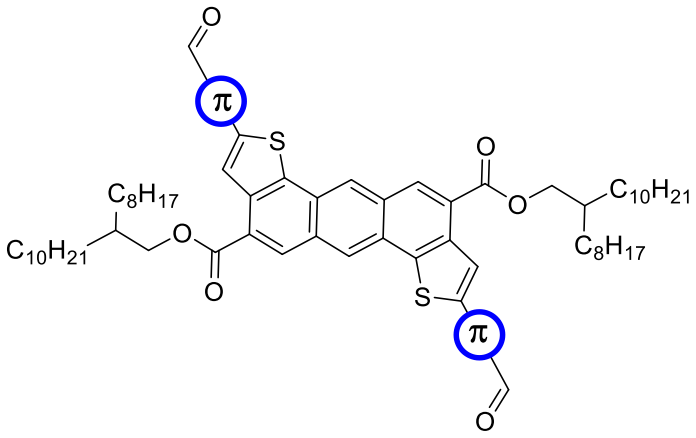

In a dried two neck round bottom flask under Ar, were compound **5** (150 mg, 0.099 mmol) and aldehyde **c** (53 mg, 0.22 mmol) in dry Toluene (7.5 mL, 0.015 M), the resulting dark brown solution was degassed for 15 min with Ar, then was added $Pd(PPh_3)_4$ (6 mg, 0.0052 mmol) and the solution was heated to reflux for 16 h. After 16 h, solvent was distilled in vacuo and the corresponding dark red solid was purified by flash chromatography (Tol. to 7:3 v/v Tol/DCM) to give pure compound **15** as red solid (110 mg, 88% yield) ^1H(400 MHz, CDCl3): δ= 10.56 (s, 2H), 9.04 (s, 2H), 8.38 (s, 2H), 8,37 (s, 2H), 7.98-7.97 (d, 2H, J= 4Hz), 7.89-7.88 (d, 2H, J= 4Hz), 4.50-4.48 (d, 4H. J= 8Hz), 2.04 (m, 2H), 1.64-1.55 (m, 64H), 0.94-0.89 (t, 12H, J= 8Hz) ppm. ^{13}C(100 MHz, CDCl3) δ= 187.97, 165.96, 153.66, 152.08, 141.18, 137.68,

134.55, 131.41, 129.85, 125.86, 124.85, 124.72, 66.84, 37.80, 32.10, 32.06, 31.72, 30.34, 29.95, 29.93, 29.90, 29.86, 29.58, 29.54, 27.99, 27.09, 27.00, 22.85, 17.67, 14.27, 13.75 ppm. MS (MALDI-TOF): [M]=1262.52)

Synthesis of intermediate (14) via DArP

In a dried 10mL microwaves vial under N_2, were added compound **3b** (100 mg, 0.106 mmol) and aldehyde **c** (65 mg, 0.266 mmol), $Pd_2(dba)_3$ (4 mg, 0.0042mmol), P(*O*-methoxyphenil)$_3$ (6 mg, 0.017 mmol), PivOH (11 mg, 0.106 mmol) and Cs_2CO_3 (104 mg, 0.318 mmol) in dry Toluene (2 mL, 0.05 M), the resulting dark brown solution was degassed for 15 min with N_2, then was heated at 100°C for 16 h. After 16 h, the resulting red solution was precipitated in cold MeOH and the corresponding red precipitate was collected by filtration and vacuum oven dried to give pure compound as red solid **15** (124 mg, 93% yield)

Synthesis of NFA 1

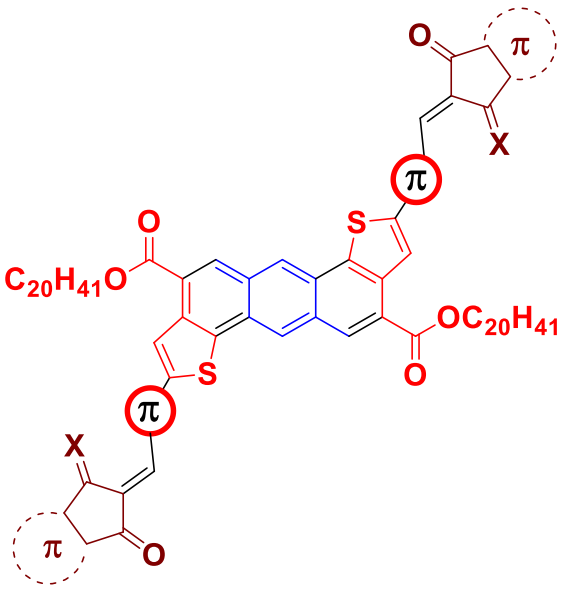

In a dried two neck round bottom flask under Ar, were added intermediate **13** (100 mg, 0.086 mmol), end-cap group (50 mg, 2.5 mmol) and piridine (200 µL) in dry $CHCl_3$ (20 mL, 0.005 M), the resulting dark red solution was degassed with Ar for 15 min. then was heated at reflux for 16. After 16 h, the resulting deep blue solution was cooled down and the resulting solution was precipitated in cold EtOH. The resulting deep blue solid was filtered off to give the desirable NFA **1** as a deep blue solid. However, further purifications were not performed due to its insolubility. MS (*MALDI-TOF*): [M]=1510.5

Synthesis of NFA 2

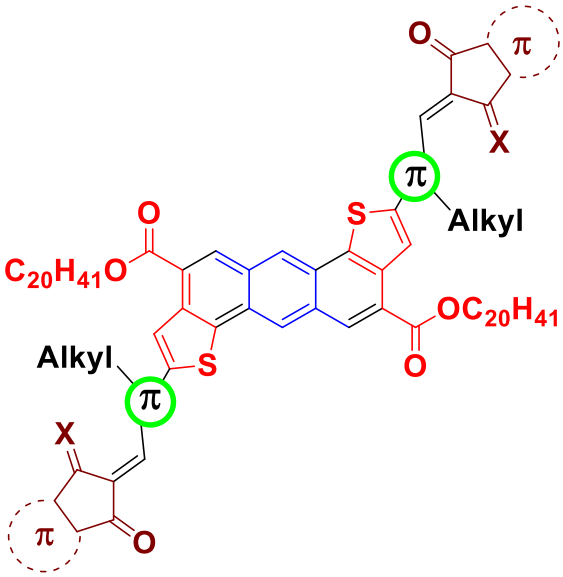

In a dried two neck round bottom flask under Ar, were added intermediate **14** (64 mg, 0.046 mmol), end-cap group (27 mg, 0.138 mmol) and piridine (100 µL) in dry CHCl3 (10 mL, 0.005 M), the resulting dark red solution was degassed with Ar for 15 min. then was heated at reflux for 16. After 16 h, the resulting deep blue solution was cooled down and the resulting solution was precipitated in cold EtOH. The resulting deep blue solid was filtered off to give the desirable **NFA 1** as a deep blue solid. However, further purifications were not performed due to its insolubility. MS (MALDI-TOF): [M]=1735.8

Synthesis of NFA 3

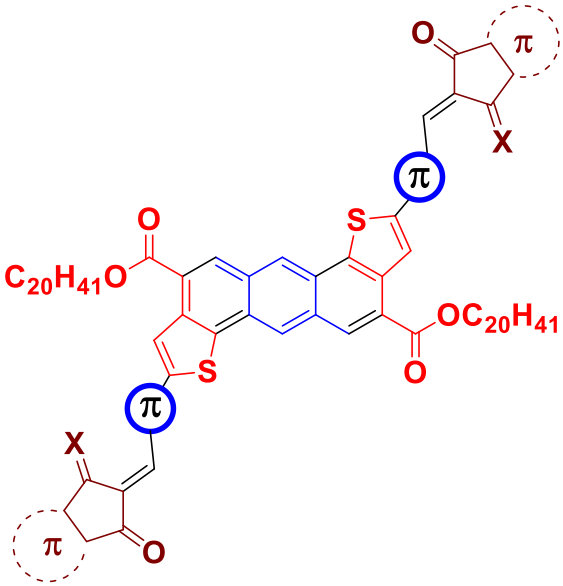

In a dried two neck round bottom flask under Ar, were added intermediate **15** (124 mg, 0.098 mmol), end-cap group (332 mg, 0.98 mmol) and piperidine (100 µL) in dry CHCl3 (2 mL, 0.05 M), the resulting dark red solution was degassed with Ar for 15 min. then was heated at reflux for 16. After 16 h, the resulting deep blue solution was cooled down and the resulting solution was precipitated in cold EtOH. The resulting deep blue solid was filtered off and dried over night to give the desirable **NFA 3** as a deep violet solid (118 mg, 70% yield). ^{1}H (400 MHz, CDCl3): δ= 8.39 (s, 2H), 7.89 (s, 2H), 7.67 (s, 2H), 7.59 (s, 2H), 7.23-7.18 (d, 2H, J= 4Hz), 6.81-6.79 (d, 2H, J= 4Hz), 4.48-4.46 (d, 4H. J= 8Hz), 3.84-3.81 (d, 4H, J=8Hz) 2.13-2.11 (m, 2H),1.64-1.24 (m, 88H), 0.94-0.89 (t, 18H, J= 8Hz) ppm. ^{13}C(100 MHz, CDCl3) δ= 192.24, 167.08, 165.56, 153.67, 150.67, 140.13, 137.23, 133.82, 130.65, 128.96, 127.37, 126.69, 125.02, 124.75, 124.13, 123.92, 68.85, 53.57, 44.90. 37.81, 32.23. 31.98, 31.17, 30.52, 30.14, 30.08, 30.00, 29.73, 29.66, 29.40, 29.27, 27.14, 27.04, 14.40, 14.32, 14.27 ppm. MS (MALDI-TOF): [M]= 1717.758

Chapter 4

Synthesis of novel polymeric nonfullerene acceptors (PMSAs) based on anthradithiophene for bulk heterojunction solar cells (BHJs)

This chapter is partly based on the following publication*: Synthesis of novel polymers no fullerene acceptors (PMSAs) based on anthradithiophene for bulk heterojunction solar cells (BHJs),* G. Forti, R. M. Pankow, A. Nitti, G. Bianchi, R. Po, D. Pasini, T. J. Marks and A. Facchetti, *in preparation*

4.1→ INTRODUCTION

Since their discovery, nonfullerene acceptors (NFAs) have significantly boosted the efficiencies of BHJ cells up to 18%,[166,168,170180] due to their high NIR absorption, and electron mobility and morphology properties, well integrating with the donor components, in the BHJ architectures. Despite their unique benefits compared to the classical fullerene acceptors components such as PCBM61 or PCBM71, they still have some downsides, limiting further improvement of their efficiencies and stability. In the last few years, a novel, promising strategy has been proposed to overcome these problems, based on a new type of solar cells called polymers solar cells (PSCs). In a classical PSC, the active layer is usually made of p and n-type polymers while in the classical BHJ usually the n-type material is a small molecule. This strategy offers several potential advantages such as: a) better thermal and mechanical properties, b)

[180] S. Ellinger, K. Graham, P. Shi, R. Farley, T. Steckler, R. Brookins, P. Taranekar, J. Mei, L. Padilha and T. Ensley, «Donor–Acceptor–Donor-based-Conjugated Oligomers for Nonlinear Op-tics and Near-IR Emission» *Chem. Mater*. **2011**, *23*, 3805.

additional channel for electrons and c) better morphological properties.[181][182] Historically, the first example of n-type polymers, ND2200 (Figure 4.1), has been proposed by Facchetti *et al* [183] in 2009; however only in the last few years firstly with the synthesis of PZ1 by Li *et al.*[184] and secondly with PJ1 by Cao *et al.*[185] the attention on this field has greatly expanded.

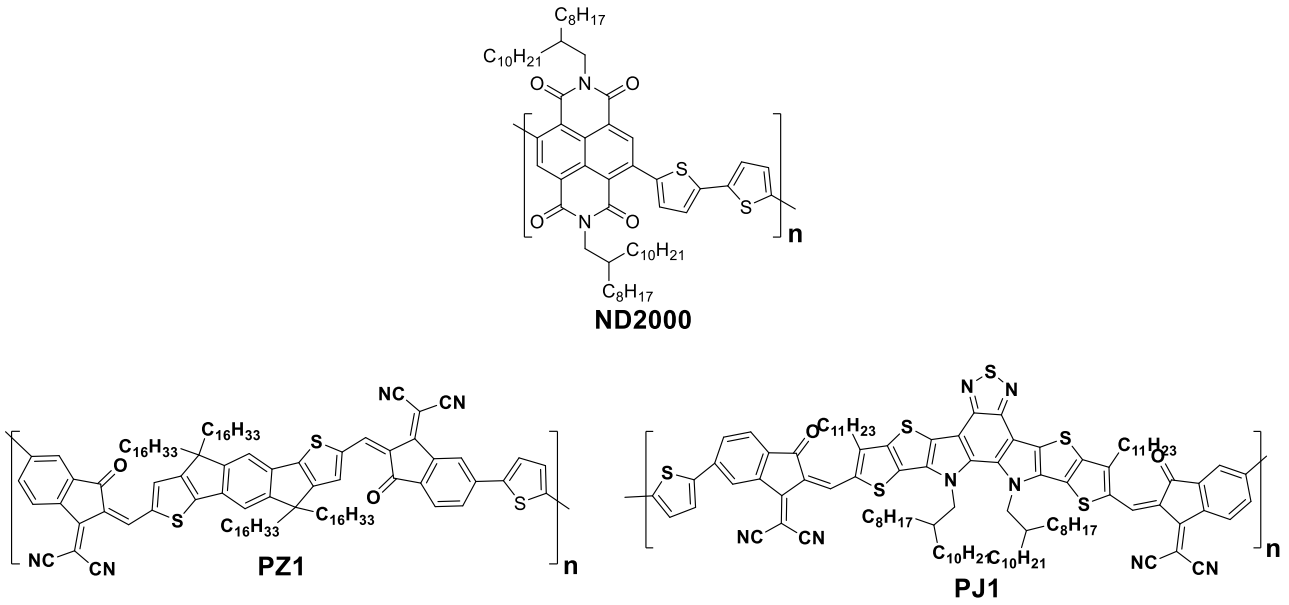

Figure 4.1. Structures of ND2000, PZ1 and PJ1.

[181] Zhang, Z-G.; Li, Y. «Polymerized Small-Molecule Acceptors for High-Performance All-Polymer Solar Cells» *Angew. Chem. Int. Ed*. **2021**, *60*, 4422–4433.

[182] Sun, H.; Guo, X.; Facchetti, A. «High-Performance n-Type Polymer Semiconductors: Applications, Recent Development, and Challenges» *Chem*, **2020**, *6*, 1310–1326.

[183] H. Yan, Z. Chen, Y. N. C. Zheng, J. R. Quinn, F. Dötz, M. Kastler and A. Facchetti, «A high-mobility electron-transporting polymer for printed transistors» *Nature,* **2009***, 457,* 679–686.

[184] Z.-G. Zhang, Y. Yang, J. Yao, L. Xue, S. Chen, X. Li, W. Morrison, C. Yang and Y. Li, «Constructing a Strongly Absorbing Low-Bandgap Polymer Acceptor for High-Performance All-Polymer Solar Cells» *Angew.Chem. Int.Ed.* **2017***, 56,* 13503–13507.

[185] Jia, J. Zhang, W. Zhong, Y. Liang, K. Zhang, S. Dong, L. Ying, F. Liu, X. Wang, F. Huang *et al*. «14.4% Efficiency All-Polymer Solar Cell with Broad Absorption and Low Energy Loss Enabled by a Novel Polymer Acceptor» *Nano Energy*, **2020**, *72*, 104718.

Since then, several examples of polymers acceptors (PMSAs) based on NFA comonomers have been synthesized, essentially varying the p-type co-monomer used. The key limitation for this approach lays in the p-type comonomers available. Despite in both PZ1 and PJ1 the p-type comonomer is thiophene, which is cheap and non-toxic, it does not offer any modulation of the photophysical and photovoltaic properties, limiting its use in PSC. Therefore, much complex and expensive co-monomers have been used to achieve higher power conversion efficiency PCE (Figure 4.2).[178186]

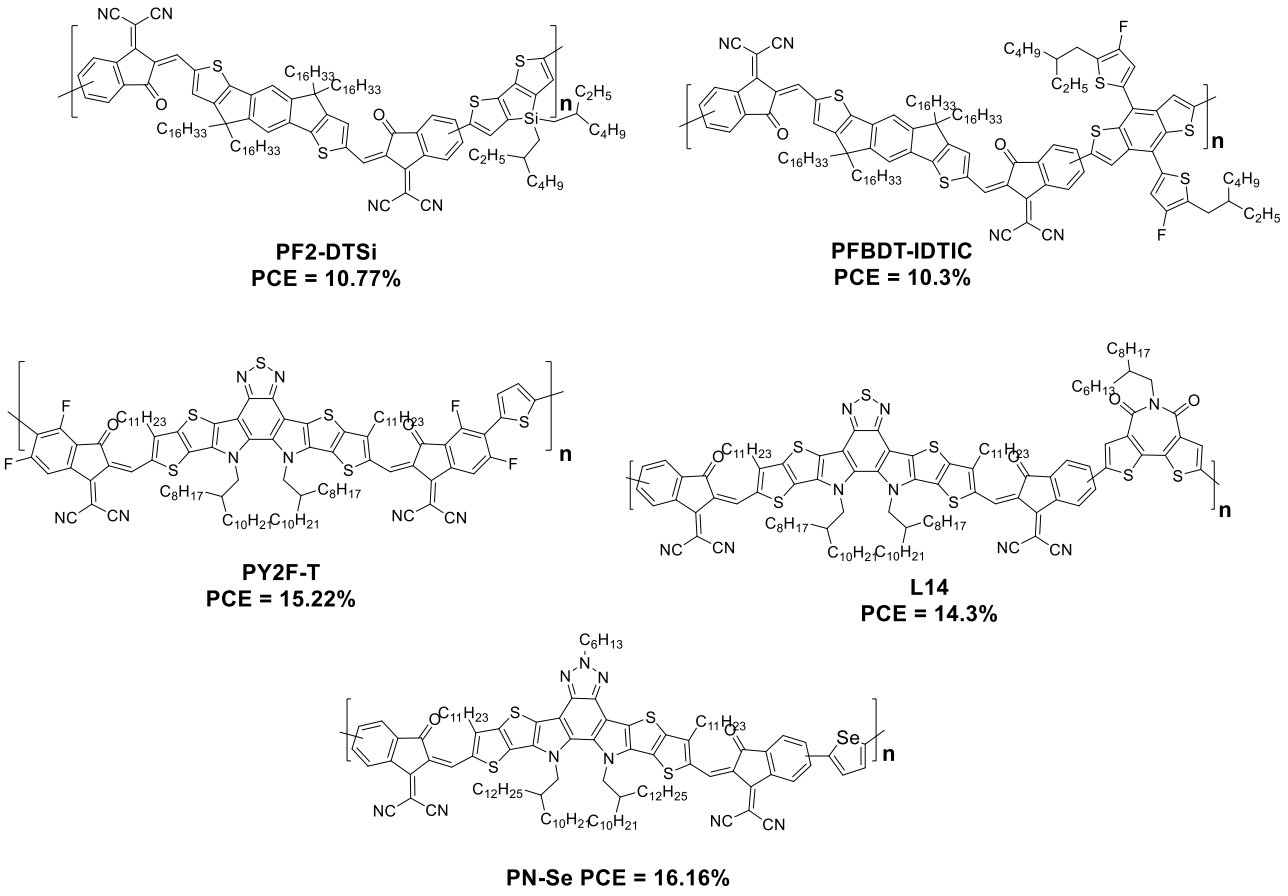

Figure 4.2. Recent PMSAs

[186] H. Yu, M. Pan, R. Sun, I. Agunawela, J. Zhang, Y. Li, Z. Qi, H. Han, X. Zou, W. Zhou, S. Chen, J. Y. L. Lai, S. Luo, Z. Luo, D. Zhao, X. Lu, H. Ade, F. Huang, J. Min and H. Yan, «A Difluoro-Monobromo End Group Enables High-Performance Polymer Acceptor and Efficient All-Polymer Solar Cells Processable with Green Solvent under Ambient Condition» *Adv. Funct. Mater.* **2021***, 31,* 2100791.

It is clear that, to achieve high efficiencies, the synthetic complexity of monomers increases, resulting in higher costs and long, difficult and not potentially scalable syntheses. Cheap and easily available co-monomers must be used to overcome the above-mentioned problems; for that reason, we decided to use ADT (Figure 4.3a),[187] already made in our group, as new co-monomer for the synthesis of novel PMSAs.

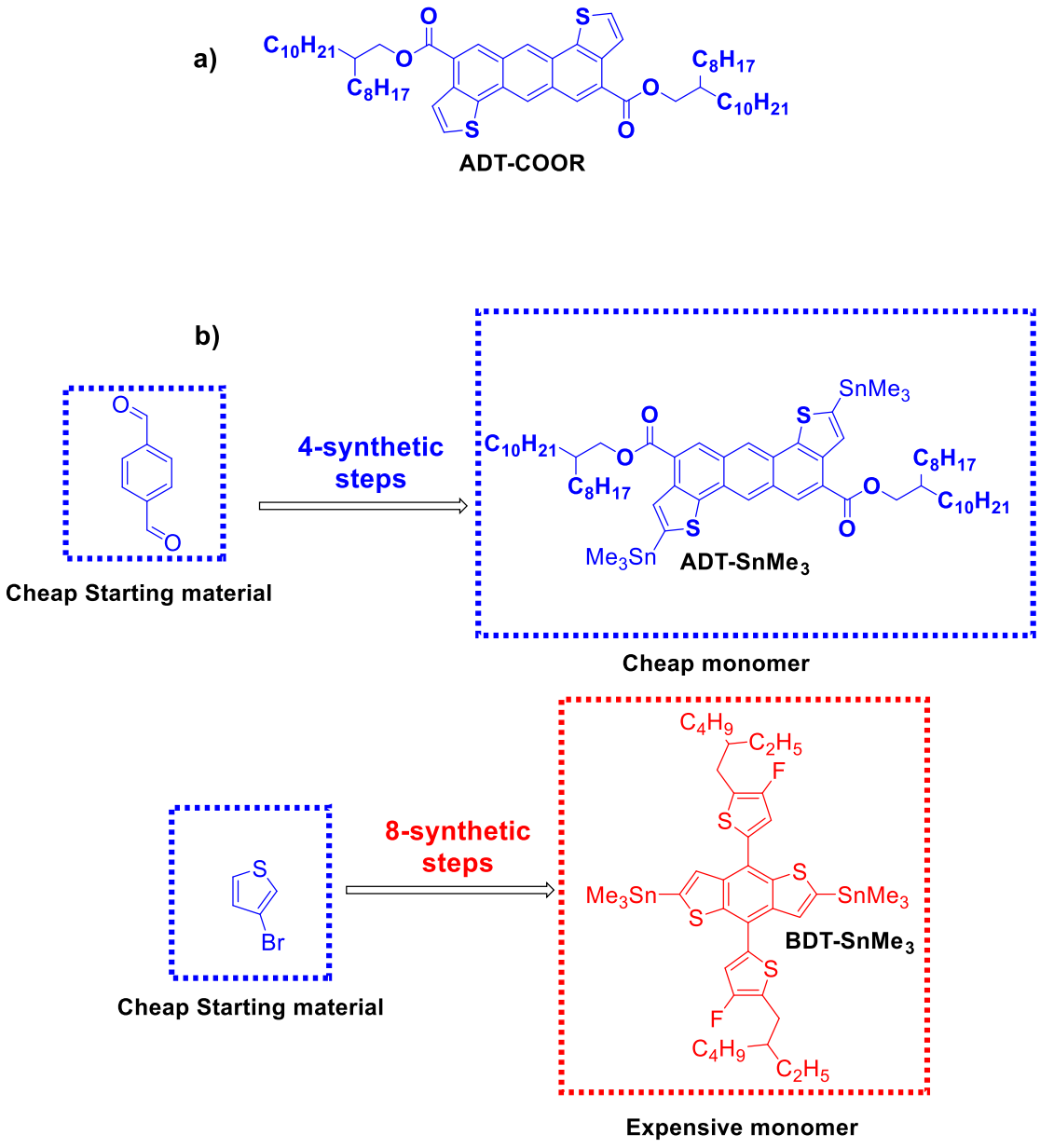

Figure 4.3: a) ADT molecule, b) BDT-SnMe$_3$ and ADT-SnMe$_3$ comparison

[187] A. Nitti, G. Forti, G. Bianchi, C. Botta, F. Tinti, M. Gazzano, N. Camaioni, R. Po and D. Pasini, «Anthradithiophene-Based Organic Semiconductors through Re-giodirected Double Annulations,» *J. Mater. Chem. C,* **2021**, *9,* 9302–9308.

Compared to BDT-$SnMe_3$ which requires at least 8 synthetic steps, ADT-$SnMe_3$ can be made in 4 steps in high yield and multi gram scale, which makes it suitable from an industrial point of view (Figure 4.3b), we decided, therefore, to co-polymerize it with the most used NFA cores such as IDIC, NDI and Y6 (Figure 4.4).

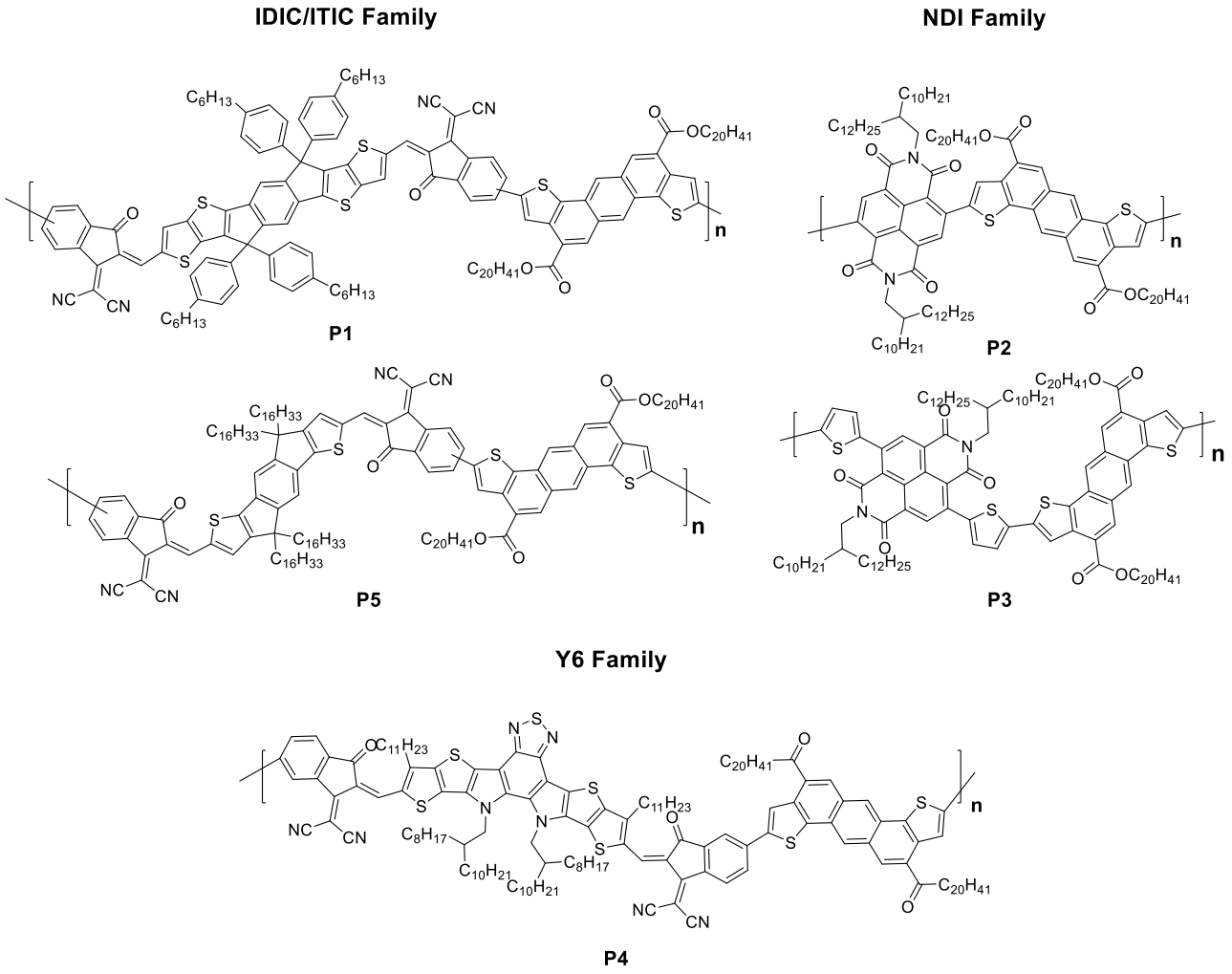

Figure 4.4. PMSAs based on ADT monomer.

4.2→ RESULTS AND DISCUSSION

The retro-synthetic pathway for ours PMSAs start from ADT-COOR which has been stannylated in presence of LDA to generate intermediate **2** followed by Stille cross-coupling with the corresponding NFAs-Br core (Scheme 4.1)

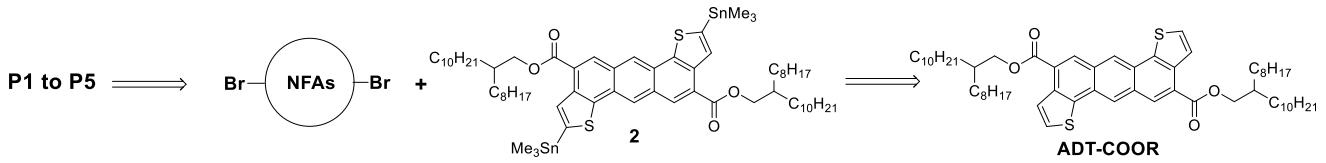

Scheme 4.1. Retrosynthetic pathway.

Intermediate 2 was obtained in high yield followed our previous work (see Chapter 3). Stille reactions were conducted in presence of $Pd_2(dba)_3$ and P(*o*-tolyl)$_3$ as palladium source and ligand respectively, allowing us to isolate in high yield polymers **P1** to **P5** (Scheme 4.2) in good to excellent yields, after purification by an initial precipitation, and several Soxhlet extractions, as detailed in the experimental section.

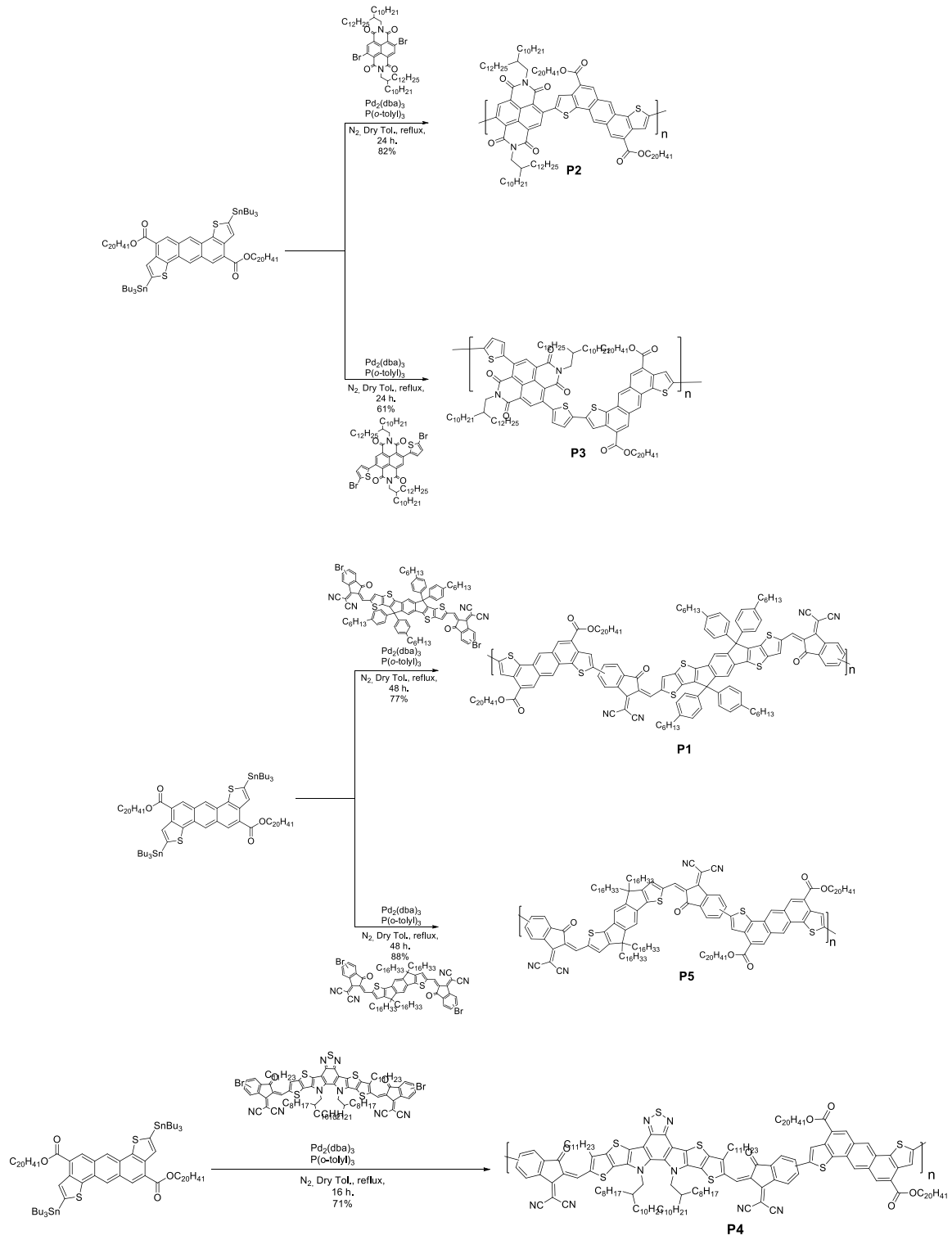

Scheme 4.2. Stille polymerization conditions for the synthesis of **P1-P5**.

Photophysical characterization. The identity and purity of **P3**,**4** and **P5** were assessed by ^{1}H NMR and elemental analysis (EA). these PSMAs show good solubility in common organic solvents such as chloroform (CF) and chlorobenzene (CB). The number-average molecular masses (M_n) of the polymers were measured to be 72.8 kDa ($Đ$ = 2.95), 34.5 kDa ($Đ$ = 2.64) and 23.3 kDa ($Đ$ = 1.76) for **P3**, **P4** and **P5**, respectively, by high-temperature GPC (150 °C), calibrated with polystyrene standards using trichlorobenzene as eluent (Figure 4.S9-11 in the appendix). Polymers **P1** and **P2**, instead, did not show an optimal solubility for GPC. **P3**, **P4** and **P5** polymers have excellent thermal stability with a decomposition temperature (Td) above 310 °C (5% weight loss onset), as shown by TGA (Figure 4.S8). Furthermore, DSC plots (Figure 4.S9) reveal no obvious thermal transitions for both polymers in the 50−300 °C range, which portend excellent blend morphological stability in APSC active layers. The optical absorption spectra of the solutions and neat films of **P1, P2, P3, P4** and **P5** are shown in Figure 4.5a and 4.5b. **P1** and **P5** show principal maxima at 691 nm (solutions) and 701 nm (films) and 695 (solution)/696 (film) nm, respectively. **P4** showed a strong near IR absorption with principal maxima at 748 nm (solution) and 775 nm (film) respectively, indicating a strong aggregation in thin film. Polymers **P2** and **P3** show remarkable differences in terms absorption profile: while **P3** shows a principal maxima at 658 nm (solution) and a 673 nm (film) respectively, **P2** shows the same principal maxima located at 577 nm in both solution and film, respectively, likely originated from a not optimal conjugation along the backbone due to a higher dihedral angle between ADT and NDI moiety. Cyclic voltammetry (CV) measurements on **P1** to **P5** were carried out to estimate the LUMO and HOMO energies of these systems (Figure 4.5c). The LUMO levels of **P1, P2, P3; P4** and **P5** are −3.83/−5.43 eV, -3.87/-5.93 eV, -3.90/-5.94 eV, -3.82/-5.71 eV and -4.06/-5.69 eV respectively. The CV data point towards the use of PM6 and PBDB-T donor polymers, which have MO energies compatible with the new acceptors, with PM6 offering an obvious advantage to increase APSC V_{oc} values.

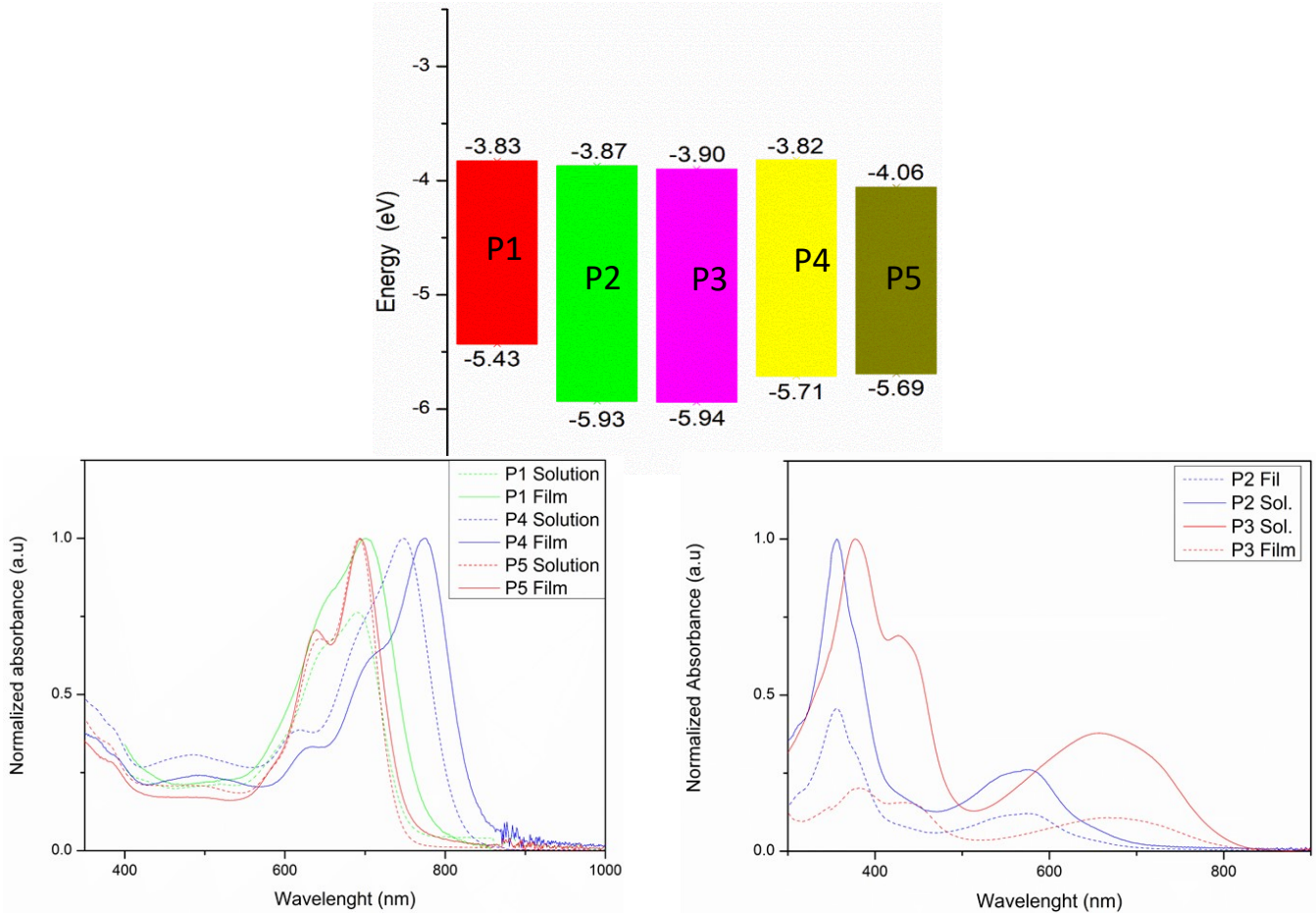

Figure 4.5. Top: HOMO/LUMO levels of polymers **P1** to **P5**. Bottom: a) UV/Vis spectra of **P1**, **P4** and **P5** in solution (dot line) and film (line); b) UV/Vis spectra of **P2** and **P3** in solution (dot line) and film (line);

Photovoltaic characterization. Polymers **P3**, **P4** and **P5** were tested to evaluate their efficiencies, with PM5 and PM6 as suitable donor materials for our devices. **P3** was tested with both conventional and inverted architecture; however, only with a conventional architecture ITO/PEDOT/**P3**:PM5/PDINN/Ag we were able to observe a PCE=1.43%. **P4** was tested with both conventional and inverted architecture; however, only with a conventional architecture ITO/PEDOT/**P4**:PM5/PDINN/Ag we were able to observe a PCE=5%. **P5** was tested with an inverted architecture ITO/ZnO/BHJ/MoO_3/Ag showing a PCE=3.95% (Table 4.1). Despite several efforts our devices did not show high efficiencies, to be mainly ascribed to the lower J_{sc} and FF(%) observed (Figure 4.S12). Generally speaking, low values of FF(%)

can be attributed to bimolecular recombination of the charges while low values of J_{sc} indicate a problem in excitons formation and dissociation.[188][189] So far, we have not found the reasons behind that, we are still investigating our polymers to understand in deep what could be the problem.

Table 4.1: Photovoltaic properties

Donor	**Acceptor**	**J_{sc}**	**V_{oc}**	**FF(%)**	**PCE**
PBDB-T	**P3**	4.70	0.87	0.35	1.43
PBDB-T	**P4**	12.69	0.87	0.46	5.00
PBDB-T-F	**P5**	8.79	0.84	0.52	3.95

Morphological characterization. The crystallinity and chain packing of **P3**, **P4** and **P5** blend films were studied by grazing incidence wide-angle X-ray scattering (GIWAXS; Figure 4.6). All polymers adopt a preferential π-face on chain orientation with (100) diffraction peaks at 0.26-0.28 $Å^{-1}$ in the in-plane direction and distinct (010) diffraction peaks at 1.61−1.68 $Å^{-1}$ in the out-of-plane direction (Figure 4.S14). The resulting lamellar and π−π stacking distances calculated from the (100) and (010) reflections are 23.92, 22.10, and 23.40. Å and 3.89, 3.77, 3.74 Å for **P3**, **P4** and **P5**, respectively (Table 4.S3). While for **P3** the latter values are significantly longer than in Y5-based PSMAs (∼3.8 Å),[190][191] **P4** and **P5** show shorter values, indicating tight π−π stacking interactions between end-cap groups and the donor materials. The lamellar and π−π crystal coherence lengths (CCL) were also calculated using the full-width at half-maxima of the corresponding reflections. **P3** shows a larger lamellar CCL of 5.41 nm than

[188] L. Wu, H. Zang, Y.-C. Hsiao, X. Zhang and B. Hu, « Wu, Lili; Zang, Huidong; Hsiao, Yu-Che; Zhang, Xitian; Hu, Bin. «Origin of the fill factor loss in bulk-heterojunction organic solar cells» *Appl. Phys. Lett.* **2014***, 104,* 153903.

[189] K. Vandewal, A. Gadisa, W. D. Oosterbaan, S. Bertho, F. Banishoied, I. V. Severen, L. Lutsen, T. J. Cleij, D. Vanderzande and J. V. Manca, «The Relation Between Open-Circuit Voltage and the Onset of Photocurrent Generation by Charge-Transfer Absorption in Polymer : Fullerene Bulk Heterojunction Solar Cells,» *Adv. Funct. Mater*. **2008**, *18*, 2064–2070.

[190] A. Tang, J. Li, B. Zhang, J. Peng and E. Zhou, «E. Low-Bandgap nType Polymer Based on a Fused-DAD-Type Heptacyclic Ring for AllPolymer Solar Cell Application with a Power Conversion Efficiency of 10.7%» *ACS Macro Lett.* **2020***, 9,* 706−712.

[191] W. Wang, Q. Wu, R. Sun, J. Guo, Y. Wu, M. Shi, W. Yang, W. H. Li and J. Min, «Controlling Molecular Mass of Low-Band-Gap Polymer Acceptors for High-Performance All-Polymer Solar Cells,» *Joule* **2020***, 4,* 1070-1086.

the 2.71 nm and 3.71 nm for **P4** and **P5** nm respectively. Furthermore, **P3** exhibits the lowest π–π CCL value of 0.98 nm than the 1.35 nm ,1.48 nm of **P4** and **P5**, indicating somewhat smaller crystallite sizes.

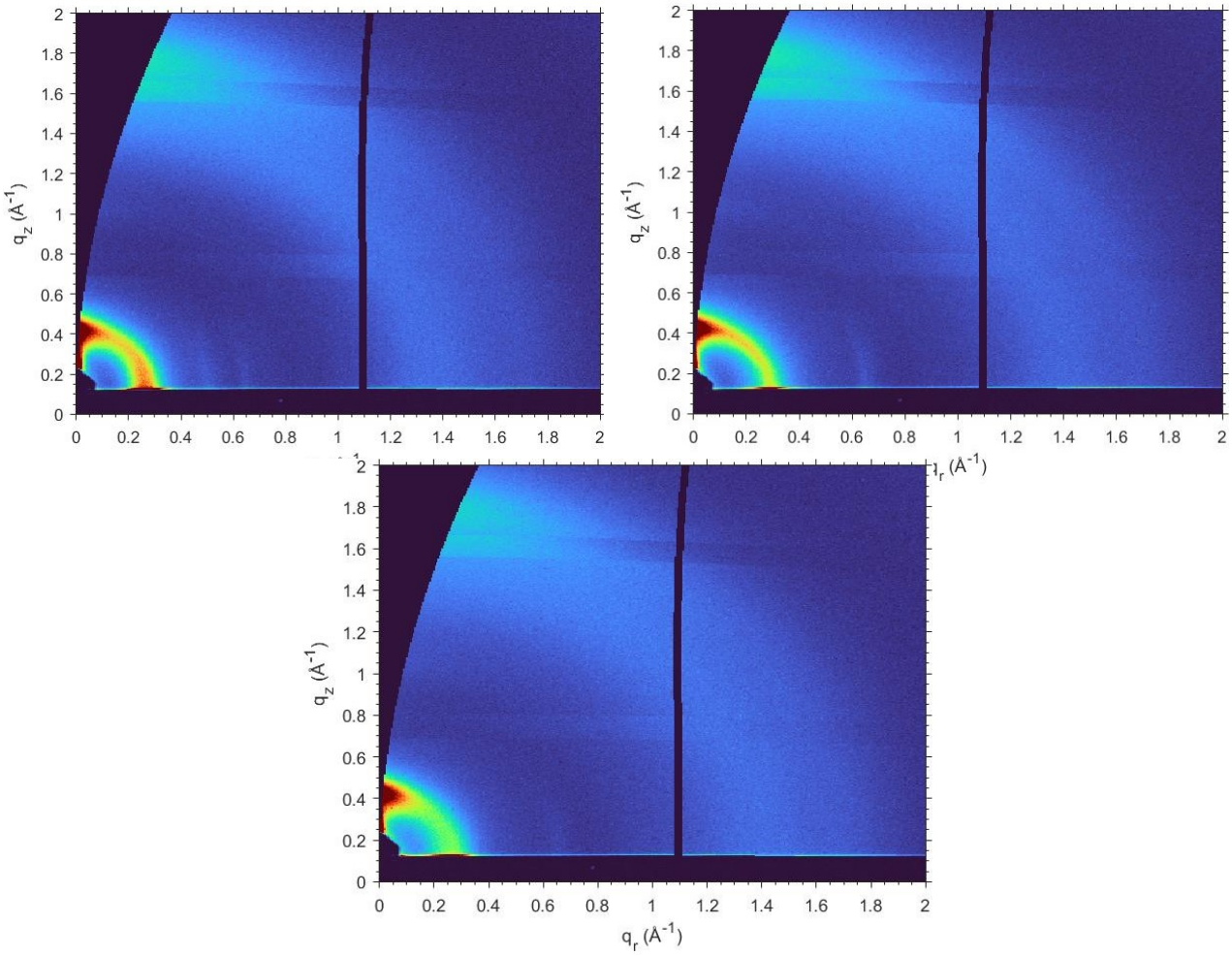

Figure 4.6. GIWAXS diffraction pattern polymers **P3** (top left), **P4** top right) and **P5 (**bottom).

4.3→ CONCLUSION

In conclusion we were able to synthesize different polymers acceptors (**P1** to **P5**) in very high yield. Polymers **P3** to **P5** were structurally characterized, showing comparable properties with the already known PMSAs in terms of HOMO/LUMO levels, absorption profile and molecular weight. Photovoltaic properties have been studied using as polymers donor PM5 and PM6; preliminary results showed a low efficiency for ADT-NFAs polymers, mainly ascribed to the low values of FF(%) and J_{sc} observed in our

devices. Polymers **P3** to **P5** are currently still under investigation and optimization, to understand in deep the origin of these low efficiencies.

4.4→ EXPERIMENTAL PART

1.General experimental

NMR spectra were recorded on a Bruker Avance III HD 500MHz system equipped with a TXO Prodigy probe. Chemical shifts for 1H and 13C spectra are referenced to residual protio-solvent signals (δ 1H = 7.26 for $CDCl_3$ and ^1H = 5.973 for $C_2D_2Cl_4$ δ 13C = 77.16 for $CDCl_3$) and chemical shifts are reported in ppm. Polymer molecular weights were measured on a Polymer Laboratories PL-GPC 220 instrument at 150 ºC calibrated with polystyrene standards and using trichlorobenzene as eluent. UV-Vis absorption spectra were recorded on a Varian Cary 100 UV-vis spectrophotometer. Elemental analyses (EA) of product polymers were carried out at Midwest Microlabs Inc. All reactions were carried out under an N2 atmosphere, and all starting materials and solvents were purchased from commercial suppliers and used without further purification. PBDB-T and PM6 were purchased from Derthon Optoelectronic Materials ScienceTechnology Co.

2. Morphology and Microstructure Analysis

Grazing-incidence wide-angle x-ray scattering (GIWAXS) measurements were performed at beamLine 8ID-E at the Advanced Photon Source at Argonne National Laboratory. The samples were irradiated at incidence angles from 0.130° to 0.140° in vacuum at 10.915 keV for two summed exposures of 2.5 s each. Signals were collected with a Pilatus 1M detector located at a distance of 228.16 mm from the samples. Blend films for GIWAXS were prepared according to the procedure for photovoltaic devices.

3. Device fabrication

Solar cells were fabricated in a conventional device configuration of ITO/PEDOT:PSS/active layers/ PDINN/Ag. The ITO substrates were scrubbed with detergent and then sonicated with deionized water, acetone, and isopropanol, then subsequently dried overnight in an oven. The glass substrates were treated with UV-ozone for 30 min before use. PEDOT:PSS (Heraeus Clevios P VP AI 4083) was spin-cast onto the ITO substrates at 4000 rpm for 30 s, and then dried at 150 °C for 15 min in air. The donor:acceptor blends (1:1 or 2:1 weight ratio) were dissolved in chloroform/chlorobenzene (total concentrations =10, 14 and 16 mg/mL for **P3**, **P4** and **P5** respectively), and stirred overnight in a nitrogen-filled glove box.

The solution was then spin-cast at 3500 rpm for 60 s onto PEDOT:PSS film, after being kept on a 65 °C hotplate for 30 min.. A thin PDINN layer was coated on the active layer, followed by the deposition of Ag (evaporated under 5×10^{-4} Pa through a shadow mask). The optimal active layer thickness measured by a Bruker Dektak XT stylus profilometer was about 110 nm. The current densityvoltage (J-V) curves of all encapsulated devices were measured using a Keithley 2400 Source Meter in the air under AM 1.5G (100 mW cm^{-2}) using a Newport solar simulator. The light intensity was calibrated using a standard Si diode (with KG5 filter, purchased from PV Measurements to bring spectral mismatch to unity). An optical microscope (Olympus BX51). Devices with an inverted device architecture of ITO /ZnO (~25 nm) /Active layer(90 -100 nm) /MoO_3 (10 nm)/Ag (100 nm) were also fabricated. Pre-patterned ITO-coated glass wafers (Thin Film Devices, Inc.) with a sheet resistance of ≈20 Ω/sq were used as substrates. The ZnO precursor solution is prepared by dissolving 220 mg of zinc acetate dehydrate (Sigma Aldrich) and 62 mg of 2-ethanolamine (Sigma Aldrich) in 2 mL 2-methoxyethanol (Sigma Aldrich), then stir overnight. The ZnO precursor is spin-coated on precleaned ITO glass at 7000 rpm after filtering through a 0.45 μm PVDF filter and 20 min at 170°C in air. Then the device is transferred into an argon glove box. After that, active layer solutions (14 to 16 mg/mL in total) were then spin-coated onto the ZnO layer (Argon filled glovebox) while spinning 3000 RPM depending on viscosity to achieve appropriate thicknesses of 90~100 nm. All the substrates were loaded into a metal-evaporation chamber and with a mask of dimensions of mm 2. Then these substrates were vapor-deposited with a molybdenum oxide interlayer (10 nm) and silver (100 nm) electrode at high vacuum (~6 x 10^{-6} Torr). All the devices were measured under simulated AM1.5G irradiation (100 mW cm^{-2}) illumination with a standard ABET Sun 2000 Solar Simulator in the air. A standard silicon solar cell was used to calibrate the light intensity. The voltage was scanned from 1.20 V to -0.20 V.

4. Synthesis of New Compounds

General procedure fot the synthesis of polymer P1 to P5

In an oven dried Schlenk tube were added intermediate 2 (1 eq.) NFA-Br (1 eq.), $Pd_2(dba)_3$ (0.04 eq) and P(*O*-Tolyl)$_3$ (0.16 eq.) in previously degassed dry Tol. (0.3M). The resulting blue solution was stirred at 110 °C for 16-48h. After cooling to room temperature, the solution was slowly added to methanol and the resulting precipitates were collected by filtration and washed in a Soxhlet extractor with methanol, hexane, acetone, dichloromethane, and chloroform. The chloroform fraction was precipitated with methanol, dried under vacuum at 50 °C overnight to obtain the polymer acceptors.

Synthesis of P1

In an oven dried Schlenk tube were added intermediate **2** (100 mg, 0.066 mmol) ITIC-Br (105 mg, 0.066), $Pd_2(dba)_3$ (1.20 mg, 0.00132 mmol) and P(*O*-Tolyl)$_3$ (1.60 mg, 0.00528 mmol) in previously degassed dry Tol. (2 ml, 0.03M). The resulting blue solution was stirred at 110 °C for 48h. **P1** was obtained as black solid (98 mg, 71% yield) after Soxhlet (CF). ^{1}H VT-NMR 120°C (600 MHz, $C_2D_2Cl_4$) δ: 9.20-9.18 (m, 1H), 8.98-8.85 (m, 7H), 8.50-8.48 (m, 2H), 8.29-8.28 (m, 1H), 8.09 (m, 1H), 7.96 (m, 1H), 7.78-7.74 (m, 3H), 7.36-7.26 (m, 22 H), 4.58-4.54 (m, 4H), 2.72 (s, 11H), 2.13-2.08 (m, 2H), 1.63-1.37 (m, 118H), 0.97 (s, 37H) ppm. Elem. Anal. calc. For $[C_{1162}H_{174}N_4O_6S_8]_n$: C, 76.92; H, 6.93; N, 2.21. Found: C, 50.52, H, 5.10, N, 1.43.

Synthesis of P2

In an oven dried Schlenk tube were added intermediate **2** (100 mg, 0.066 mmol) NDI-Br (73mg, 0.066 mmol), $Pd_2(dba)_3$ (1.20 mg, 0.00132 mmol) and P(*O*-Tolyl)$_3$ (1.60 mg, 0.00528 mmol) in previously degassed dry Tol. (2 ml, 0.03M). The resulting blue solution was stirred at 110 °C for 24h. **P2** was obtained as violet solid (101 mg, 82% yield) after Soxhlet (Hexane). ^{1}H VT-NMR 120°C (600 MHz, $C_2D_2Cl_4$) δ: 9.02-8.58 (m, 10H), 4.43-4.40 (m, 4H), 4.19-4.15 (m, 4H), 2.02 (m, 4H), 1.57-0.84 (m, 303H) ppm. Elem. Anal. calc. For $[C_{130}H_{194}N_2O_8S_4]_n$: C, 76.49; H, 9.58; N, 1.37. Found: C, 75.62, H, 9.49, H, 1.65.

Synthesis of P3

In an oven dried Schlenk tube were added intermediate **2** (84.2 mg, 0.055 mmol) NDI-T-BR (70 mg, 0.055 mmol), $Pd_2(dba)_3$ (1.0 mg, 0.0011 mmol) and P(*O*-Tolyl)$_3$ (1.35 mg, 0.0044 mmol) in previously degassed dry Tol. (1.7 ml, 0.03M). The resulting blue solution was stirred at 110 °C for 24h. **P3** was obtained as black deep violet solid (75 mg, 61% yield) after Soxhlet (CF). ^{1}H VT-NMR 120°C (600 MHz, $C_2D_2Cl_4$) δ: 8.97-8.70 (m, 7H), 8.70-8.40 (m, 4H), 7.66-7.22 (m, 7H), 4.56(s, 4H), 4.24-4.21 (m, 4H), 2.23-2.10 (m, 4H), 1.51-1.33 (m, 157H), 0.98-0.93 (m, 27H) ppm. Elem. Anal. calc. For $[C_{138}H_{198}N_2O_8S_6]_n$: C, 75.15; H, 9.05; N, 1.27. Found: C, 74.58, H, 8.94, N, 1.65.

Synthesis of P4

In an oven dried Schlenk tube were added intermediate **2** (81 mg, 0.053 mmol)) Y6-Br (100 mg, 0.053 mmol), $Pd_2(dba)_3$ (1.0 mg, 0.0011 mmol) and P(*O*-Tolyl)$_3$ (1.3 mg, 0.0043 mmol) in previously degassed dry Tol. (1.6 mL, 0.03 M). The resulting blue solution was stirred at 110 °C for 16h. **P4** was obtained as

black solid (93 mg, 71% yield) after Soxhlet (CF). ^{1}H VT-NMR 120°C (600 MHz, $C_2D_2Cl_4$) δ: 9.29-7.65 (m, 15H), 4.93-4.90 (m, 4H), 4.62-4.55 (m, 4H), 3.37 (s, 2H), 2.27-2.07 (m, 4H), 1.70-0.92 (m, 171H) ppm. Elem. Anal. calc. For $[C_{174}H_{230}N_8O_6S_9]_n$: C, 74.15; H, 8.23; N, 3.98. Found: C, 74.01, H, 8.37, N, 4.48.

Synthesis of P5

In an oven dried Schlenk tube were added intermediate **2** (220 mg, 0.145 mmol) IDIC-Br (250 mg, 0.145 mmol), $Pd_2(dba)_3$ (2.7 mg, 0.003 mmol) and P(*O*-Tolyl)$_3$ (3.5 mg, 0.0116 mmol) in previously degassed dry Tol. (4 mL). The resulting blue solution was stirred at 110 °C for 48h. **P5** was obtained with 85% yield after Soxhlet. ^{1}H VT-NMR 120°C (600 MHz, $C_2D_2Cl_4$) δ: 9.28-9.25 (m, 2H), 9.09-8.87 (m, 8H), 8.49 (s, 2H), 8.33 (s, 3H), 8.14 (s, 3H), 7.98-7.89 (m, 3H), 7.79-7.76 (m, 3H), 4.60 (s, 4H), 2.24-2.12 (m, 10H), 1.62-0.94 (m, 168H) ppm. Elem. Anal. calc. For $[C_{174}H_{238}N_4O_6S_6]_n$: C, 78.15; H, 8.97; N, 2.10. Found: C, 73.49, H, 8.89, N, 2.38.

Chapter 5

Synthesis of novel polymeric nonfullerene acceptors (PMSAs) via DARP

5.1→ INTRODUCTION

Polymers small molecule acceptors (PMSAs) are a promising new type of acceptors that combine a small NFA into a polymer chain, leading to some unique properties.[185] [186] From a synthetic point of view, PMSAs require a Stille cross-coupling between an NFA-Br and the corresponding tin intermediate (the π-spacer, Figure 5.1); this often results in complicated and long synthesis to afford the tin intermediates, which also have the downsides to be toxic and not very stable. The development of a new sustainable route to achieve these molecules can help us to avoid the mentioned above problems and increase the overall sustainability for PMSAs. Among the possible polymerization method, the most promising so far is the direct arylation polymerization (DARPs), due to its capability to perform a C-C coupling without using any intermediate (Figure 5.1).[192][193][194] Despite this huge step forward to the reduction of waste and

[192] Pouliot, J-R.; Grenier, F.; Blaskovits, J. T.; Beaupré, S.; Leclerc, M. «Direct (Hetero)arylation Polymerization: Simplicity for Conjugated Polymer Synthesis, » *Chem. Rev.* **2016**, *116*, 14225–14274.

[193] Bohraa, H; Wang, M. «Direct C–H arylation: a "Greener" approach towards facile synthesis of organic semiconducting molecules and polymers, » J. Mater. Chem. A, **2017**, *5*, 11550-11571.

[194] Kuwabara, J.; Kanbara, T. «Step-Economical Synthesis of Conjugated Polymer Materials Composed of Three Components: Donor, Acceptor, and π Units, » *Macromol. Rapid Commun.* **2021***, 42,* 200493.

synthetic steps, DARPs has some significant drawbacks such as a) substrate dependency, b) low molecular weights obtained, and c) defects, which still limit its uses.[195][196][197][198][199]

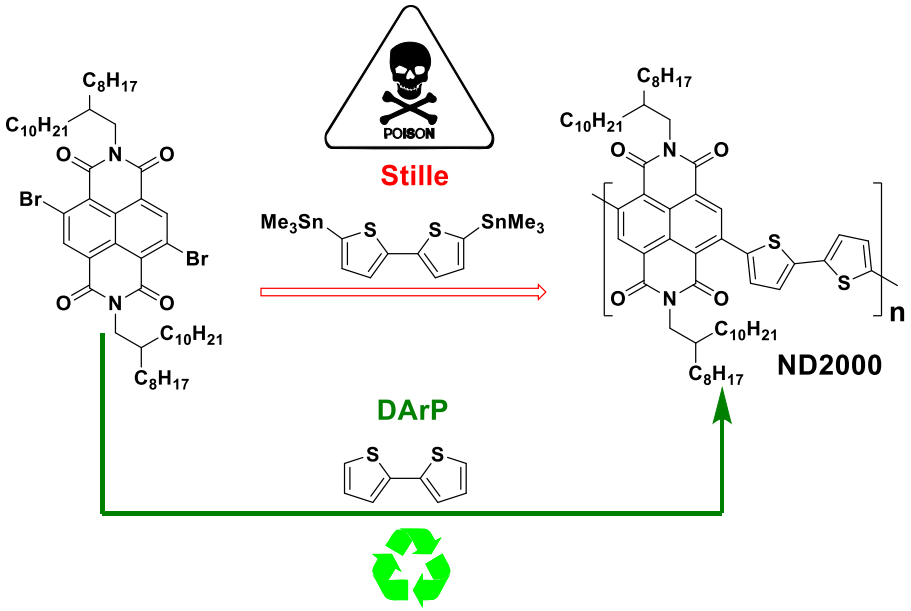

Figure 5.1. A comparison between the Stille reaction and the DARP reaction for ND2000.

[195] N. S. Gobalasingham and B. C. Thompson, «Direct arylation polymerization: A guide to optimal conditions for effective conjugated polymers» *Progress in Polymer Science,* **2018***, 83,* 135-201.

[196] R. M. Pankow and B. C. Thompson, «Approaches for improving the sustainability of conjugated polymer synthesis using direct arylation polymerization (DArP)» *Polym. Chem.* **2020***, 11,* 630-640.

[197] M. Leclerc, S. Brassard and S. Beaupré, *Polym. J.* **2020**, *52*, *13–20*.

[198] K. Nakabayashi, «Direct arylation polycondensation as conjugated polymer synthesis methodology» *Polym. J.* **2018**, *50*, 475–483.

[199] A. Nitti, R. Po, G. Bianchi and D. Pasini, «Direct Arylation Strategies in the Synthesis of π-Extended Monomers for Organic Polymeric Solar Cells» *Molecules* **2017***, 22,* 21.

While, DARP has been extensively used for the synthesis of donor polymers,[200][201][202] showing in some case better results than Stille ones, it has rarely been applied, despite few examples[203][204], to high performance acceptor polymers. The main reason behind this choice is related to the intrinsic structures of NFAs, which have side reaction sites that may lead to defects (Figure 5.2). Taking this into account, we decided to pursue this strategy to evaluate the feasibility for this type of reaction over NFAs cores.

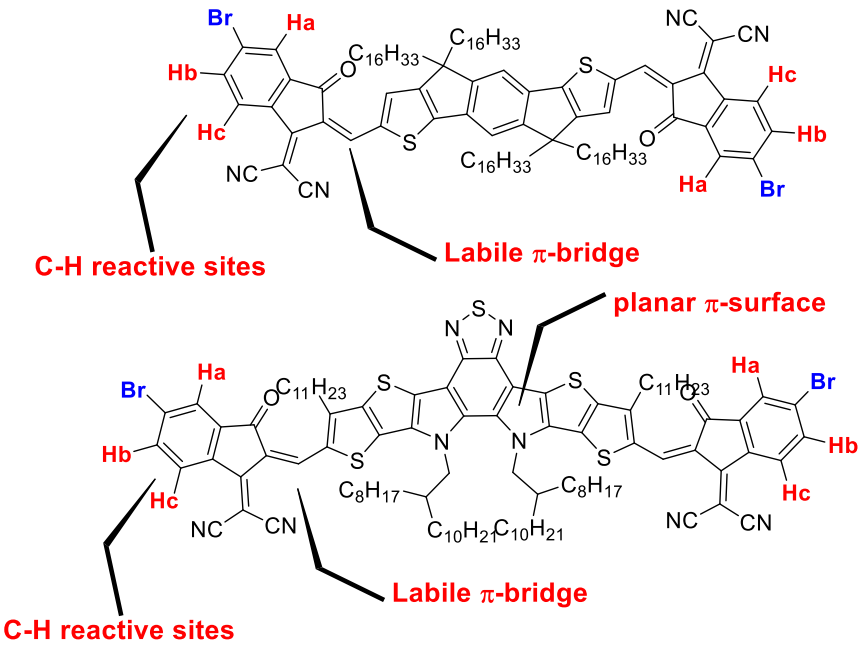

Figure 5.2. Reaction sites in NFAs which may lead to defects.

[200] X. Wanga and M. Wang, «Synthesis of donor–acceptor conjugated polymers based on benzo[1,2-b:4,5-b′]dithiophene and 2,1,3-benzothiadiazole via direct arylation polycondensation: towards efficient C–H activation in nonpolar solvents» *Polym. Chem.* **2014**, *5,* 5784-5792.

[201] N. S. Gobalasingham, R. M. Pankow, S. Ekiza and B. C. Thompson, «Evaluating structure–function relationships toward three-component conjugated polymers via direct arylation polymerization (DArP) for Stille-convergent solar cell performance» *J. Mater. Chem. A* **2017**, *5,* 14101-14113.

[202] M. Zhang, X. Guo, S. Zhang and J. Hou, «Synergistic Effect of Fluorination on Molecular Energy Level Modulation in Highly Efficient Photovoltaic Polymers» *Adv. Mater.* **2014**, *26,* 1118–1123.

[203] R. Matsidik, H. Komber, A. Luzio, M. Caironi and M. Sommer, «Defect-free Naphthalene Diimide Bithiophene Copolymers with Controlled Molar Mass and High Performance via Direct Arylation Polycondensation» *J. Am. Chem. Soc.* **2015**, *137,* 6705–6711.

[204] A. Robitaille, S. A. Jenekhe and M. Leclerc, «Poly(naphthalene diimide-alt-bithiophene) Prepared by Direct (Hetero)arylation Polymerization for Efficient All-Polymer Solar Cells» *Chem. Mater.* **2018**, *30,* 5353–5361.

5.2→ RESULTS AND DISCUSSION

We have chosen to consider as PMSAs the following polymers already made via Stille polymerization (Figure 5.3).

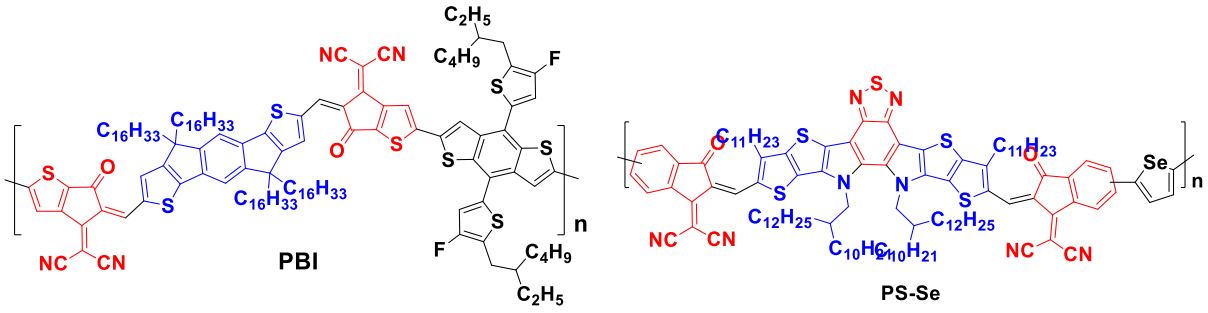

Figure 5.3. Reference PMSAs

We decided to investigate the DARPs feasibility for PBI due to its simpler end-cap groups, and we decided to use 2,2 -bithiophene as model substrate instead of BDT due to its excessive cost. We used "modified Ozawa conditions" to perform this reaction as reported in the following Scheme 5.1.

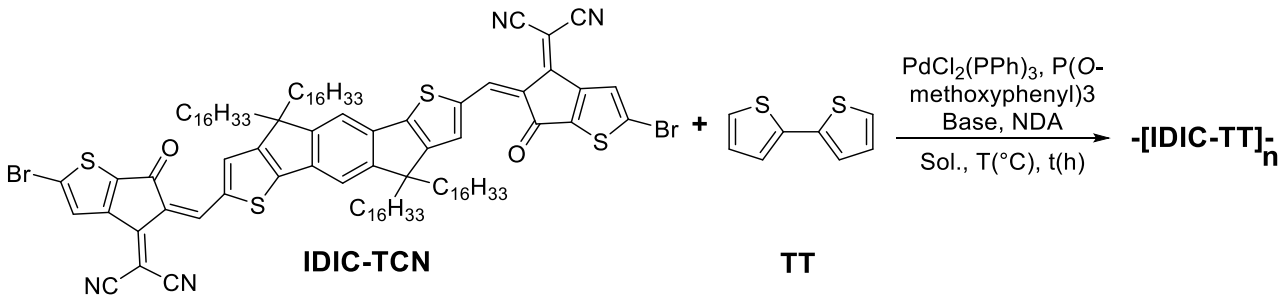

Scheme 5.1. Test reaction 1

We tested different bases, temperatures, and concentrations; however, from Table 5.1 we can clearly see that in all entries, a small amount of -CHO defects were observed.

Table 5.1. Conditions for test reaction 1

Entry	*Base*[a]	*Solv.*[b]	*T(°C)*	*t(h)*	*Reaction yield (%)*[c]	*-CHO(%) defect*[d]
1	Na_2CO_3	Tol. (0.5M)	110	16	40%	3
2	K_2CO_3	Tol. (0.5M)	90	16	50%	6
3	K_2CO_3	Tol. (0.3M)	110	16	43%	7
4	K_2CO_3	Tol. (0.3M)	110	8	25%	2

a) Dry base; b) Dry solvent; c) Calculated after Soxhlet; d) Calculated from ^{1}H-NMR.

In order to understand the presence of defects, we synthesized the corresponding homocoupling and Stille polymers (Scheme 5.2a and b) as references to perform an ^{1}H NMR analysis (Figure 5.4a). From ^{1}H NMR analysis we can clearly see a similar profile between Stille and DARPs polymers despite the presence of -CHO defects, while no apprectiable homocoupled polymer has been observed. To investigate in deep the presence of defects, we performed an UV/Vis analysis to evaluate the absorption profile for the mentioned above polymers (Figure 5.4b). From UV/Vis analysis we can clearly see that polymers obtained with DARPs have lost the typical vibrionic shoulder respect to Stille ones meaning, in other words, huge amount of defects likely ascribed to bithiophene.

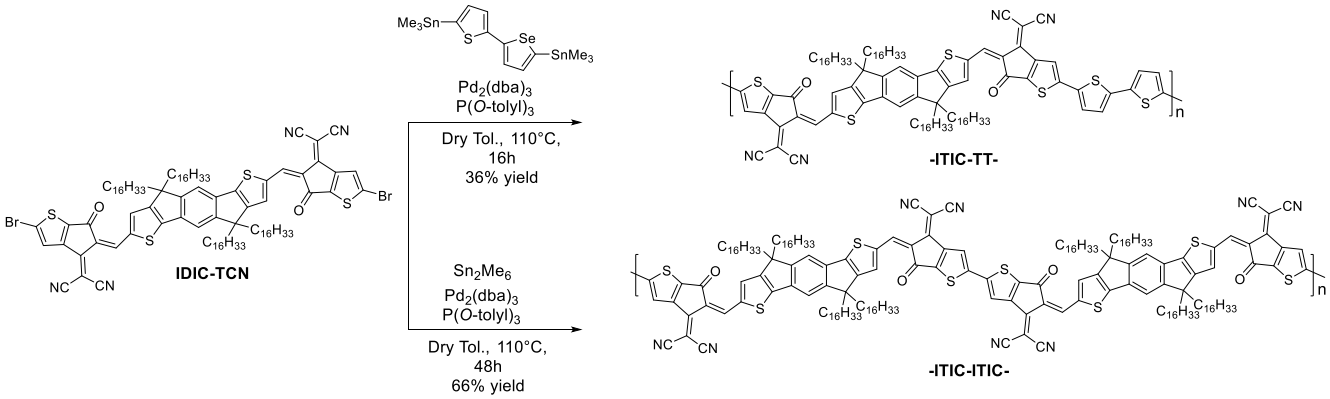

Scheme 5.2. Stille and homocoupled polymers

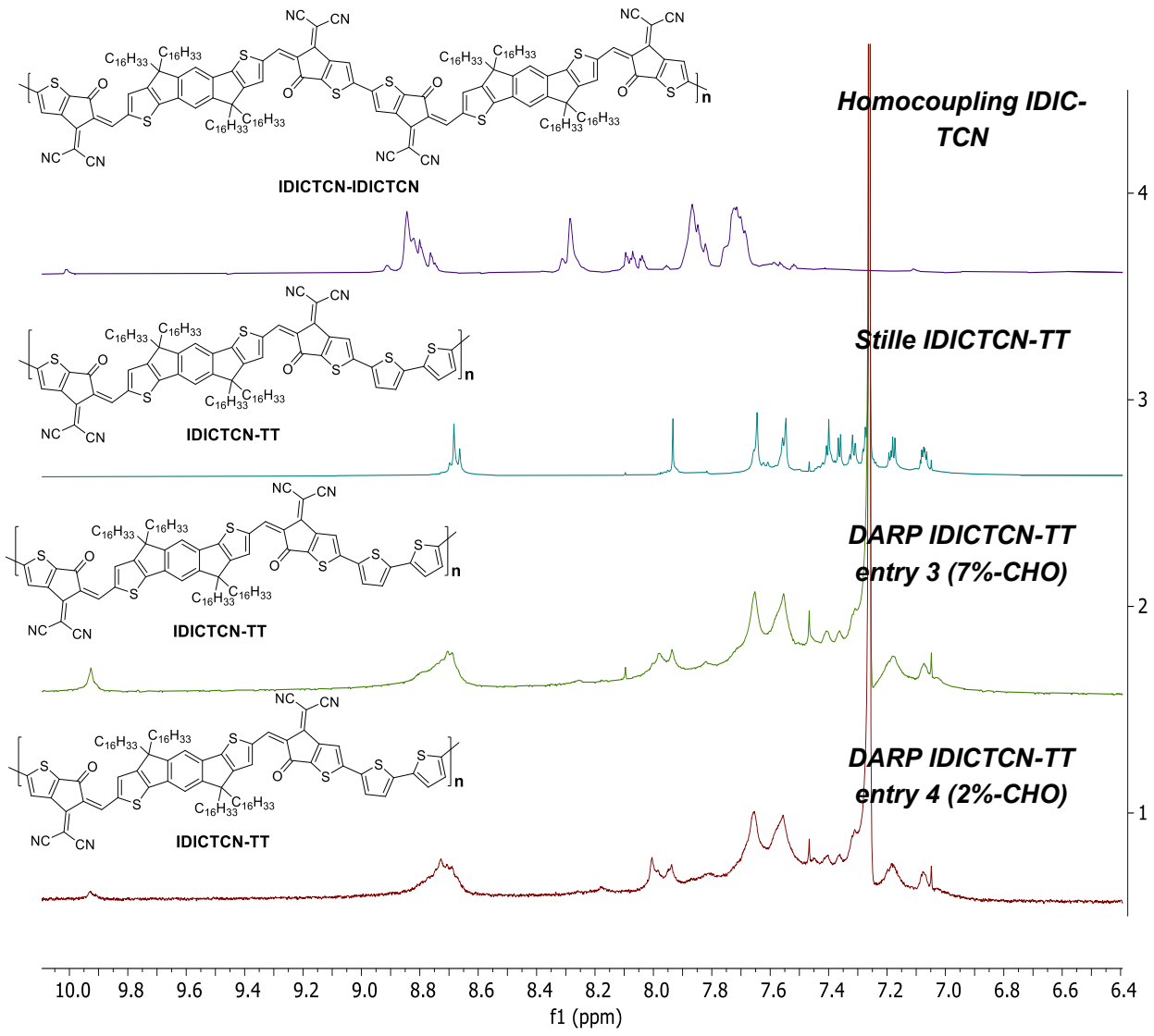
IDICTCN-IDICTCN
Homocoupling IDIC-TCN
IDICTCN-TT
Stille IDICTCN-TT
IDICTCN-TT
DARP IDICTCN-TT entry 3 (7%-CHO)
IDICTCN-TT
DARP IDICTCN-TT entry 4 (2%-CHO)
4
3
2
1
10.0 9.8 9.6 9.4 9.2 9.0 8.8 8.6 8.4 8.2 8.0 7.8 7.6 7.4 7.2 7.0 6.8 6.6 6.4
f1 (ppm)

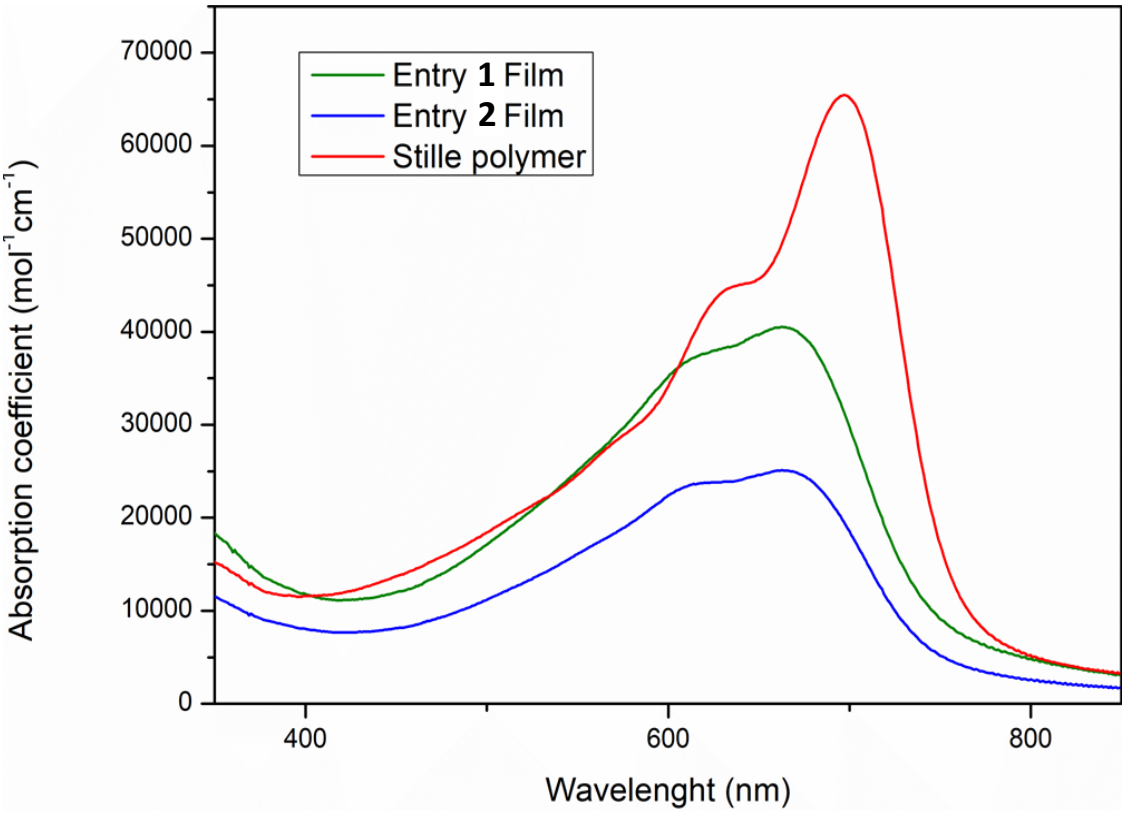

Figure 5.4. a) ^{1}H NMR analysis of homocoupling; Stille coupling and highest and lowest defects; b) UV/Vis of DARPs polymers and Stille

Nevertheless, since the mentioned above DARPs conditions allowed us to obtain polymers, we decided to try these conditions for the synthesis of PS-Se. PS-Se has not only shown high efficiency but also, as π-spacer, selenophene possesses much more more reactive α-positions compared to thiophene (Scheme 5.3).

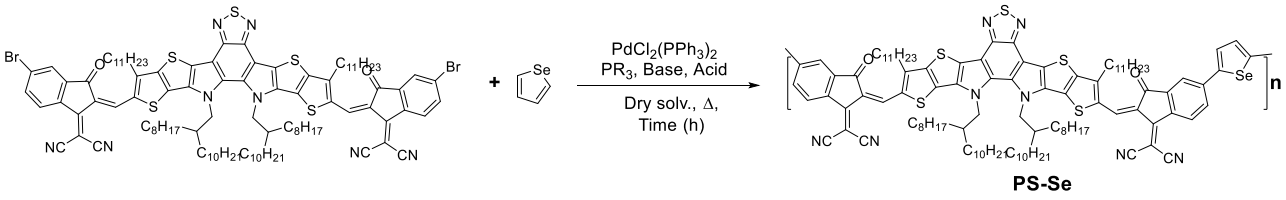

Scheme 5.3: test reaction 2

The reaction was thoroughly investigated, as reported in Table 5.2. Firstly, we used the above mentioned conditions (entry 1), but we did not isolate any product. We then decided to change solvent as well as molarity (entries 2 and 3) but no one of these strategies worked. We decided to test the classic Ozawa conditions in presence of TMEDA as additive (entries 4 and 5), since Ozawa reported some beneficial effects for the reduction of defects, but we did not isolate any product. Last, we decided to use a bulky phosphine (entry 6) to reduce side reactions, but unfortunately we did not isolate any product. According to us, the problems may arise from the IC end-cap group.

Table 5.2. Conditions for test reaction 2

Entry	***Pd***	***PR_3***	***Acid***	***Base[a]***	***TMEDA***	***Solv.[b]***	***T(°C)***	***t(h)***	***Yield (%)[c]***
1	$PdCl_2(PPh_3)_2$	P(*O*-methoxyphenil)$_3$	NDA	K_2CO_3	-	Tol (0.135M)	90	16	**
2	$PdCl_2(PPh_3)_2$	P(*O*-methoxyphenil)$_3$	NDA	K_2CO_3	-	CB (0.135M)	90	16	**
3	$PdCl_2(PPh_3)_2$	P(*O*-methoxyphenil)$_3$	NDA	K_2CO_3	Yes	Tol. (0.3M)	100	16	**
4*	$PdCl_2(PPh_3)_2$	P(*O*-Tolyl)$_3$	PivOH	Cs_2CO_3	Yes	Tol (0.25M)	100	16	**
5*	$PdCl_2(PPh_3)_2$	P(*O*-Tolyl)$_3$	PivOH	Cs_2CO_3	-	Tol (0.033M)	85	16	**
6	$PdCl_2(PPh_3)_2$	RuPhos	NDA	K_2CO_3	-	Tol. (0.3M)	100	16	**

*a) Dry base; b) Dry solvents; c) Calculated upon Soxhlet. All the reactions were carried out with 50 mg of Y6-Br, *Entry 3,4 classic Ozawa conditions in presence of TMEDA, **Entry 1 to 6 showed very high intensity of degradation products from precipitation step to Soxhlet*

According to the literature, in the presence of strong electron-withdrawing groups two possible degradative pathways could be observed (Figure 5.6) [205206207]

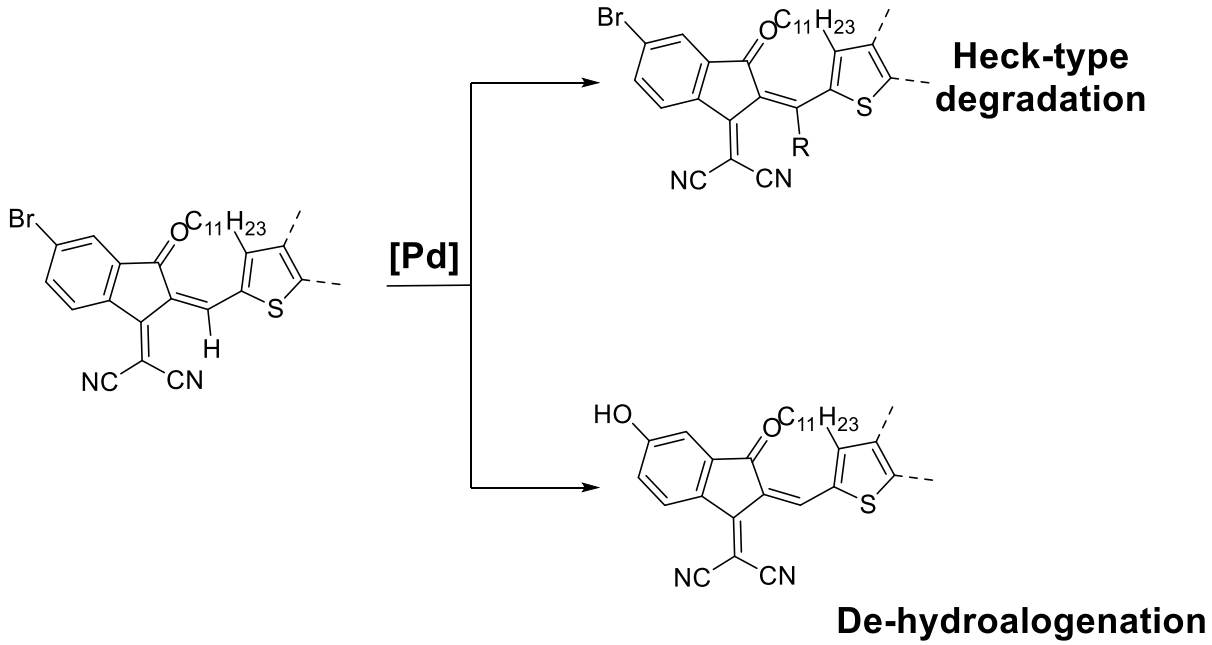

Figure 5.5. Degradative pathways

The first degradative pathway is related to the vinyl bridge, which can promote Heck-type degradation followed by nucleophilic insertion. The second one was observed for strongly deactivated aryl ring, and more precisely a deactivated aryl halide undergoes substitution of its halide with a hydroxy group. Likely,

[205] B. Zhu, L. Guo, P. Deng and S. Liu, «Comparison of two side-chain design strategies for indacenodithienothiophene–naphthalene diimide polymer photovoltaic acceptors prepared by direct (hetero)arylation polycondensation» *J. Mater. Chem. C* **2021***, 9,* 2198-2204.

[206] S. Mao, X. Shi, J.-F. Soulé and H. Doucet, «Pd/C as Heterogeneous Catalyst for the Direct Arylation of (Poly)fluorobenzenes» *Chem. Eur. J.* **2019***, 25,* 9504-9513.

[207] L. Chen, J. Roger, C. Bruneau, P. H. Dixneuf and H. Doucet, «Phosphine-Free Palladium Catalytic System for the Selective Direct Arylation of Furans or Thiophenes bearing Alkenes and Inhibition of Heck-Type Reaction» *Adv. Synth. Catal.* **2011***, 353,* 2749–2760.

what happened in our case, as seen by Sommers for **ND2000** synthesis via DARPs, has been a De-hydrohalogenation of IC groups resulting in chain's propagation steps (Figure 5.7).[203]

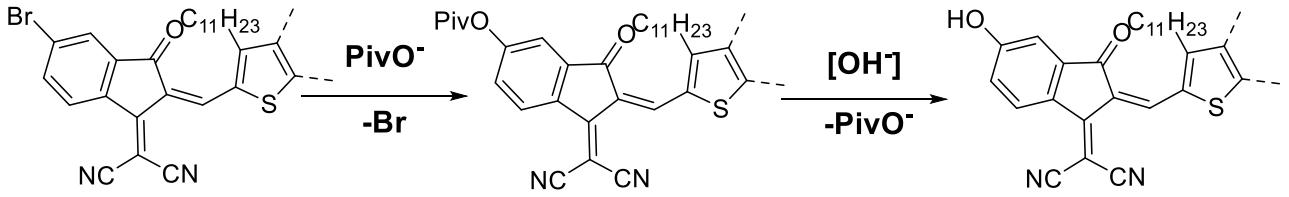

Figure 5.6: De-hydrohalogenation mechanism

We decided to use the classical Sommers conditions for our target polymer (Scheme 5.4); surprisingly we were able to isolate a deep blue solid after Soxhlet without any appreciable sign of degradation.

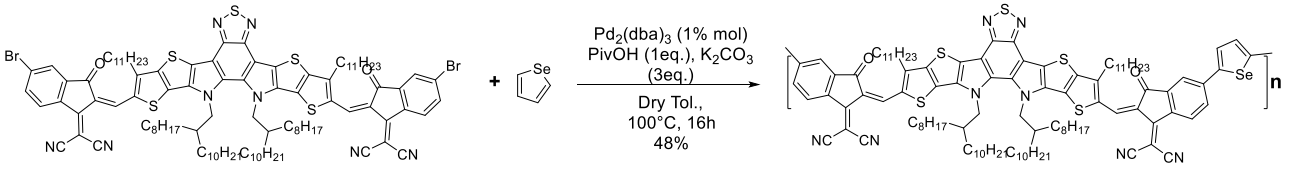

Scheme 5.4. Sommers condition

We characterized the resulting deep blue solid with UV and ^{1}H NMR (Figure 5.8a and b), with the UVanalyses showing a good match with the polymer obtained by Stille, and the NMR instead pointing to an oligomeric/dimeric structure. We further evaluated our polymer via high temperature GPC, from GPC analysis, but we clearly see a lower molecular weight (3 KDa) for DARPs than Stille ones (39 KDa) (Figure 5.S1-2 in the appendix), indicating the formation of a dimer (Figure 5.8c).

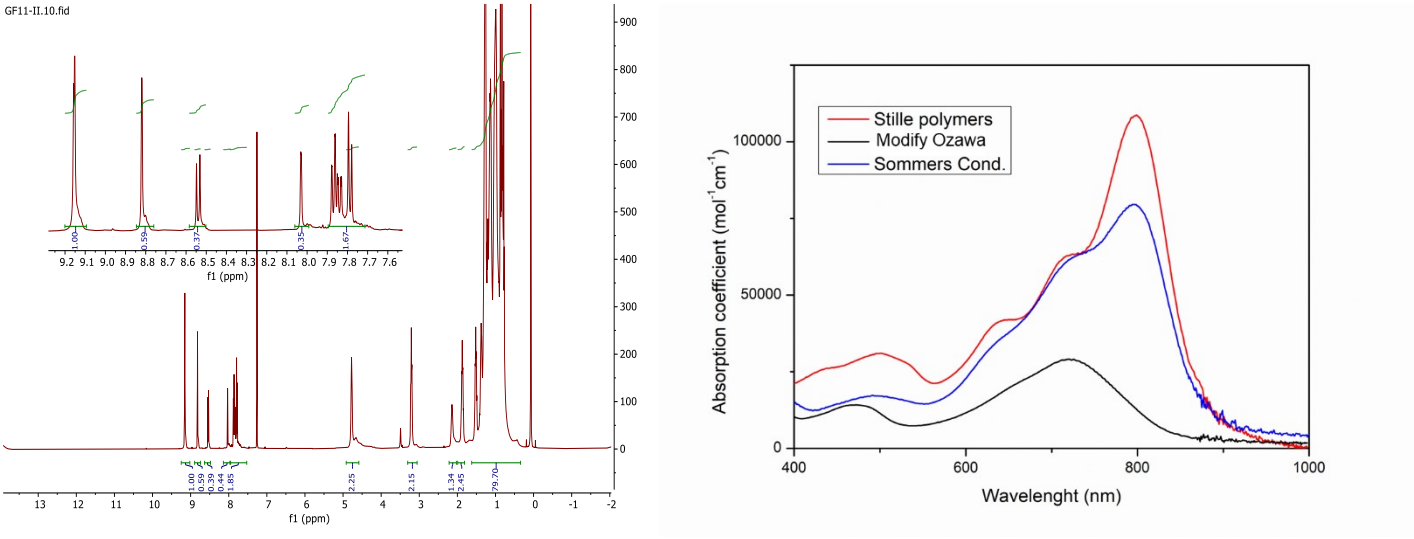

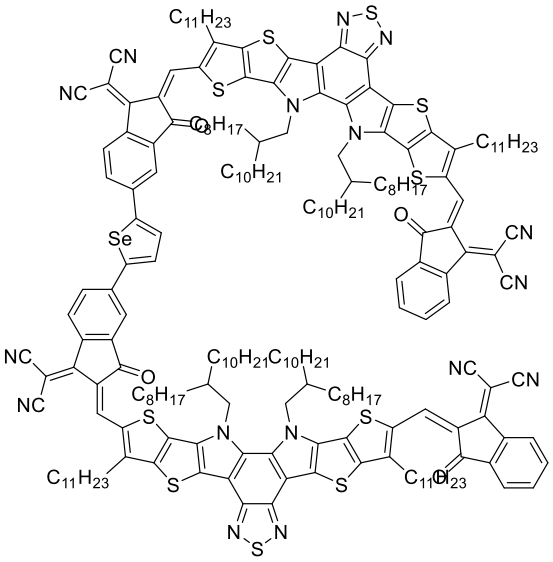

Y6-Se-Y6

Figure 5.7: a) 1H-NMR of dimer; b) UV/Vis of dimer and c) dimer structure.

5.3→ CONLCUSION

In conclusion we investigated the feasibility of DARPs for complex NFAs. Despite several efforts, we were only able to isolate the resulting Y6-Se-Y6 dimer. NFAs, such as ITIC/Y6 families, have some intrinsic limitation related to their end-cap groups and electron-deficiency, which still limit DARPs, but the synthesis of the dimer is noteworthy and confirm the possibility of this route. Currently, we are

investigating new Sommers-like conditions to avoid the degradative problems mentioned above, pushing instead the synthesis of desired products.

5.4→ EXPERIMENTAL SECTION

1.General experimental

NMR spectra were recorded on a Bruker Avance III HD 500MHz system equipped with a TXO Prodigy probe. Chemical shifts for 1H and 13C spectra are referenced to residual protio-solvent signals (δ 1H = 7.26 for $CDCl_3$ and 1H = 5.973 for $C_2D_2Cl_4$ δ 13C = 77.16 for $CDCl_3$) and chemical shifts are reported in ppm. Polymer molecular weights were measured on a Polymer Laboratories PL-GPC 220 instrument at 150 ºC calibrated with polystyrene standards and using trichlorobenzene as eluent. UV-Vis absorption spectra were recorded on a Varian Cary 100 UV-vis spectrophotometer. All commercially available reagents and solvents were purchased from Sigma-Aldrich, TCI, Alfa Aesar. and Derthon Optoelectronic Materials ScienceTechnology Co. IDIC-TCN and Y6-Br were were synthesized according to literature. [21-22]

2.Synthesis of new compounds

General conditions for test reaction 1

In an oven dried screw-cap vial (2 ml), under glovebox, were added ITIC-TCN (50 mg, 0.029 mmol), bithiophene (4.8 mg, 0.029 mmol), $PdCl_2(PPh_3)_2$ (0.81 mg, 0.0012 mmol), P(*O*-methoxyphenyl)$_3$ (1.63 mg, 0.0046 mmol), NDA (5 mg, 6.30 μL, 0.029 mmol) and base (0.087 mmol) in dry Tol. (0.3-0.5 M). the resulting solution was stirred at 90-110°C for 8 to 16h. After cooling to room temperature, the solution was slowly added to methanol and the resulting precipitates were collected by filtration and washed in a Soxhlet extractor with methanol, hexane, acetone, dichloromethane, and chloroform. The chloroform fraction was precipitated with methanol, dried under vacuum at 50 °C overnight to obtain the polymer acceptor (25 to 50% yield).

General conditions for –[ITIC-TT]- synthesis via Stille

In an oven dried Schlenk tube, under Ar, were added, ITIC-TCN (40 mg, 0.023 mmol), 5,5'-bis(trimethylstannyl)-2,2'-bithiophene (21.6 mg, 0.023 mmol) $Pd_2(dba)_3$ (1 mg, 0.0011 mmol) and P(*O*-tolyl)$_3$ (2.1 mg, 0.007 mmol) in in previously degassed dry Tol. (2 mL, 0.012 M). The resulting blue

solution was stirred at 110 °C for 16h. After cooling to room temperature, the solution was slowly added to methanol and the resulting precipitates were collected by filtration and washed in a Soxhlet extractor with methanol, hexane, acetone, dichloromethane, and chloroform. The chloroform fraction was precipitated with methanol, dried under vacuum at 50 °C overnight to obtain the polymer acceptors (16 mg, 36% yield) . ^{1}H NMR (500 MHz, CDCl3) δ: 8.68 (s, 4H), 7.93 (s, 2H), 7.65 (s, 2H), 7.56-7.55 (m, 2H), 7.41-7.40 (m, 2H), 7.36-7.32 (m, 2H), 7.32-7.31 (m, 2H), 7.27-7.26 (m, 6H), 7.19-7.17 (m, 2H) 7.08-7.07 (m, 2H), 2.05-1.93 (m, 16H), 1.55 (s, 16H), 1.25-0.86 (m, 232H) ppm.

General conditions for –[ITIC-ITIC]- homocoupled compound via Stille

In an oven dried Schlenk tube , under Ar, were added, ITIC-TCN (50 mg, 0.028 mmol), hexamethylditin (32.5 mg, 28.3 μL, 0.056 mmol), $Pd_2(dba)_3$ (0.51 mg, 0.00056 mmol) and P(*O*-tolyl)$_3$ (0.7 mg, 0.00224) in previously degassed dry Tol. (1 mL, 0.03 M). The resulting blue solution was stirred at 110 °C for 48h. After cooling to room temperature, the solution was slowly added to methanol and the resulting precipitates were collected by filtration and washed in a Soxhlet extractor with methanol, hexane, acetone, dichloromethane, and chloroform. The chloroform fraction was precipitated with methanol, dried under vacuum at 50 °C overnight to obtain the polymer acceptors (32 mg, 68% yield). VT-^{1}H NMR (600 MHz, $C_2D_2Cl_4$) δ: 8.84-8.76 (m, 4H), 8.29 (m, 2H), 8.10-8.07 (m, 2H), 7.90-7.68 (m, 10 H), 2.11 (s, 8H), 2.08 (s, 8H), 1.76 (s, 4H), 1.52-0.97 (m, 232H) ppm.

General conditions for test reaction 2

In an oven dried screw-cap vial (2 ml), under glovebox, were added Y6-Br (50 mg, 0.027 mmol), selenophene (3.5 mg, 2.45 μL, 0.029 mmol), $PdCl_2(PPh_3)_2$ (0.81 mg, 0.0010 mmol), PR_3 (0.0046 mmol), Acids (0.029 mmol), base (0.087 mmol) and TMEDA (if required) (0.029mmol) in dry solv. (0.1-0.5 M). the resulting solution was stirred at 85-100°C for 16h. After the desired time, the resulting deep blue solution was precipitaed in acidify cold MeOH under stirring. Due to degrdation, no further purification have been made.

PS-Se via Stille polymerization

In an oven dried Schlenk tube, under Ar, were added, Y6 (50 mg, 0.027 mmol), Selenophene-($SnMe_3$) (12.2 mg, 0.028 mmol), $Pd(PPh_3)_4$ (1.34 mg, 0.0012 mmol) in previously degassed dry Tol. (2.5 mL, 0.01 M). The resulting blue solution was stirred at 110 °C for 48h. After cooling to room temperature, the solution was slowly added to methanol and the resulting precipitates were collected by filtration and

washed in a Soxhlet extractor with methanol, hexane, acetone, dichloromethane, and chloroform. The chloroform fraction was precipitated with methanol, dried under vacuum at 50 °C overnight to obtain the polymer acceptors (6 mg, 12% yield). ^{1}H NMR (500 MHz, $C_2D_2Cl_4$) δ: 8.84-8.76 (m, 4H), 8.29 (m, 2H), 8.10-8.07 (m, 2H), 7.90-7.68 (m, 10 H), 2.11 (s, 8H), 2.08 (s, 8H), 1.76 (s, 4H), 1.52-0.97 (m, 232H) ppm.

Sommers condition for PS-Se

In an oven dried screw-cap vial (2 ml), under glovebox, were added Y6-Br (50 mg, 0.027 mmol), selenophene (3.5 mg, 2.45 μL, 0.029 mmol), $Pd_2(dba)_3$ (0.28 mg, 0.0003 mmol), PivOH (0.029 mmol), K_2CO_3 (0.087 mmol) in dry Tol. (55 μL, 0.5 M). the resulting solution was stirred at 100°C for 16h. After cooling to room temperature, the solution was slowly added to methanol and the resulting precipitates were collected by filtration and washed in a Soxhlet extractor with methanol, hexane, acetone, dichloromethane, and chloroform. The hexane fraction was precipitated with methanol, dried under vacuum at 50 °C overnight to obtain the resulting dimer (32 mg, 64% yield). ^{1}H NMR (500 MHz, CDCl3) δ: 9.18 (s, 2H), 8.85 (s, 1H), 8.55-8.53 (d, 2H, J = 10 Hz), 8.79 (s, 1H), 7.88-7.78 (m, 4H), 4.78 (s, 4H), 3.21 (s, 4H), 2.15-2.13 (m, 2H), 1.90-1.84 (m, 6H), 1.53-1.50 (m, 8H), 1.26-0.79 (m, 178 H) ppm.

6. Appendix

6.2. Chapter 2

6.2.1. Spectra of New Compounds

Intermediate 1a

^{1}H NMR (400 MHz, $CDCl_3$)

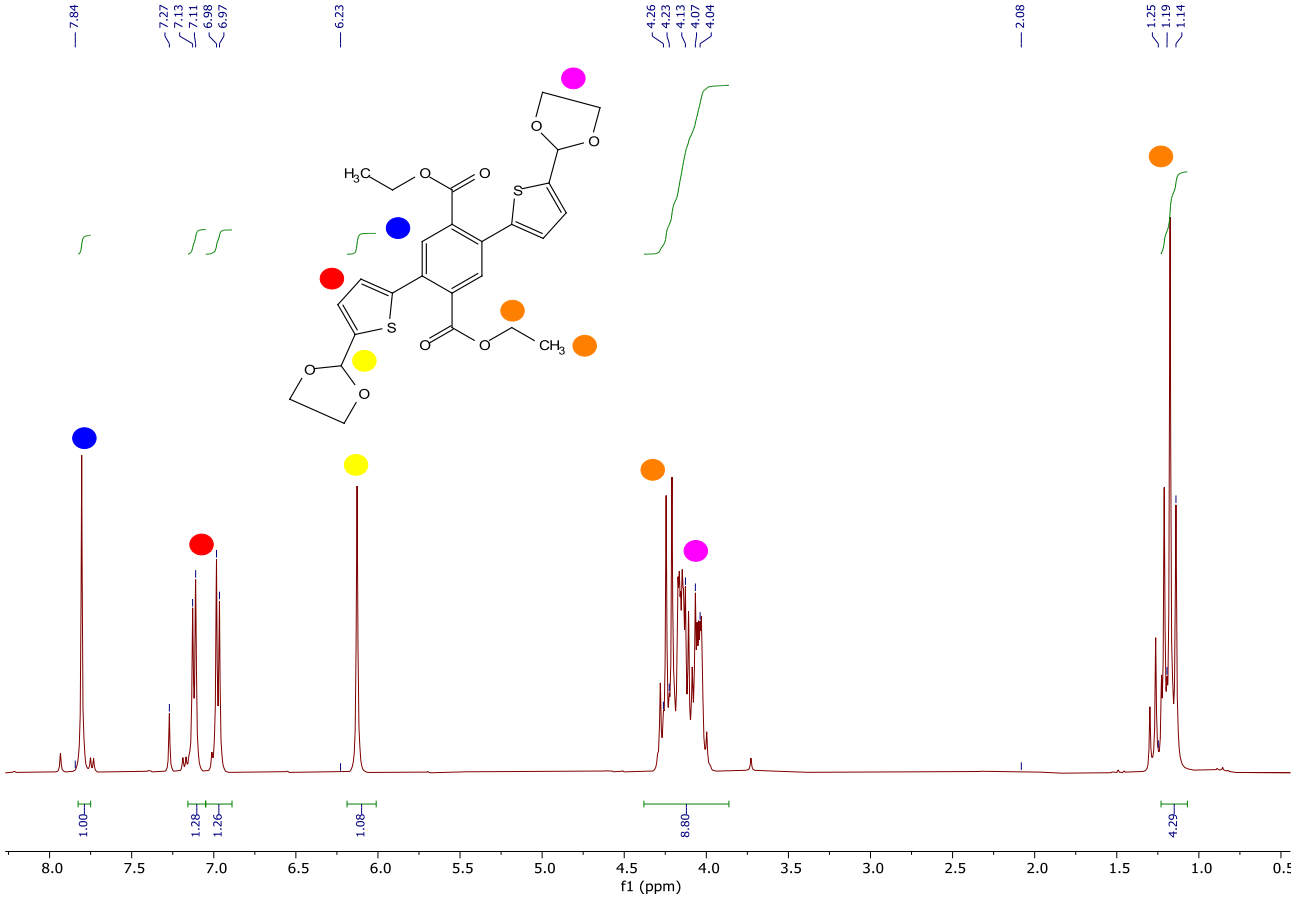

^{13}C NMR (75 MHz, $CDCl_3$)

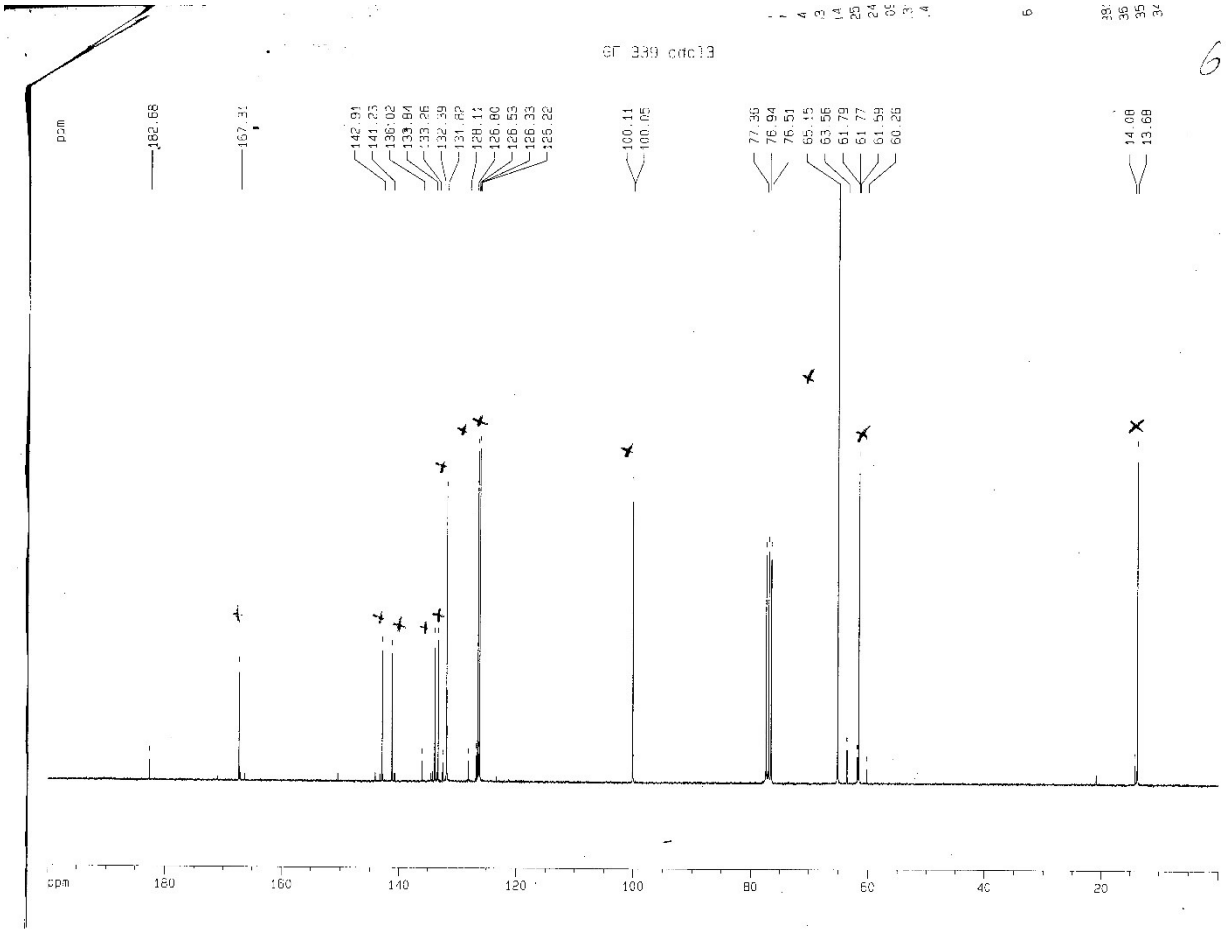
GT 339 cdcl3
6
ppm
182.68
167.31
142.91
141.23
136.02
133.84
133.26
132.39
131.82
128.11
126.80
126.53
126.33
125.22
100.11
100.05
77.36
76.94
76.51
65.15
63.56
61.79
61.77
61.59
60.26
14.08
13.68
ppm
180
160
140
120
100
80
60
40
20

ESI-MS

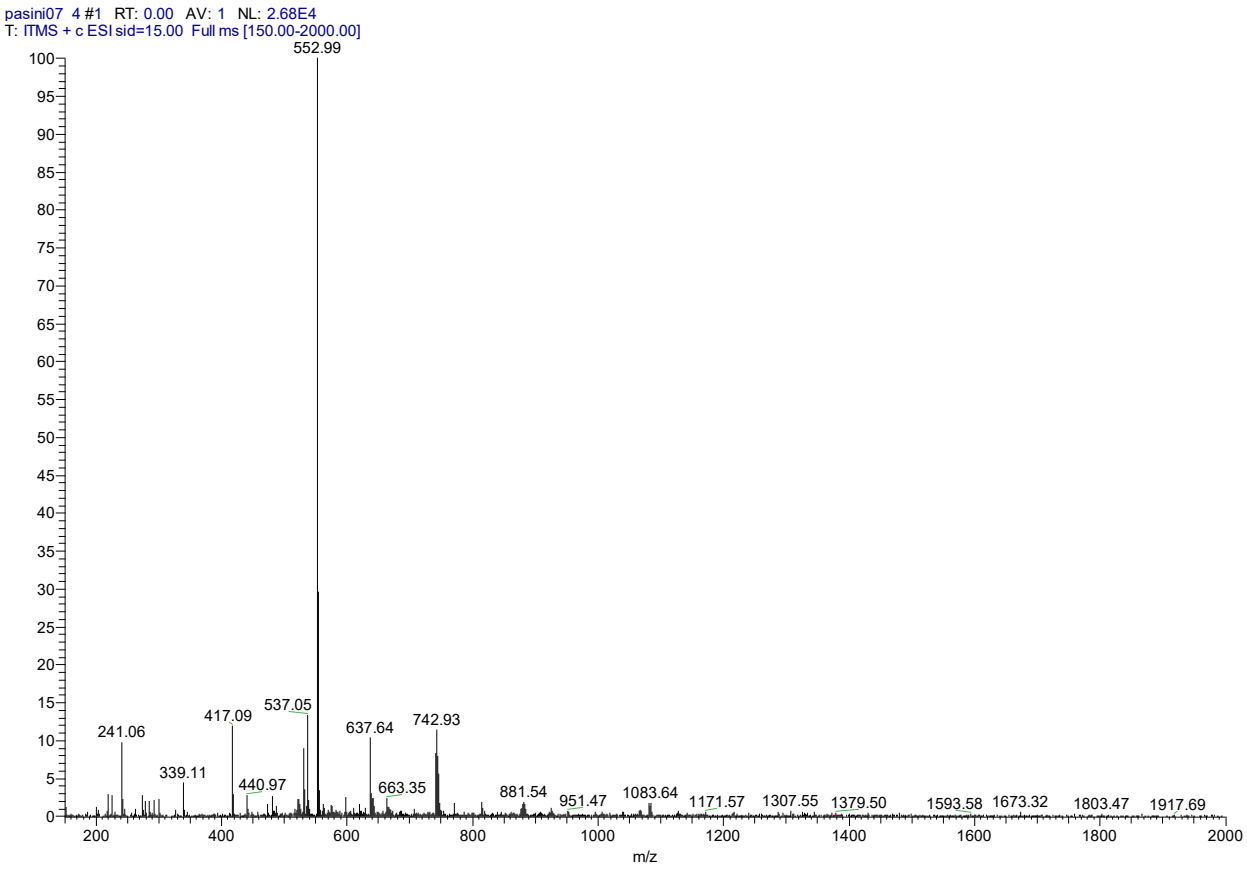

Intermediate 1b

^{1}H NMR (400 MHz, $CDCl_3$)

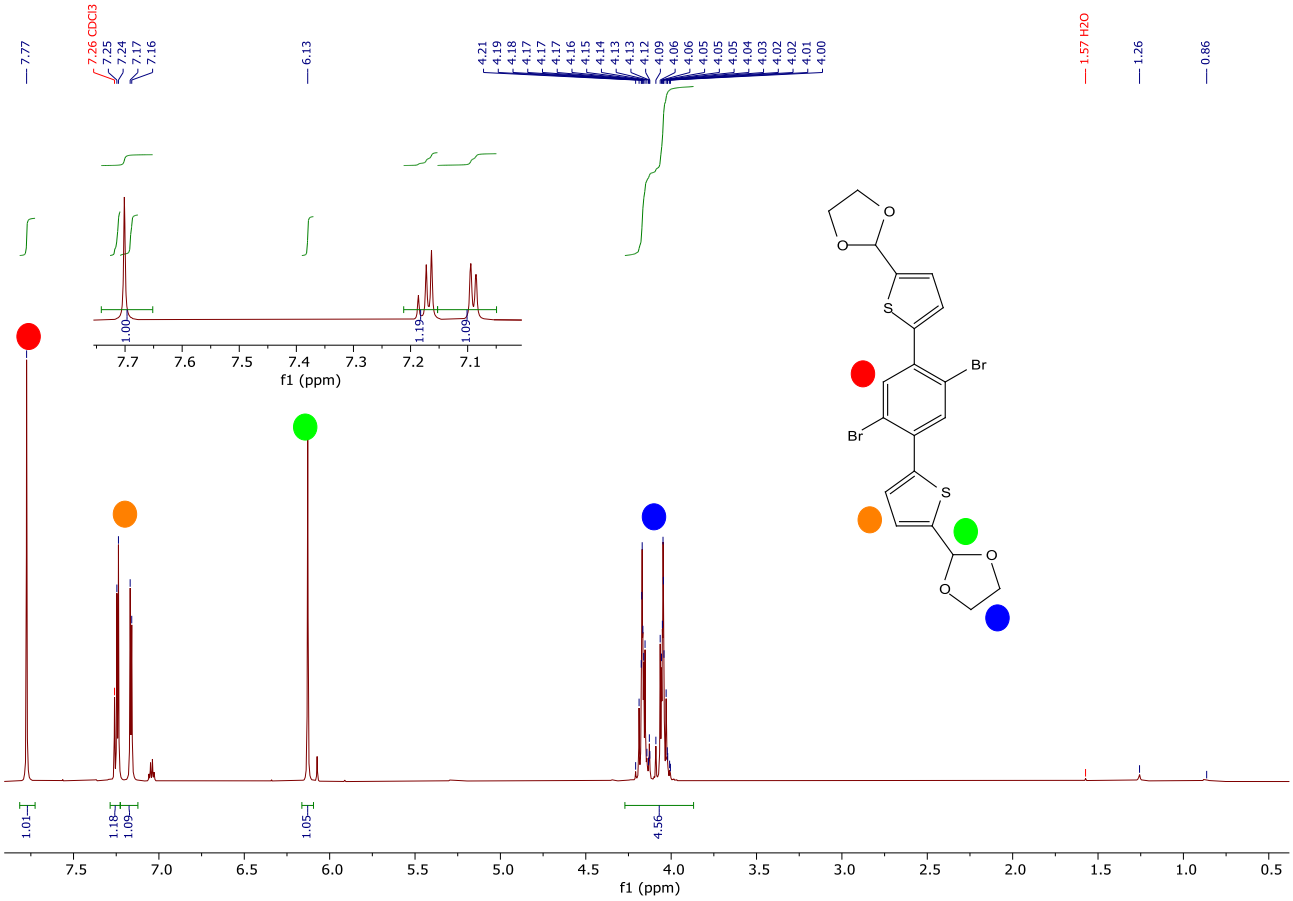

^{13}C NMR (101 MHz, $CDCl_3$)

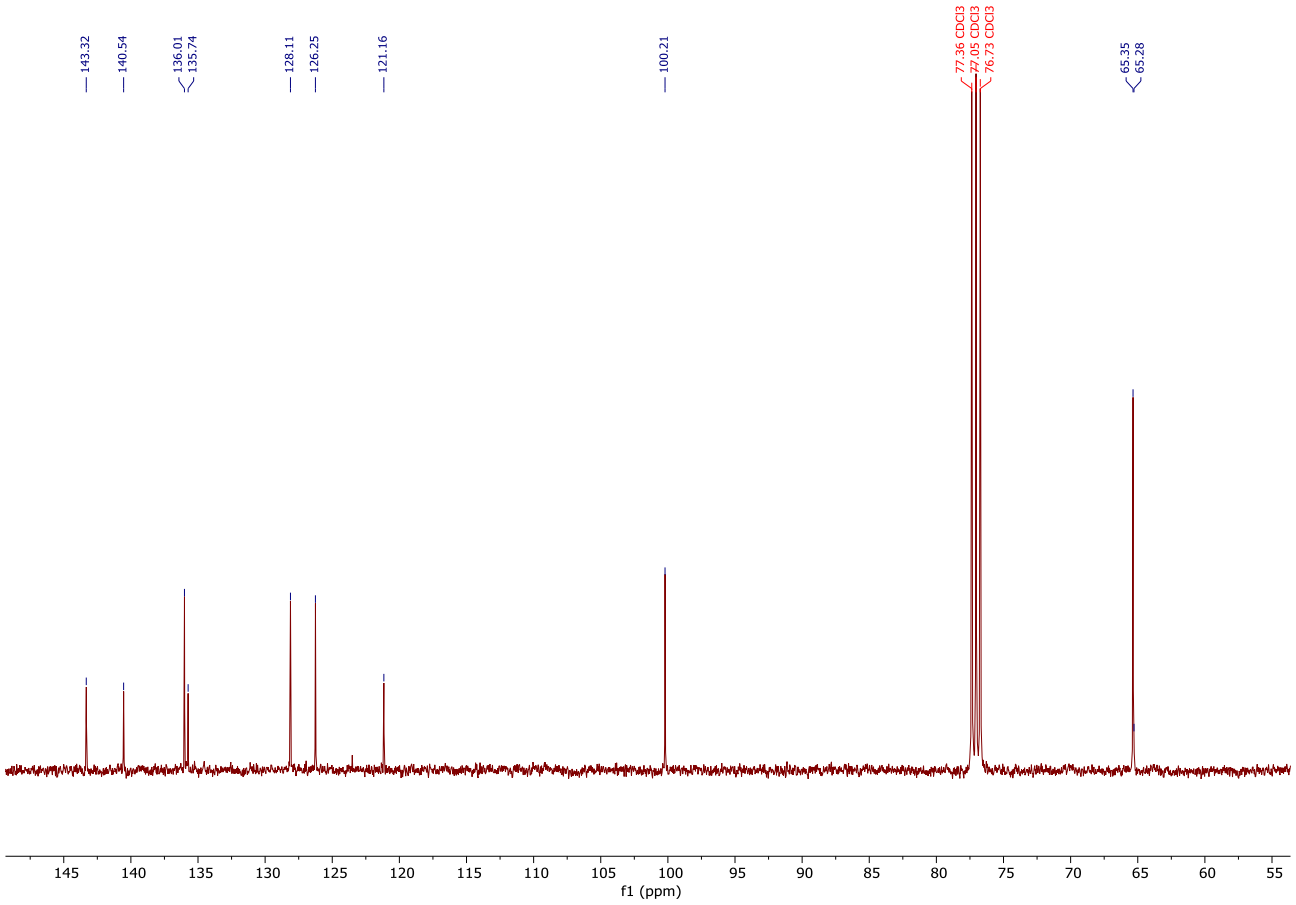
143.32
140.54
136.01
135.74
128.11
126.25
121.16
100.21
77.36 CDCl3
77.05 CDCl3
76.73 CDCl3
65.35
65.28
145
140
135
130
125
120
115
110
105
100
95
90
85
80
75
70
65
60
55
f1 (ppm)

ESI-MS

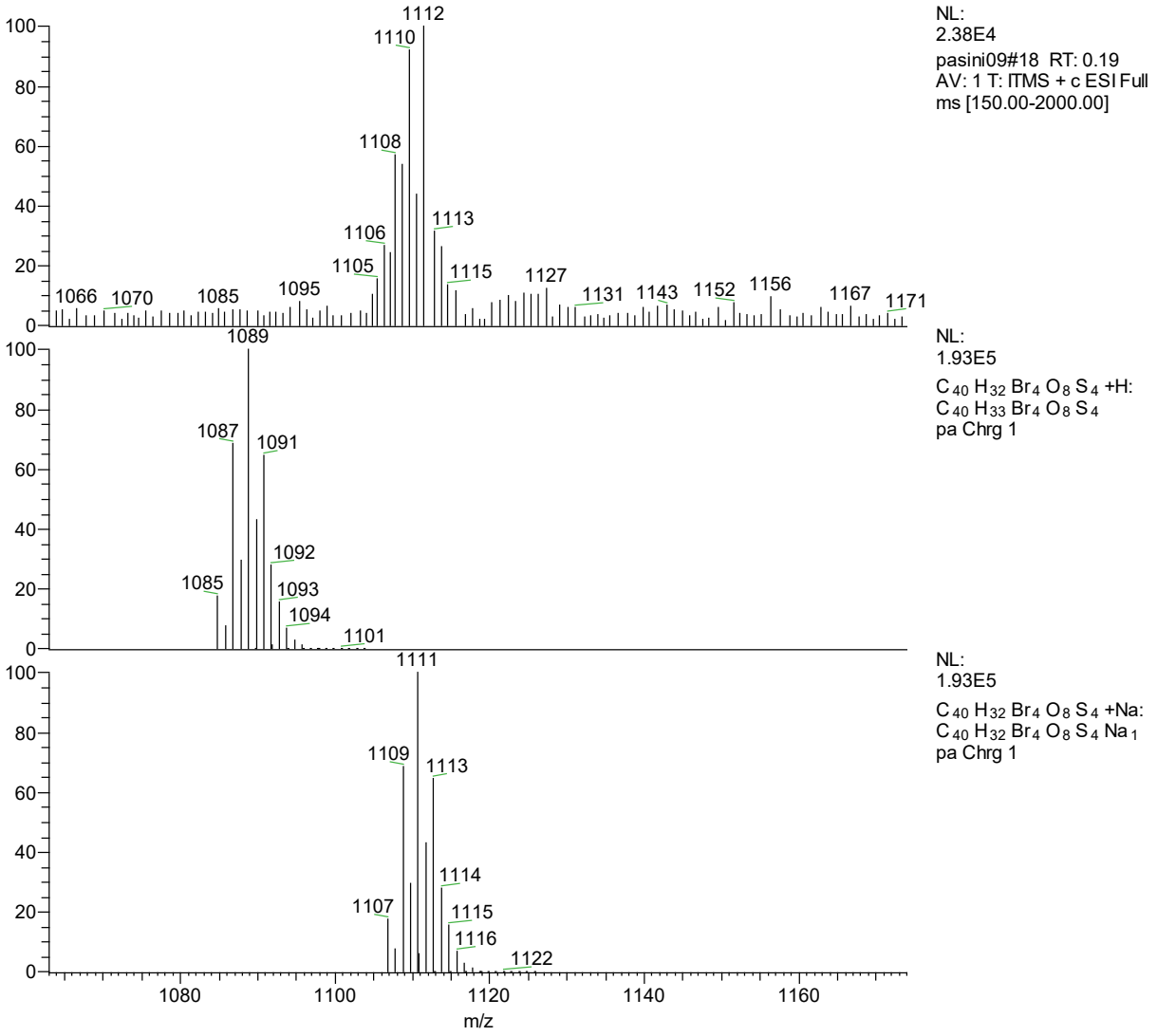

Intermediate 3a

^{1}H NMR (300 MHz, $CDCl_3$)

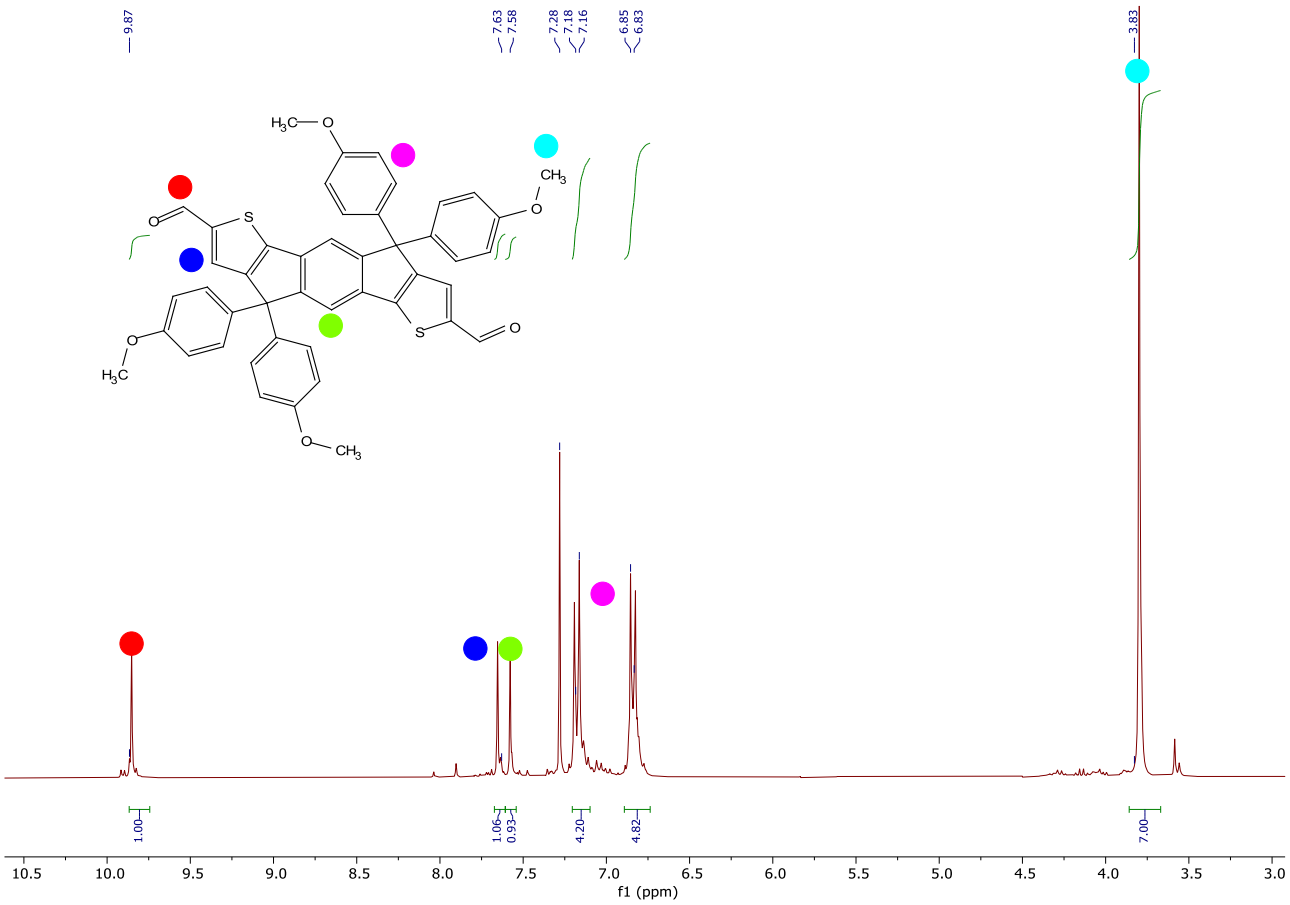

^{13}C NMR (75 MHz, $CDCl_3$)

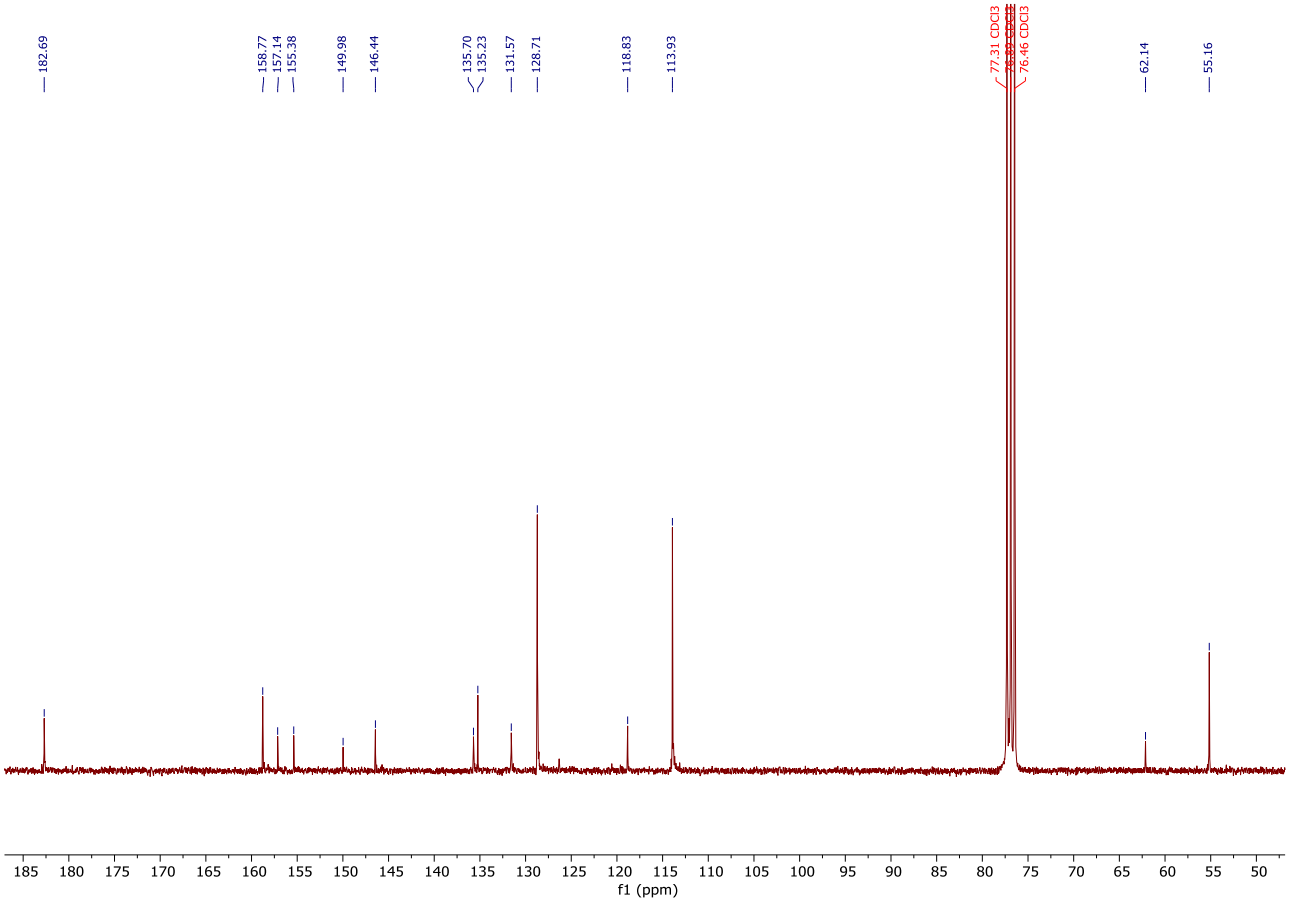

ESI-MS

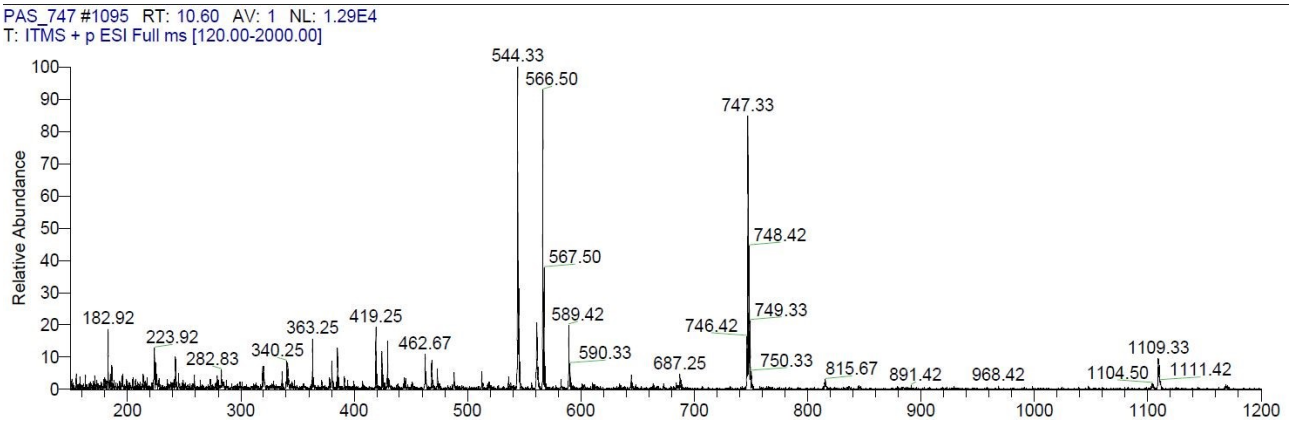

Intermediate 4a

^{1}H NMR (300 MHz, Acetone-D6)

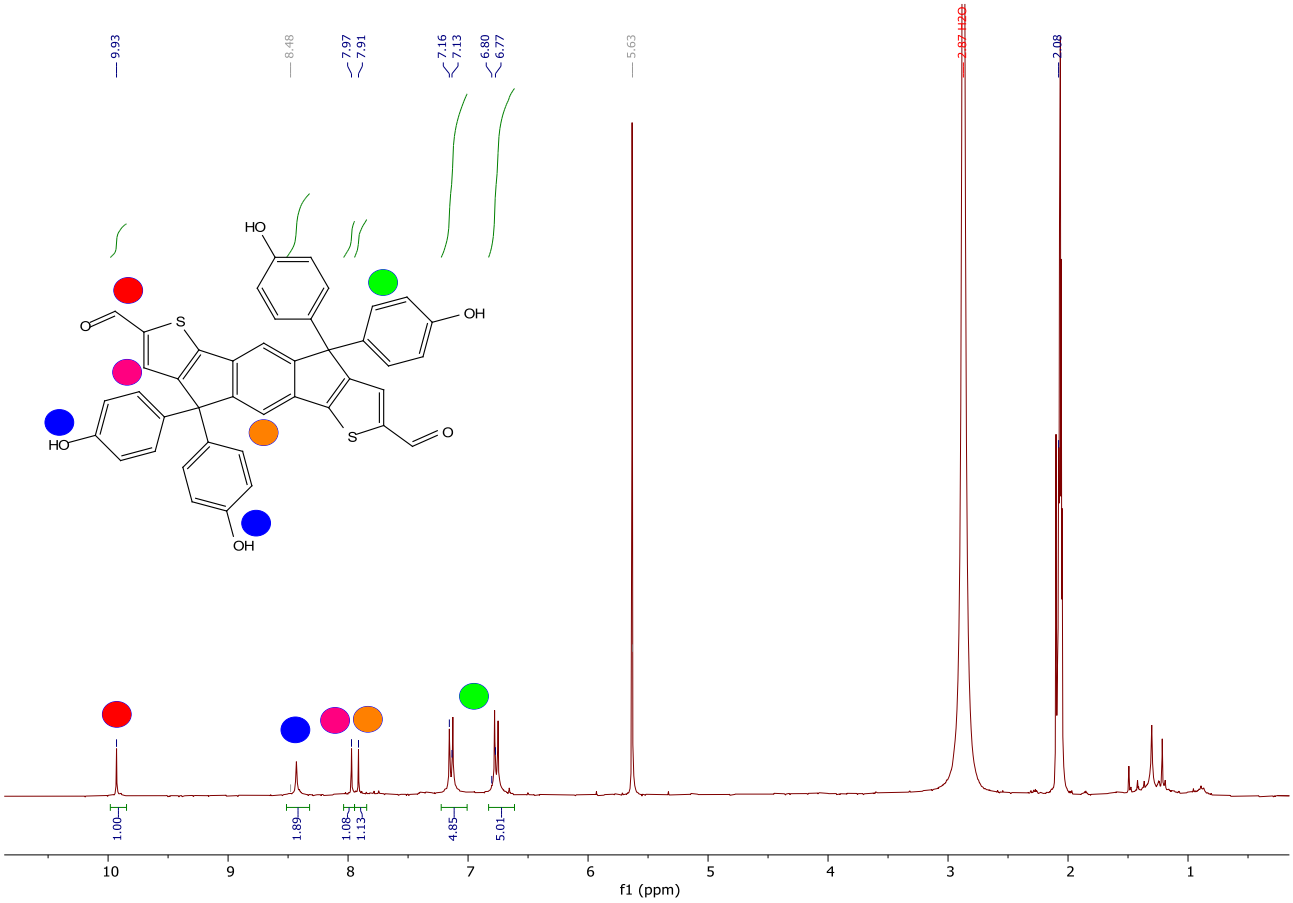

^{13}C NMR (75 MHz, Acetone-D6)

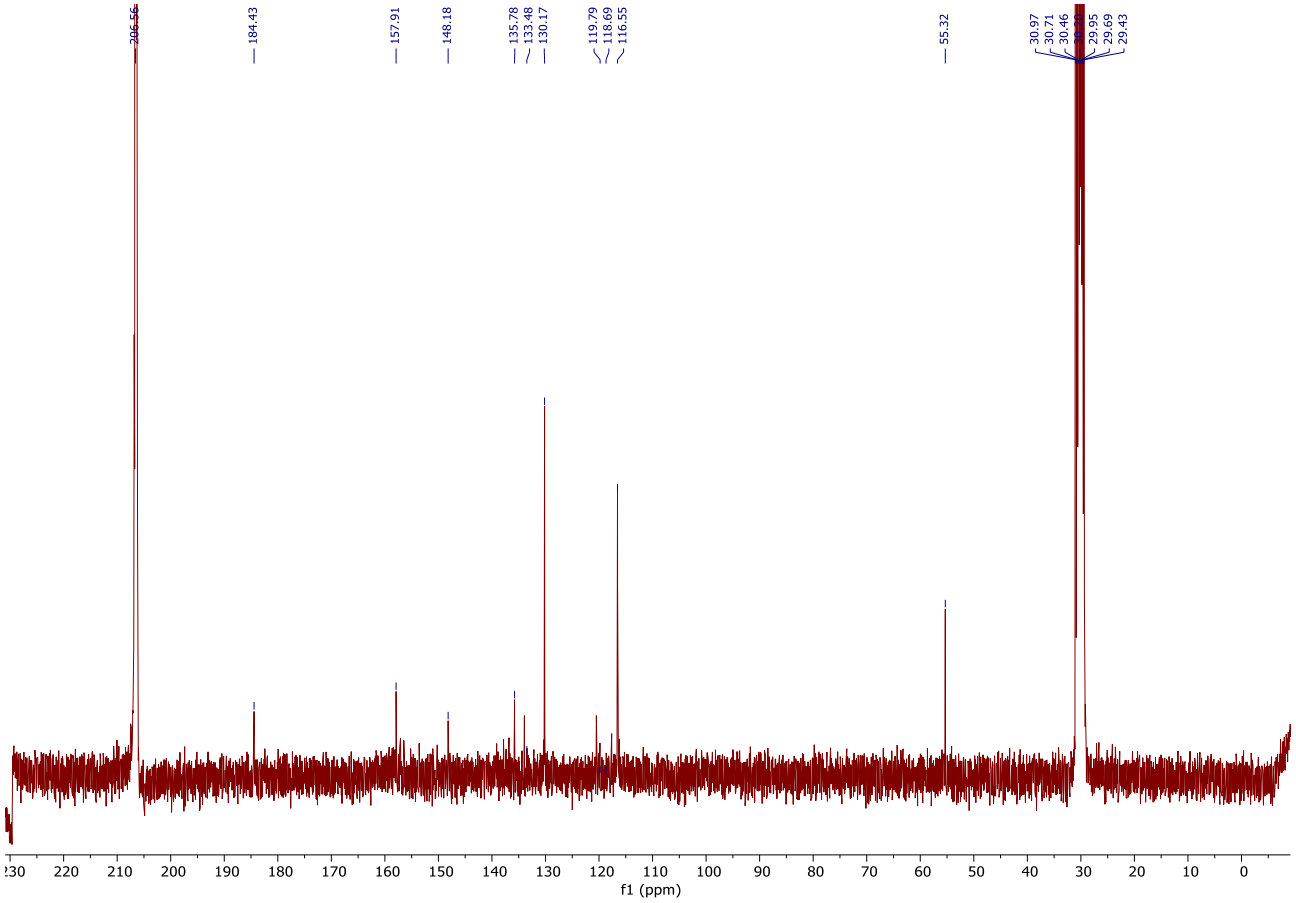

6.2.2 Additional Tables and Figures

Table 2.S1. E-*f*actor for molecule **1a**

	Amount (g)	*Waste (g)*
diethyl 2,5-dibromoterephthalate	1	-
(5-(1,3-dioxolan-2-yl)thiophen-2-yl)zinc(II) chloride	1.5	-
$Pd(PPh_3)_4$	0.122	0.122
$NaHCO_3$	20	20
Na_2SO_4	5	5
Silica gel	20	20
Total	47.66	45.122

Total waste = 45.122g; Compound obtained = 1.46g

E-*f*actor = 30.90

Table 2.S2. E-*f*actor for molecule **3a**

	Amount (g)	*Waste (g)*
1a	0.246	0.178
(4-methoxyphenyl) magnesium bromide	0.432	0.311
$NaHCO_3$	2.5	2.5
Na_2SO_4	2	2
AcOH	5.25	5.25
H_2SO_4	1	1
Silica gel	5	5
Total	16.36	16.239

Total waste = 16.239g; Compound obtained = 0.095g

E-*f*actor = 170.93

Table 2.S3. E-*f*actor for reported **IDIC** [208]

	Amount (g)	*Waste (g)*
diethyl 2,5-dibromoterephthalate	4.48	1.21
2-Bromothiophene	1.66	0.44
Mg°	0.702	0.702
Zinc chloride	3.91	3.91
$Pd(PPh_3)_4$	0.266	0.266
Celite	20	20
Mg_2SO_4	10	10
Silica gel	80	80
Total	121.02	116.53

Total waste = 116.53g; Compound obtained = 3.3g

E-*f*actor = 35.31

Table 2.S4. E-*f*actor for reported **IDIC** [213]

	Amount (g)	*Waste (g)*
diethyl 2,5-di(thiophen-2-yl)terephthalate	1	0.350
4-bromotoluene	2.64	0.92

[208] Wang, Y. *et al. Org. Lett.* **2006**, *8,* 5033–5036.

Mg°	0.378	0.378
Mg_2SO_4	5	5
AcOH	100	100
H_2SO_4	2	2
Silica	40	40
Total	151.02	148.65

Total waste = 148.65g; Compound obtained = 1.05g

E-*f*actor = 141.57

Table 2.S5. E-*f*actor comparison

Molecule	**E-*Factor tot***
3a	201.83
Reference	176.88

6.3. Chapter 3

6.3.1. Additional Tables and Figures

Table 3.S1. Optimization for the formation of ester derivatives **3**

Entry	Compound	Reaction conditions	Yield [%]
1	**3c**	$C_8H_{17}Br$, K_2CO_3, DMAc, 70 °C	8
2	**3c**	$C_8H_{17}Br$, KOH, H_2O, 100 °C	0
3	**3c**	(a) oxalyl chloride in DMF, 100°C, then (b) $C_8H_{17}OH$ Et_3N, $CHCl_3$, 40°C	0
4	**3c**	(a) $SOCl_2$, toluene, at reflux, then (b) $C_8H_{17}OH$, Et_3N, THF, 60°C	24
5	**3c**	$C_8H_{17}Br$ (2 eq), K_2CO_3 (3 eq), Bu_4NBr (3 eq), DMAc, 130°C	48
6	**3d**	1-bromo-2-ethylhexane (2 eq), K_2CO_3 (3 eq), Bu_4NBr (3 eq), DMAc, 130°C (one pot)	41
7	**3b**	9-(bromomethyl)nonadecane, K_2CO_3 (3 eq), Bu_4NBr (3 eq), DMAc, 130°C (one pot)	41
8	**3b**	9-(bromomethyl)nonadecane, K_2CO_3 (3 eq), Bu_4NBr (3 eq), DMAc, 130°C (from isolated **3a**)	51

Table 3.S2. *E* factor calculations for compounds **3a** and **3b**.

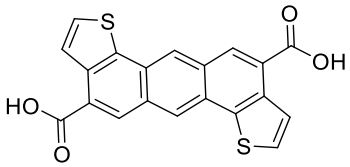

	Amount (g)	Waste (g)
2,5-dibromoterephthalaldehyde	29.19	0
3-thiopheneacetic acid	28.43	0
$Pd(OAc)_2$	2.25	2.25
PPh_3	5.25	5.25
K_2CO_3	55.28	55.28
DMAc	8.71	0
HCl	14.58	0
Total	**143.69**	**62.78**

Total waste = 62.78 g; Compound obtained = 26,87 g

E-factor = 2.34

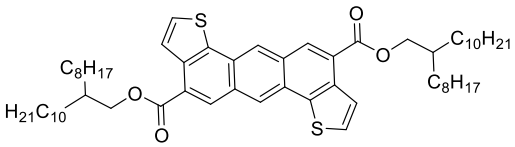

	Amount (g)	Waste (g)
Compound **3a**	18.92	0
9-(bromomethyl)nonadecane	36.14	0
K_2CO_3	27.64	27.64
DMAc	8.71	0
Silica gel	80.00	80
Hexane	131.00	131
Ethyl acetate	18.04	18.04
iPrOH	157.20	157.20

Total	**477.65**	**256.68**

Total waste = 256.68 g; Compound obtained = 24,42 g

E-factor = 16.9

Table 3.S3. Bromination experiments on esters **3**

Entry	Starting ADT	Reaction condition	Yield
1	3b	NBS, $CHCl_3$, rt	0
2	3b	NBS, DMF, 100°C	0
3	3b	NBS, $CHCl_3$:AcOH 8:2, rt	0
4	3b	Br_2, $CHCl_3$, rt	0
5	3b	Br_2, DMF, rt	0
6	3d	NBS, DMF, 100°C	0
7	3d	NBS, $CHCl_3$:AcOH 8:2, rt	25
8	3d	NBS, $CHCl_3$:AcOH 1:1, rt	0
9	3a	Br_2, NaOH, H_2O, reflux	0

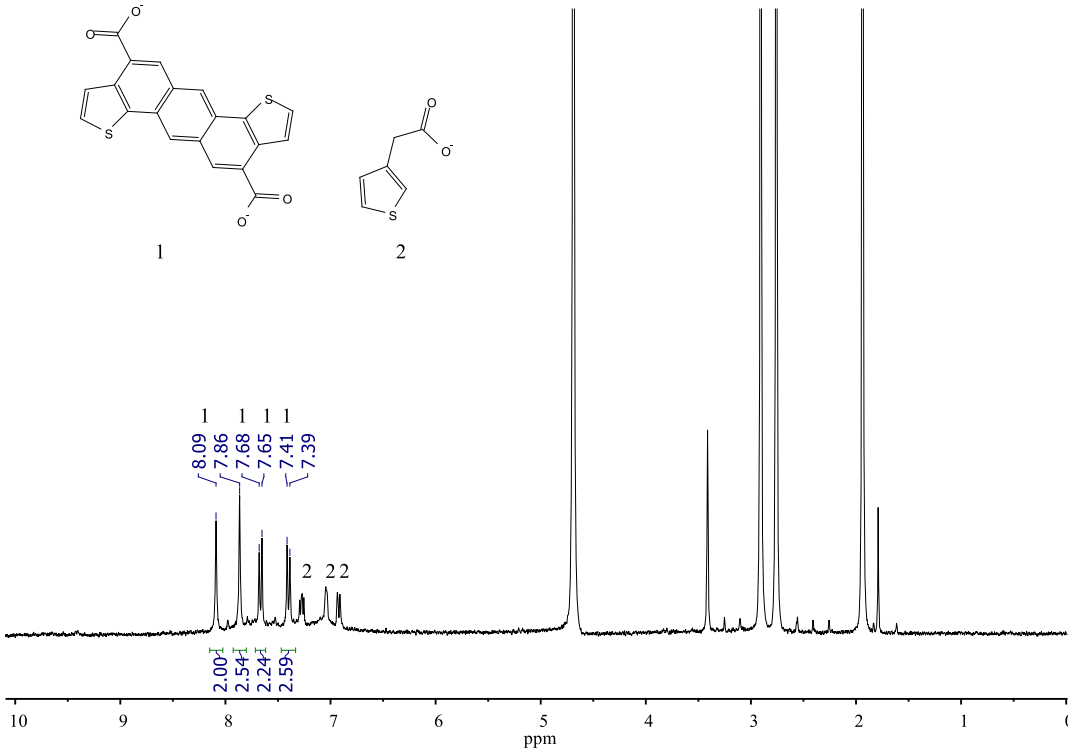

Figure 3.S1. ^{1}H NMR spectra (D_2O, 400 MHz, 298 K) of the crude reaction mixture for the preparation of compound **3a**. The crude reaction mixture was obtained removing the reaction solvent (DMAc) under reduced pressure.

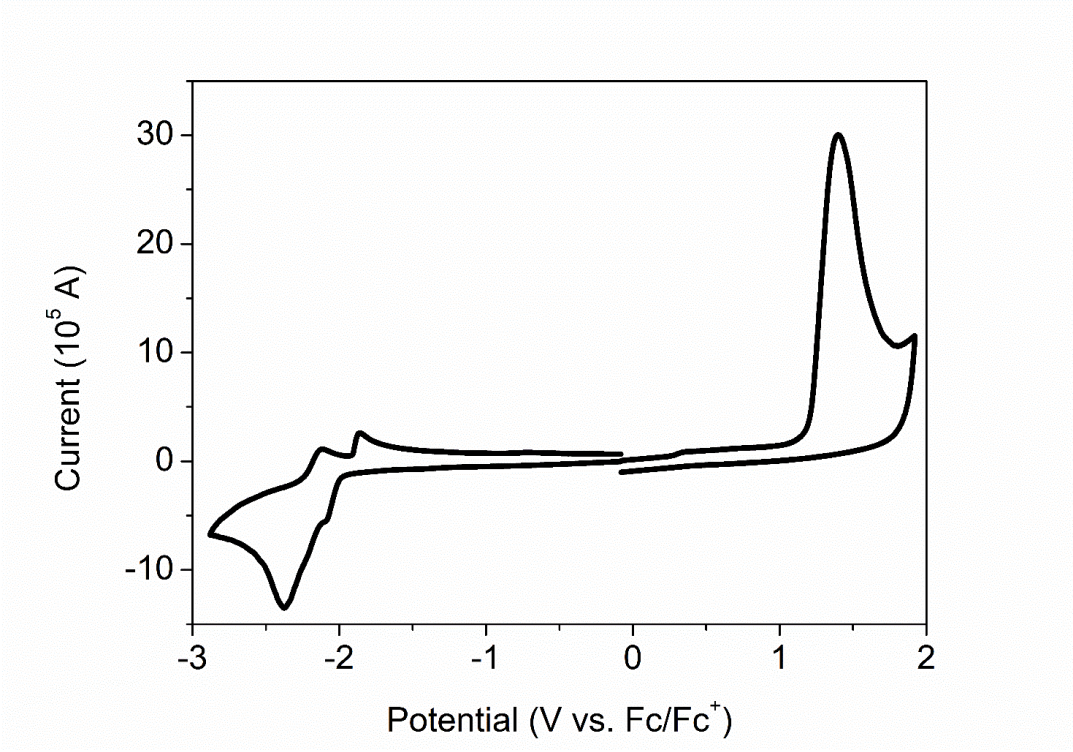

Figure 3.S2. Cyclic voltammogram of compound **3b**.

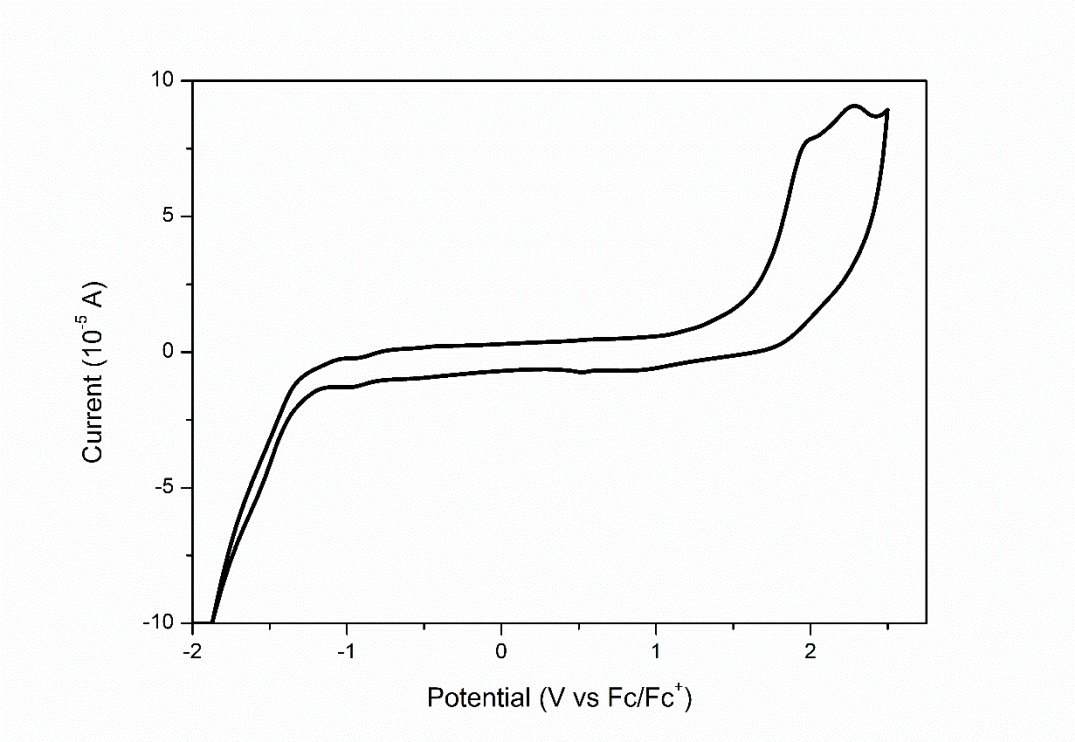

Figure 3.S3. Cyclic voltammogram of compound **9**.

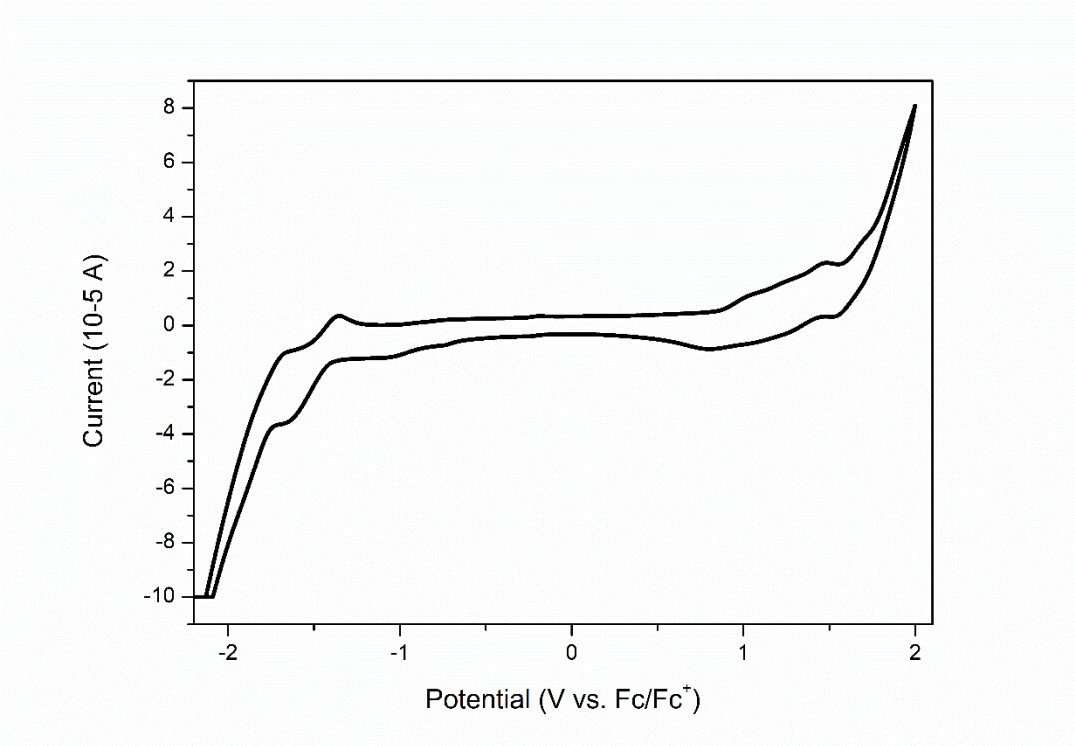

Figure 3.S4. Cyclic voltammogram of compound **10**.

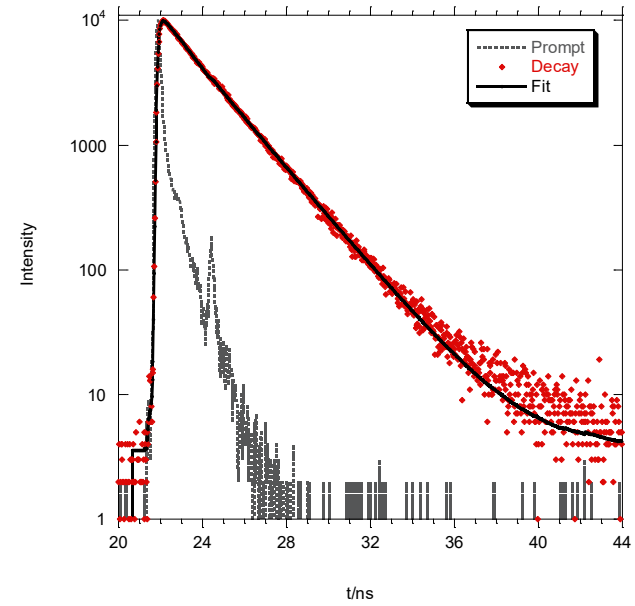

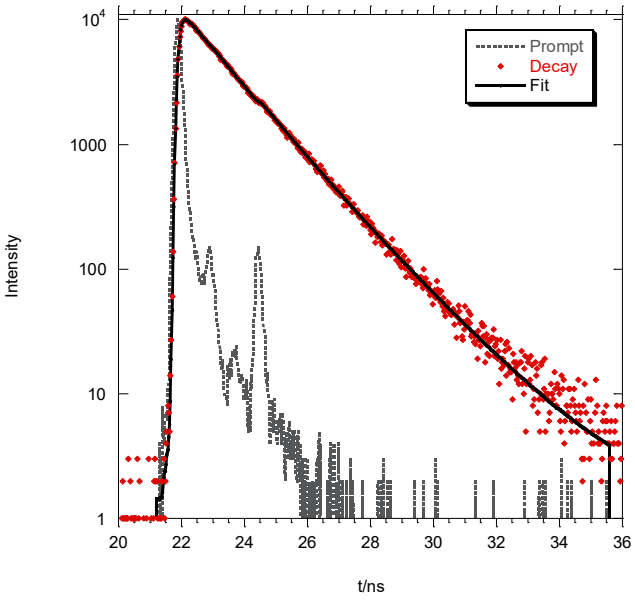

Figure 3.S5. PL decay (λ_{ex}=407 nm) in chloroform of compounds **9** (top, λ_{em}@560nm) and **10** (bottom, λ_{em}@590nm)

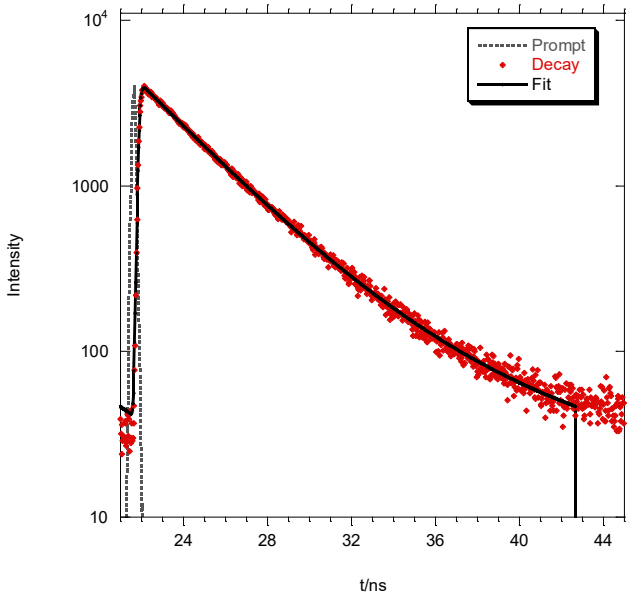

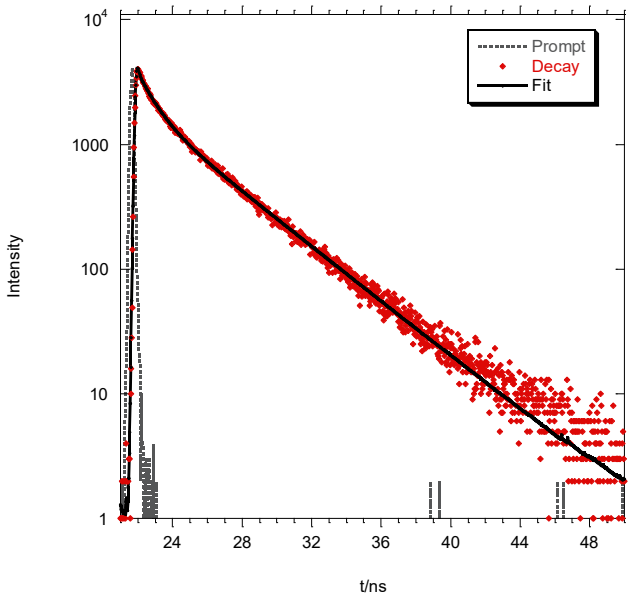

Figure 3.S6. PL decay (λ_{ex}=407 nm) in film cast of compounds **9** (top, λ_{em}@766nm) and **10** (bottom, λ_{em}@725nm)

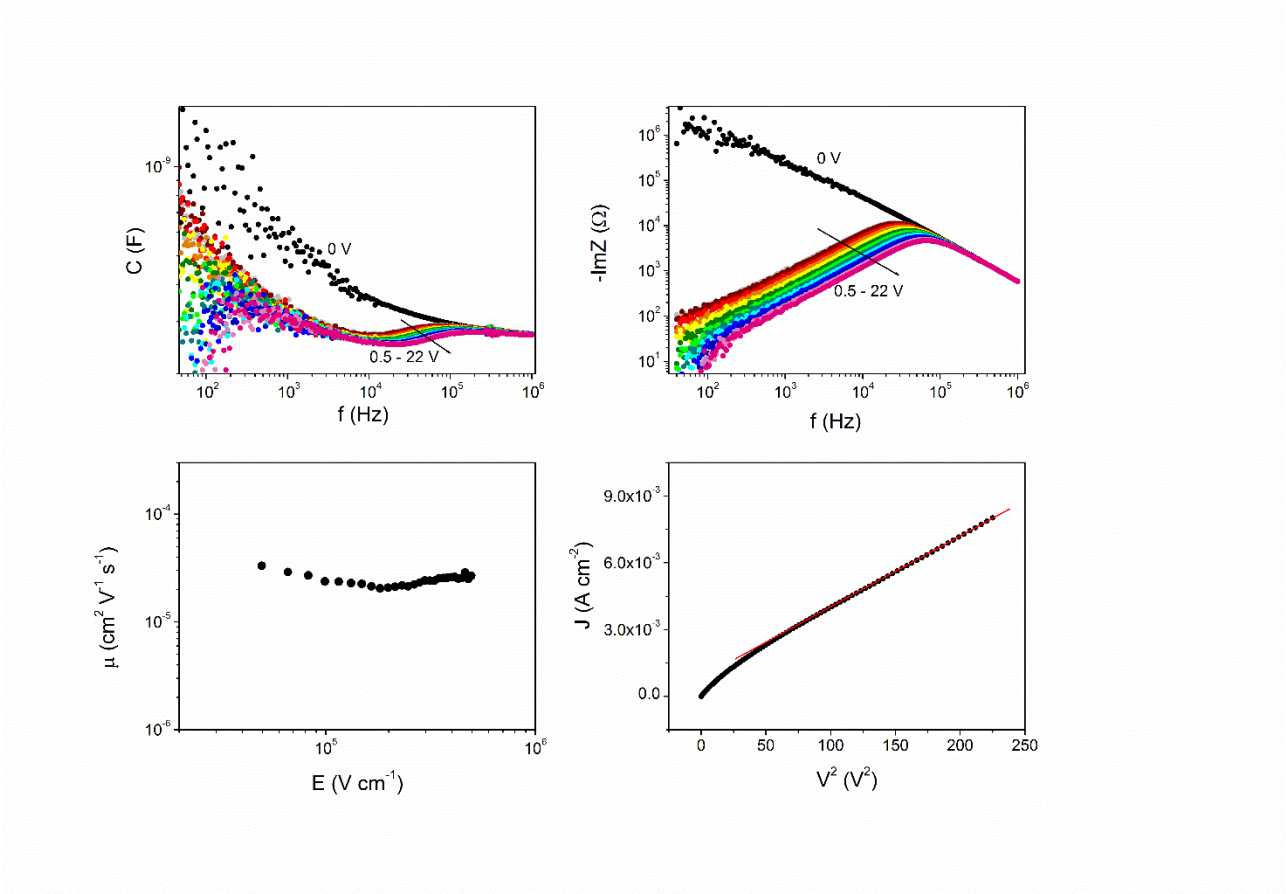

Figure 3.S7. *Top:* Variation of the capacitance (left) and of the imaginary part of impedance (right) with frequency and for various values of the dc bias for a hole-only device made of oligomer **8** (600 nm thick). *Bottom:* Bulk hole mobility as a function of the electric field (left), obtained from impedance measurements, and current-density versus square voltage (right) (the red line indicates the linear fit to the experimental data)

6.3.2. Spectra of New Compounds

Compound **3a**

^{1}H NMR (300 MHz, DMSO-d_6)

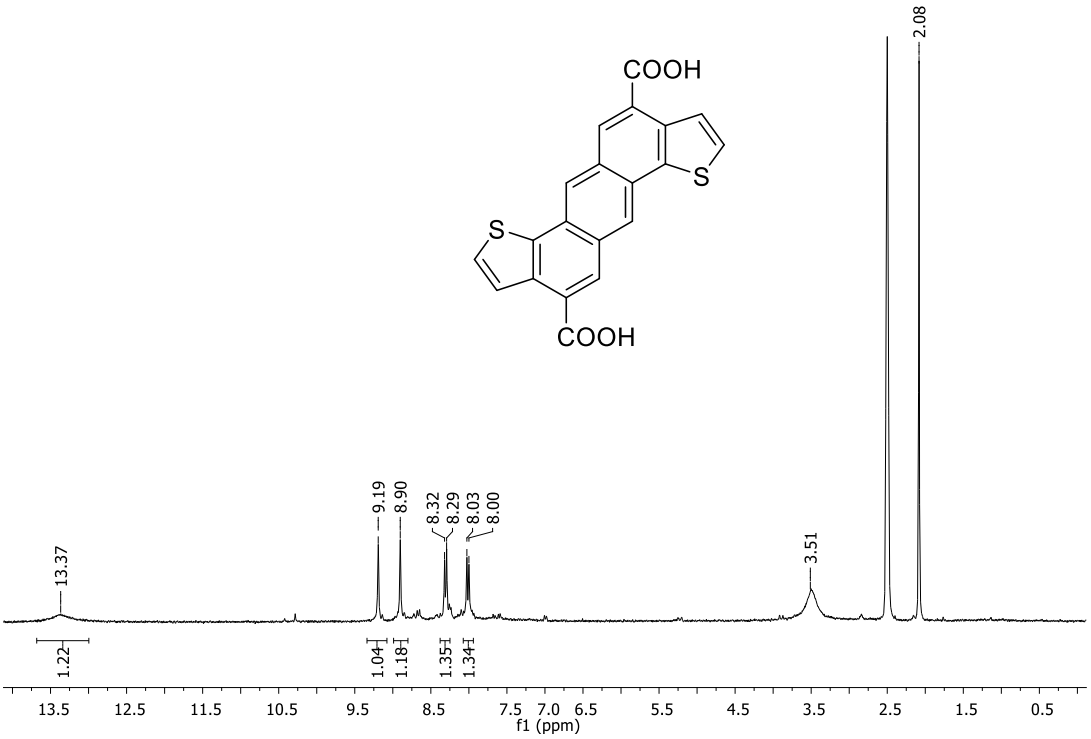

^{13}C NMR (101 MHz, DMSO-d_6)

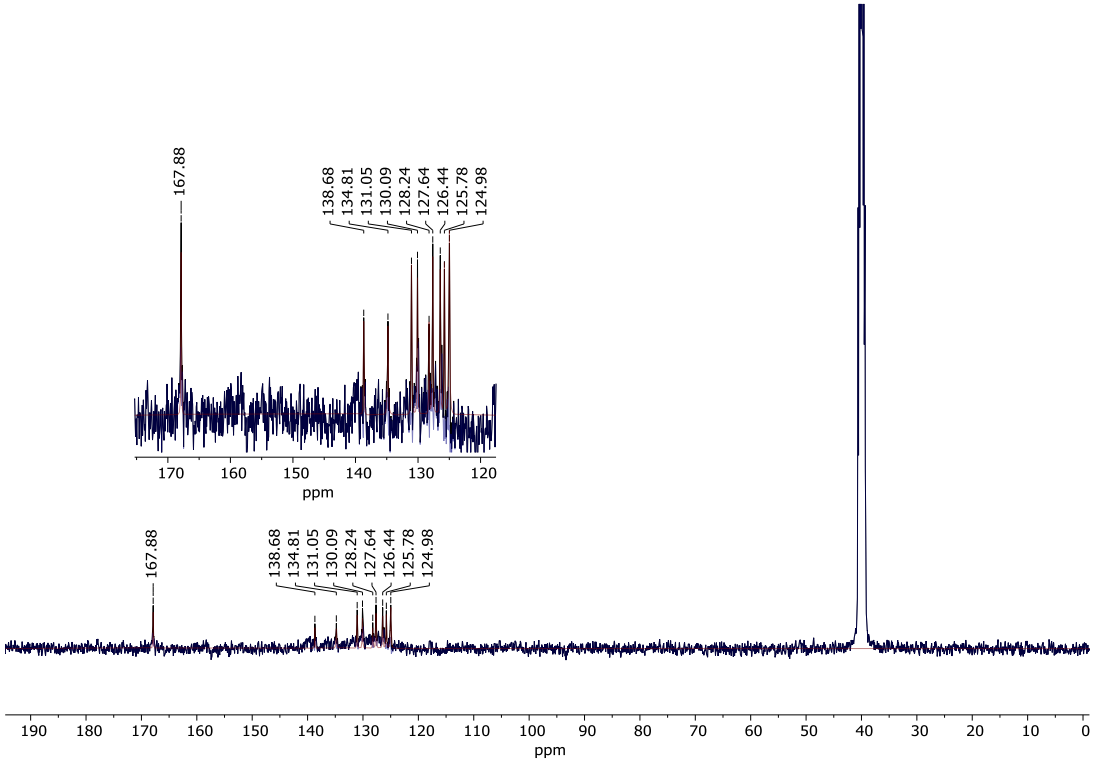
167.88
138.68
134.81
131.05
130.09
128.24
127.64
126.44
125.78
124.98
170
160
150
140
130
120
ppm
167.88
138.68
134.81
131.05
130.09
128.24
127.64
126.44
125.78
124.98
190
180
170
160
150
140
130
120
110
100
90
80
70
60
50
40
30
20
10
0
ppm

Compound **3b**

^{1}H NMR (300 MHz, $CDCl_3$)

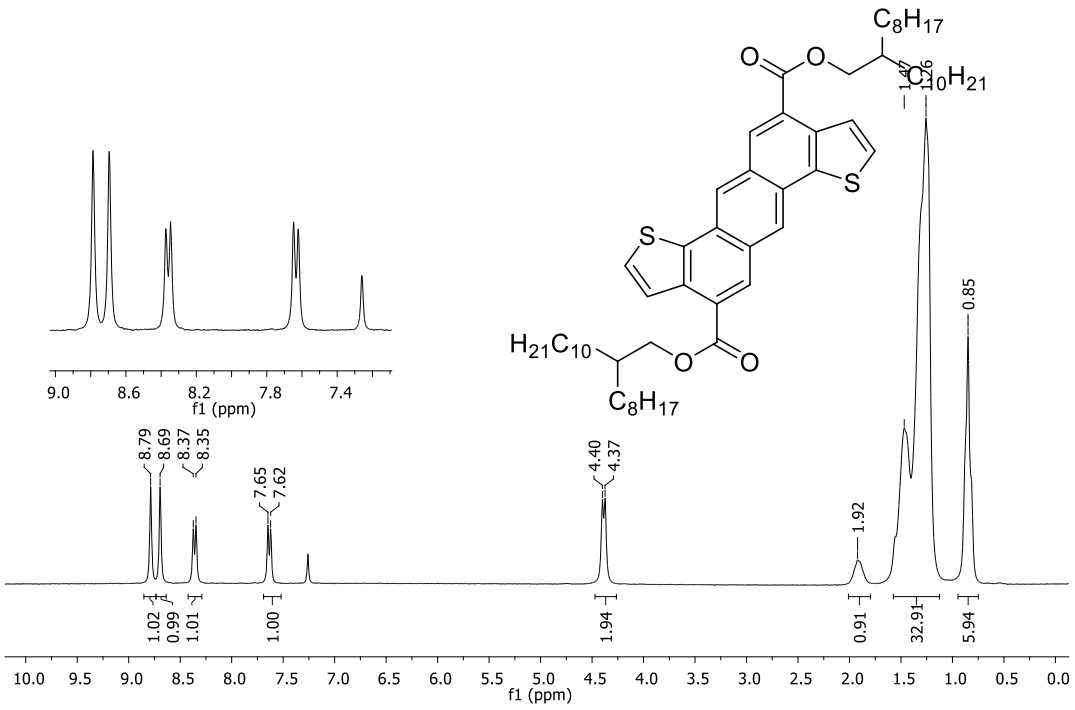

^{13}C NMR (101 MHz, $CDCl_3$)

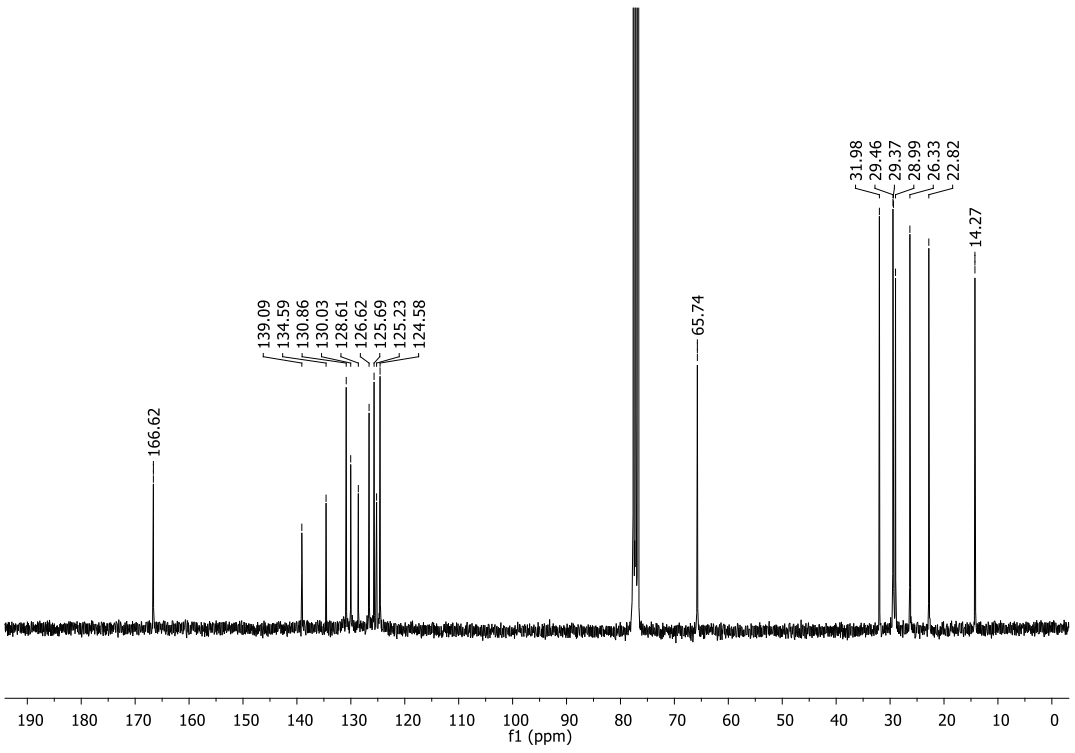

Compound **3c**

[1]H NMR (300 MHz, $CDCl_3$)

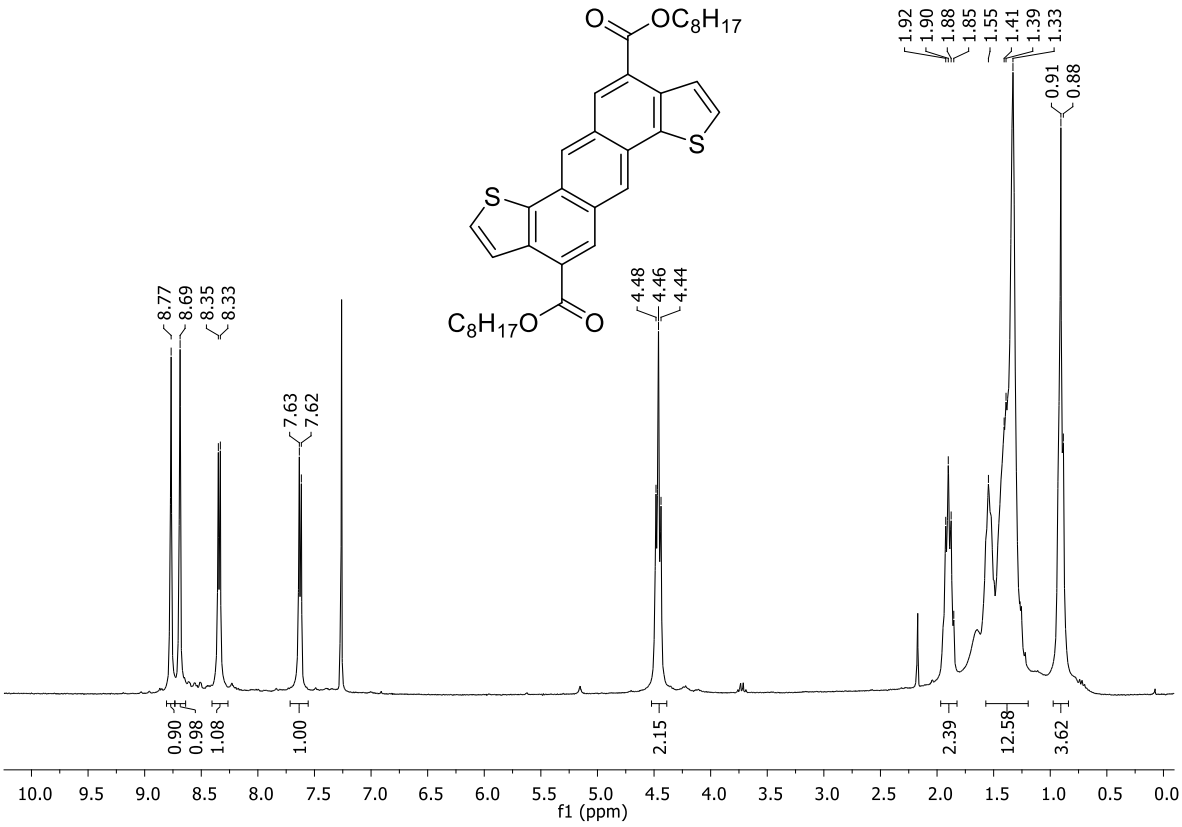

[13]C NMR (101 MHz, $CDCl_3$)

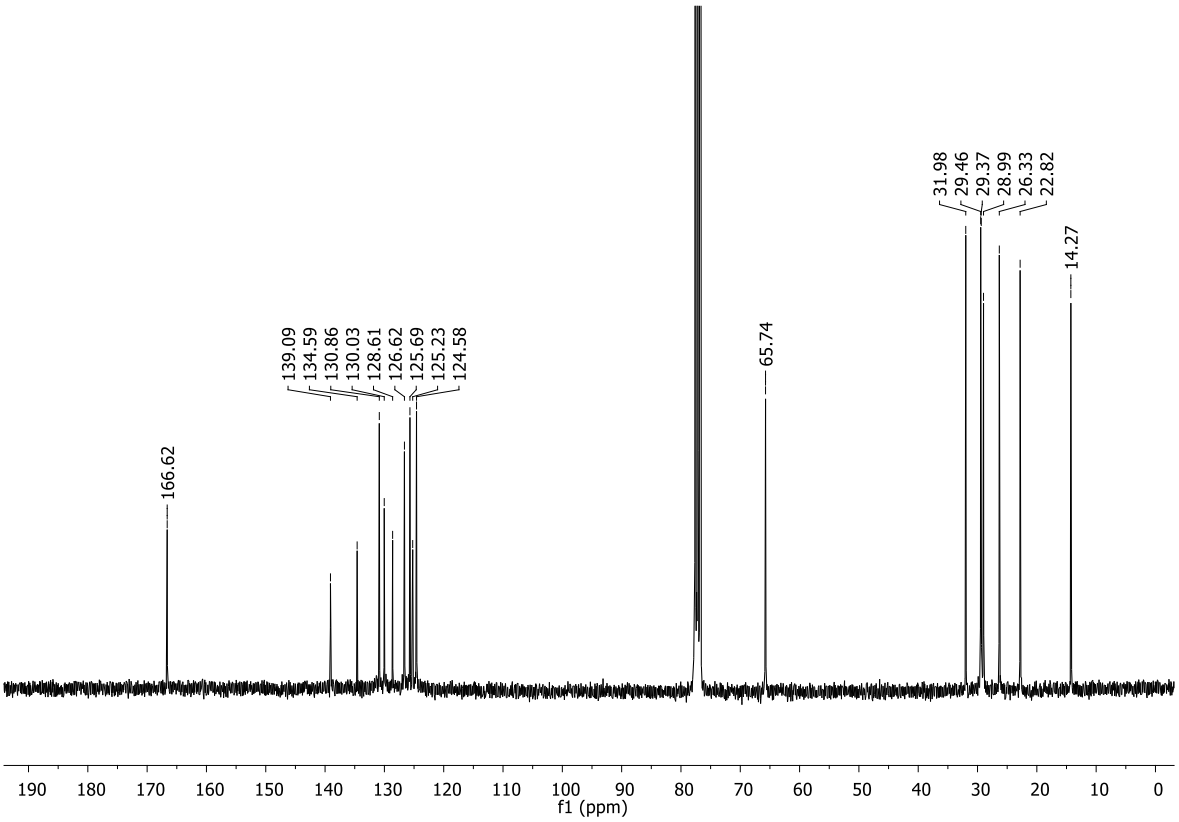
166.62
139.09
134.59
130.86
130.03
128.61
126.62
125.69
125.23
124.58
65.74
31.98
29.46
29.37
28.99
26.33
22.82
14.27
190 180 170 160 150 140 130 120 110 100 90 80 70 60 50 40 30 20 10 0
f1 (ppm)

DEPT

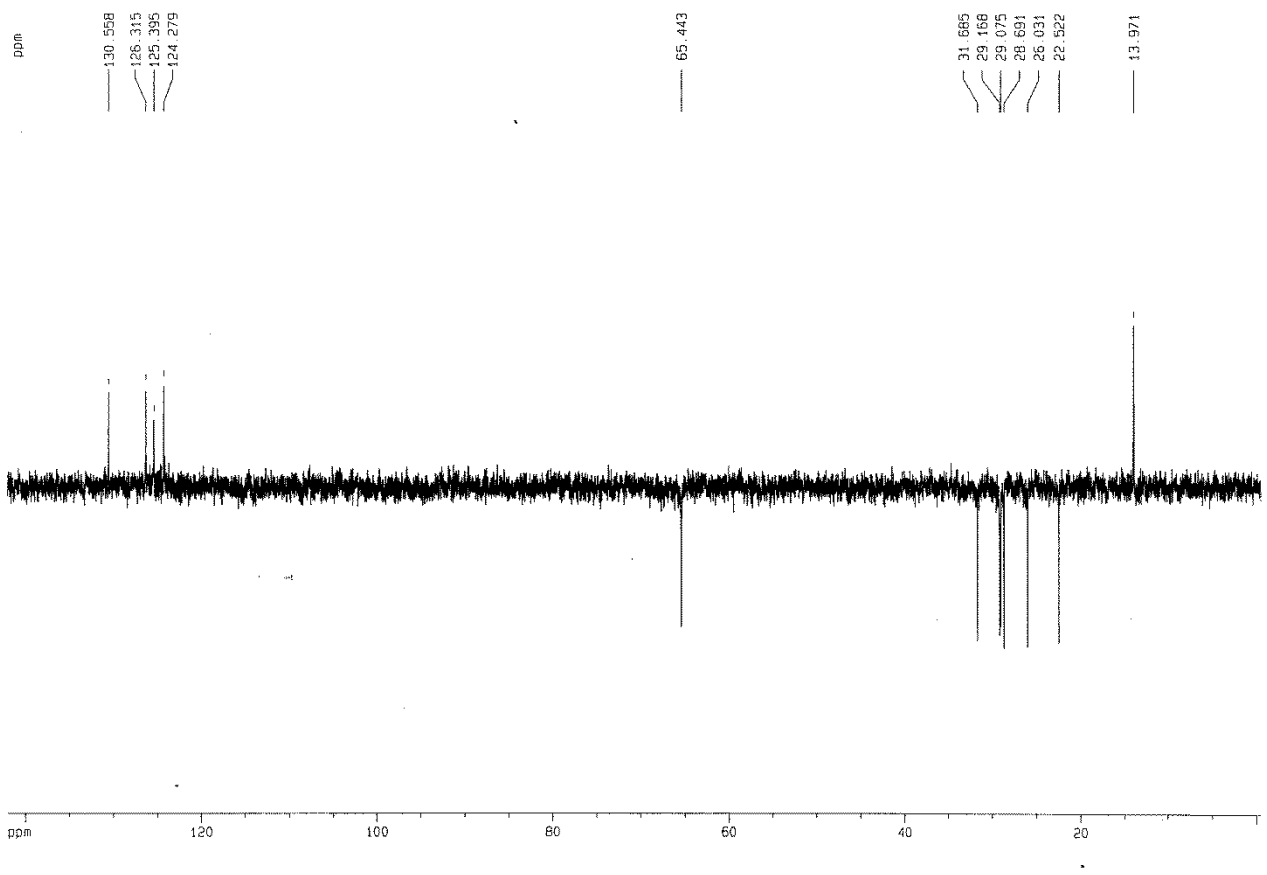
ppm
130.558
126.315
125.395
124.279
65.443
31.685
29.168
29.075
28.691
26.031
22.522
13.971
ppm
120
100
80
60
40
20

DEP-MS

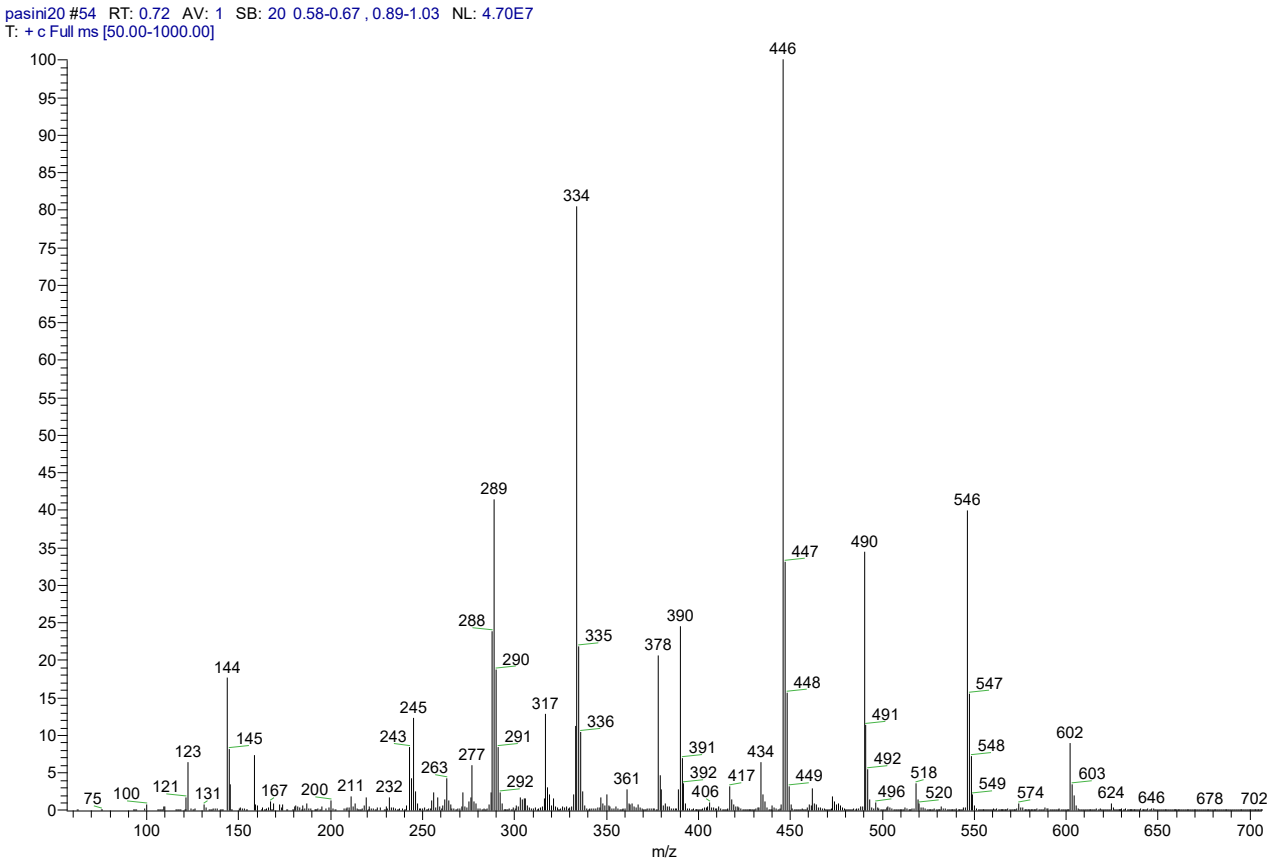
pasini20 #54 RT: 0.72 AV: 1 SB: 20 0.58-0.67 , 0.89-1.03 NL: 4.70E7
T: + c Full ms [50.00-1000.00]
m/z

Compound **3d**

[1]H NMR (300 MHz, $CDCl_3$)

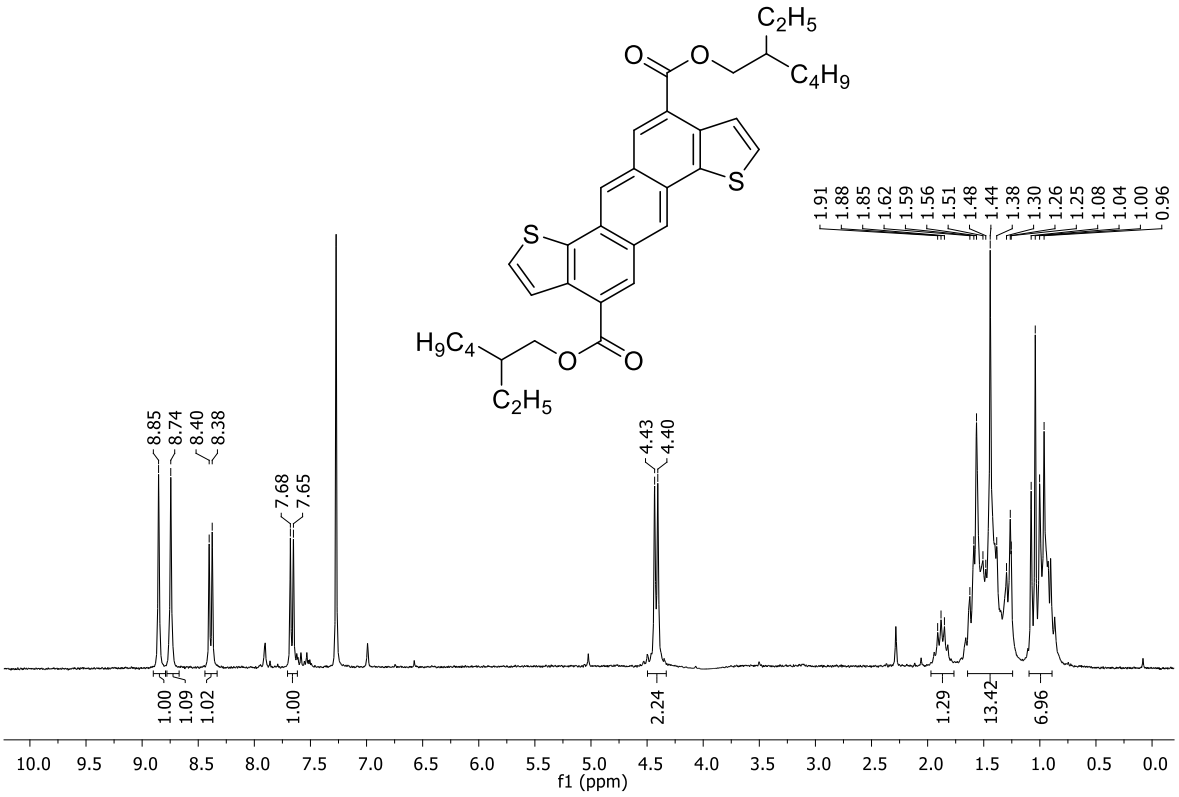

[13]C NMR (101 MHz, $CDCl_3$)

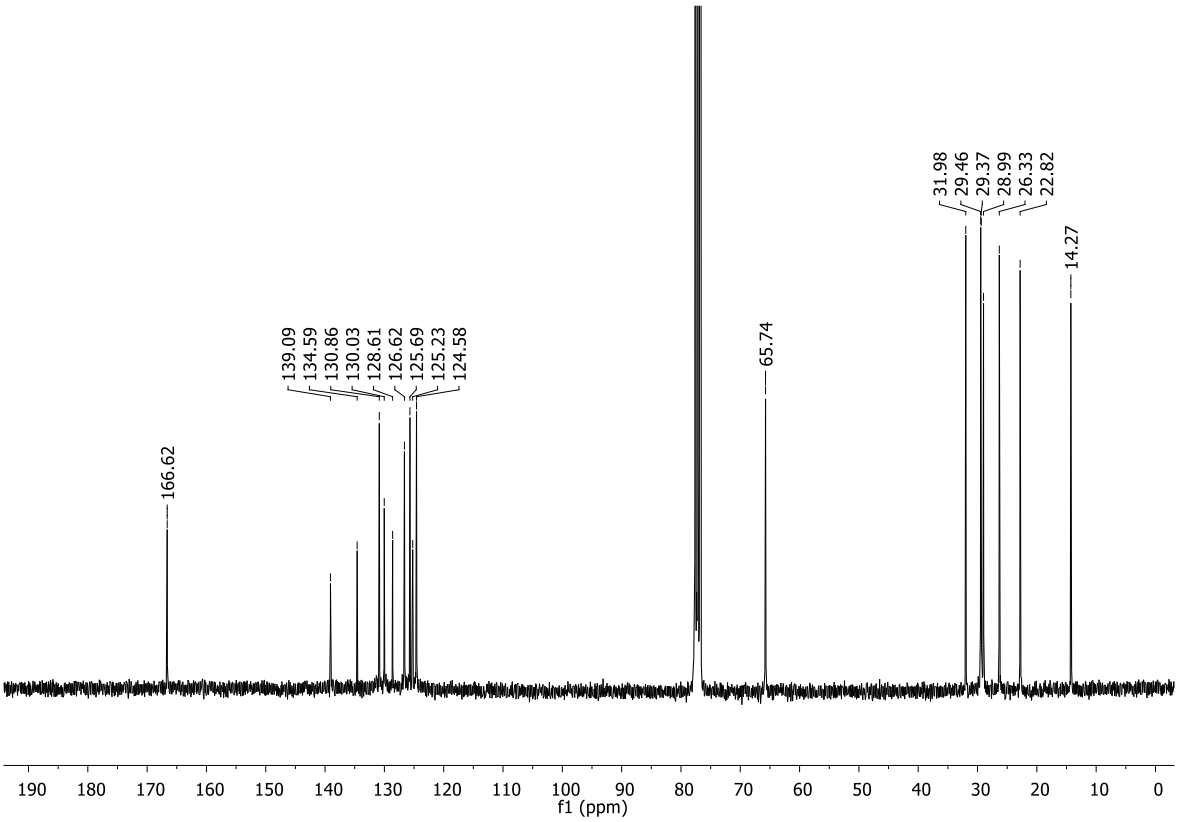
166.62
139.09
134.59
130.86
130.03
128.61
126.62
125.69
125.23
124.58
65.74
31.98
29.46
29.37
28.99
26.33
22.82
14.27
190 180 170 160 150 140 130 120 110 100 90 80 70 60 50 40 30 20 10 0
f1 (ppm)

DEPT

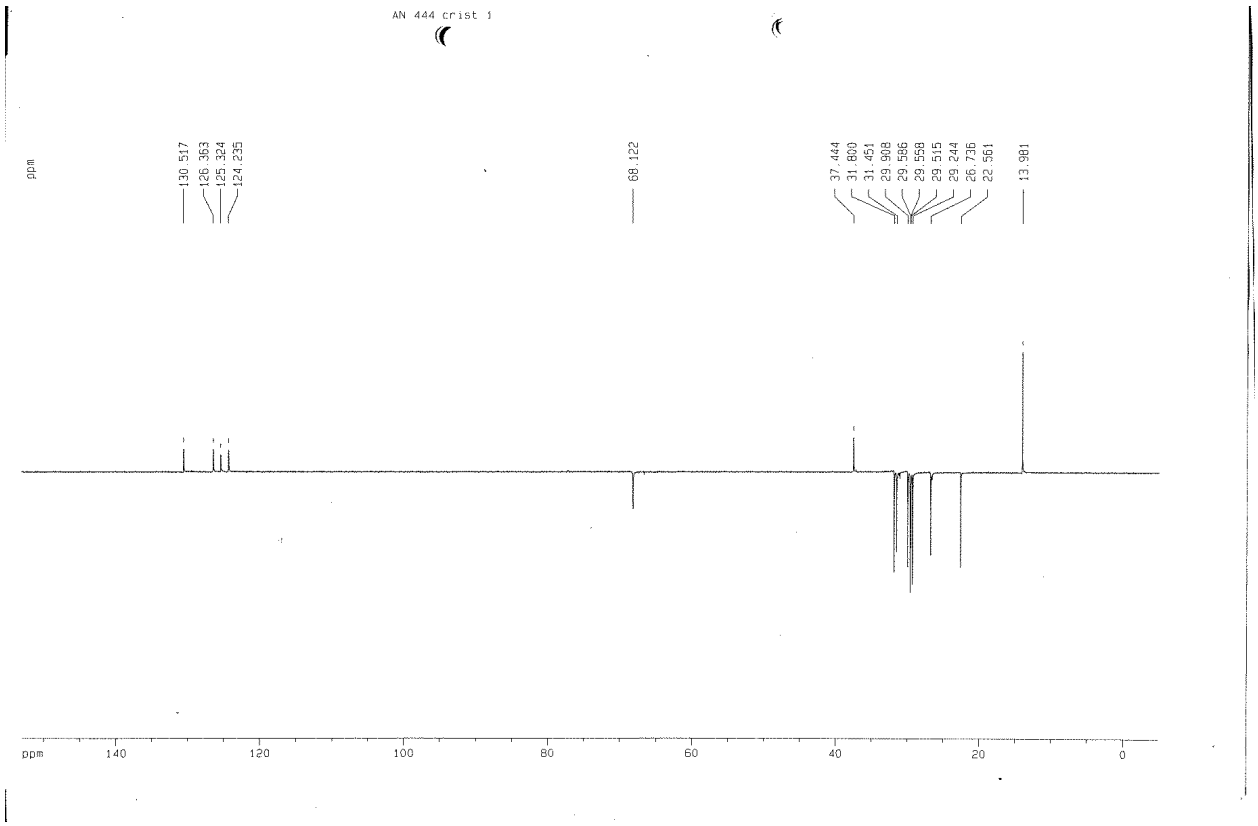
AN 444 crist 1
ppm
130.517
126.363
125.324
124.235
68.122
37.444
31.800
31.451
29.908
29.586
29.558
29.515
29.244
26.736
22.561
13.981
ppm 140 120 100 80 60 40 20 0

DEP-MS

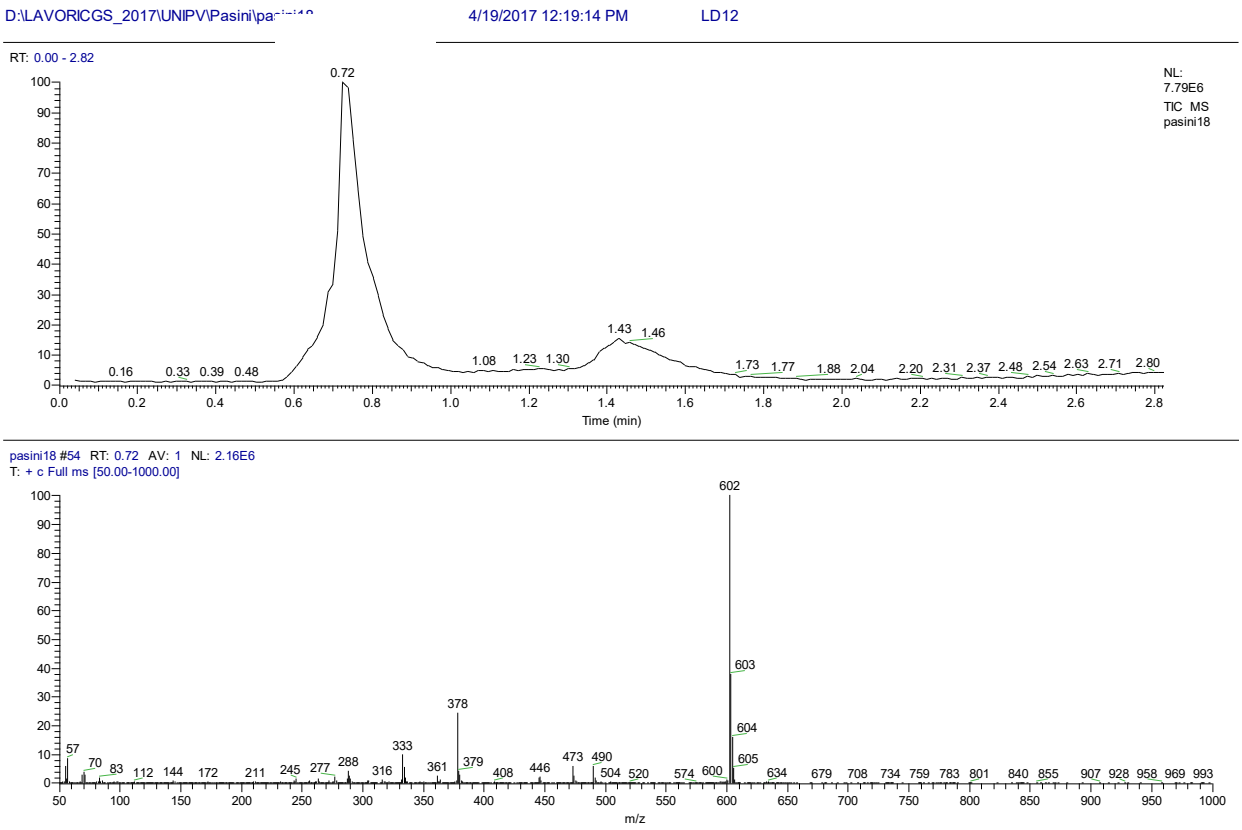
D:\LAVORICGS_2017\UNIPV\Pasini\pa
4/19/2017 12:19:14 PM
LD12
RT: 0.00 - 2.82
NL:
7.79E6
TIC MS
pasini18
Time (min)
pasini18 #54 RT: 0.72 AV: 1 NL: 2.16E6
T: + c Full ms [50.00-1000.00]
m/z

Compound **4**

^{1}H NMR (300 MHz, $CDCl_3$)

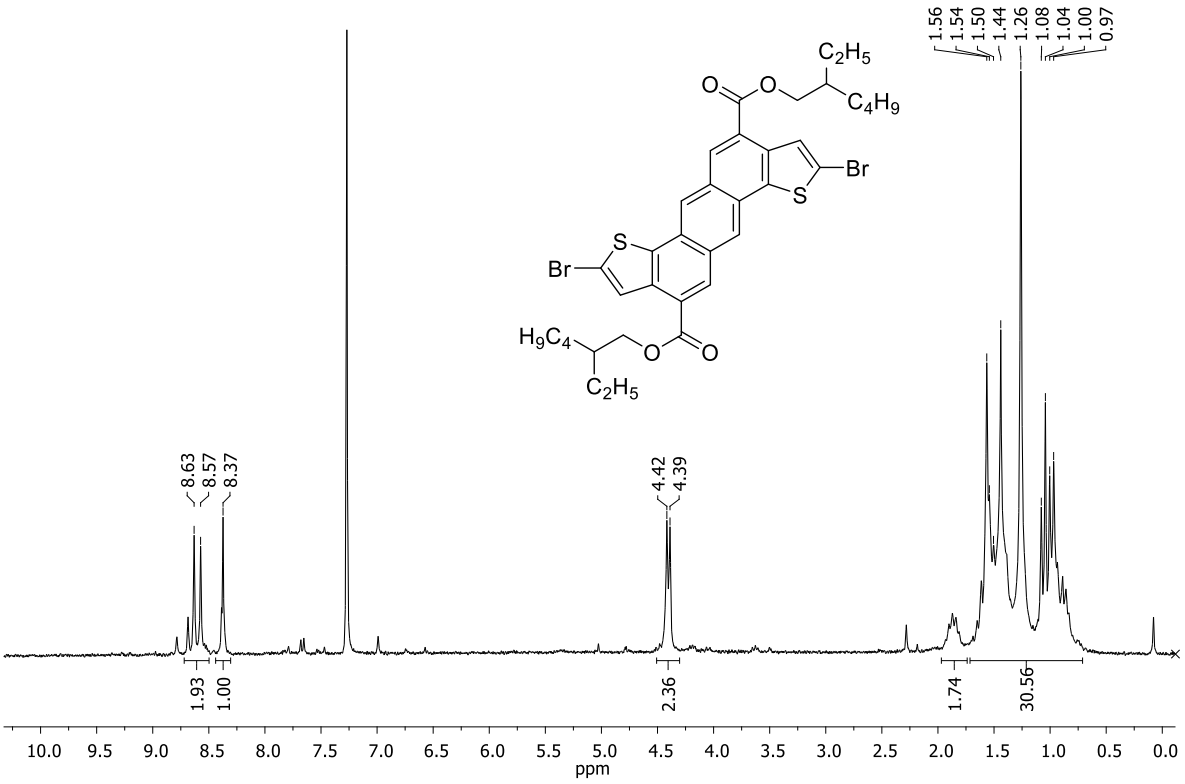

^{13}C NMR (101 MHz, $CDCl_3$)

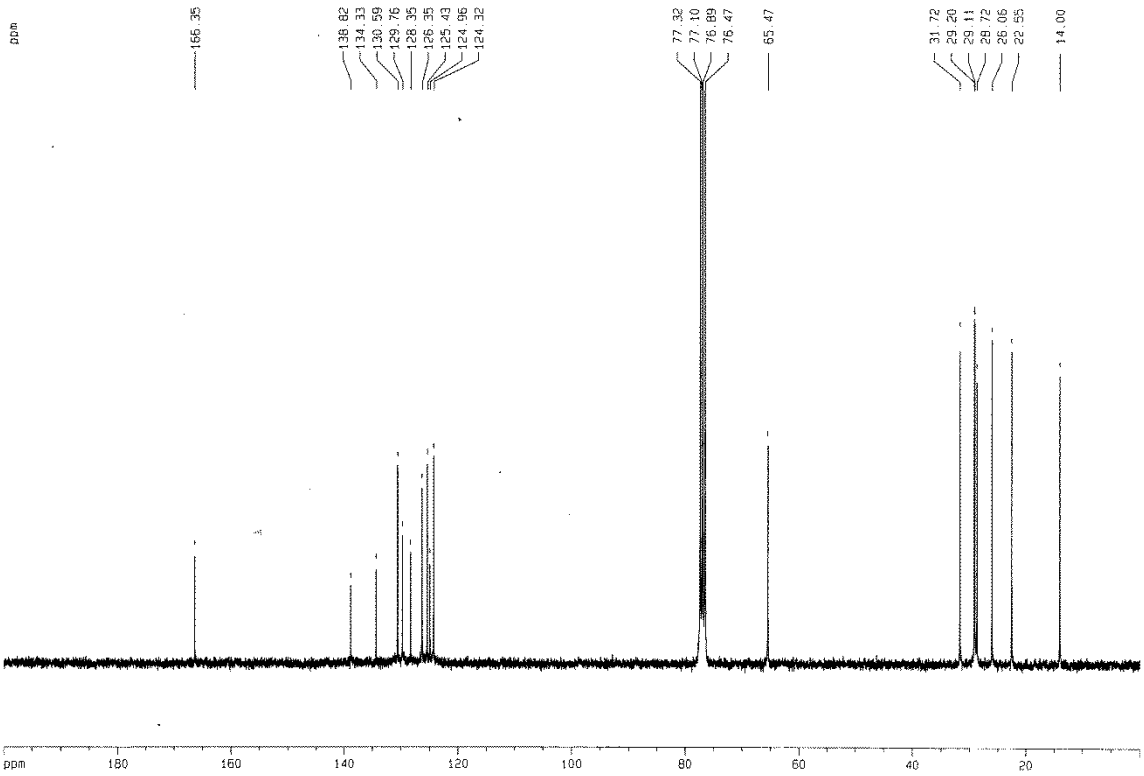
ppm
166.35
138.82
134.33
130.59
129.76
128.35
126.35
125.43
124.96
124.32
77.32
77.10
76.89
76.47
65.47
31.72
29.20
29.11
28.72
26.06
22.55
14.00
ppm
180
160
140
120
100
80
60
40
20

DEP-MS

pasini24_170607120158 6/7/2017 12:01:58 PM LD28

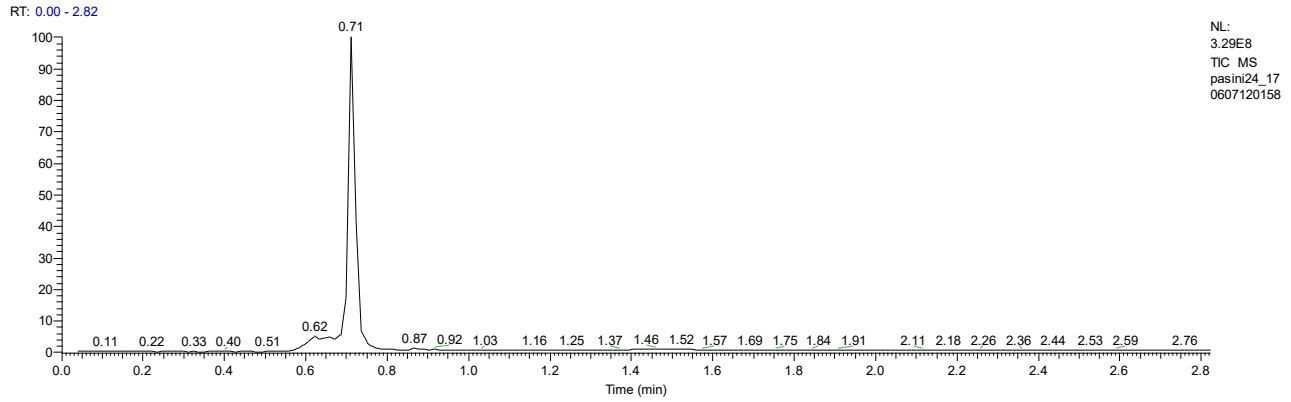

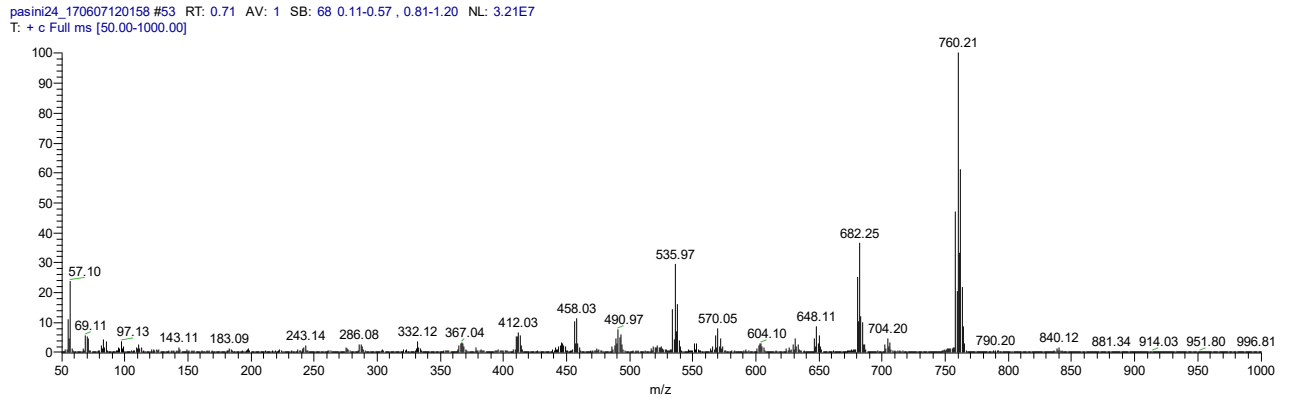

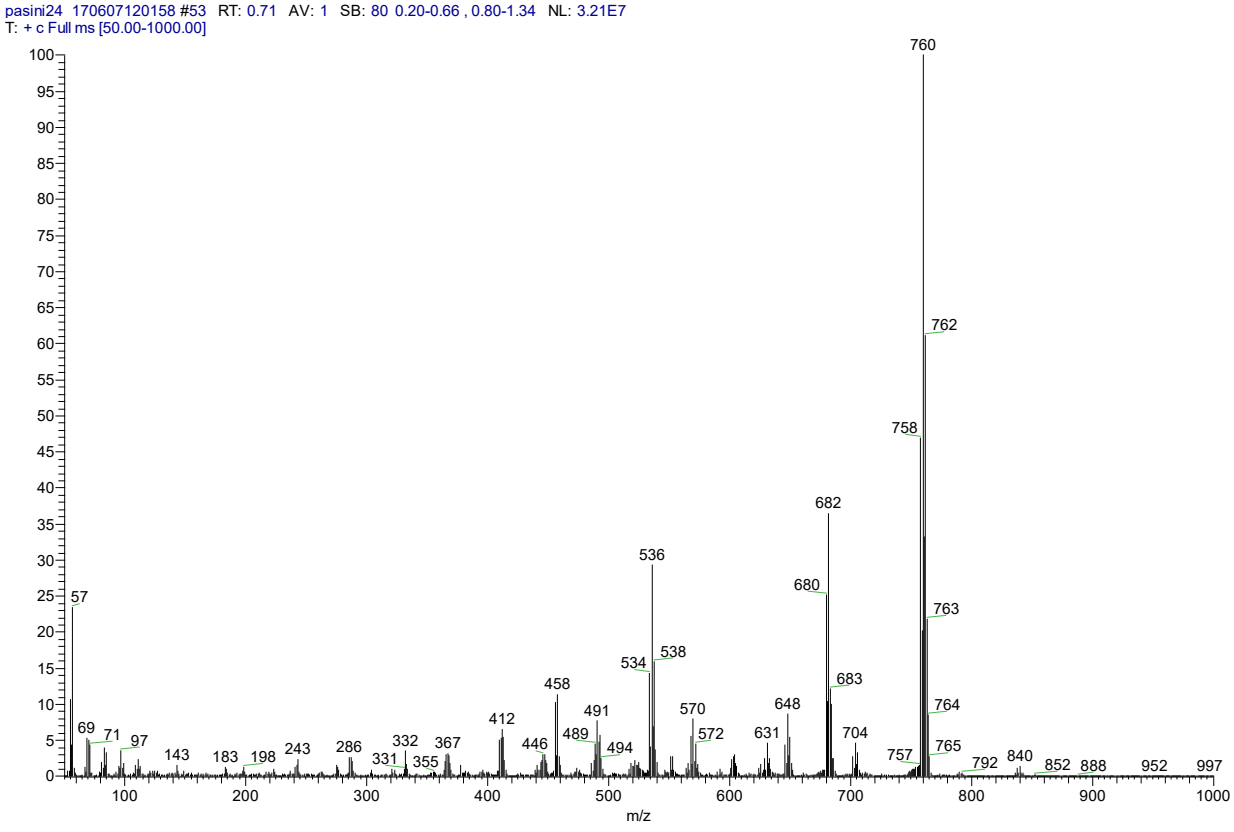

Compound **5**

^{1}H NMR (300 MHz, $CDCl_3$)

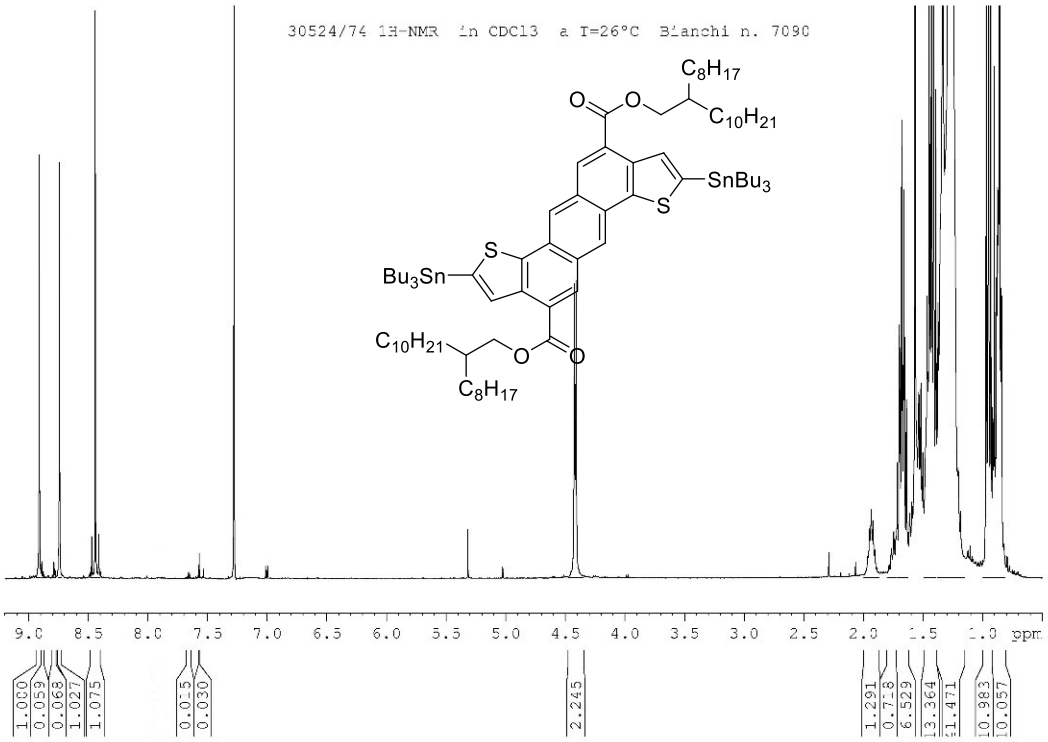

^{13}C NMR (101 MHz, $CDCl_3$)

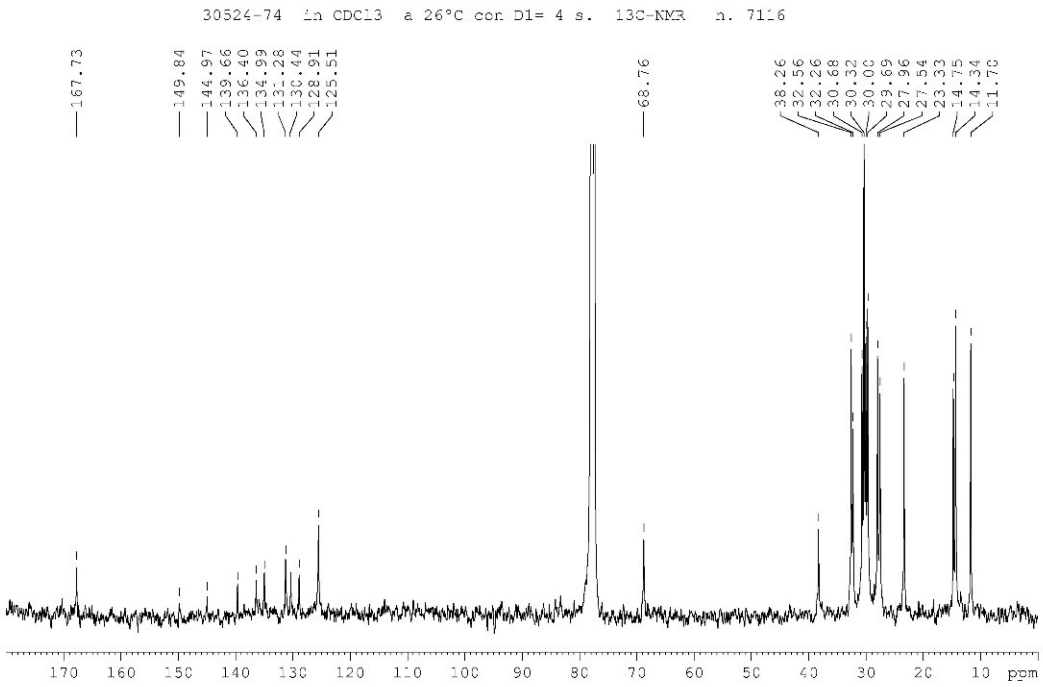

APCI FTICR MS

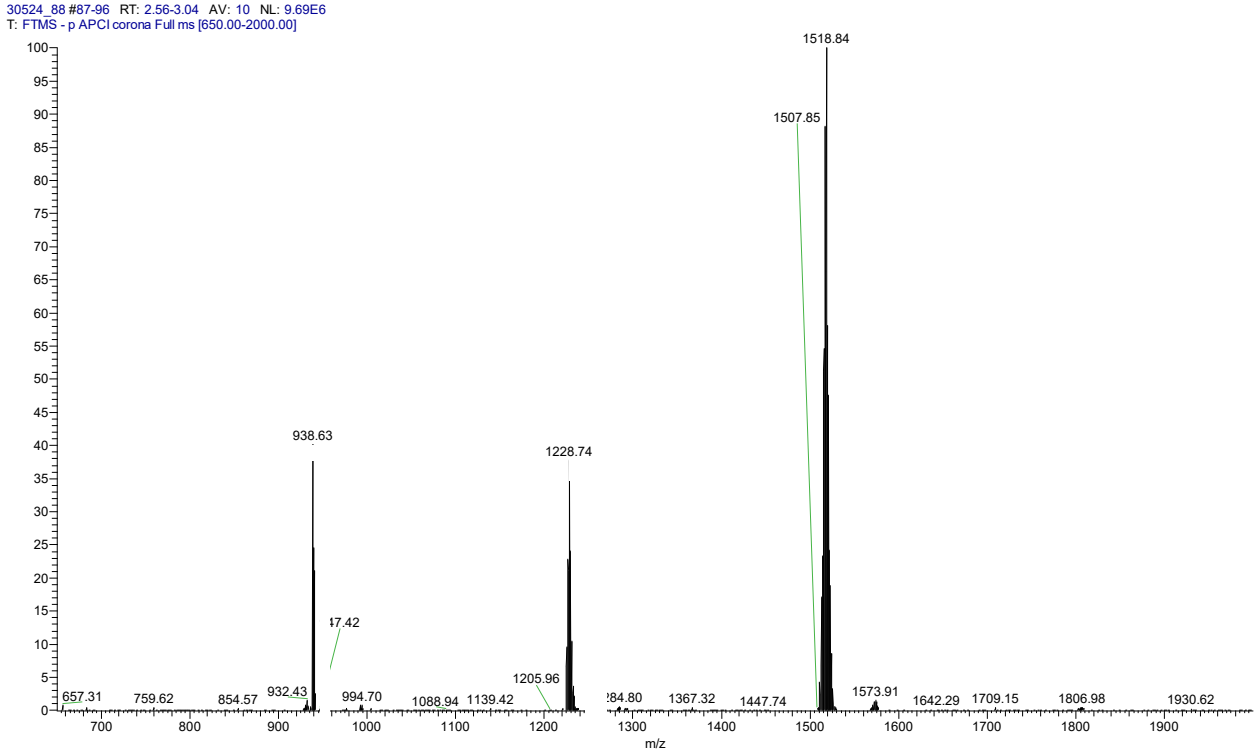

Compound **6**

^{1}H NMR (300 MHz, $CDCl_3$)

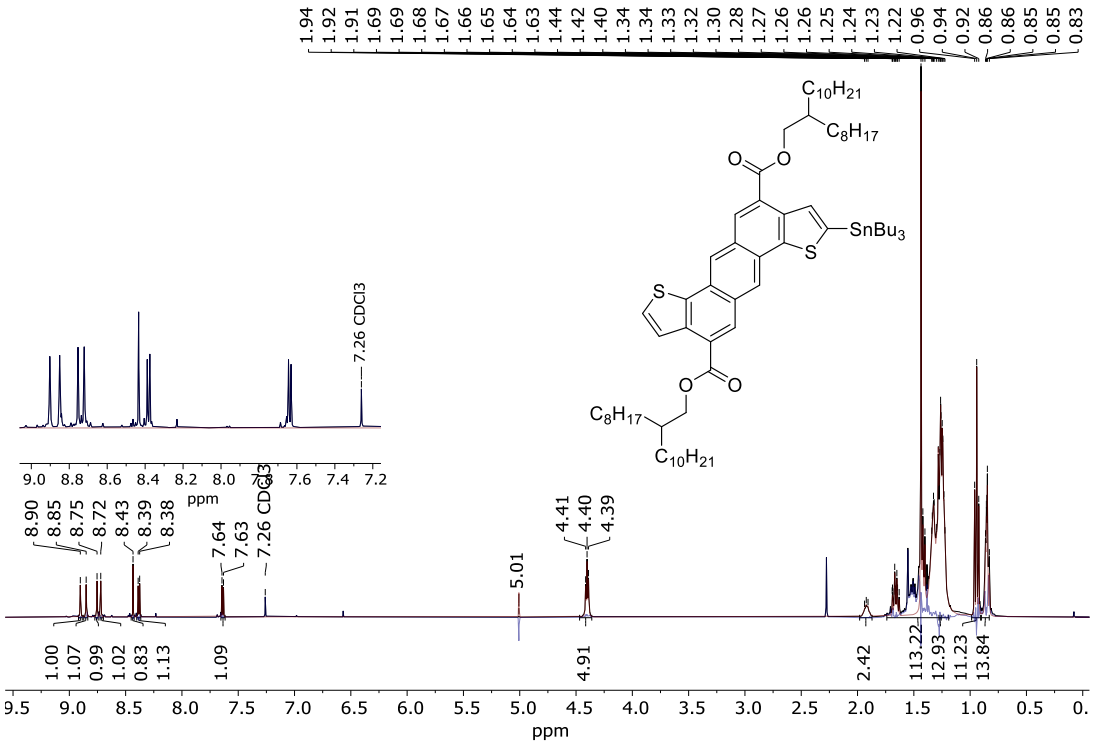

^{13}C NMR (101 MHz, $CDCl_3$)

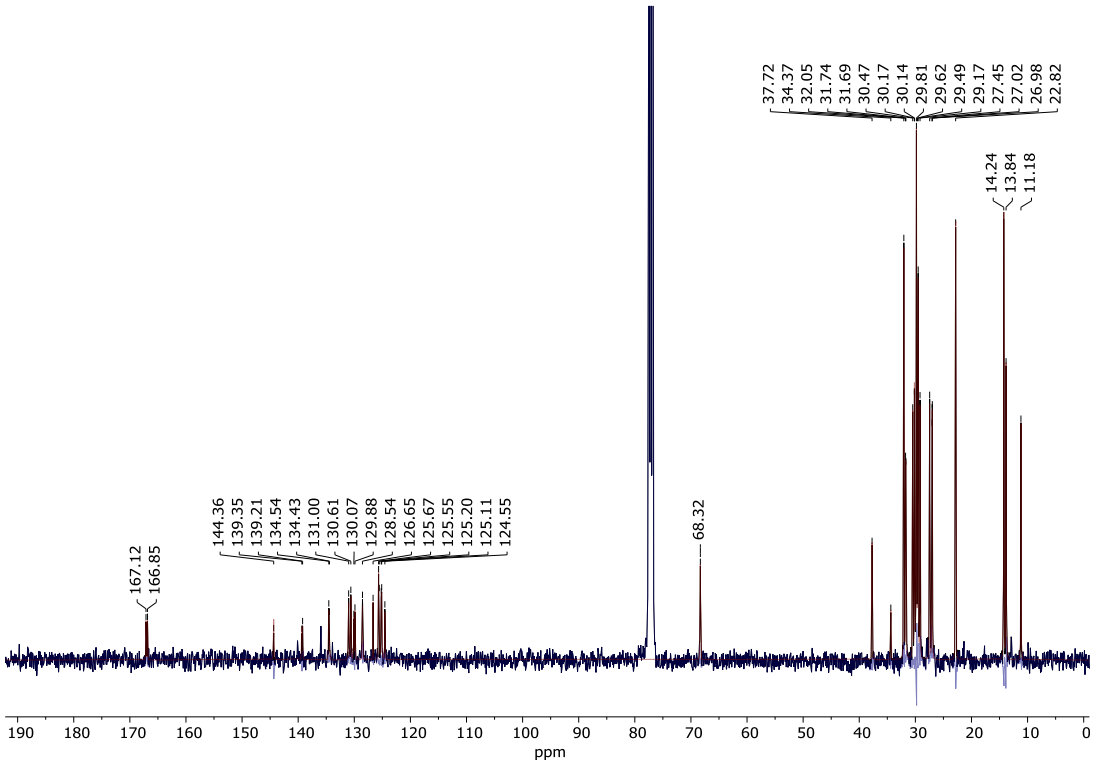

Compound **9**

^{1}H NMR (400 MHz, $CDCl_3$)

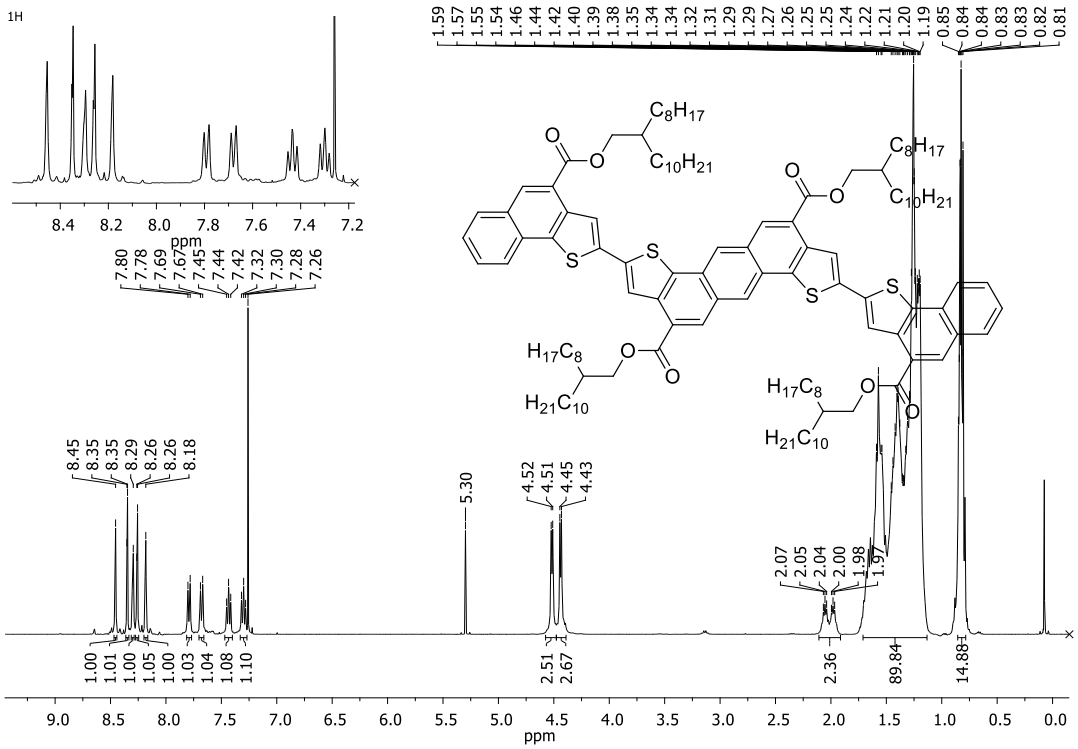

^{13}C NMR (400 MHz, $CDCl_3$)

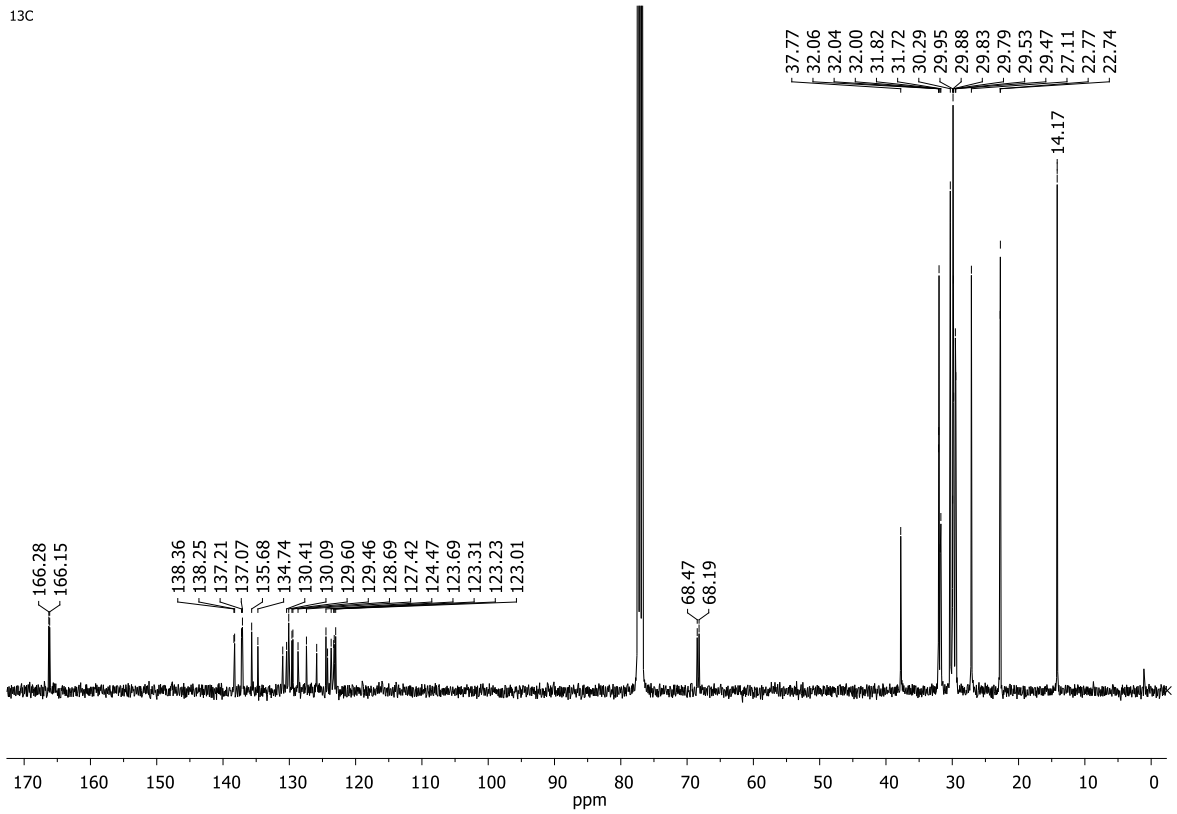
13C
37.77
32.06
32.04
32.00
31.82
31.72
30.29
29.95
29.88
29.83
29.79
29.53
29.47
27.11
22.77
22.74
14.17
166.28
166.15
138.36
138.25
137.21
137.07
135.68
134.74
130.41
130.09
129.60
129.46
128.69
127.42
124.47
123.69
123.31
123.23
123.01
68.47
68.19
170 160 150 140 130 120 110 100 90 80 70 60 50 40 30 20 10 0
ppm

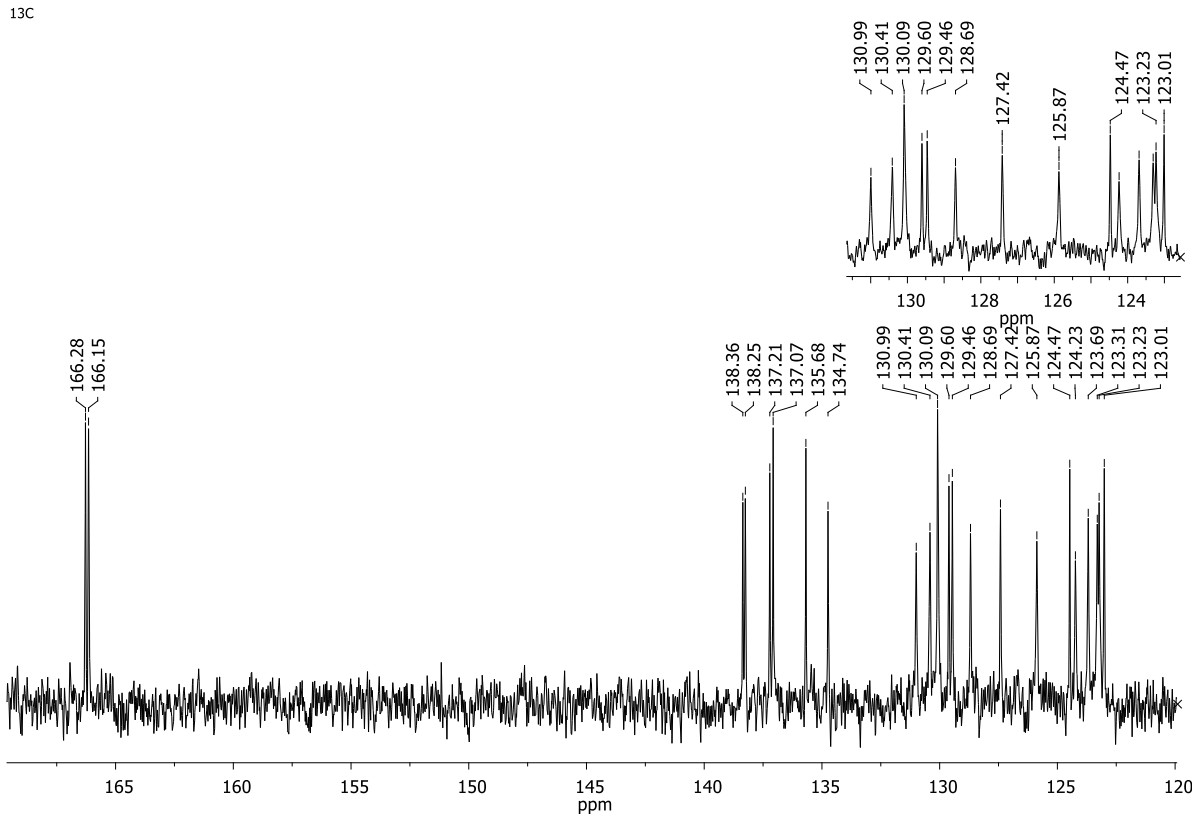
13C
130.99
130.41
130.09
129.60
129.46
128.69
127.42
125.87
124.47
123.23
123.01
130 128 126 124
ppm
166.28
166.15
138.36
138.25
137.21
137.07
135.68
134.74
130.99
130.41
130.09
129.60
129.46
128.69
127.42
125.87
124.47
124.23
123.69
123.31
123.23
123.01
165 160 155 150 145 140 135 130 125 120
ppm

DEPT135deg

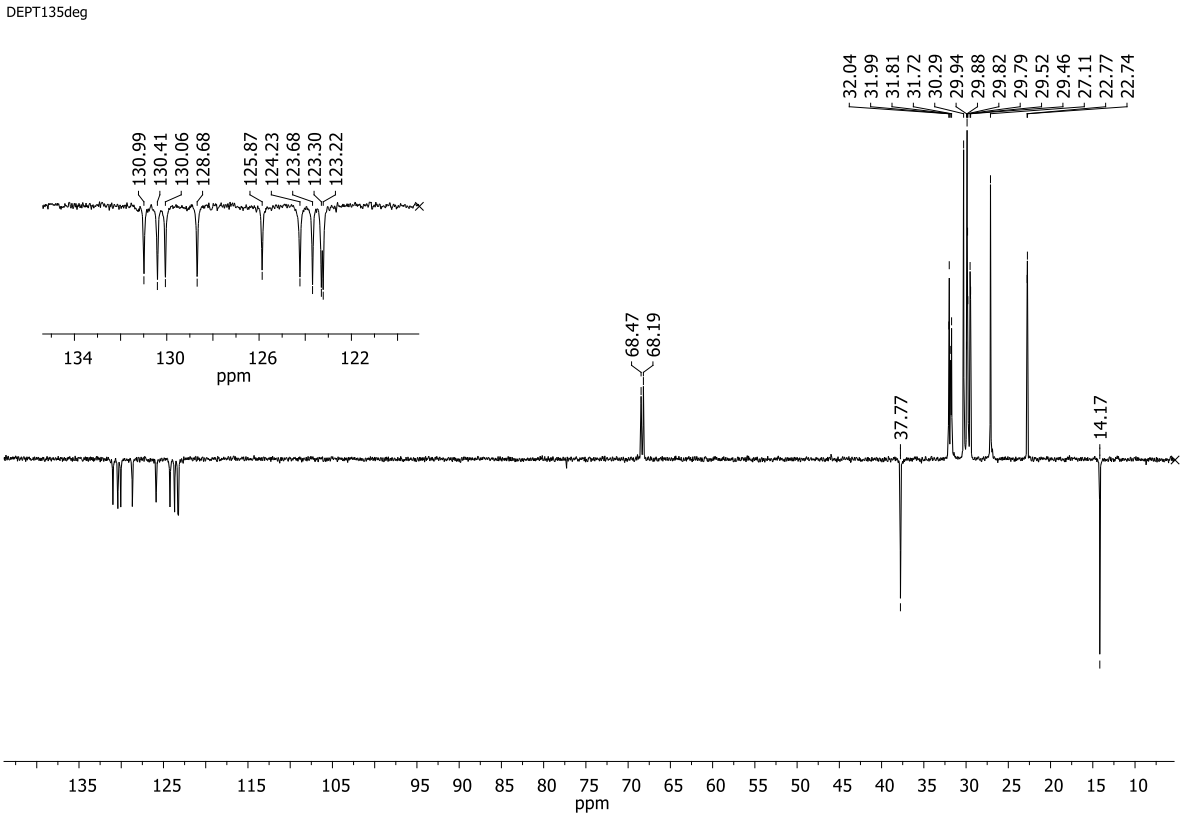
DEPT135deg
32.04
31.99
31.81
31.72
30.29
29.94
29.88
29.82
29.79
29.52
29.46
27.11
22.77
22.74
130.99
130.41
130.06
128.68
125.87
124.23
123.68
123.30
123.22
134
130
126
122
ppm
68.47
68.19
37.77
14.17
135
125
115
105
95
90
85
80
75
70
65
60
55
50
45
40
35
30
25
20
15
10
ppm

COSY

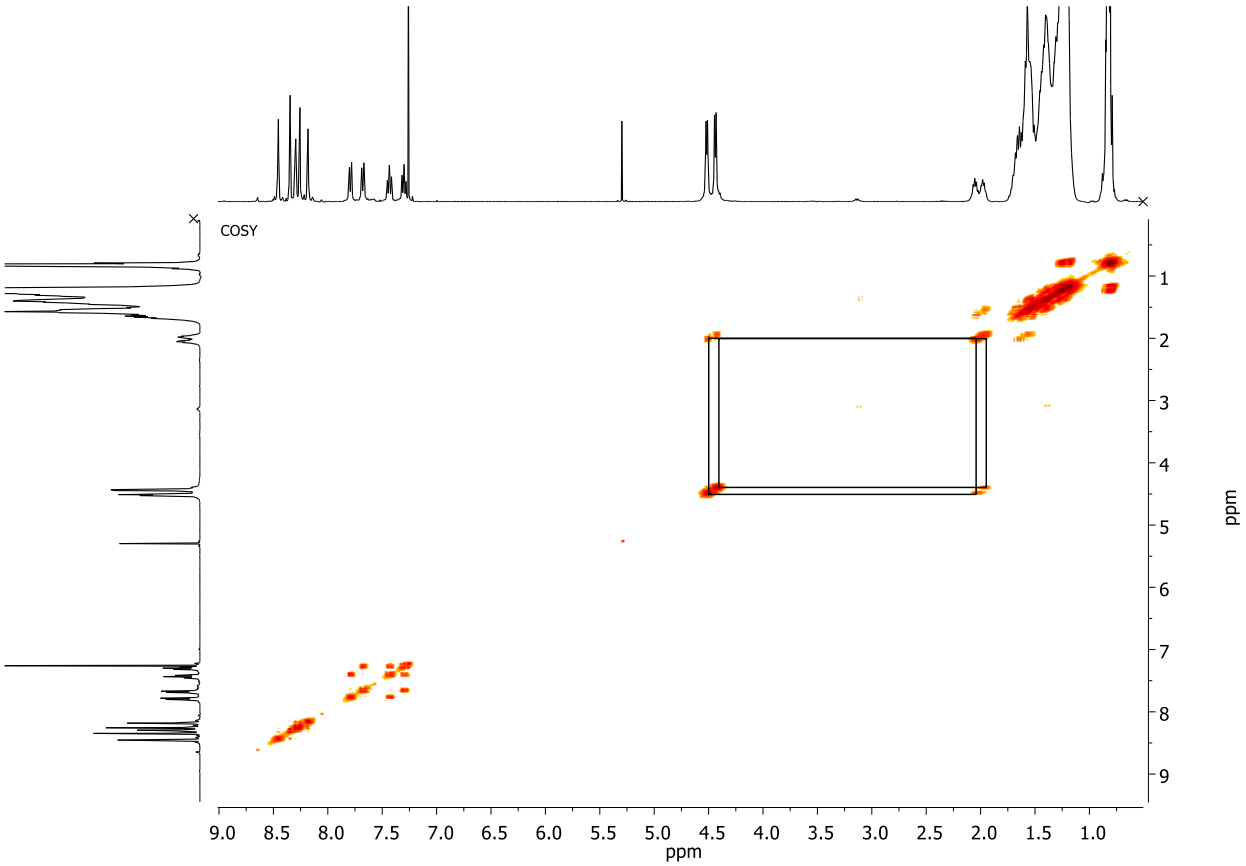
COSY
9.0 8.5 8.0 7.5 7.0 6.5 6.0 5.5 5.0 4.5 4.0 3.5 3.0 2.5 2.0 1.5 1.0
ppm
1 2 3 4 5 6 7 8 9
ppm

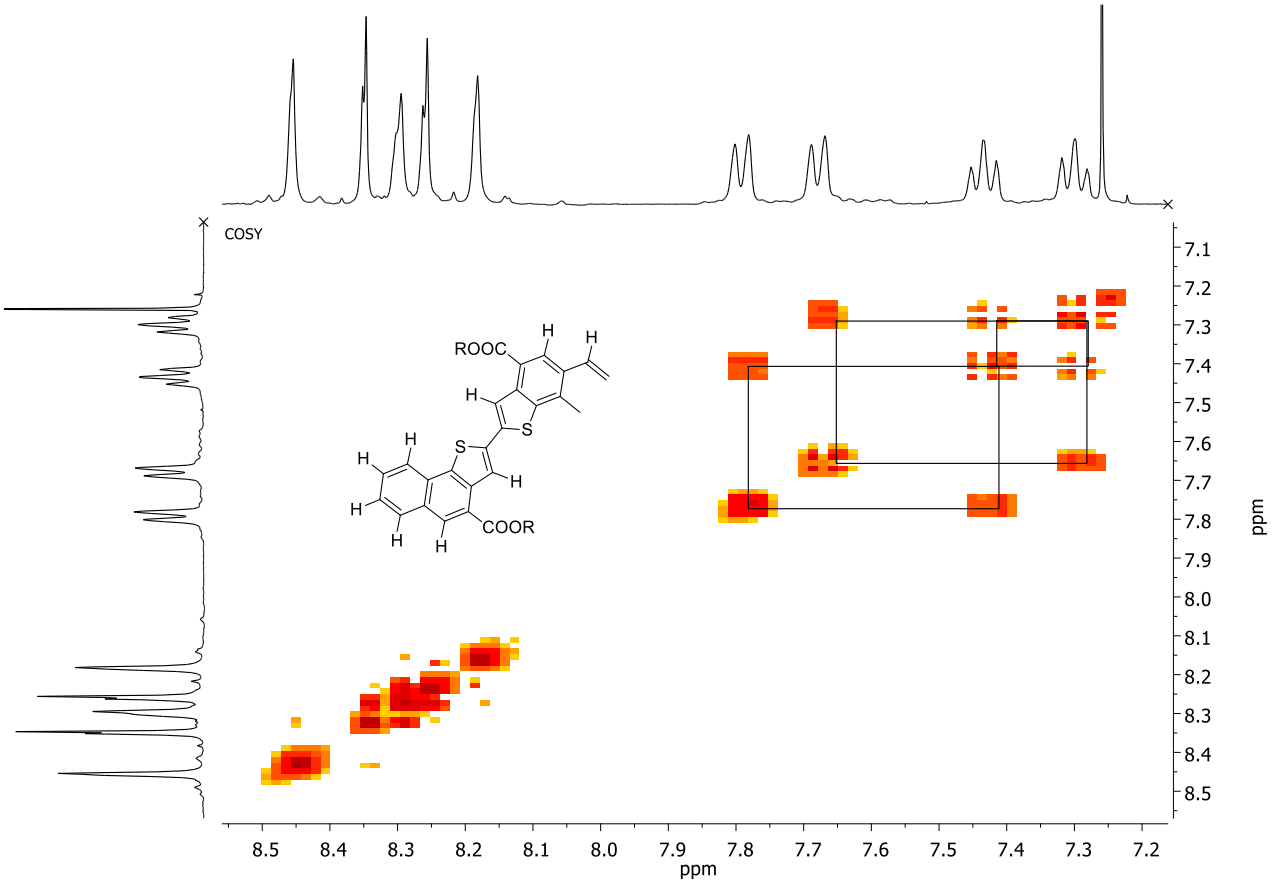
COSY
ROOC
COOR
S
S
H
8.5
8.4
8.3
8.2
8.1
8.0
7.9
7.8
7.7
7.6
7.5
7.4
7.3
7.2
ppm
7.1
7.2
7.3
7.4
7.5
7.6
7.7
7.8
7.9
8.0
8.1
8.2
8.3
8.4
8.5
ppm

HMQC

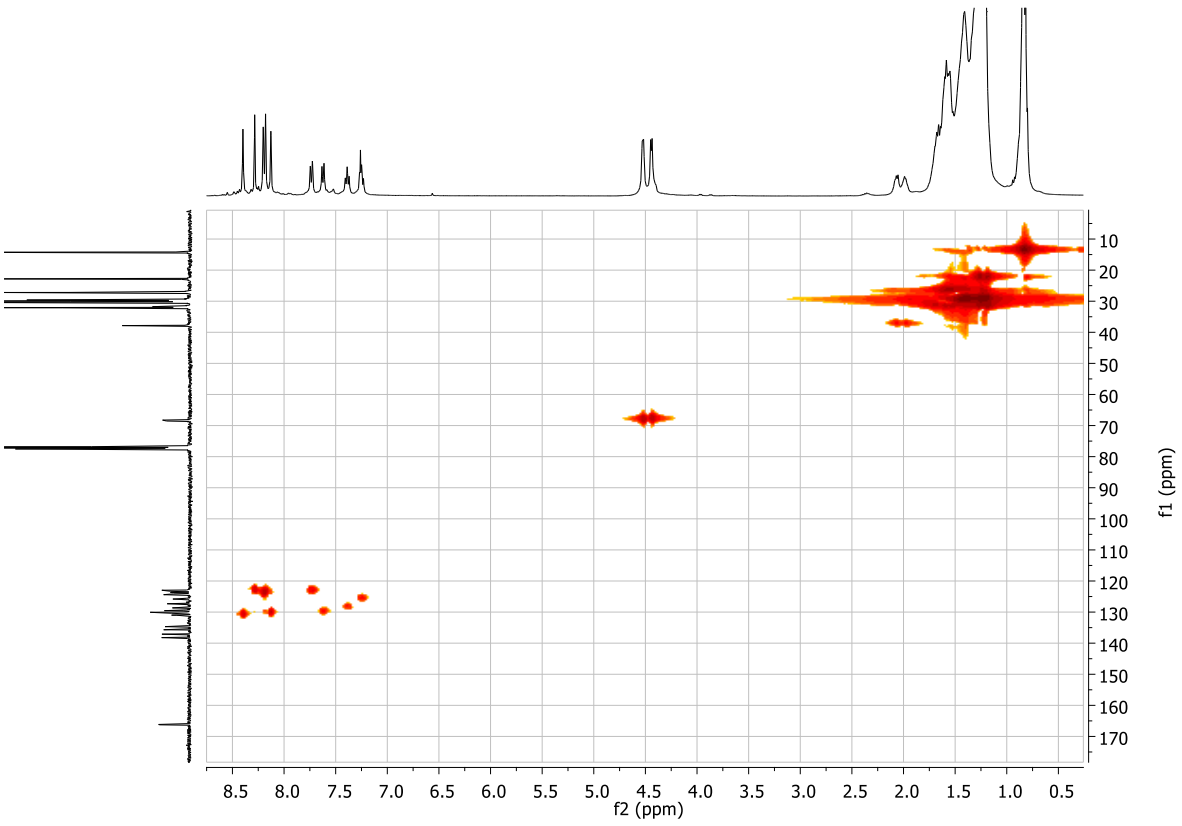
f2 (ppm)
f1 (ppm)

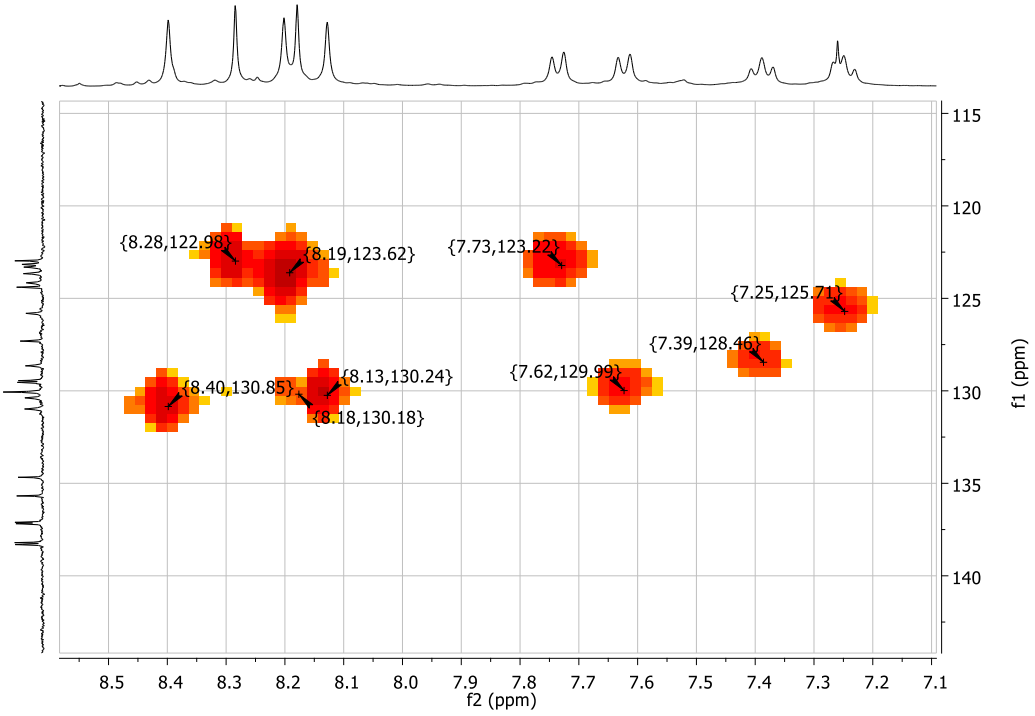
{8.28,122.98}
{8.19,123.62}
{7.73,123.22}
{7.25,125.71}
{7.39,128.46}
{7.62,129.99}
{8.40,130.85}
{8.13,130.24}
{8.18,130.18}
f2 (ppm)
f1 (ppm)

HMBC

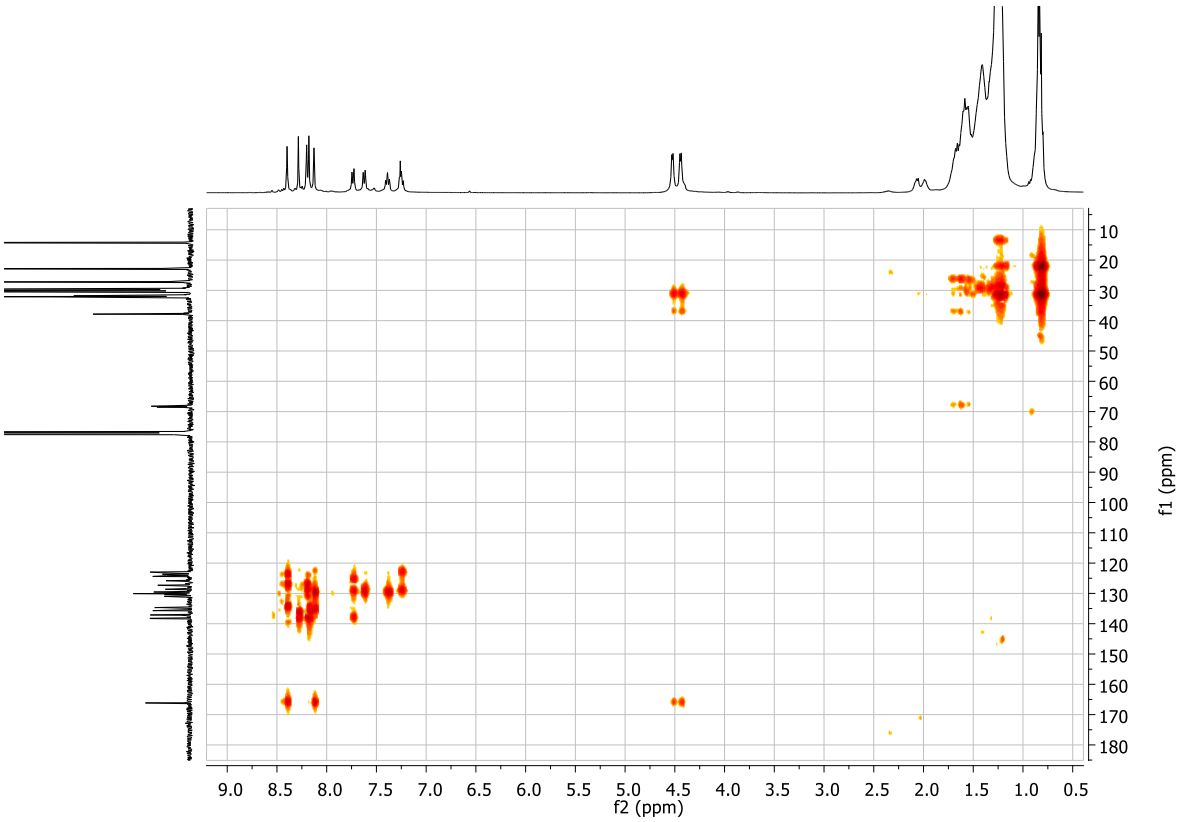

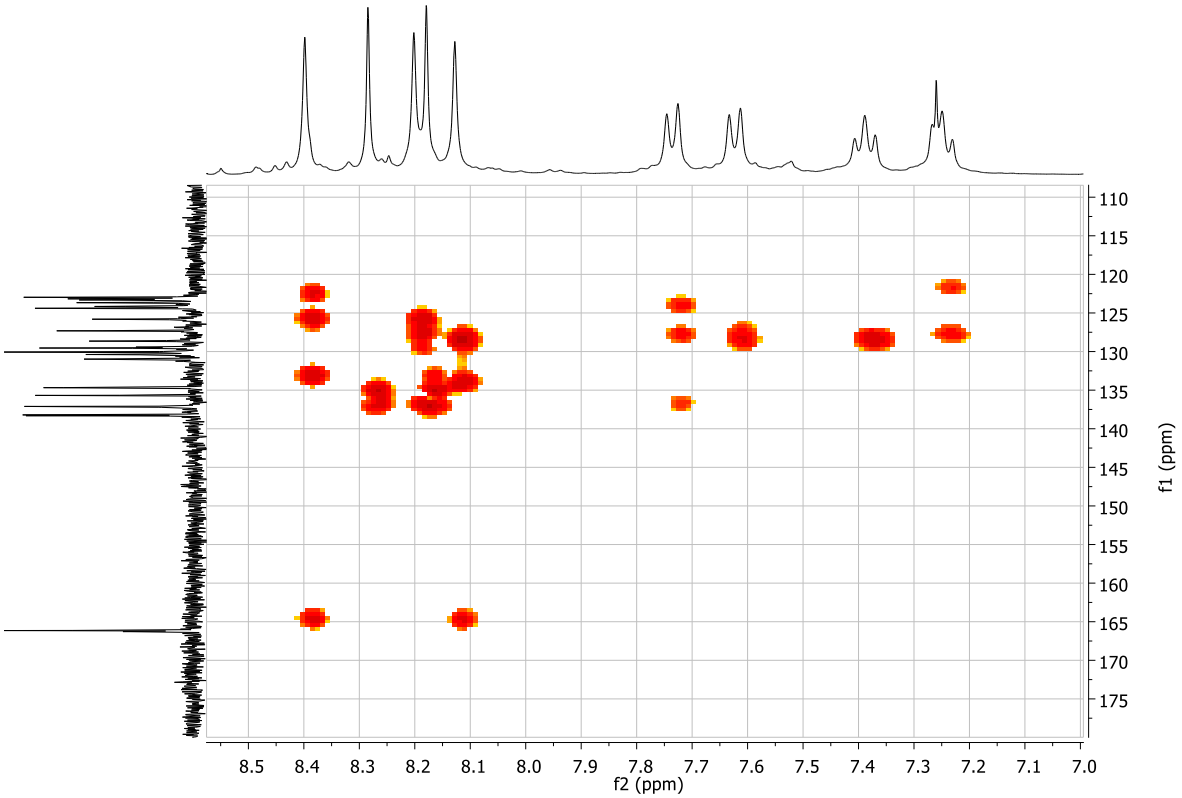

MALDI-TOF

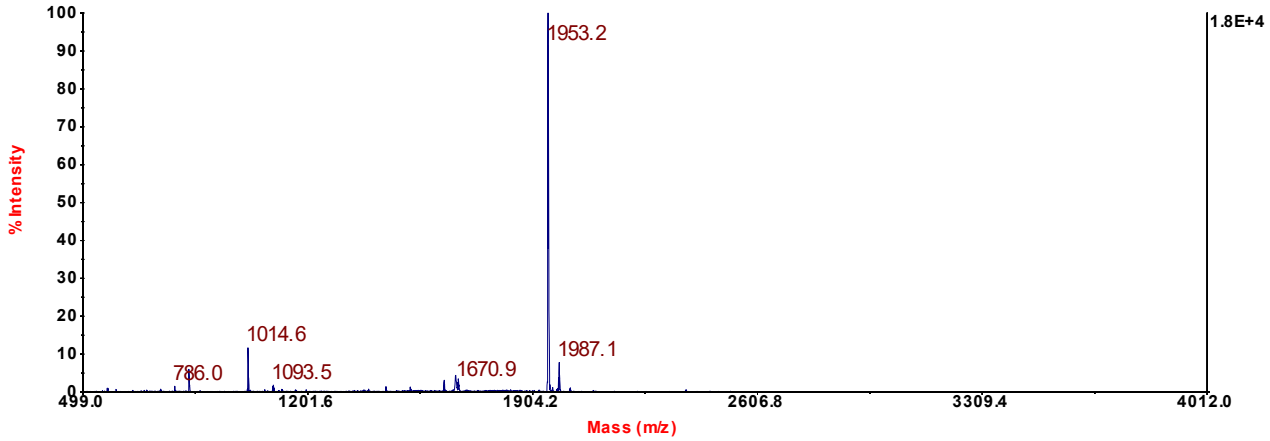
100
90
80
70
60
50
40
30
20
10
0
% Intensity
1953.2
1.8E+4
1014.6
1987.1
786.0
1093.5
1670.9
499.0
1201.6
1904.2
2606.8
3309.4
4012.0
Mass (m/z)

Compound **10**

^{1}H NMR (400 MHz, $CDCl_3$)

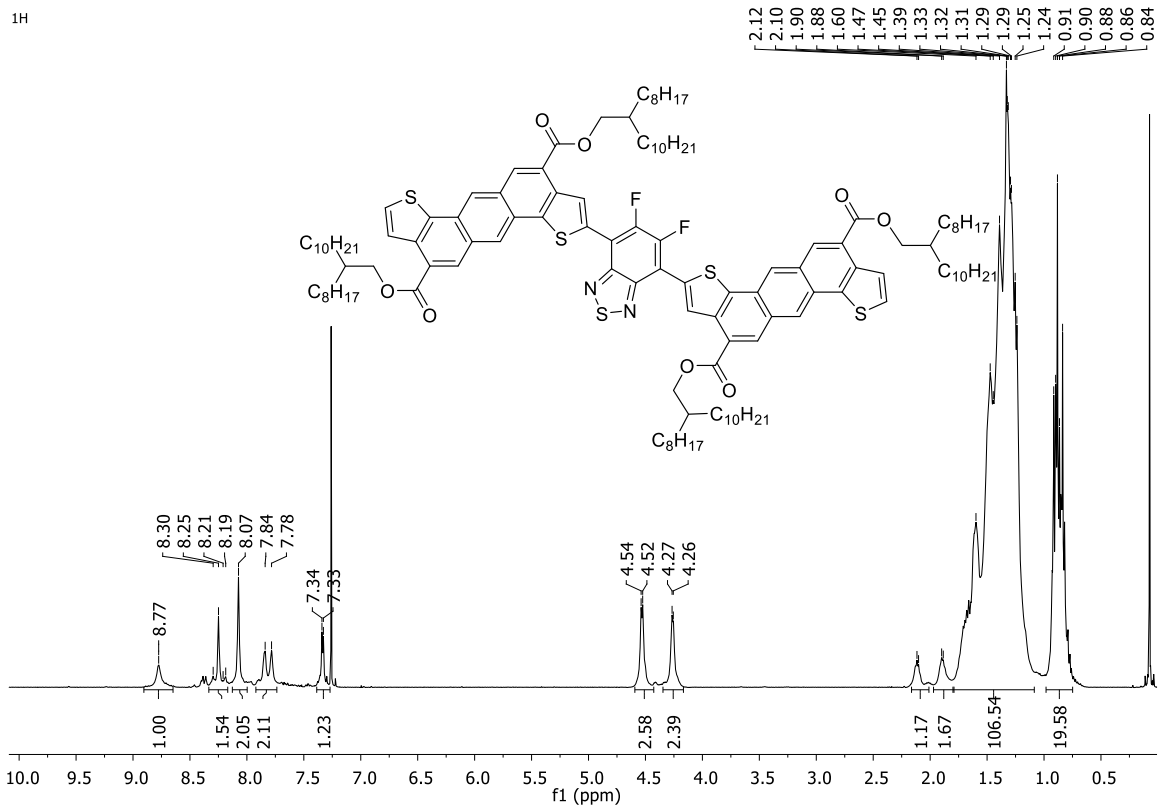

^{19}F NMR

19F

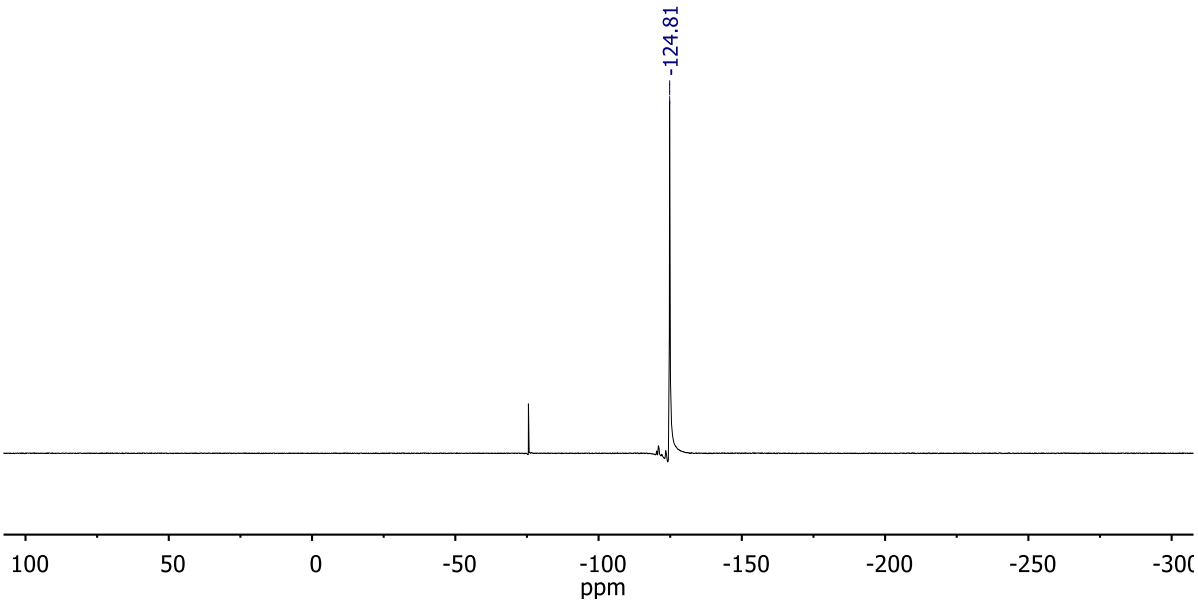

^{13}C NMR (101 MHz, $CDCl_3$)

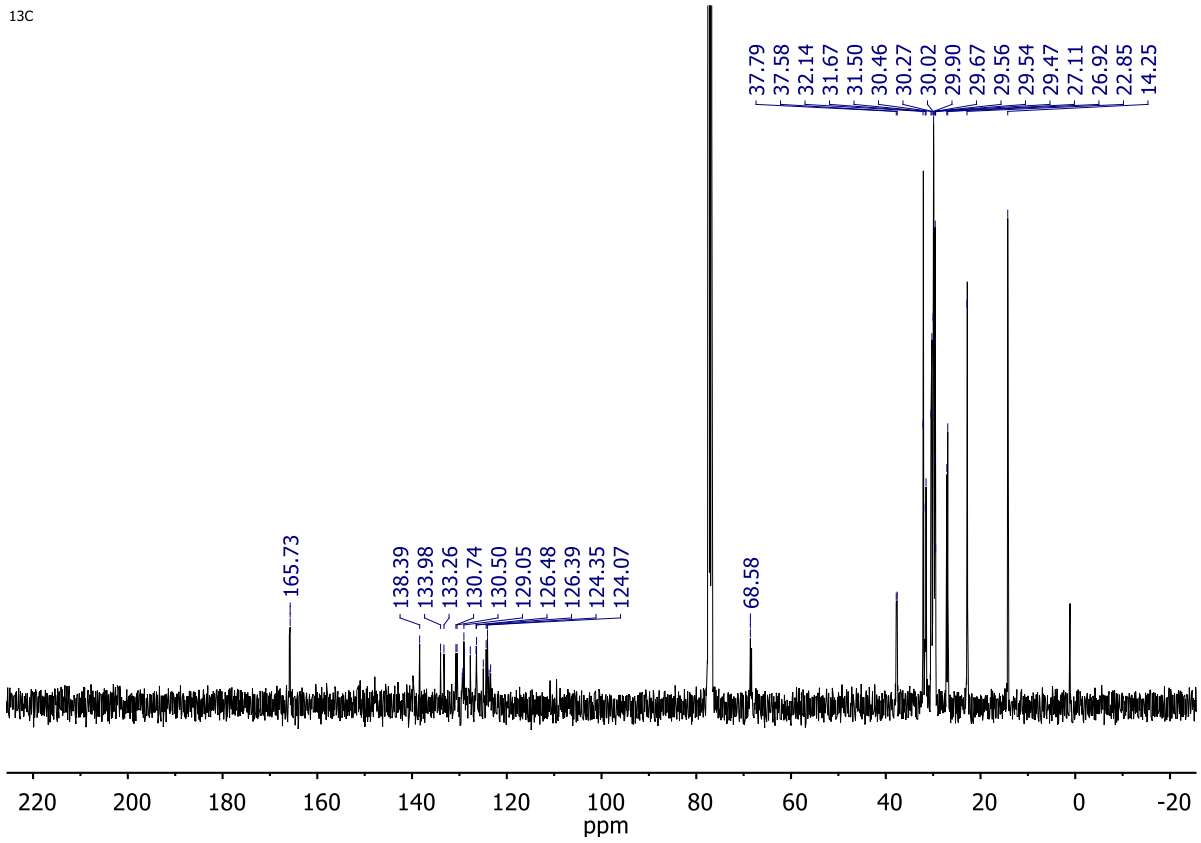

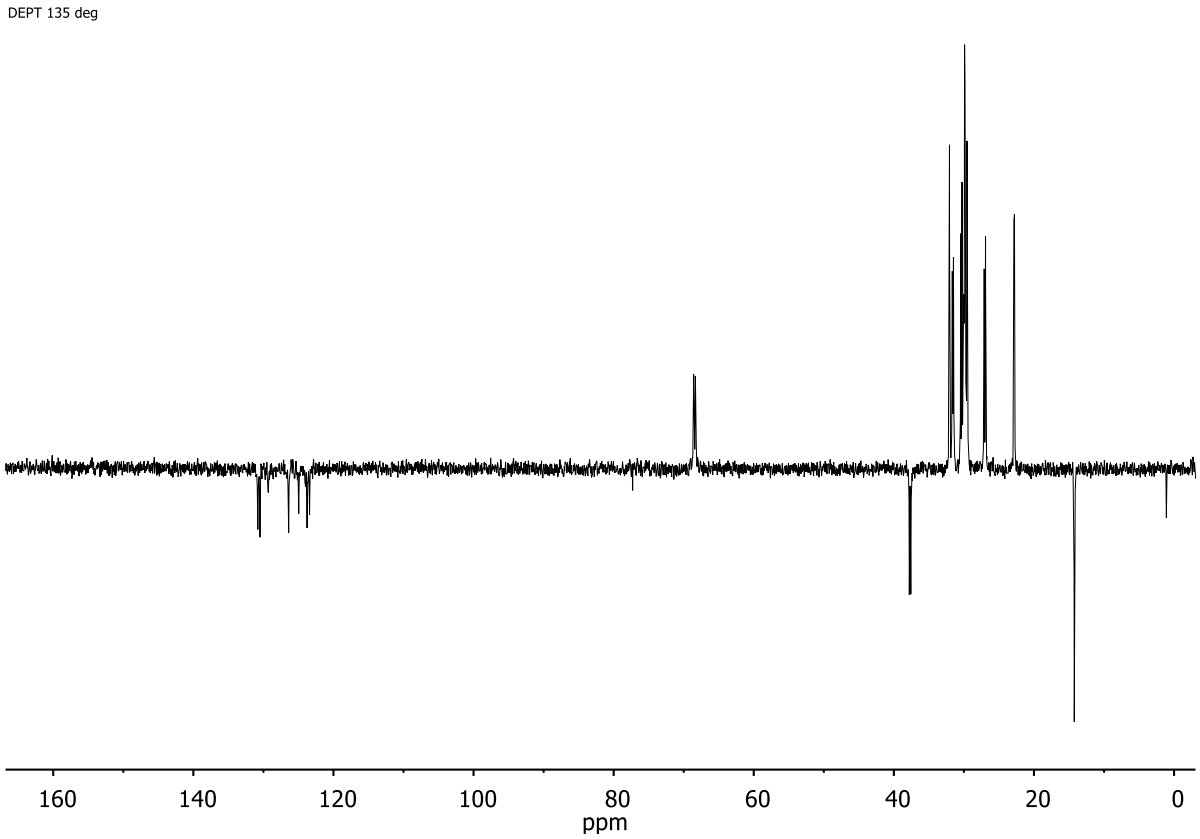
DEPT 135 deg
160
140
120
100
80
60
40
20
0
ppm

COSY

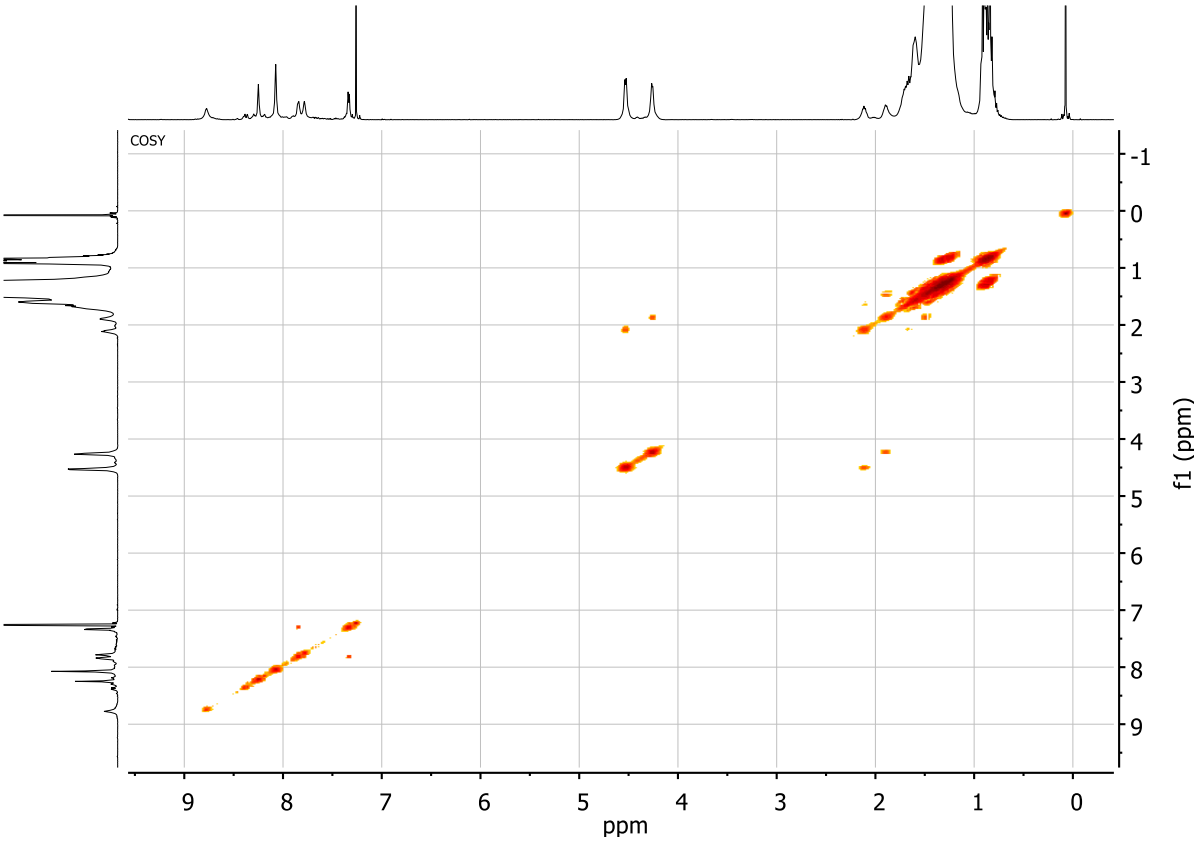

HSQC

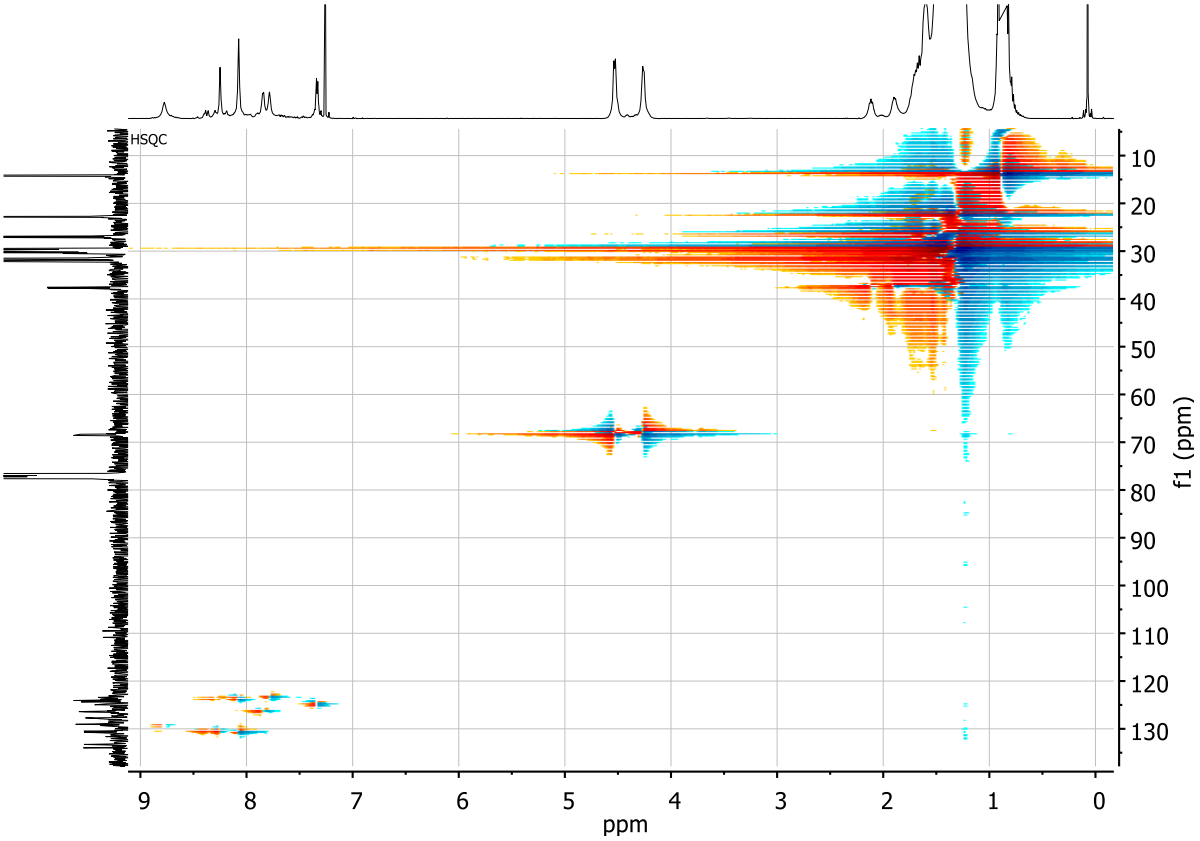
HSQC
10
20
30
40
50
60
70
80
90
100
110
120
130
f1 (ppm)
9
8
7
6
5
4
3
2
1
0
ppm

HMBC

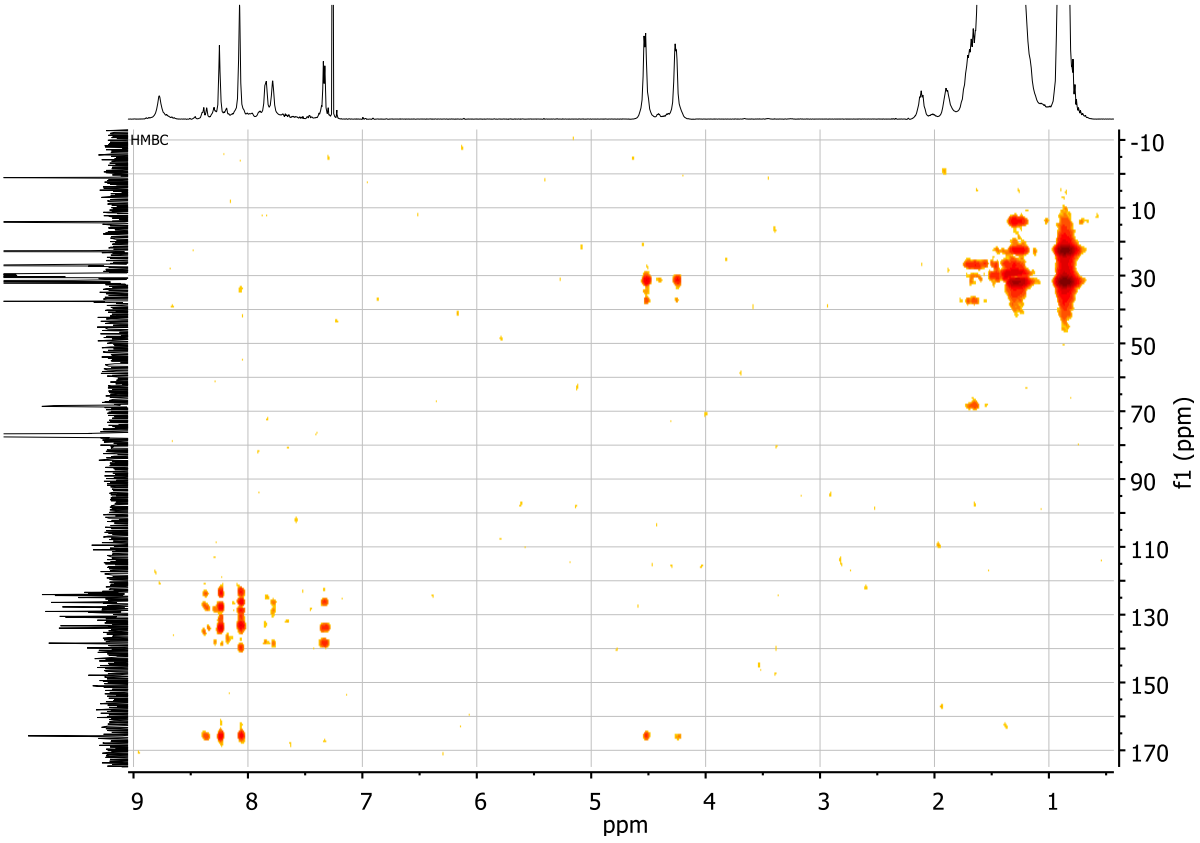
HMBC
-10
10
30
50
70
90
110
130
150
170
f1 (ppm)
9
8
7
6
5
4
3
2
1
ppm

Intermediate 13

^{1}H NMR (300 MHz, $CDCl_3$)

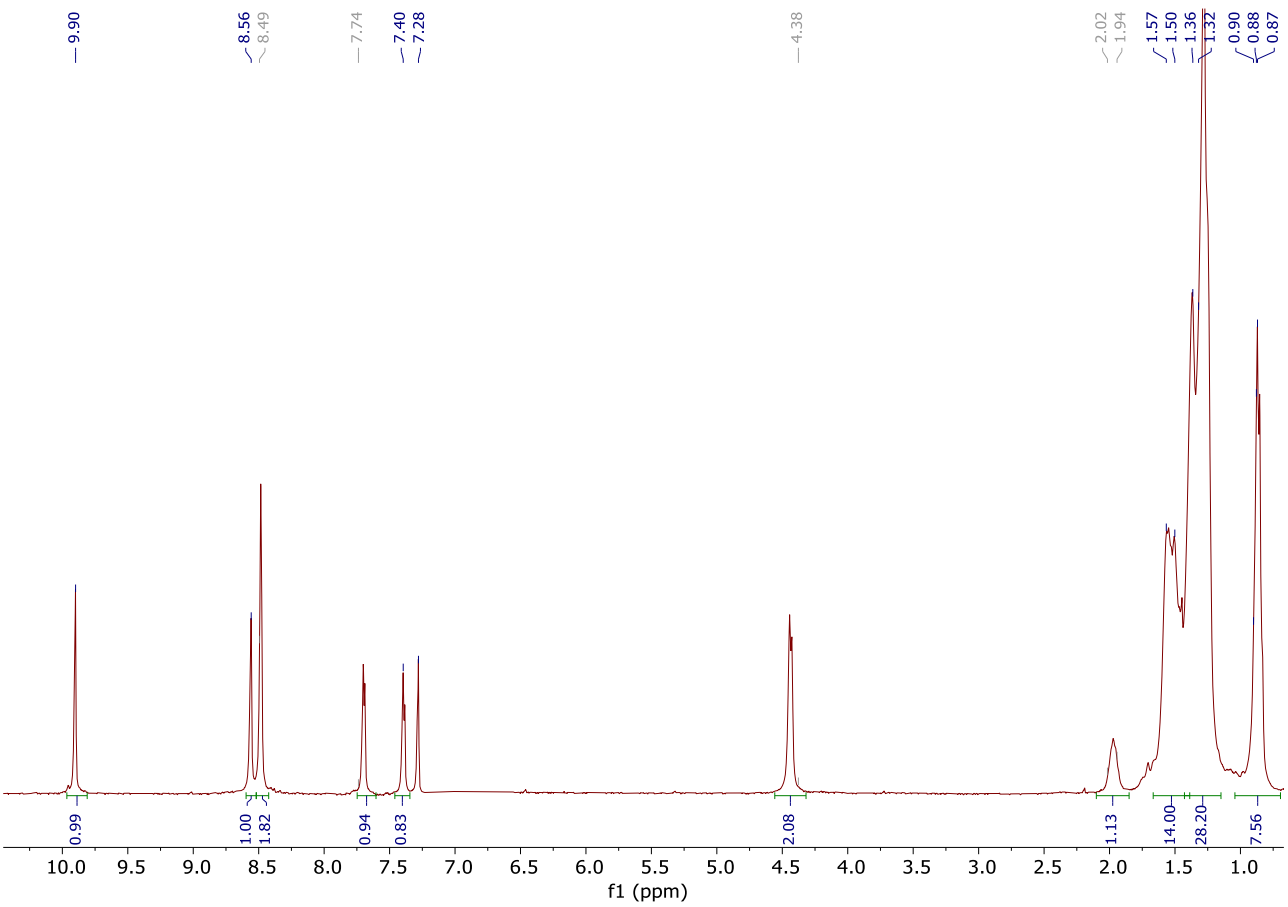

^{13}C NMR (75 MHz, $CDCl_3$)

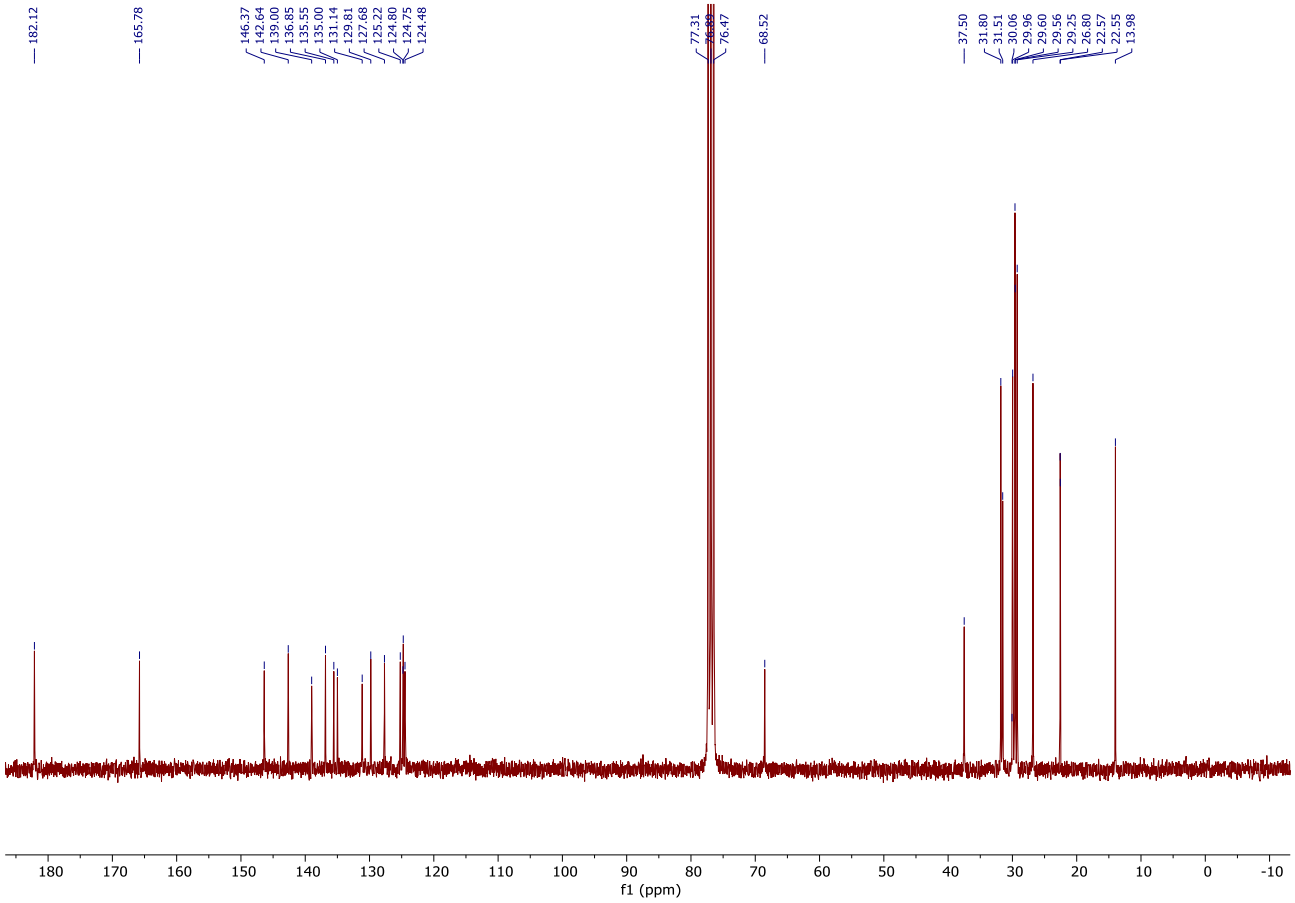

MALDI ANALYSIS

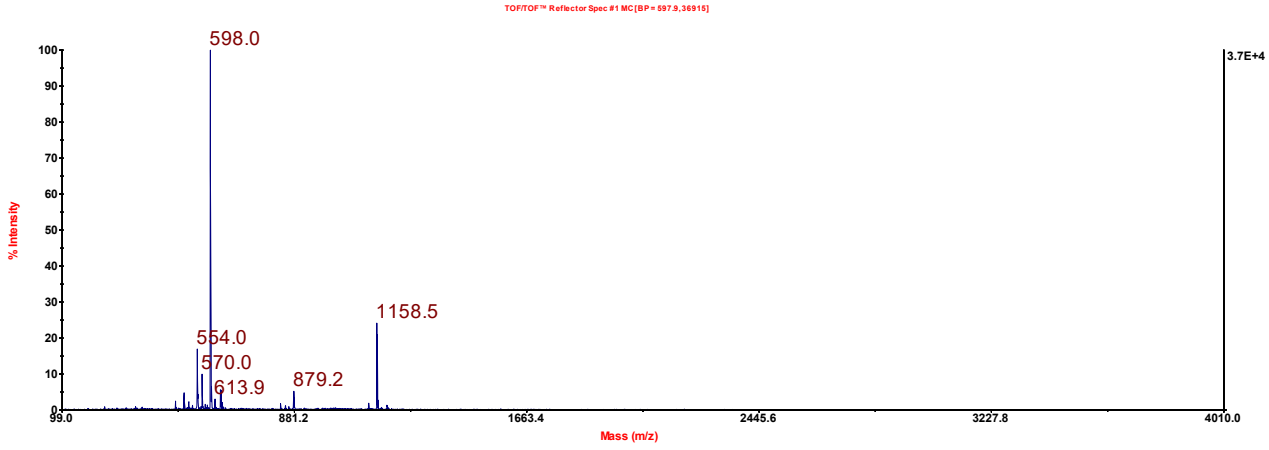

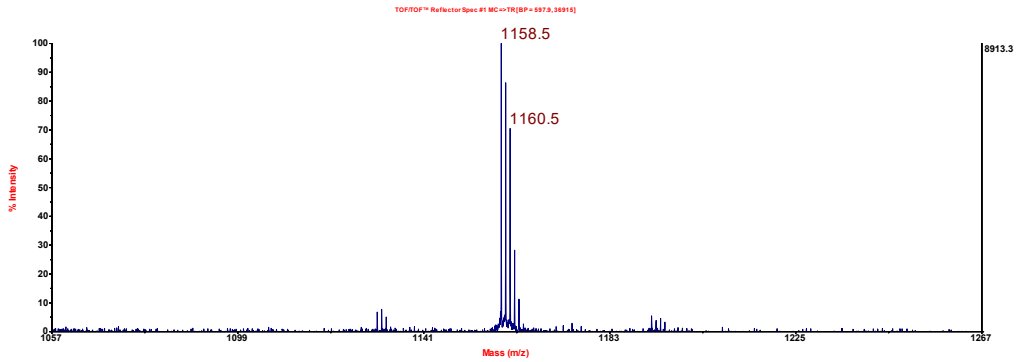

NFA 1

MALDI ANALYSIS

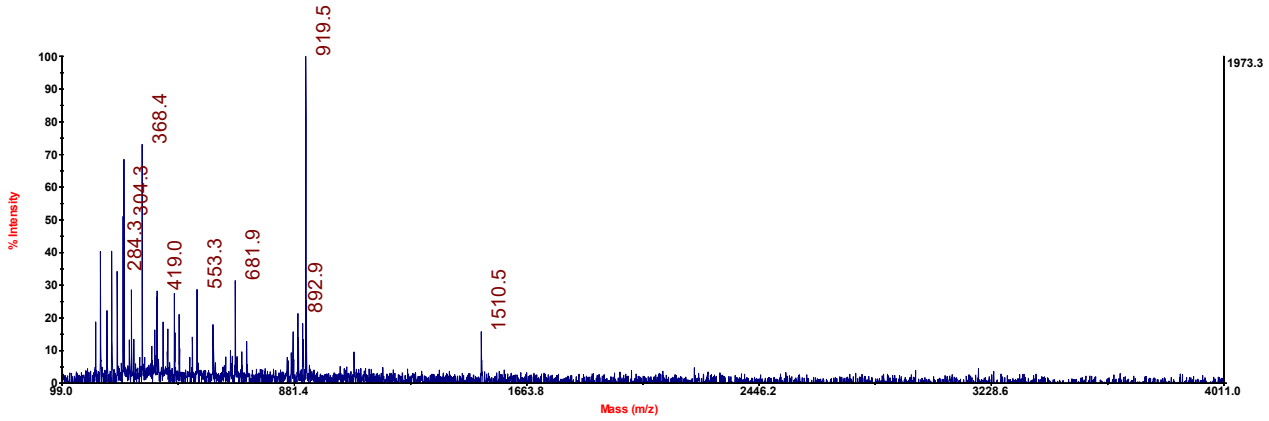

Intermediate 14

^{1}H NMR (300 MHz, $CDCl_3$)

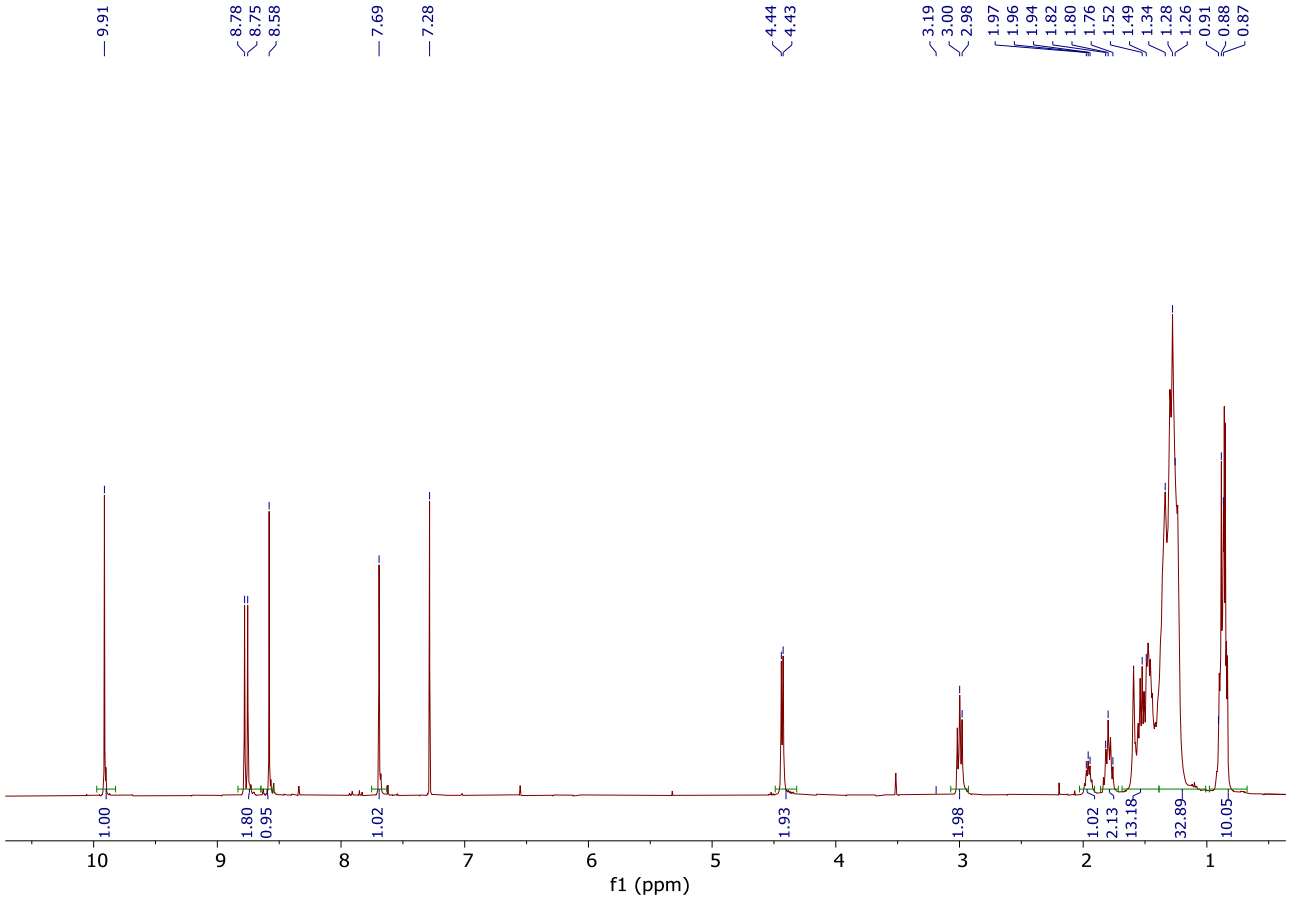

^{13}C NMR (75 MHz, $CDCl_3$)

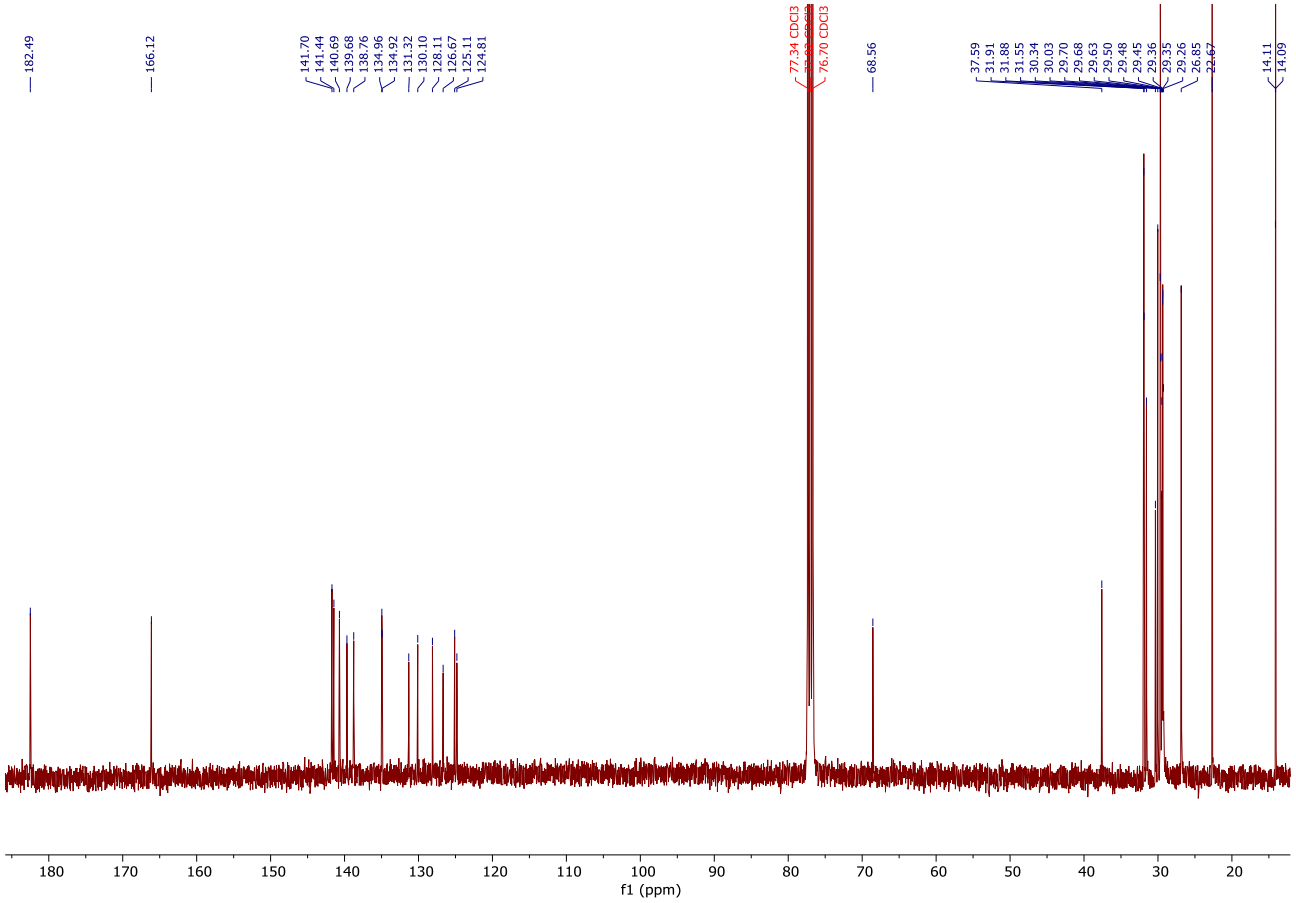

MALDI ANALYSIS

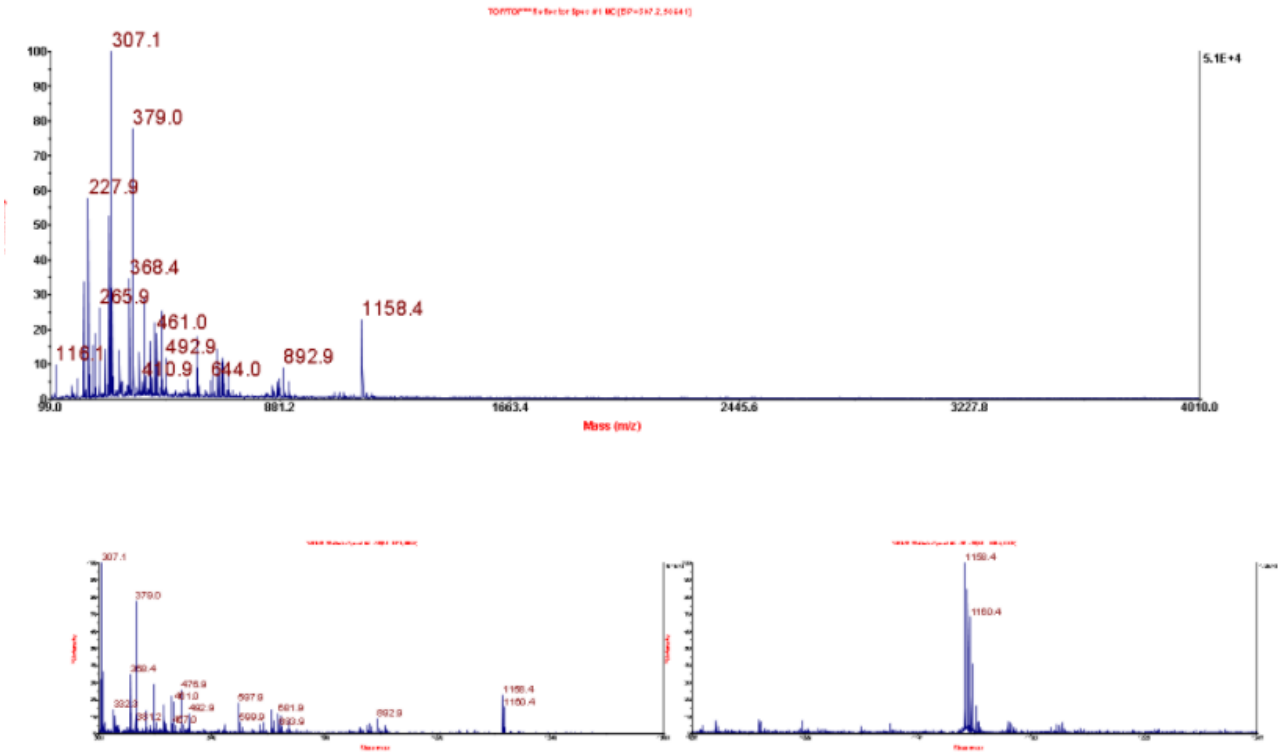

NFA 2

MALDI ANALYSIS

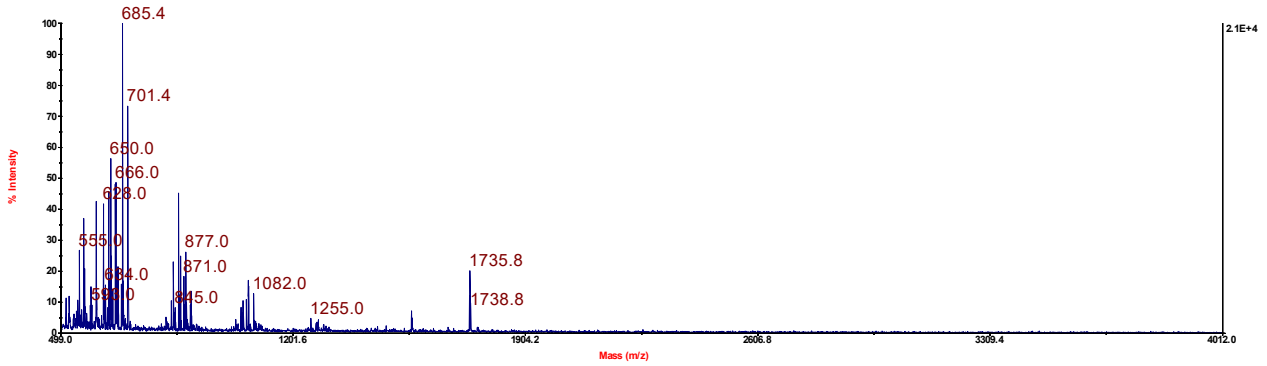

Intermediate 15

^{1}H NMR (400 MHz, $CDCl_3$)

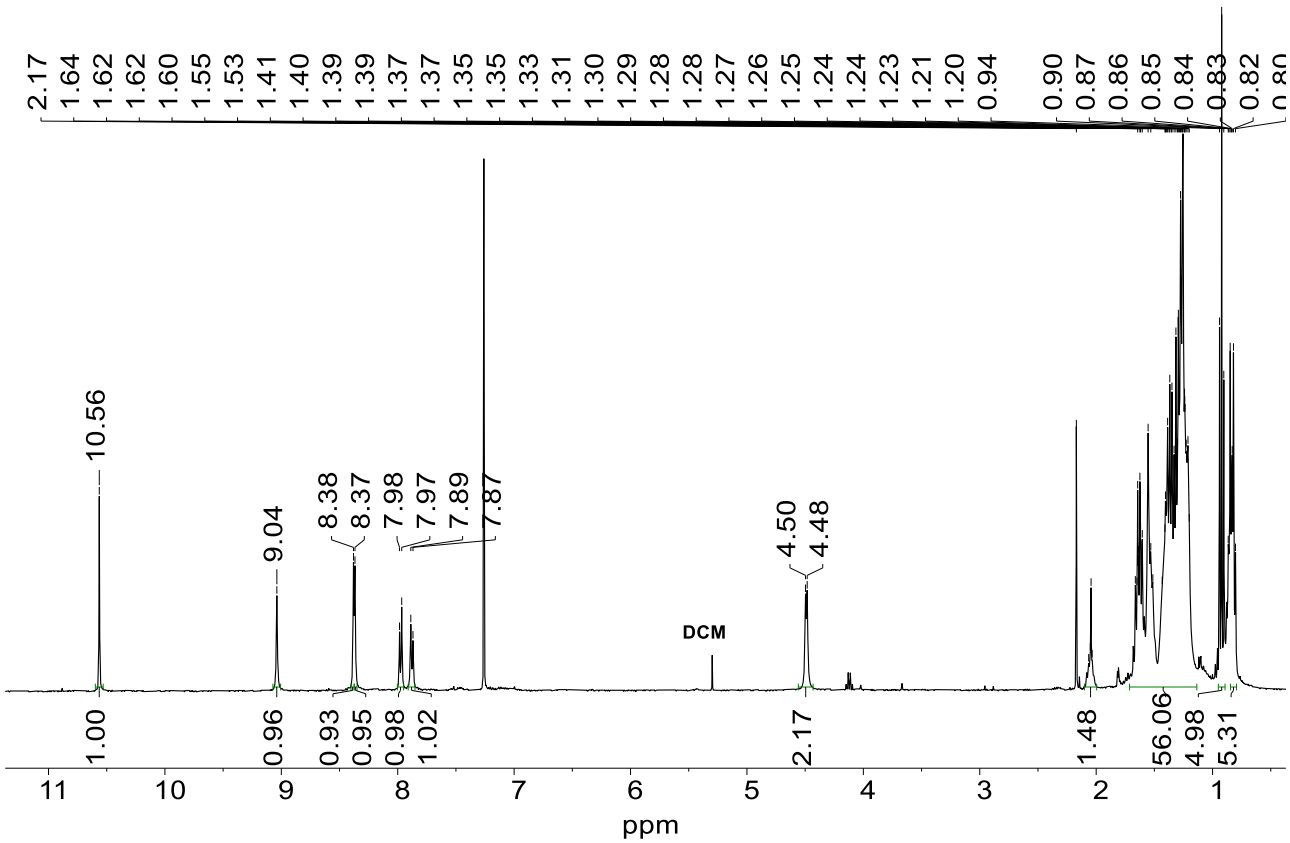

^{13}C NMR (101 MHz, $CDCl_3$)

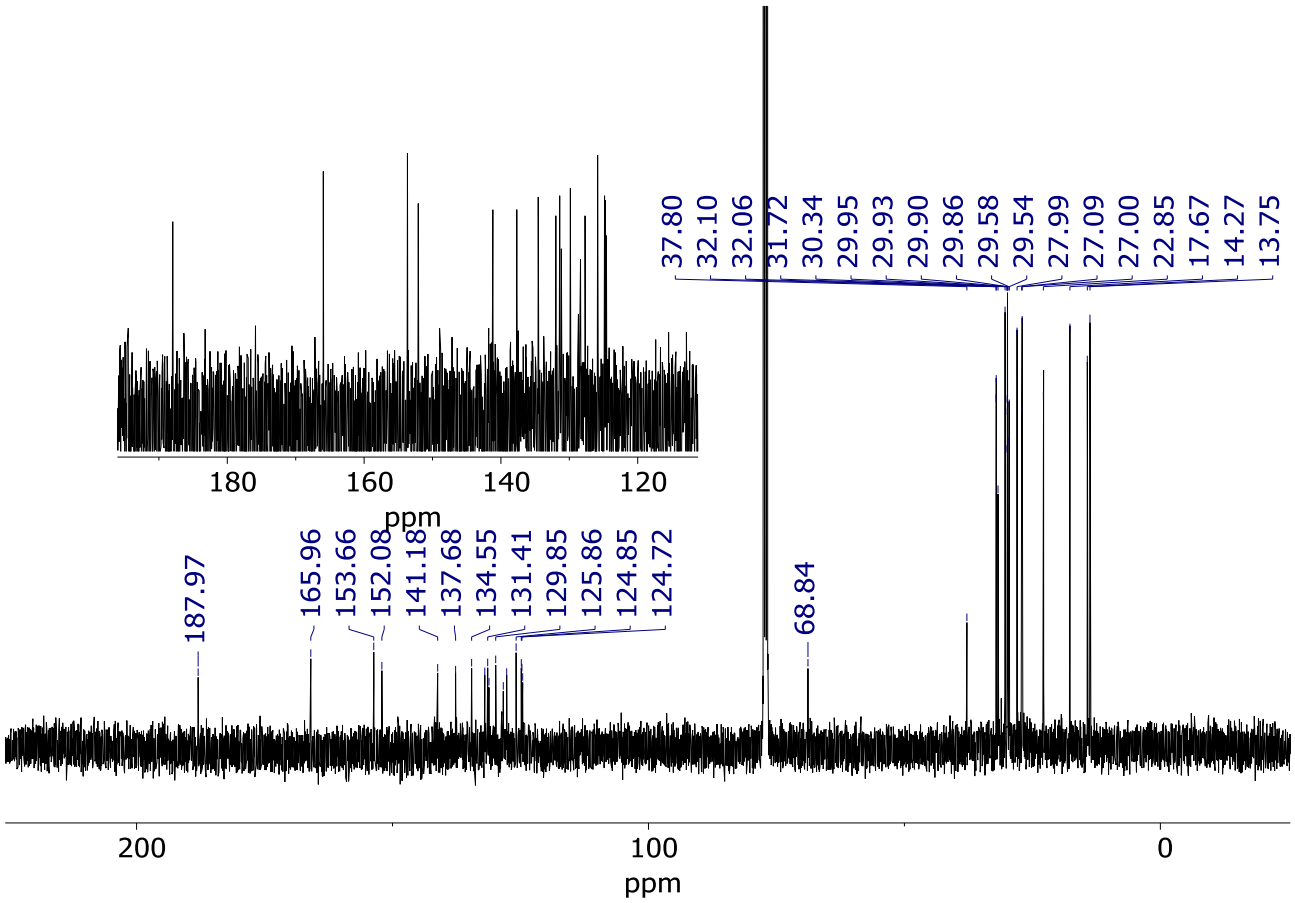

MALDI ANALYSIS

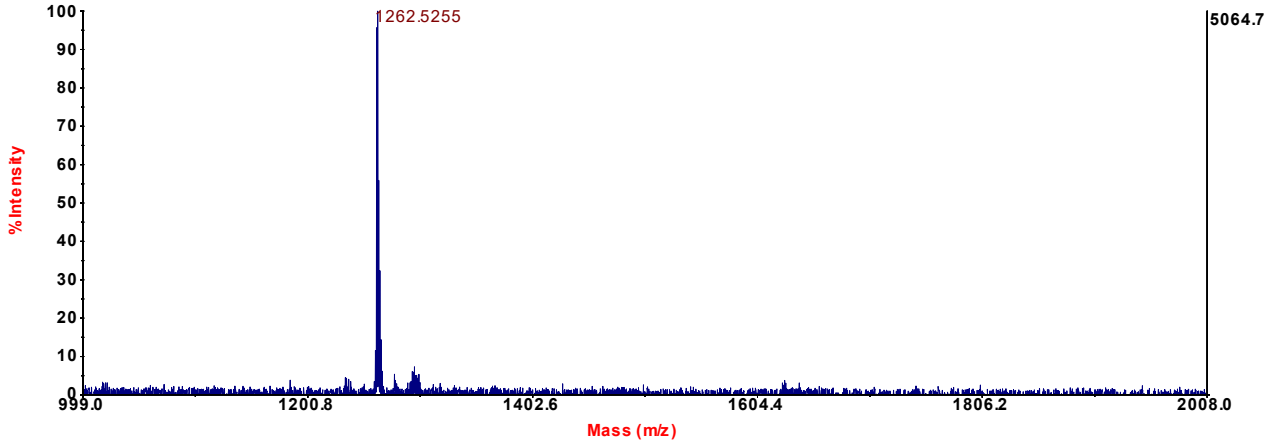

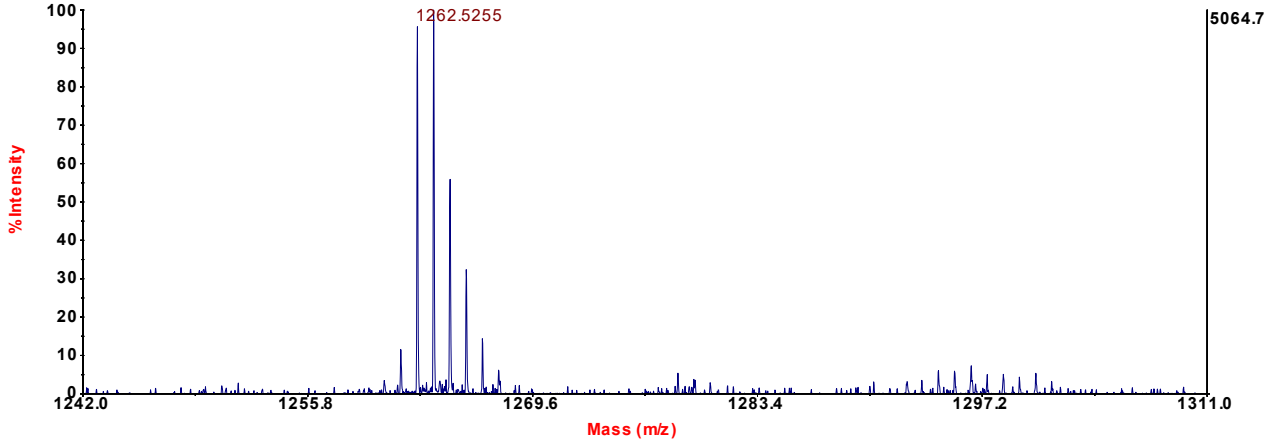

NFA 3

^{1}H NMR (400 MHz, $CDCl_3$)

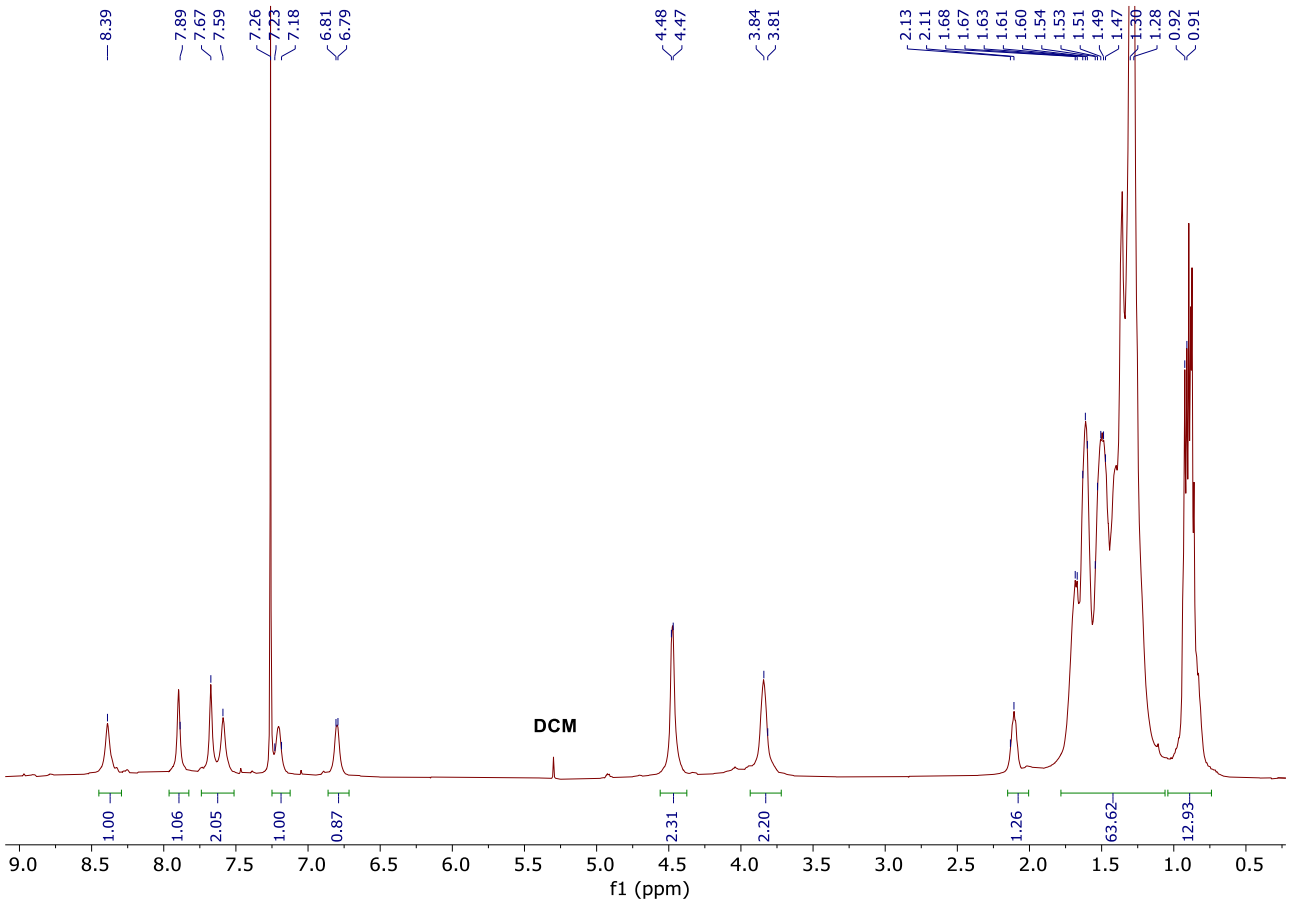

^{13}C NMR (100 MHz, $CDCl_3$)

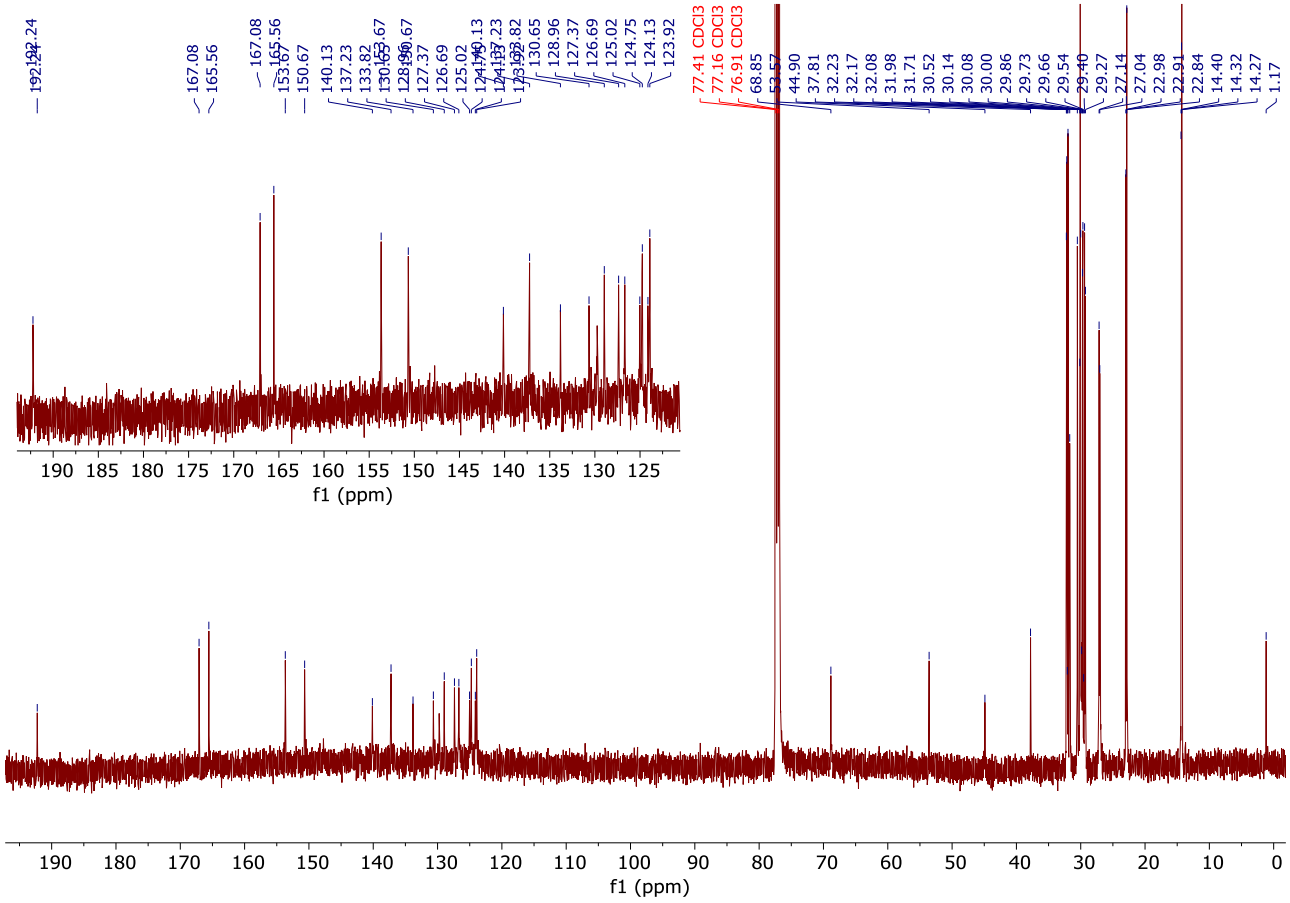

MALDI ANALYSIS

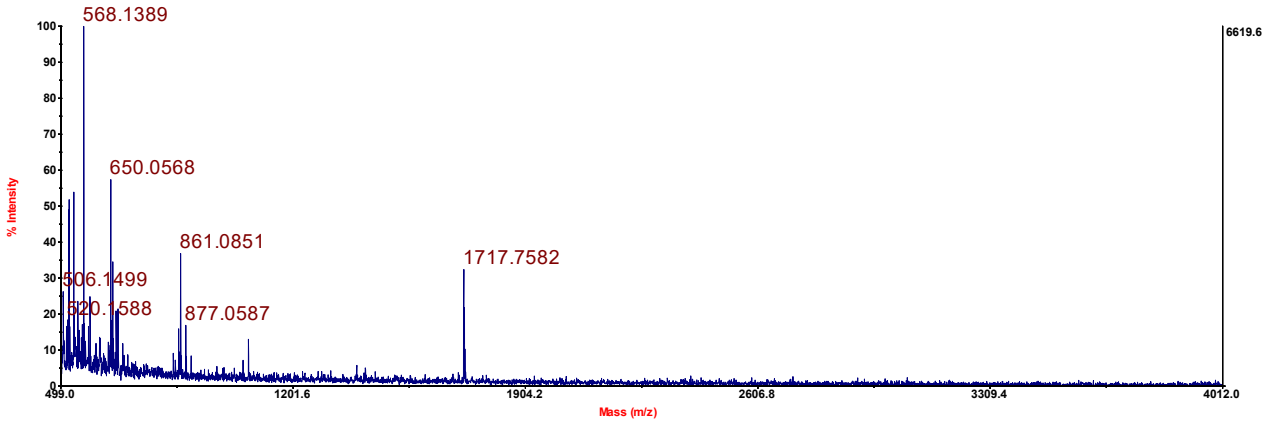

6.4. Chapter 4

6.4.1. Spectra of New Compounds

Polymer P1

^{1}H VT-NMR at 120°C (600 MHz, $C_2D_2Cl_4$)

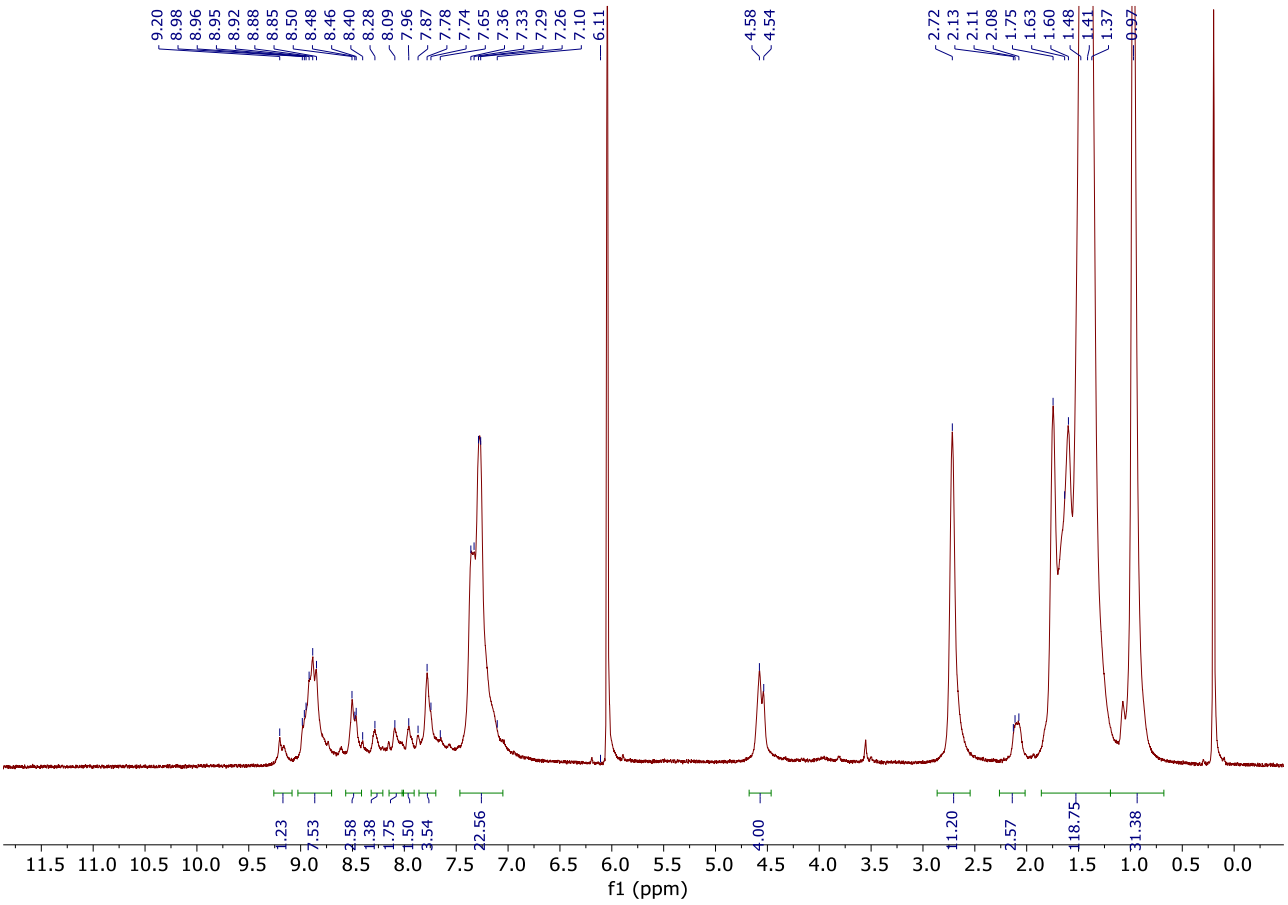

Polymer P2

^{1}H VT-NMR at 120°C (600 MHz, $C_2D_2Cl_4$)

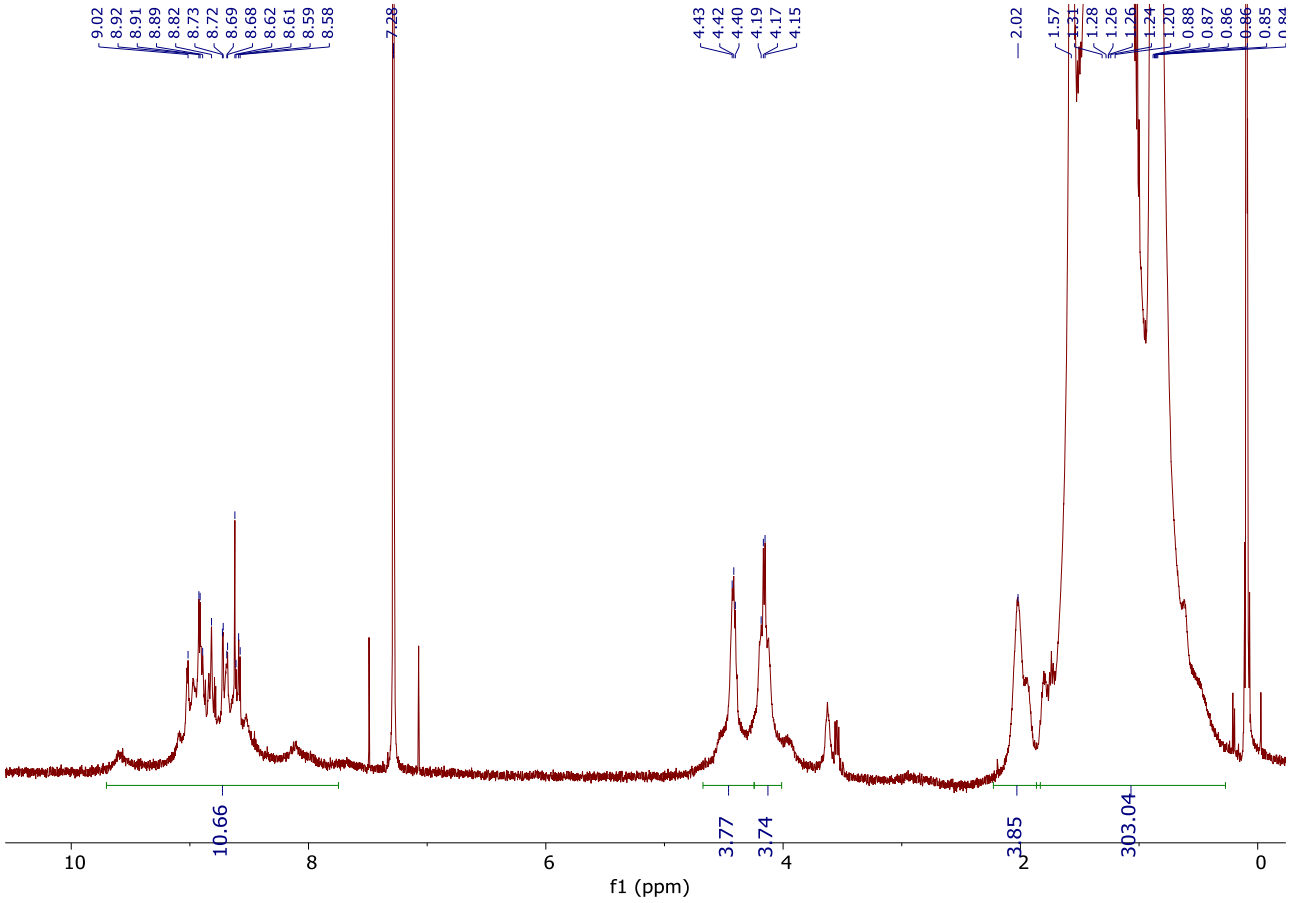

Polymer P3

^{1}H VT-NMR at 120°C (600 MHz, $C_2D_2Cl_4$)

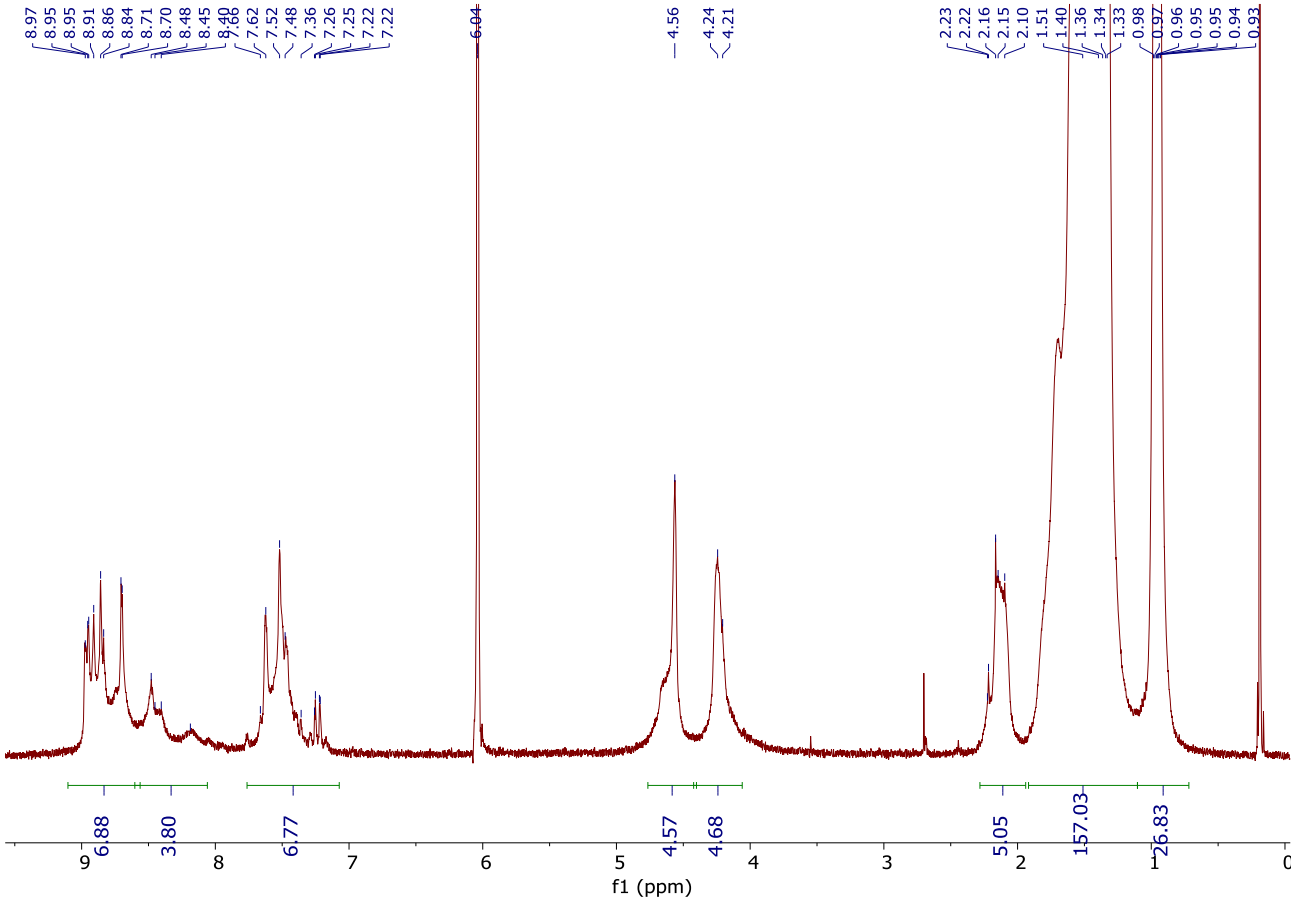

Polymer P4

^{1}H VT-NMR at 120°C (600 MHz, $C_2D_2Cl_4$)

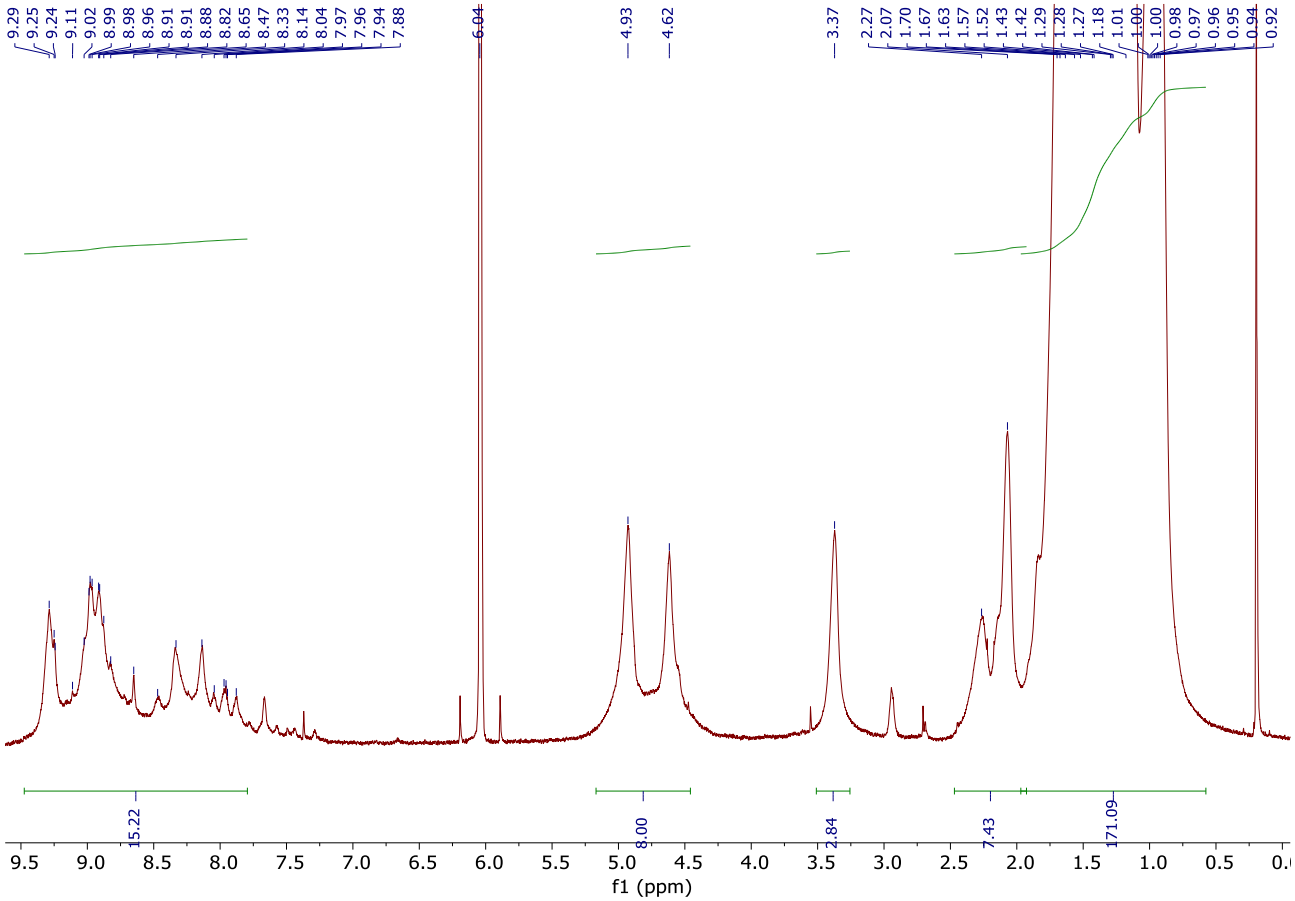

Polymer P5

^{1}H VT-NMR at 120°C (600 MHz, $C_2D_2Cl_4$)

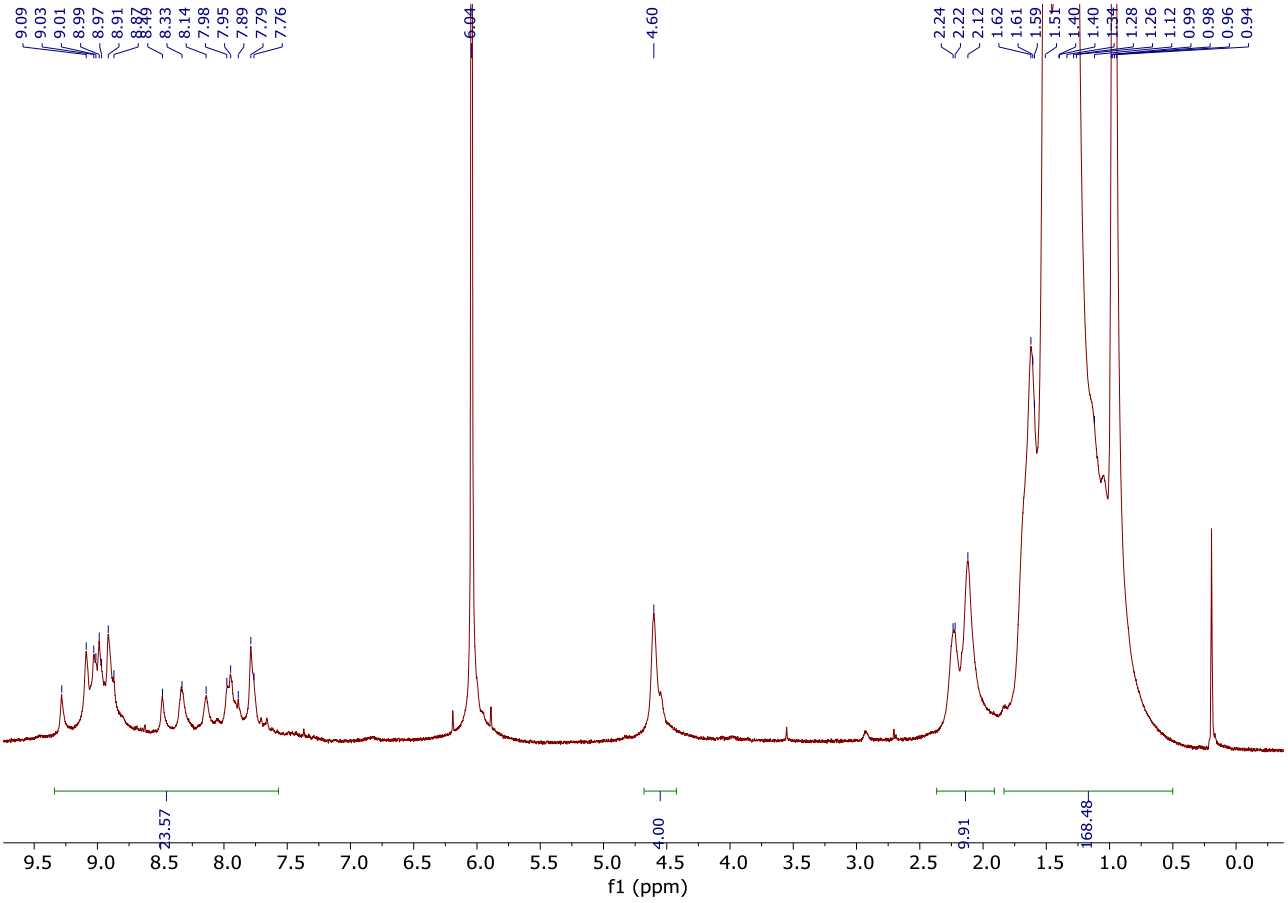

6.4.2. Additional Tables and Figures

Photophysical properties (Table 4.S1)

Entry	*Solution (nm)*	*Film (nm)*	*λ_{onset} (nm)*	*Egopt (eV)*	*HOMO^{cv} (eV)*	*LUMO^{cv} (eV)*	*M_n (kg/mol)*	*M_w (kg/mol)*	*Đ*
P1	691	701	776	1.60	-5.43	-3.83	*	*	*
P2	577	577	714	1.73	-5.93	-3.87	*	*	*
P3	658	673	810	1.53	-5.94	-3.90	53312	214835	2.95
P4	748	775	849	1.46	-5.71	-3.82	23296	41148	1.76

P5	695	696	760	1.63	-5.69	-4.06	34504	91313	2.64

**P1 and P2 difficult to be analyzed due to their low solubility*

TGA of polymers P3 to P5 (Figure 4.S7)

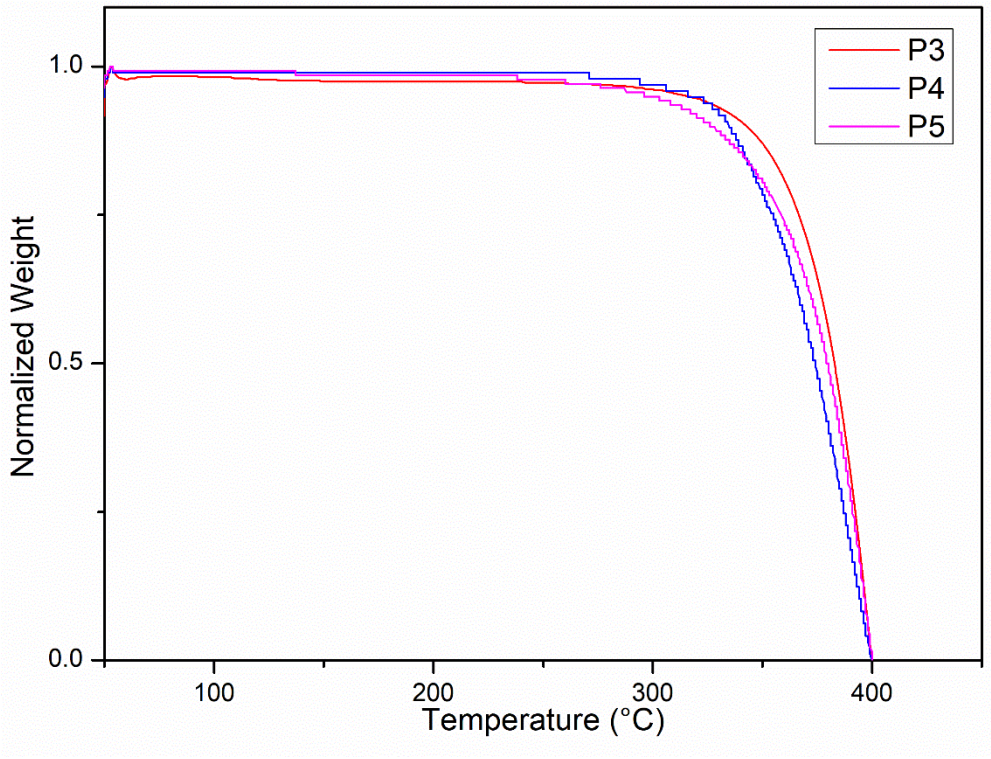

Figure 4.S7: TGA profiles for polymers P3 to P5

DSC of polymers P3 to P5 (Figure 4.S8)

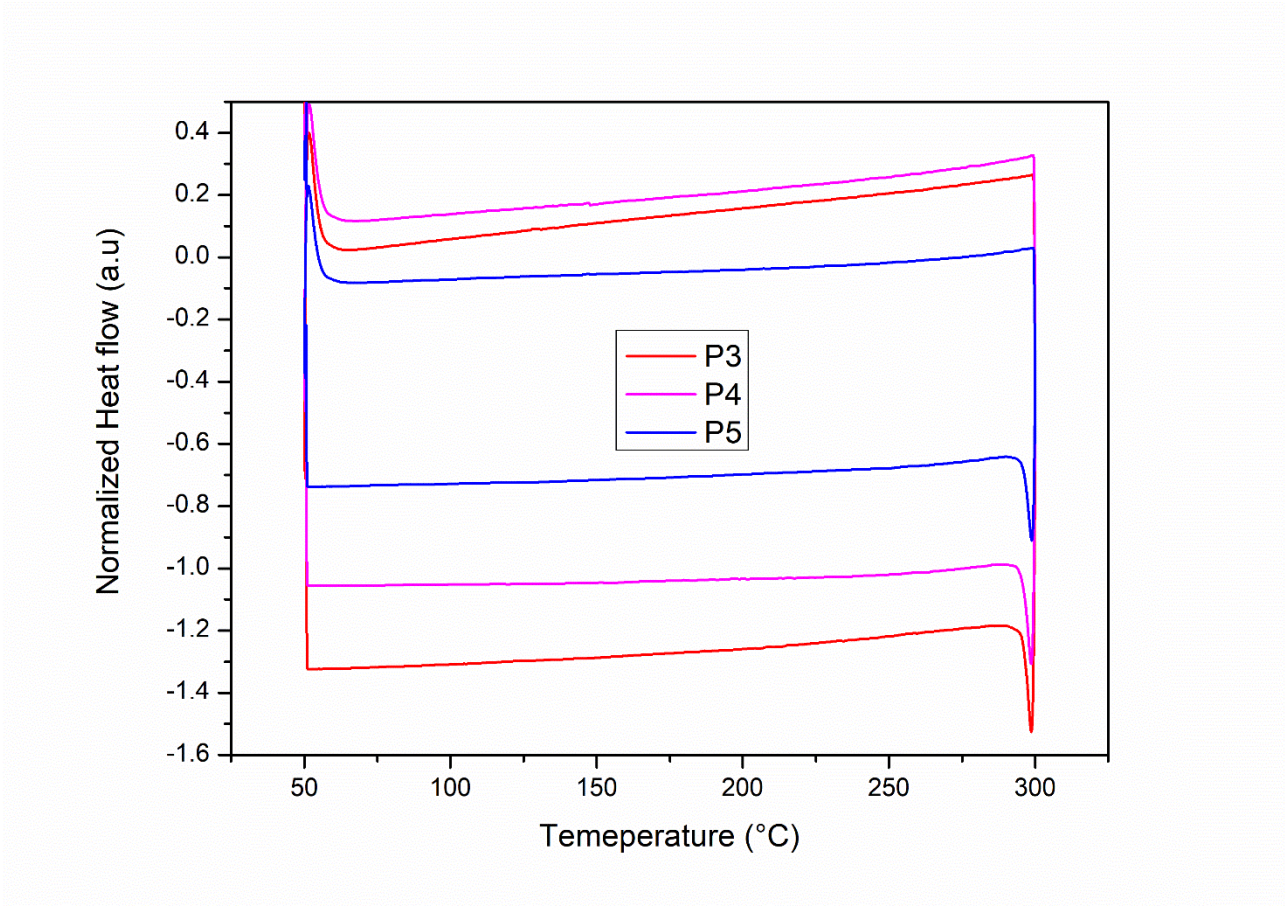

Figure 4.S8: DSC profiles for polymers P3 to P5

GPC P3 (Figure 4.S9)

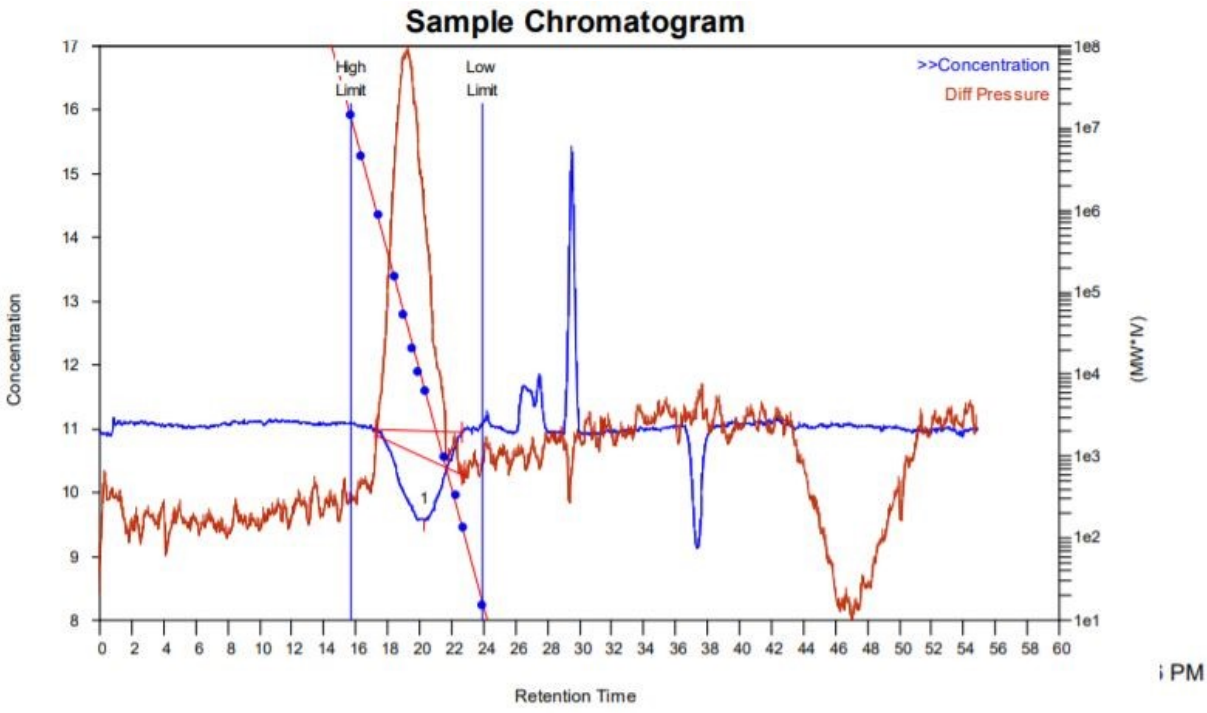
Sample Chromatogram
High Limit
Low Limit
>>Concentration
Diff Pressure
Concentration
(MW*V)
Retention Time
1
PM

Cirrus GPC Sample Injection Report

Generated by: Tobin Marks — Wednesday, August 25, 2021 5:06 PM
Workbook: F:\Cirrus Workbooks\GPC-VS-08192021\GPC-VS-08192021.mplw

Sample Details

Sample Name: GF58
Acquired: 8/25/2021 11:28:47 AM — By Analyst: Tobin Marks
Batch Name: Gf58
Filename: F:\Cirrus Workbooks\GPC-VS-08192021\gf58-0001.cgrm
Concentration: 1.00 mg/ml — K of Sample: 14.1000
Injection Volume: 100.0 ul — Alpha of Sample: 0.7000
LIMS ID: — Bottle ID:

Workbook Details

Eluent: TCB stabilised with 0.0125% BHT — Flow Rate: 1.00 ml/min
Column Set: PLgel 10um MIXED-B LS 300 x 7.5 mm — Column Set Length: 900 mm
Detector: — Temperature: 150

Analysis Using Method: Universal Calibration

Comments:

Results File: F:\Cirrus Workbooks\GPC-VS-08192021\gf58-0001-Repeat (04).rst

Calibration Used: 8/21/2021 11:18:47 AM

Calibration Type: Universal — Curve Fit Used: 1
Calibration Curve: y = 18.414619 - 0.718238x^1

High Limit MW RT: 15.72 mins — Low Limit MW RT: 23.90 mins
High Limit MW: 3752000 — Low Limit MW: 860
K: 14.1000 — FRM Name:
Alpha: 0.7000 — Flow Marker RT: 0.00 mins
FRCF: 0.0000

Sample Injection Report

MW Averages

Peak No	Mp	Mn	Mw	Mz	Mz+1	Mv	PD
1	70311	53312	156191	363858	586956	126849	2.92976

Processed Peaks

Peak No	Name	Start RT (mins)	Max RT (mins)	End RT (mins)	Pk Height (mV)	% Height	Area (mV.secs)	% Area
1	Concentration	17.27	20.32	22.62	-1.39776	0	239.953	100
2	Diff Pressure	17.27	19.23	22.62	3.00843	0	441.085	100

Peak Detection

Baseline Detection

No	Start RT (mins)	End RT (mins)	Start Height	End Height	Is St Mod	Is End Mod
1	17.27	22.62	10.98	10.96	No	No
2	17.27	22.62	0.23	-0.07	No	No

GPC P4 (Figure 4.S10)

Cirrus GPC Narrow Standard Report

Generated by: Tobin Marks — Wednesday, August 25, 2021 5:08 PM
Workbook: F:\Cirrus Workbooks\GPC-VS-08192021\GPC-VS-08192021.mplw

Sample Details

Sample Name: GF77
Acquired: 8/25/2021 12:26:37 PM — By Analyst: Tobin Marks
Batch Name: GF77
Filename: F:\Cirrus Workbooks\GPC-VS-08192021\gf77-0001.cgrm
Concentration: 1.00 mg/ml — K of Sample: 14.1000
Injection Volume: 100.0 ul — Alpha of Sample: 0.7000
LIMS ID: — Bottle ID:

Workbook Details

Eluent: TCB stabilised with 0.0125% BHT — Flow Rate: 1.00 ml/min
Column Set: PLgel 10um MIXED-B LS 300 x 7.5 mm — Column Set Length: 900 mm
Detector: — Temperature: 150

Analysis Using Method: Universal Calibration

Comments:

Results File: F:\Cirrus Workbooks\GPC-VS-08192021\gf77-0001-Repeat (02).rst

Calibration Generated: 8/21/2021 11:18:47 AM

Calibration Type: Universal — Curve Fit Used: 1
Calibration Curve: y = 18.414619 - 0.718238x^1

High Limit MW RT: 15.72 mins — Low Limit MW RT: 23.90 mins
High Limit MW: 3752000 — Low Limit MW: 860
K: 14.1000 — FRM Name:
Alpha: 0.7000 — Flow Marker RT: 0.00 mins
FRCF: 0.0000

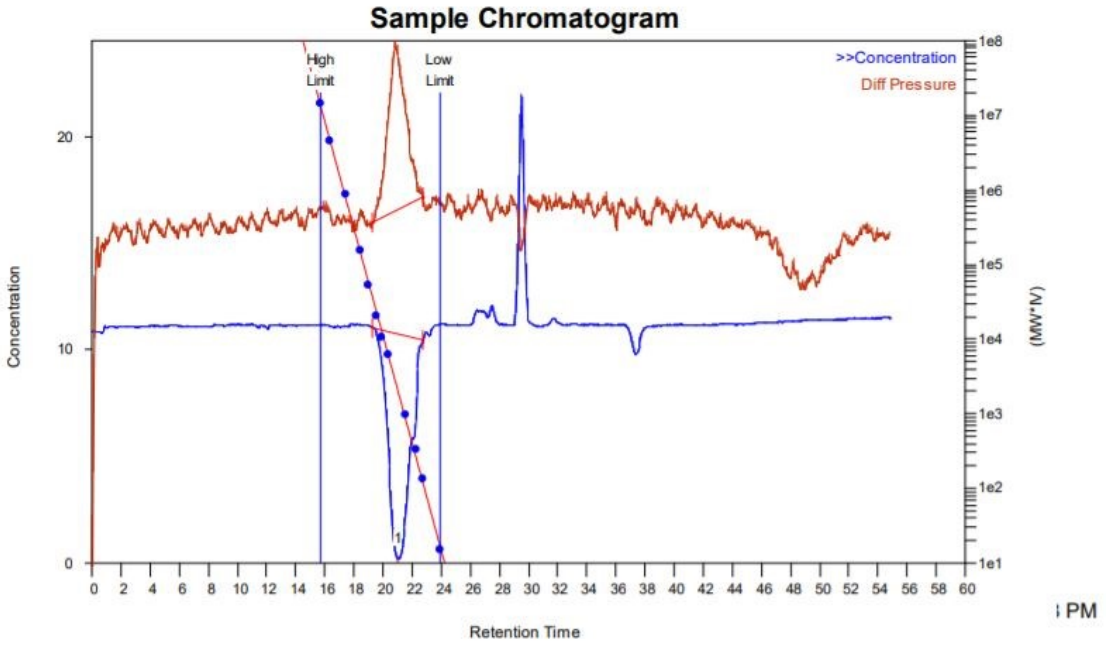

Narrow Standard Report

Processed Peaks

Peak No	Name	Start RT (mins)	Max RT (mins)	End RT (mins)	Pk Height (mV)	% Height	Area (mV.secs)	% Area
1	Concentration	19.25	21.03	22.73	-10.5697	0	1012.47	100
2	Diff Pressure	19.25	20.80	22.73	2.01641	0	176.652	100

GPC P5 (Figure 4.S11)

Cirrus GPC Narrow Standard Report

Generated by: Tobin Marks — Wednesday, August 25, 2021 5:11 PM
Workbook: F:\Cirrus Workbooks\GPC-VS-08192021\GPC-VS-08192021.mplw

Sample Details

Sample Name: GF86
Acquired: 8/25/2021 1:24:25 PM — By Analyst: Tobin Marks
Batch Name: GF86
Filename: F:\Cirrus Workbooks\GPC-VS-08192021\gf86-0001.cgrm
Concentration: 1.00 mg/ml — K of Sample: 14.1000
Injection Volume: 100.0 ul — Alpha of Sample: 0.7000
LIMS ID: — Bottle ID:

Workbook Details

Eluent: TCB stabilised with 0.0125% BHT — Flow Rate: 1.00 ml/min
Column Set: PLgel 10um MIXED-B LS 300 x 7.5 mm — Column Set Length: 900 mm
Detector: — Temperature: 150

Analysis Using Method: Universal Calibration

Comments:

Results File: F:\Cirrus Workbooks\GPC-VS-08192021\gf86-0001-Repeat (01).rst

Calibration Generated: 8/21/2021 11:18:47 AM

Calibration Type: Universal — Curve Fit Used: 1
Calibration Curve: y = 18.414619 - 0.718238x^1

High Limit MW RT: 15.72 mins — Low Limit MW RT: 23.90 mins
High Limit MW: 3752000 — Low Limit MW: 860
K: 14.1000 — FRM Name:
Alpha: 0.7000 — Flow Marker RT: 0.00 mins
FRCF: 0.0000

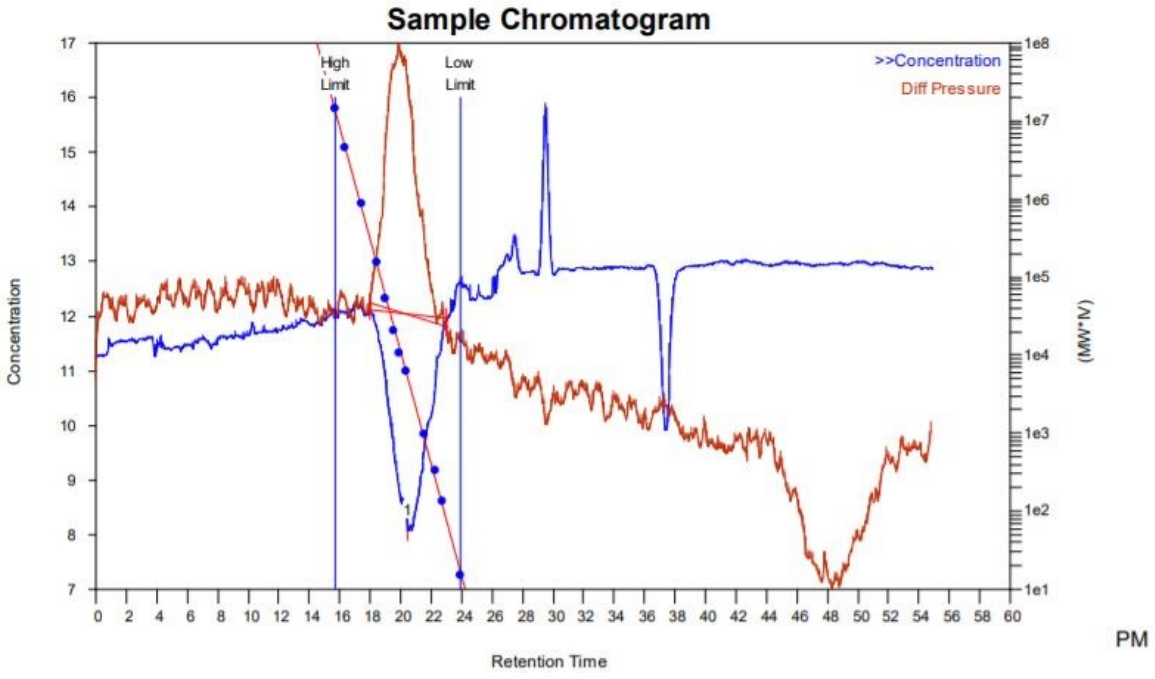

Narrow Standard Report

Processed Peaks

Peak No	Name	Start RT (mins)	Max RT (mins)	End RT (mins)	Pk Height (mV)	% Height	Area (mV.secs)	% Area
1	Concentration	17.95	20.42	23.02	-3.98219	0	589.422	100
2	Diff Pressure	17.95	19.82	23.02	2.34164	0	324.409	100

J/V curves P3 to P5 (Figure 4.S12)

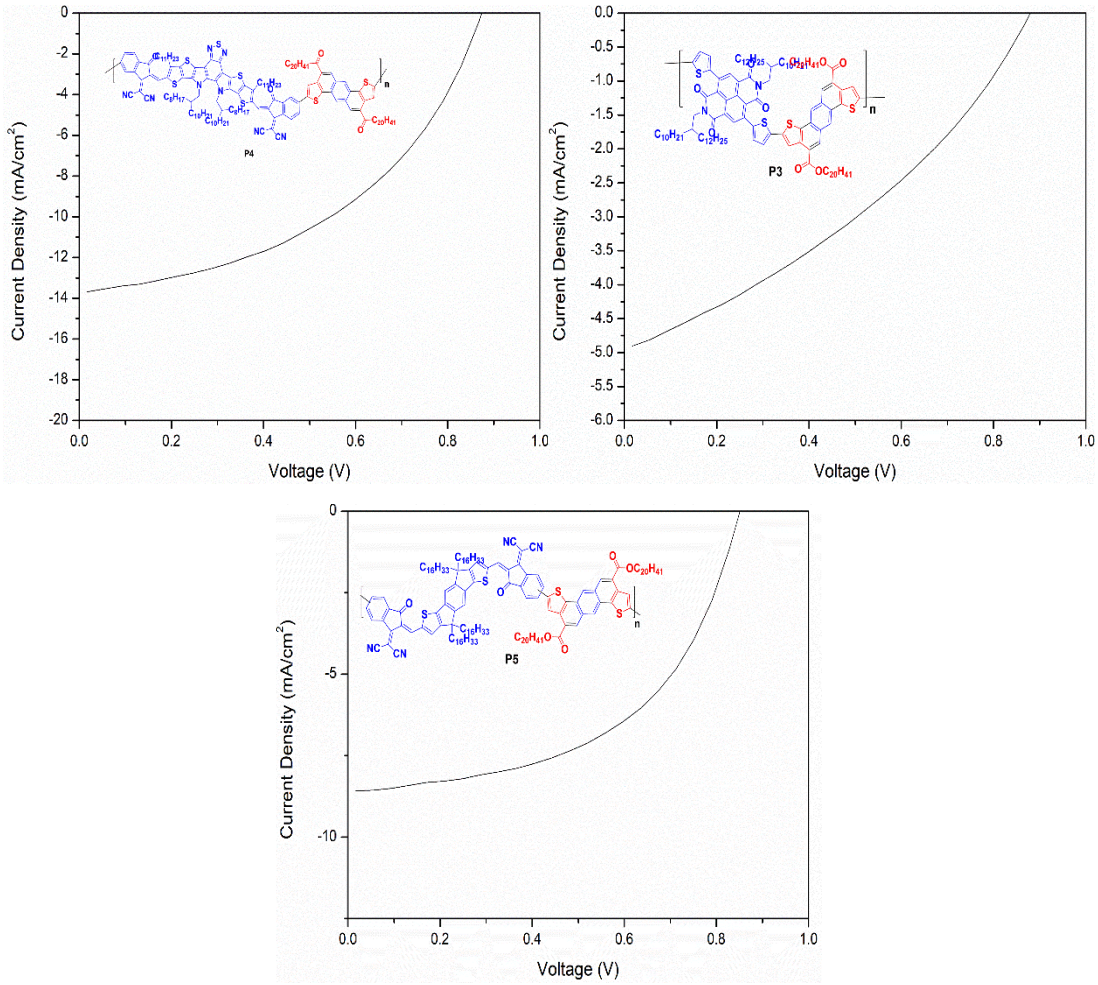

Figure 4.S12: J/V curves P3 to P5

Figure 4.S13: diffraction pattern for P3 and P4 top and P5 bottom

Line cut for polymers P3 to P5 (Figure 4.S14)

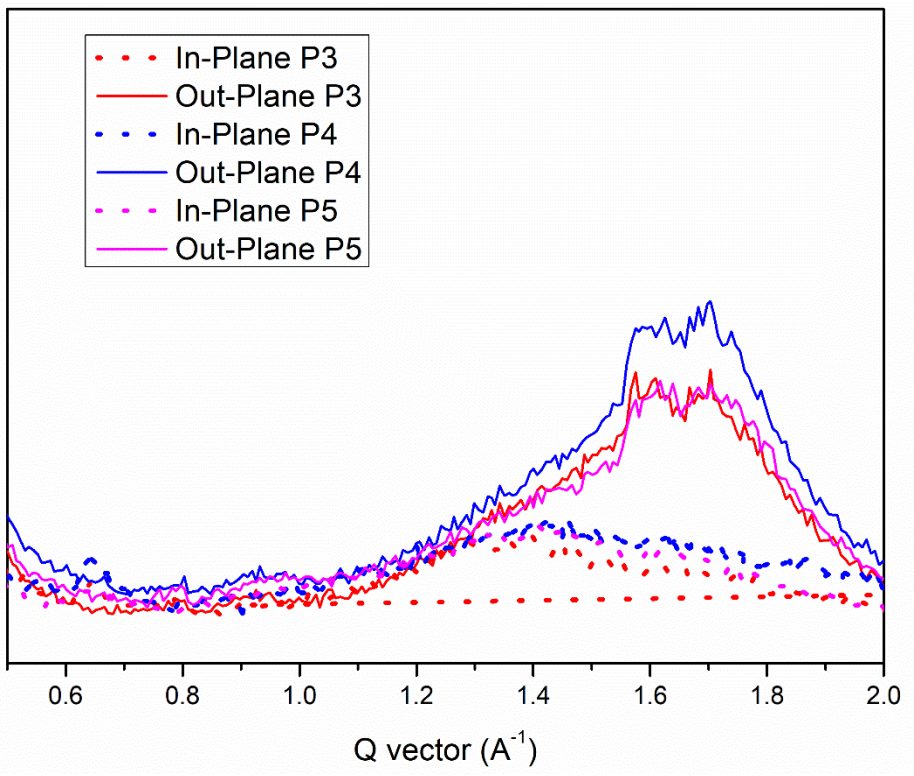

Figure 4.S13: the corresponding IP and OOP line-cut profiles for the indicated blend films

Summary of reflection position, d-spacing, and correlation length (CL) of theindicated films from GIWAXS measurements (Table 4.S2).

Film	In-Plane (100)				Out-of-plane (010)			
	q_{xy} (Å^{-1})	*d*-spacing (Å)	FWHM (Å^{-1})	CCL (Å)	q_z (Å^{-1})	π-π distance (Å)	FWHM (Å^{-1})	CCL (Å)
PBDB-T	0.290	21.64	0.106	55.34	1.685	3.73	0.217	26.91
P1	0.262	23.92	0.107	54.41	1.615	3.89	0.599	9.76
P2	0.284	22.10	0.216	27.06	1.666	3.77	0.432	13.53
P3	0.269	23.40	0.157	37.14	1.682	3.74	0.394	14.83

6.5 Chapter 5

6.5.1. Spectra of New Compounds

^{1}H NMR (500 MHz, $CDCl_3$) comparison between Homocoupling, Stille and DARPs polymers (Figure S1)

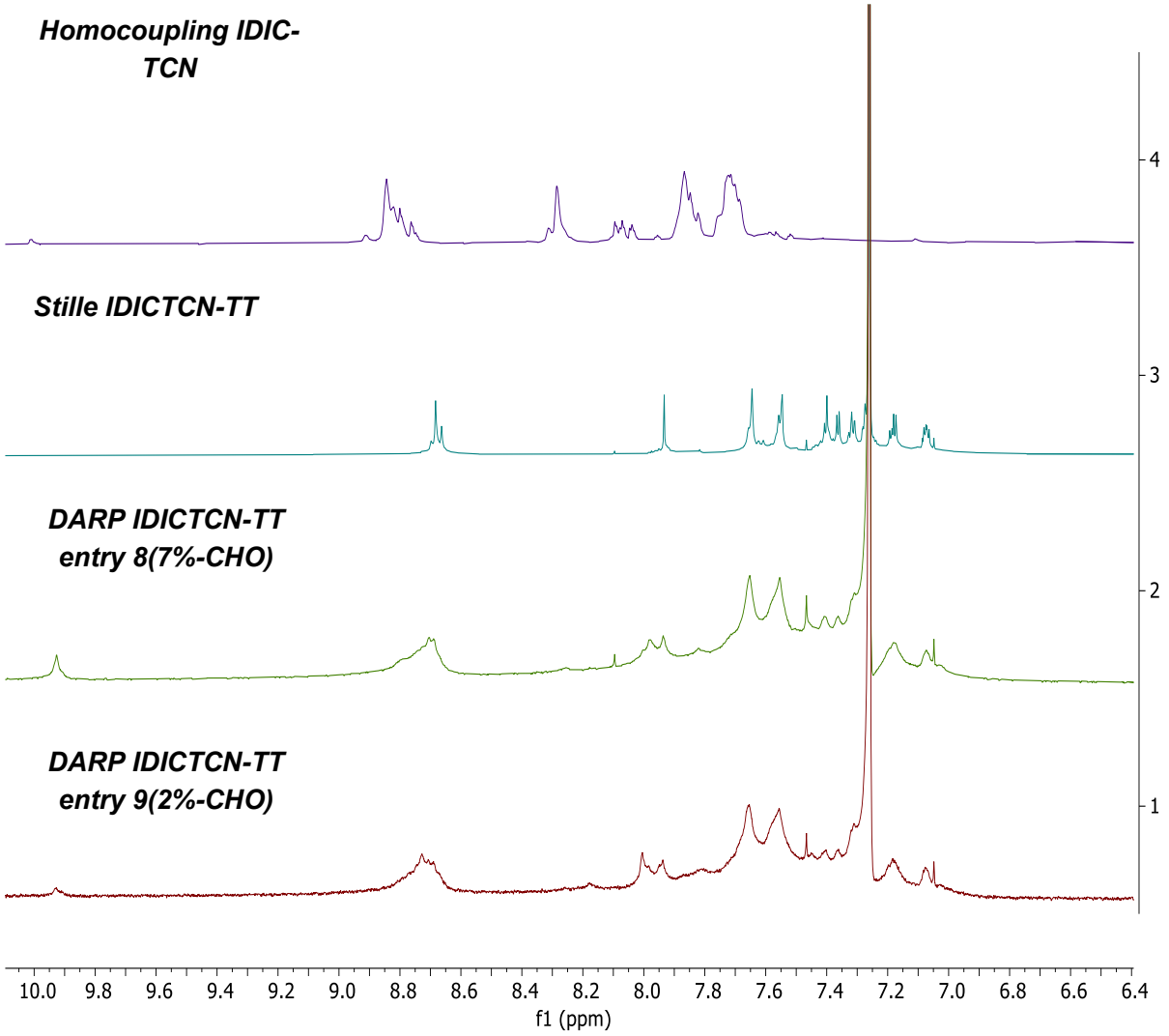

ITICTCN-TT via Stille

^{1}H NMR (500 MHz, $CDCl_3$)

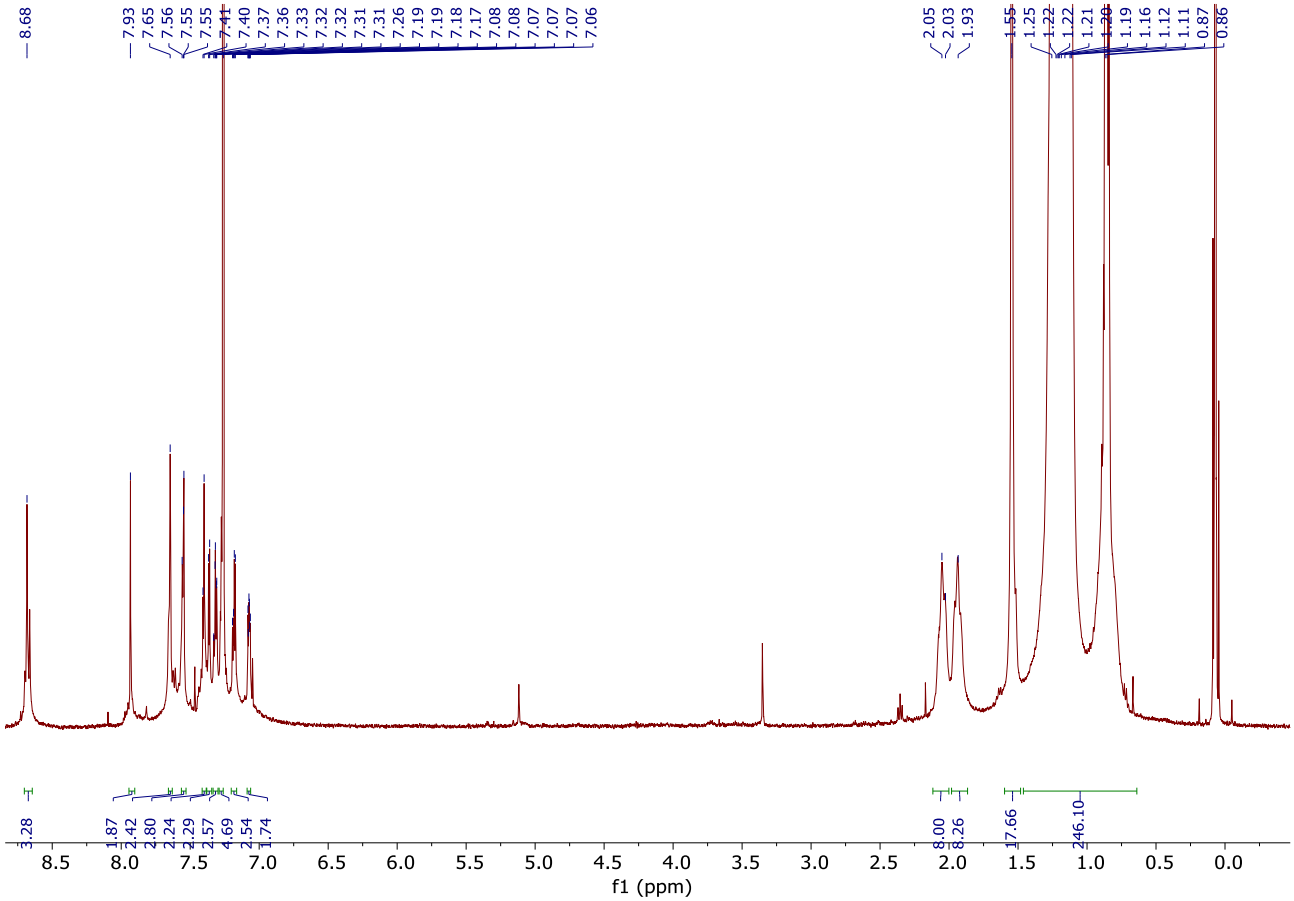

ITIC-ITIC homo-coupled compound via Stille

^{1}H NMR (500 MHz, $CDCl_3$)

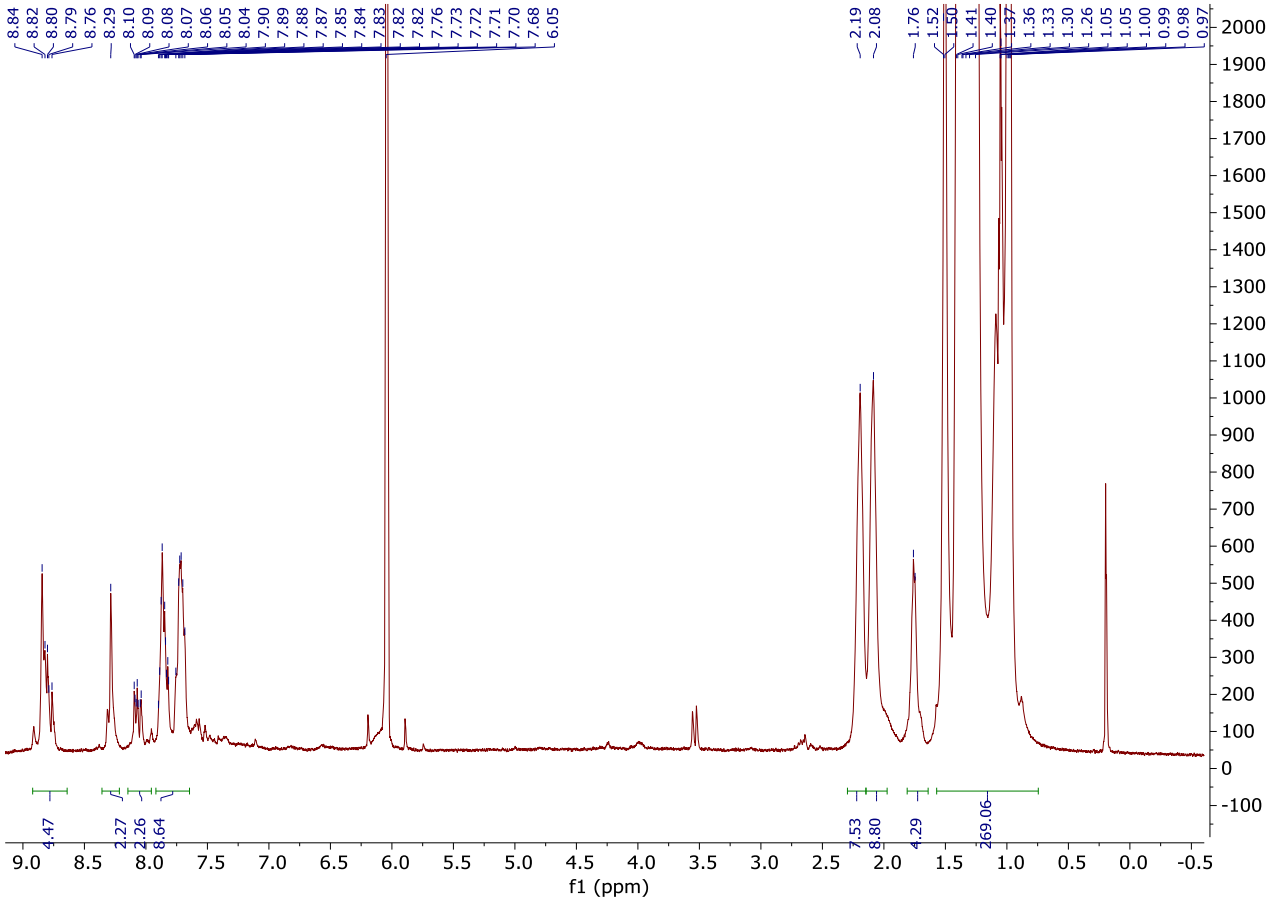

PS-Se via DARP

^{1}H NMR (500 MHz, $CDCl_3$)

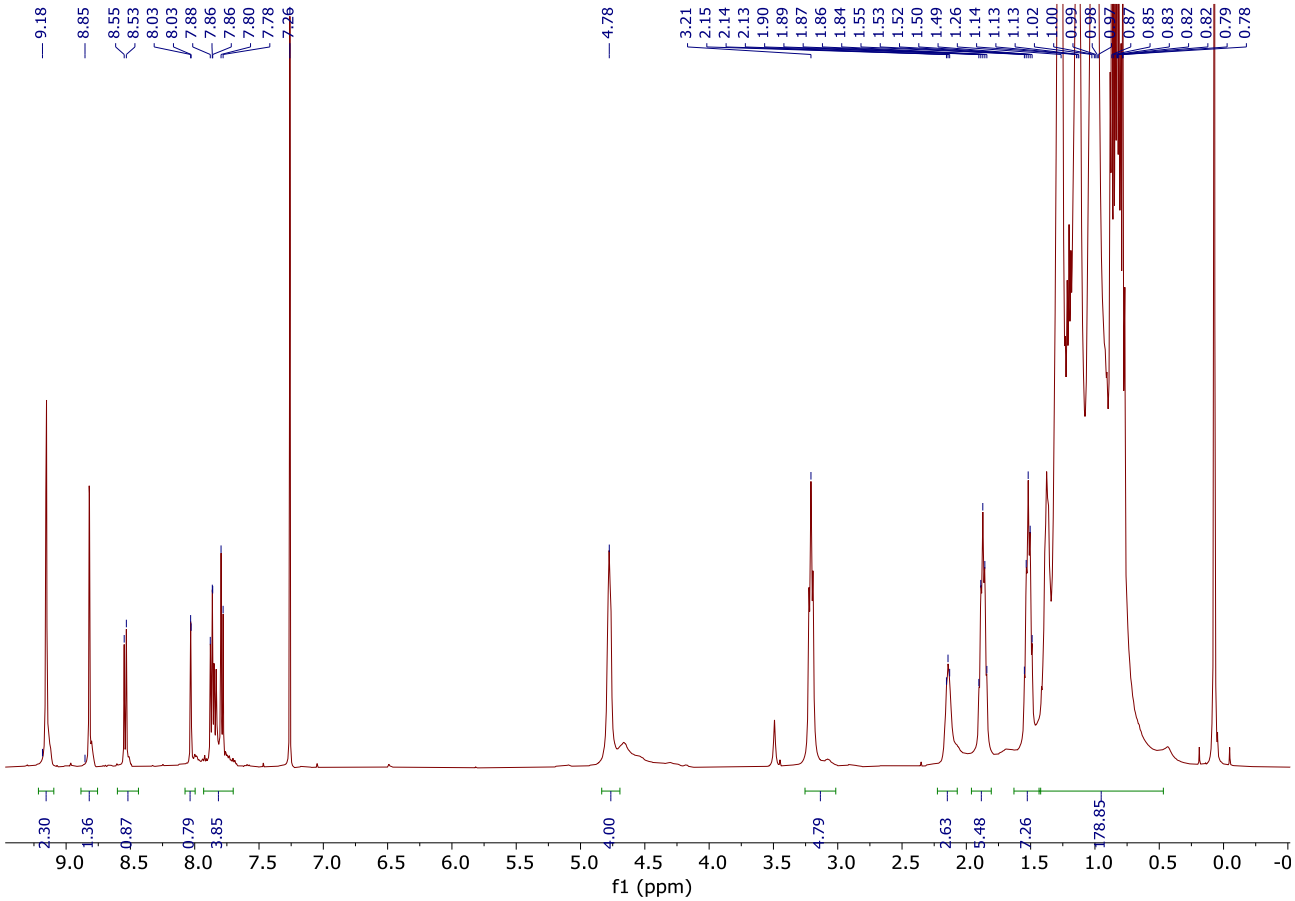

PS-Se via Stille

^{1}H NMR (500 MHz, $CDCl_3$)

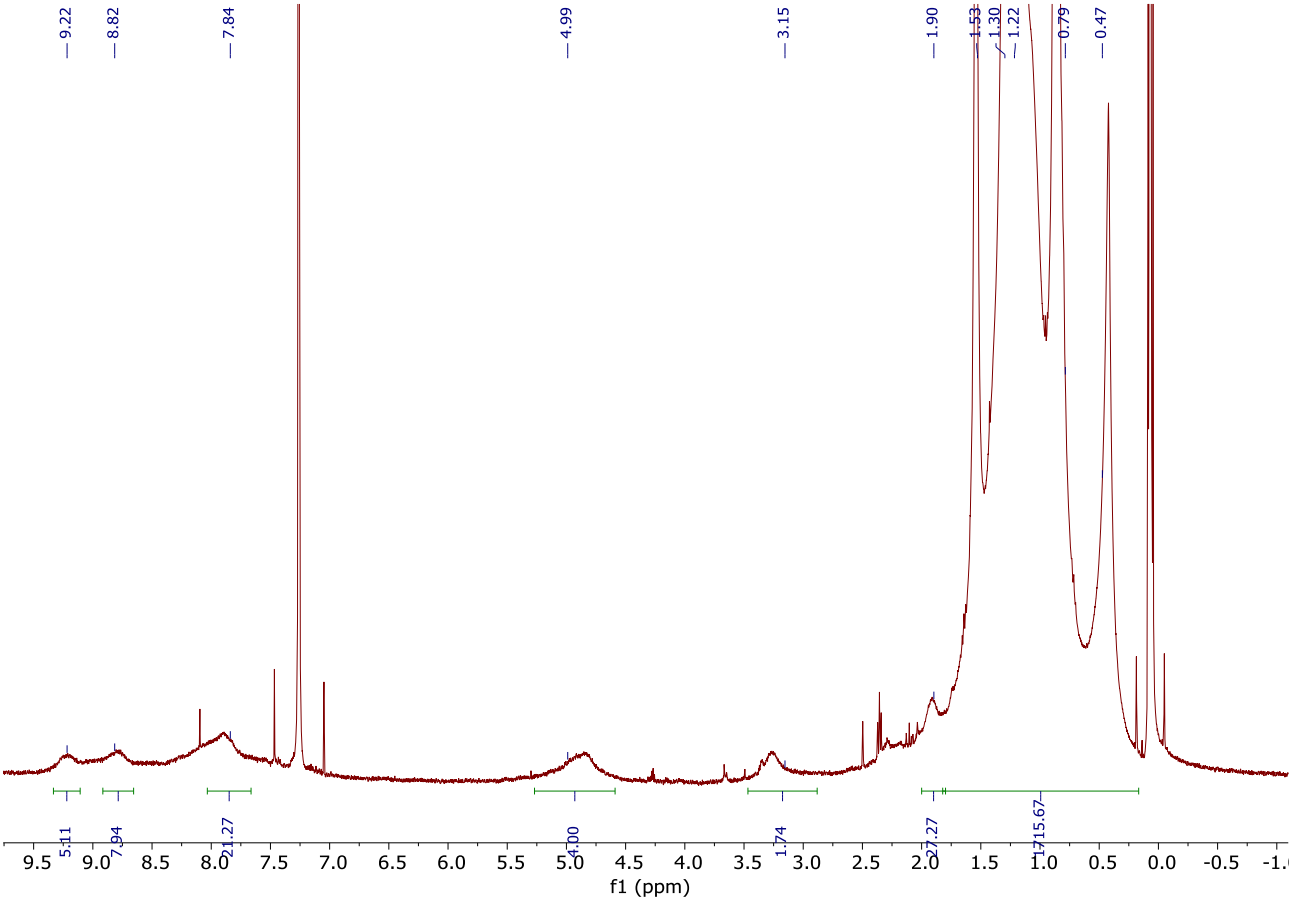

6.5.2. Additional Tables and Figures

GPC of PS-Se DARP$_S$ polymer (Figure 5.S1)

Cirrus GPC Sample Injection Report

Generated by: Tobin Marks — Monday, January 10, 2022 7:29 PM

Workbook: F:\Cirrus Workbooks\GPC-VS-08192021\GPC-VS-08192021.mplw

Sample Details

Sample Name: GF11-II

Acquired: 11/2/2021 9:44:36 PM — By Analyst: Tobin Marks

Batch Name: 11-02-21

Filename: F:\Cirrus Workbooks\GPC-VS-08192021\11-02-21-0003.cgrm

Concentration: 1.00 mg/ml — K of Sample: 14.1000

Injection Volume: 100.0 ul — Alpha of Sample: 0.7000

LIMS ID: — Bottle ID:

Workbook Details

Eluent: TCB stabilised with 0.0125% BHT — Flow Rate: 1.00 ml/min

Column Set: PLgel 10um MIXED-B LS 300 x 7.5 mm — Column Set Length: 900 mm

Detector: — Temperature: 150

Analysis Using Method: Universal Calibration

Comments:

Results File: F:\Cirrus Workbooks\GPC-VS-08192021\11-02-21-0003-Repeat (01).rst

Calibration Used: 8/21/2021 11:18:47 AM

Calibration Type: Universal — Curve Fit Used: 1

Calibration Curve: y = 18.414619 - 0.718238x^1

High Limit MW RT: 15.72 mins — Low Limit MW RT: 23.90 mins

High Limit MW: 3752000 — Low Limit MW: 860

K: 14.1000 — FRM Name:

Alpha: 0.7000 — Flow Marker RT: 0.00 mins

FRCF: 0.0000

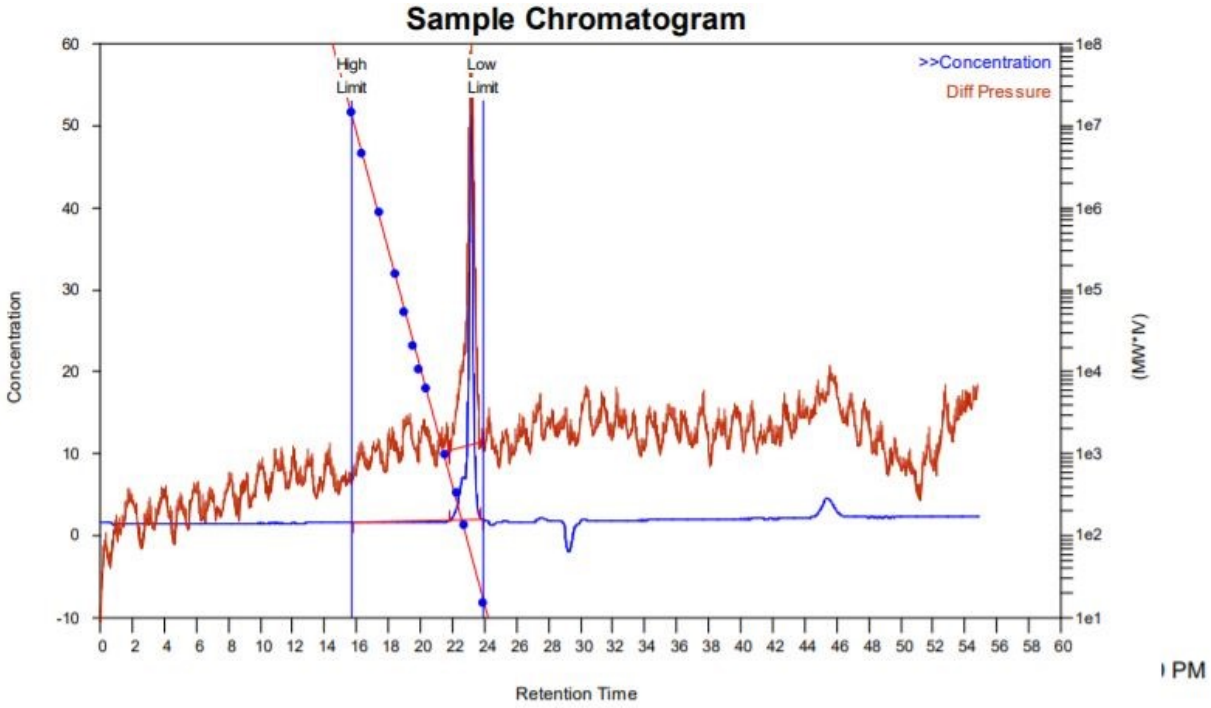

Sample Injection Report

MW Averages

Peak No	Mp	Mn	Mw	Mz	Mz+1	Mv	PD
1	2511	2589	2805	3161	3738	2744	1.08331

Processed Peaks

Peak No	Name	Start RT (mins)	Max RT (mins)	End RT (mins)	Pk Height (mV)	% Height	Area (mV.secs)	% Area
1	Concentration	21.80	23.13	23.72	51.4938	0	1262.35	100
2	Diff Pressure	21.80	23.15	23.90	2.12443	0	73.1626	100

Peak Detection

Baseline Detection

No	Start RT (mins)	End RT (mins)	Start Height	End Height	Is St Mod	Is End Mod
1	15.78	23.90	1.62	1.99	No	No
2	21.80	23.90	9.61	9.66	No	No

Figure 5.S1: GPC of PS-Se DARPS polymer

GPC of PS-Se Stille polymer (Figure 5.S2)

Cirrus GPC Sample Injection Report

Generated by: Tobin Marks — Monday, January 10, 2022 7:27 PM

Workbook: F:\Cirrus Workbooks\GPC-VS-08192021\GPC-VS-08192021.mplw

Sample Details

Sample Name: PS-Se stille

Acquired: 11/2/2021 8:46:48 PM — By Analyst: Tobin Marks

Batch Name: 11-02-21

Filename: F:\Cirrus Workbooks\GPC-VS-08192021\11-02-21-0002.cgrm

Concentration: 1.00 mg/ml — K of Sample: 14.1000

Injection Volume: 100.0 ul — Alpha of Sample: 0.7000

LIMS ID: — Bottle ID:

Workbook Details

Eluent: TCB stabilised with 0.0125% BHT — Flow Rate: 1.00 ml/min

Column Set: PLgel 10um MIXED-B LS 300 x 7.5 mm — Column Set Length: 900 mm

Detector: — Temperature: 150

Analysis Using Method: Universal Calibration

Comments:

Results File: F:\Cirrus Workbooks\GPC-VS-08192021\11-02-21-0002-Repeat (02).rst

Calibration Used: 8/21/2021 11:18:47 AM

Calibration Type: Universal — Curve Fit Used: 1

Calibration Curve: y = 18.414619 - 0.718238x^1

High Limit MW RT: 15.72 mins — Low Limit MW RT: 23.90 mins

High Limit MW: 3752000 — Low Limit MW: 860

K: 14.1000 — FRM Name:

Alpha: 0.7000 — Flow Marker RT: 0.00 mins

FRCF: 0.0000

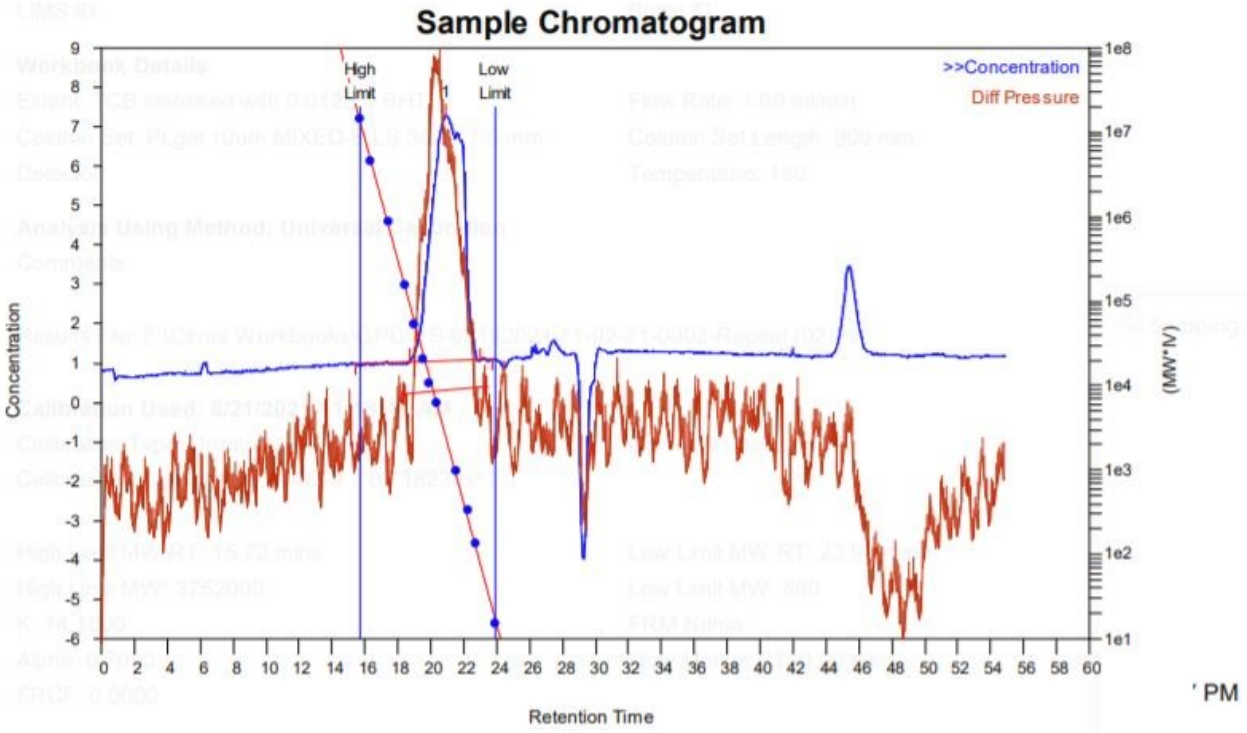

Sample Injection Report

MW Averages

Peak No	Mp	Mn	Mw	Mz	Mz+1	Mv	PD
1	63498	39606	91533	195885	324139	69657	2.31108

Processed Peaks

Peak No	Name	Start RT (mins)	Max RT (mins)	End RT (mins)	Pk Height (mV)	% Height	Area (mV.secs)	% Area
1	Concentration	18.75	20.90	23.02	6.25375	0	848.1	100
2	Diff Pressure	18.32	20.50	23.37	0.989159	0	121.894	100

Peak Detection

Baseline Detection

No	Start RT (mins)	End RT (mins)	Start Height	End Height	Is St Mod	Is End Mod
1	15.43	23.72	0.97	1.09	No	No
2	18.32	23.37	9.39	9.41	No	No

Figure 5.S2: GPC of PS-Se Stille polymer